ANALYSIS AND PATTERN MAPPING OF ORGANIC INTERFACES BY MEANS OF SEISMIC GEOPHYSICAL TECHNOLOGIES TO INVESTIGATE ARCHAEOLOGICAL PALAEOLANDSCAPES BENEATH THE SOUTHERN NORTH SEA

A.I. FRASER

PhD

2021

ANALYSIS AND PATTERN MAPPING OF ORGANIC INTERFACES BY MEANS OF SEISMIC GEOPHYSICAL TECHNOLOGIES TO INVESTIGATE ARCHAEOLOGICAL PALAEOLANDSCAPES BENEATH THE SOUTHERN NORTH SEA

Andrew Iain Fraser

Submitted for the degree of Doctor of Philosophy

Department of Archaeological & Forensic Sciences

School of Life Sciences

University of Bradford

ANALYSIS AND PATTERN MAPPING OF ORGANIC INTERFACES BY MEANS OF SEISMIC GEOPHYSICAL TECHNOLOGIES TO INVESTIGATE ARCHAEOLOGICAL PALAEOLANDSCAPES BENEATH THE SOUTHERN NORTH SEA

Abstract

Keywords: archaeology, environment, sea-level, palaeolandscape, seismic, marine geophysics, peat, Holocene, Mesolithic,

Investigating the archaeology of submerged landscapes beneath many metres of sea and buried under modern sands requires an understanding of the terrestrial surface as it may have been prior to the inundation. To do this, environmental evidence is required from contextualised in-situ locations and the best material evidence for preservation of archaeology, organic remains, dating proxies, pollen, diatoms, microfossils, coleoptera etc. is peat.

This research supports the search for peat in submarine environments by interpreting seismic surveys of the sub-sea floor and analysing reflective signals for distinctive organic responses. By means of sedimental analysis and ground observation, the research sets out to differentiate between organic signals, to allow for the identification and location of shallow peat beds within features of a palaeolandscape. Using these results should provide an opportunity to target such peat beds in an archaeologically focused coring programme.

The research also examines ways in which organic responses may be mapped over larger areas in order to integrate the results into a wider scale landscape model identifying potential peatland, marsh, valley fen and lowland areas.

Finally, the research introduces an artificial intelligence neural networking technology for the identification of organic interfaces in seismic surveys, examining three different ways in which this could be accomplished using specialist computer tools and software.

Declaration

This dissertation is the result of my own work and includes aspects of collaboration only where expressly indicated in the text. It has not been previously submitted, in part or whole, to any university of institution for any degree, diploma, or other qualification.

In accordance with Departmental guidelines, this thesis does not exceed 80,000 words.

Signed:____ 

Date:_____27th November 2020

Post Viva Corrections: _____7th June 2021

Andrew Iain Fraser BA, MSc

University of Bradford

Acknowledgements

Thank you to my supervisors, Professor Vincent Gaffney and Dr Simon Fitch, whose advice kept me sane through the process and to the ERC funded Europe's Lost Frontiers Project whose support and experience was always valued. I would also like to thank Dr Tine Missiaen and her team from VLIZ in Belgium along with the crew of the Belgica from whom I learned much about onboard live surveying operations.

Thank you to the University of Bradford for the use of their facilities and software applications.

Thank you to the University of Hull for the Word template this thesis has been formatted on.

On a personal front, I am extremely thankful for the support of my family, to Dave for his keen eye and encouragement and, always, to my wife Joyce without whom I would not have been able to get through the process motivationally, emotionally or financially.

CONTENTS

1 INTRODUCTION 1

1.1 Introduction to Thesis 1
1.2 The Aims of the ERC Europe's Lost Frontiers Project 2
1.3 Aim of Research 4
1.4 Objectives (6) 5

2 LITERATURE REVIEW OF CURRENT RESEARCH 9

2.1 Introduction 9
2.2 Significance of Doggerland and its Archaeology 9
2.3 The Geology of the North Sea 15
2.4 Evolution of the Holocene Landscape: Sea Level Change 24
2.5 The Archaeology of the southern North Sea 32
2.5.1 Archaeological Evidence – Offshore and Intertidal 33
2.5.2 Archaeological Evidence – Coastal Sites 38
2.5.3 Palaeolandscape Modelling 42
2.5.4 Climatic Change 47
2.6 An Overview of Marine Geophysics 52
2.6.1 Non-Acoustic Methods 54
2.6.2 Acoustic Mapping 55
2.7 An Overview of the Archaeological uses of a Geographical Information System 58

3 SEISMIC INTERPRETATION METHOD 61

3.1 The Acquisition and Usage of Data: 2D Seismic Data 61
3.2 Interpretation of 2D survey data 63
3.3 Depth Conversion 68
3.4 The Acquisition and Usage of Data: 3D Seismic Data 71
3.5 3D Geomorphological Interpretation 76
3.6 Creating terrain surfaces from 3D seismic data 77
3.7 Discussion – issues with interpolating to bathymetry 80

4 SPATIAL MAPPING & MODELLING 82

4.1 Introduction 82
4.2 Comparison of Differing data types, scales, projections and geo-spatial references. 84
4.2.1 Temporality: 84
4.2.2 Scale: 84
4.2.3 Projection: 84

4.2.4 Resolution: *88*
4.3 An Overview of Qualitative and Predictive Modelling 89
4.3.1 Predictive Modelling *90*
4.3.2 Deductive & Inductive Modelling *91*
4.3.3 Qualitative vs Quantitative Modelling *91*
4.4 Methods of integrating Seismic Interpretation into ArcGIS 92
4.4.1 Use of Digital Elevation Models in GIS: *94*
4.4.2 Raster Grid Definition: *94*
4.5 Spatial Analysis and Mapping of Seismic Data within ArcGIS 95

5 CASE STUDY - PEAT IDENTIFICATION IN GROUND OBSERVED SEISMIC SURVEYS 98

5.1 An Introduction to Submerged Peat and its Formation 98
5.2 Knowledge and Skillsets 103
5.3 Methods 105
5.4 A New Velocity Model 114
5.5 Vertical Resolution and Fresnel Zones 118
5.6 Facias and Signal Strength 121
5.7 Q Factor and Attenuation 122
5.8 Phase Analysis 126

6 CASE STUDY RESULTS 129

6.1 Environmental Core Analysis & Initial Interpretation 129
6.2 Seismic Interpretations of Horizons & Identification of Holocene Features 132
6.3 Line 18 Core Interpretations 133
6.3.1 ELF005B & HRVC49 ..... *133*
6.3.2 Core ELF002 ..... *138*
6.4 Line 11A Core Interpretations 141
6.4.1 Core ELF009 ..... *142*
6.4.2 ELF007, HRVC29 & ELF020 ..... *144*
6.5 Line 5 BM_1A Interpretations 149
6.5.1 ELF054 ..... *150*
6.6 Results for the New Velocity Model 153
6.7 Q Factor and Phase Analysis Results 157
6.8 Core Analysis by Depth and Phase Polarity 159
6.8.1 HRVC49 & ELF005B *159*
6.8.2 ELF002 ..... *162*
6.8.3 ELF009 ..... *165*
6.8.4 ELF007, HRVC29, ELF020 ..... *167*
6.8.5 ELF054 ..... *171*

7 SPATIAL ANALYSIS OF POTENTIAL PEAT BEDS IN SOUTHERN NORTH SEA 177

7.1 A Characterisation of the Study Area from a Spatial Perspective 177
7.2 Mapping the Organic Signature 177

8 DATA ANALYSIS & NEURAL NETWORKS 185

8.1 Introduction to Analysis by means of Neural Networks 185
8.2 Available technologies for the automation of geophysical machine learning 185
8.3 Supervised Machine Learning – Theoretical Models 187
8.4 Unsupervised Machine Learning (via an SOM) 193
8.5 Methods and Requirements for machine learning. 194
8.6 Method 1: Image Recognition (Python & Tensorflow) 195
8.7 Method 2: Unsupervised Vector Quantiser (via OpendTect) 202
8.8 Method 3: Supervised Artificial Neural Networking (via OpendTect) 210
8.9 Discussion on improving neural networking model results 218

9 CASE STUDY CONCLUSIONS – PEAT IDENTIFICATION IN INUNDATED PALAEOLANDSCAPES.....220

9.1 Identification and Classification of Organic Reflectors 220
9.2 Interpretation of boundary facies and depth precision employing a new velocity model 230
9.3 Phase Variance Signature Research used for the location of Peat 237
9.4 Acoustic Attenuation.....238

10 OVERALL CONCLUSIONS & DISCUSSIONS 245

10.1 Introduction 245
10.2 Summary of Results 247
10.2.1 Outline Process for Peat Bed Location:.....248
10.3 Industrial Uses for Marine Organic Seismic Modelling 250
10.3.1 Construction.....250
10.3.2 Aggregate Excavation 250
10.3.3 Windfarms.....251
10.3.4 Energy Prospection 252
10.4 Potentials for Archaeological Investigation 253

11 FUTURE WORK.....255

11.1 Use of Technologies for further Study – An Introduction 255
11.2 North Sea Research 255

11.2.1 Bright Reflectors *255*
11.2.2 Peat Location *256*
11.2.3 Parametric Echosounder Integration *256*
11.2.4 Artificial Intelligence *257*
11.3 Worldwide Application 258
11.4 Sea-Level Rise & Peat Cores 259
11.5 Collection & Context of Samples 260
11.6 Impact of this Research 261

12 WORK CITED 264

12.1 Websites Referenced: 286

13 APPENDICES 287

13.1 APPENDIX 1 – SEDIMENT CLASSIFICATION SYSTEMS 288
13.2 APPENDIX 2 – VELOCITY MODEL COMPUTATIONS 290
13.3 APPENDIX 3 – PYTHON SCRIPT FOR KERAS IMAGE RECOGNITION 291
13.4 APPENDIX 4 – LEGISLATION SURROUNDING MARINE ARCHAEOLOGY 293
13.4.1 Terrestrial Legislation of Concern: *293*
13.4.2 UK Marine Legislation and Guidance: *294*
13.4.3 European or International Waters Legislation: *294*
13.5 APPENDIX 5 – DIGITAL EXPANDED VERSIONS OF KEY IMAGES 296
13.6 APPENDIX 6 – NEW CALIBRATED DATES FOR OFFSHORE ARCHAEOLOGICAL FINDS 297

LIST OF TABLES

Table 2.1 Holocene Primary Unit Descriptions (Cotterill et al. 2017) 21

Table 2.2 Regional sea level indicators used around the world (Milne et al. 2009) 28

Table 2.3 Archaeological Dating Divisions for North Western Europe with Mesolithic and Neolithic focus in bold (Bicket and Tizzard 2015) 34

Table 2.4 Upper Palaeolithic and Mesolithic radiocarbon calibrated dates on human and worked faunal remains dredged from the North Sea (Weninger et al. 2008). Collation and new calibrated dates of all finds by author. 37

Table 2.5 Techniques in Marine Geophysics (after Bates et al., 2007; Verhegge et al. 2016) 53

Table 3.1 Source data acquired for the Europe's Lost Frontiers Project. Shot at differing resolutions and bin size ratios. 61

Table 4.1 GIS DEM toolkit (Conolly and Lake 2006) 94

Table 5.1 The Von Post Scale of Humification (Ekono 1981) 105

Table 5.2 Brief description of all cores containing organic material within study area 106

Table 5.3 Cores containing organic material and proximity to verifiable seismic survey data 109

Table 5.4 Breakdown of descriptive classifications for velocity models (Ekono 1981) 116

Table 5.5 (Wang 2016) showing primary conclusions. 123

Table 6.1 Data from the Humber REC Environment Report by Dr Benjamin R. Gearey and Emma-Jayne Hopla adapted by the author to correspond to seismic interpreted colours. 136

Table 6.2 HRVC29 Data from the Humber REC Environment Report by Dr Benjamin R. Gearey and Emma-Jayne Hopla adapted by the author to correspond to seismic interpreted colours 146

Table 6.3 Velocities based on Hamilton's porosity and bulk density calculations (Hamilton 1970) classified by grain size based on the Udden-Wentworth Scale (Wentworth 1922). 154

LIST OF FIGURES

Figure 1.1 Scope of Europe's Lost Frontiers Project and this Thesis.....3

Figure 2.1 Reid's proposed representation of Mesolithic lands and riverine routes (Reid 1913: p.40).....10

Figure 2.2 Examples of Dredges and Beam Trawling. Note the lip (left) and spikes (right) which can expose potentially eroded archaeology (Dixon 2015 p.27) 14

Figure 2.3 Important areas of the southern North Sea as referenced in this thesis 16

Figure 2.4 Salt Dome causing gas chimney which has repercussions to the shallowest levels (Müller et al. 2018 p.145).....18

Figure 2.5 The North Sea during the Neogene was a deep marine channel fed by rivers on either side (after Rasmussen et al. 2010 p.20) 20

Figure 2.6 Global sea levels as measured over stratified deposits from the last 7 marine oxygen isotope stages from two sites in Persian Gulf (Stevens et al. 2014 p.182) 25

Figure 2.7 Early Holocene Sea-Level Curves as represented by Jelgersma and Behre, (Jelgersma 1979; Behre 2007) with mean line of all intertidal dates by the author. Including data from Ward (Ward et al. 2006) from previous work by the author.....27

Figure 2.8 GIA Model of sea level rise in years BP at 500 year intervals from (Sturt et al. 2013) 29

Figure 2.9 Europe's Lost Frontiers mapping of land extent 2020 (Walker et al., 2021 in press).....30

Figure 2.10 The Leman and Ower Point Photograph: Anthony Kelly Norfolk Museum Services.....33

Figure 2.11 After (Maarleveld 2020) in The Archaeology of Europe's Drowned Landscapes (pp. 521-535)Drawing by Thijs Maarleveld 36

Figure 2.12 Sites of Mesolithic significance taken from the SplashCOS database (splashcosviewer.net). Black outline shows approximate coastline at 8.2ky.....39

Figure 2.13 Clark's map of northern Europe shows Doggerland closely resembling the extent we propose today (Clark 1936: insert.) 43

Figure 2.14 Morrison's Mesolithic UK coastline with lakes and rivers reproduced by author (Morrison 1980 p.85).....44

Figure 2.15 Global Sea-Level Rise in phased responses (from Li et al. 2014). Red lines mark the range of interpreted sea-level data (from Lambeck and Chappell 2001). 49

Figure 2.16 Differing acoustic technologies that can be employed. After Stoker et al. 1997.....57

Figure 3.1 Feature overlay from Humber REC marked on seismic above (including suggested core location in red) and sequence interpretation below (after Fitch 2011).....64

Figure 3.2 Coloured Interpretation showing clinoform sequences of fill deposition. Green - horizon of final terrestrial landscape, gold - modern Holocene sands. Between these are clinoforms demonstrating the inundation deposition. Data from FUGRO\RVO.nl (Thal et al. 2018).....67

Figure 3.3 Sound Speed Curve based on salinity over temperature (Lurton 2002) 69

Figure 3.4 Figure 3.4 Historical surface salinity (‰ in red) and temperature (°C in blue) of Southern Bight and English Channel in the 20th Century. Data provided by VLIZ (L van Meel 1975).....70

Figure 3.5 The extent of the PGS 3D MEGA MERGE Blocks (geo-referenced from PGS data).....72

Figure 3.6 Bathymetry, palaeochannels, glacial and geological features may be highlighted and overlaid as cultural layers in IHS Kingdom..74

Figure 3.7 Timeslicing and Gridding of 3D Blocks and highlighting of features allows correlation of 2D vertical data associated with even small features. 75

Figure 3.8 The ICES grid overlying PGS southern North Sea data blocks. .78

Figure 4.1 Above, the 3 representations of a sphere on a flat surface; Azimuthal, Conical and Cylindrical and below, examples of these projections and how they distort (source: MapProjections.net) 85

Figure 4.2 European UTM North Zones 29 – 35 shown in longitude. (Source: K Bellis, Creative Commons Wikimedia).....87

Figure 4.3 DEM, Culture and Timeslice (0.07s) data in a palimpsest layered GIS. Also included as Digital Appendix 13.5 Section 5 97

Figure 5.1 Kivenen's general classification scheme for peat (Kivinen 1980) 100

Figure 5.2 Types of Peat development. First 3 images show cross-sectional development, Final image is top-down view of saddle fen (Kivinen 1980). 103

Figure 5.3 Spatial representation of cores to survey lines to establish a study area 108

Figure 5.4 Surface temperature & salinity of southern North Sea over 40 years (data source: Cefas 2019) 110

Figure 5.5 Process of acoustic attenuation (WA) and the attenuation coefficient μ through material χ (after Kearey et al. 2013) 113

Figure 5.6 Simplification of Hamilton's continental shelf min-max variability of porosity vs grain size and porosity vs bulk density in material type with added potential peat ranges. 117

Figure 5.7 Left lateral Fresnel Zone represented by A to A' (Whitewright 2015) calculated dependent on frequency of individual survey. In the case of survey line 11A Frequency range shown right from 2.5Hz to a max of 6 kHz. 120

Figure 5.8 Applying spectral analysis for Q Estimation with bandpass filters in IHS Kingdom. 122

Figure 5.9 Trace Analysis from Upper Horizon As to Lower Horizon A_R 125

Figure 5.10 four types of phase wavelet and their corresponding polarity: a) Minimum Phase, b) Linear Phase, c) Maximum Phase, d) Zero Phase (Sheriff 2012) 127

Figure 6.1 Study Area within larger coring environment 129

Figure 6.2 Close up of the study area with prominent cores and survey lines marked 130

Figure 6.3 Survey Line_18 in its entirety. Vertical scales have been exaggerated for clarity 132

Figure 6.4 *Line 18 100N* showing similar high quantities of reflective signals on shallow slopes 134

Figure 6.5 ELF005B photograph and Lithography courtesy of M Bates, Lost Frontiers 2017. Adapted by author 135

Figure 6.6 Basic Interpretation of HRVC49 and ELF005B showing unit lithology as per Table 6.1 137

Figure 6.7 Core ELF002 (Photograph and lithology courtesy of M Bates, Lost Frontiers 2018 Adapted by author. 139

Figure 6.8 Basic Interpretation of ELF002 Core Lithography 140

Figure 6.9 Line_11A in its entirety. Vertical scales are exaggerated for clarity 141

Figure 6.10 Core ELF009 Photograph and lithology courtesy of M Bates, Lost Frontiers 2018 adapted by author 143

Figure 6.11 Initial interpretation of the area surrounding core ELF009 showing bright reflectors (white) 144

Figure 6.12 Basic Interpretation of feature containing cores ELF007, HRVC29 and ELF020 with the bed of bright reflectors below and laminated units above 145

Figure 6.13 ELF007 Photograph and lithology courtesy of M Bates, Lost Frontiers 2018 adapted by author 147

Figure 6.14 ELF020 photograph and Lithography courtesy of M Bates, Lost Frontiers 2017 adapted by author 148

Figure 6.15 Line 5 BM_1A with Core ELF054 approx. midway. Vertical scales exaggerated for clarity 149

Figure 6.16 ELF054 photograph and Lithography courtesy of M Bates, Lost Frontiers 2017 151

Figure 6.17 Basic Interpretation around core ELF054. The poor imaging is due to interference from weather 152

Figure 6.18 Three distinct bands of unweighted velocities grouped from new sedimental models 155

Figure 6.19 Velocities weighted by material volume within the core evidence. Average velocities favoured sandy shallower sediment obscuring deeper organic and silty / clayey sediments thus required weighting 156

Figure 6.20 A (left) Q Time banding between 45 and 65, while in Q against Frequency B (Whitewright 2015) a strong correlation between negative and positive phase is evident 158

Figure 6.21 Depth Converted Seismic Data magnified to show precision of analysis 160

Figure 6.22 Phase Function shows very strong defined polarity between negative (blue) and positive and the zero charge variance peaks 161

Figure 6.23 Depth Conversion and Ground Observation of Core ELF002 163

Figure 6.24 Phase Function with Variance reveals 2 layers of organic boundaries (in white) 164

Figure 6.25 ELF009 Depth conversion. Note the error bars are 5.5cm either side of core measurements or 11cm in total 165

Figure 6.26 Phase function with inset showing possible peat bed and deeper boundary within core ELF009 166

Figure 6.27 Depth analysis including error bars for vertical resolution & bright reflectors (Whitewright 2015). 168

Figure 6.28 Phase Function and picked peat horizons(white). Hatched area shows extent of potential peat bed 171

Figure 6.29 Depth analysis for ELF054. Initial interpretations made difficult due to inclement weather 172

Figure 6.30 The phase Function is of poor quality but shows distinct variance peaks below clay limit. 173

Figure 6.31 Cycle frequency (time) against target percentage frequency achieved 174

Figure 7.1 Organic Signature Occurrences by Amplitude Intensity 179

Figure 7.2 Depth of potential Peat beds below modern sea level. This may give some indication of locations where peat may be eroding onto the seabed 181

Figure 7.3 Extrapolated heatmap of Organic Signature by intensity. These contours are not topographic but by frequency of signal. 182

Figure 8.1 An illustrative model of an ANN or MLP neural network with 4 levels of logical depth. 188

Figure 8.2 Using a sigmoid bias to weight neurons allows integer outputs (Smith 2013). 189

Figure 8.3 2 x examples of the 4 seismic facies divisions from the 100x100 pixel image catalogue (Wrona et al. 2018). 191

Figure 8.4 Simple image recognition using Tensorflow based on 28x28 pixel imagery and 10 outputs with one hidden neural layer (after collaborative model Pytorch hub) 196

Figure 8.5 The same section of survey line V5-X-S3000 in phase view with variance peak overlay. A) on OpendTect B) and C) on IHS Kingdom on different PCs. Data courtesy of FUGRO RVO (Thal et al. 2018). ..197

Figure 8.6 (above) Employing a uniform and simplified colour bar and (below) variance peaks set to white may still obstruct detail. Therefore

there needs to be a function to run with variance on, variance off and compare 198

Figure 8.7 The Phase Degree against frequency of a typical Sparker survey (Thal et al. 2018) 199

Figure 8.8 Three examples of input data for image recognition ANN. a) direct 28x28pixel capture. b) Capture downsized to 28x28pixels in photo-editing software c) 128x128 pixel direct capture. 200

Figure 8.9 Manual picked vector sea horizon on crossline and inline, for SOM pattern recognition 203

Figure 8.10 The sample UVQ claimed to return a 55% match over 10 samples and 12 classes. However, the wave sample comparison only matched in 35% samples and classes. 204

Figure 8.11 Training the UVQ by samples, steady at 37% Average match after 141800 vectors trained 205

Figure 8.12 Sea Horizon as a UVQ 2.5D surface 206

Figure 8.13 Study Area in simplified Q-Factor and Band-pass Filter view with picked features 207

Figure 8.14 Line 11A picksets and horizons in phase view in OpendTect 208

Figure 8.15 Creation of UVQ surface was unsuccessful and failed to identify the organic deposits (in white, circled). 209

Figure 8.16 Diagrammatical representation of the OpendTect Supervised Neural Network as an MLP 213

Figure 8.17 The Event Attribute Set workflows. 214

Figure 8.18 Organic / Clay Silt interface locations as picked in IHS Kingdom and OpendTect 217

Figure 8.19 Training monitor showing dropping RMS but highly erratic percentage of misclassification 218

Figure 9.1 A (above) p-wave amplitude and B (below) the same data in phase function. Survey data by Fugro (Thal et al. 2018) 221

Figure 9.2 ELF005B analysis by depth 224

Figure 9.3 Analysis of HRVC49 bright reflectors and depth 227

Figure 9.4 ELF002 Analysis by Depth 229

Figure 9.5 ELF054 with good matches for the peat to silt definition but poor definition elsewhere 233

Figure 9.6 Depth Analysis of ELF020 235

Figure 9.7 Bright boundaries smear at HRVC49 but sharp and defined at ELF005B 240

Figure 9.8 Fugro Windfarm data reinterpreted using this thesis research for same survey line V5-S63000C (Thal et al. 2018) 242

Figure 10.1 Potential palaeo environment predicted by the phase variance process (study area) and spatial analyses of wider potential. 249

Figure 10.2 UK Aggregate Extraction Sites (Bicket and Tizzard 2015) 251

Figure 11.1 Grabs and dredging were tried at two locations interpreted as high potential for erosional or outcropping of peat.....260

Figure 11.2 Bottom Left flint debitage, Above and Right, worked fragment, probably from hammer stone (3D Scan courtesy of Tom Sparrow, Visual Heritage University of Bradford) 262

Figure 13.1 Classification by sediment class (derived from Folk - left, 1954 and Troels-Smith – right, 1955) 288

List of Abbreviations and Acronyms

Acronym	Full Descriptor
2.5D	Representation of X, Y & Z dimensions on a 2-dimensional surface.
ANN	Artificial Neural Network
BGR	Federal Institute for Geosciences (Germany)
BGS	British Geological Society
°C	degrees Centigrade
C20th	Twentieth Century
Cal BC(E) / Cal BP	radiocarbon dates calibrated against proxy dating methods e.g. tree rings giving calendar dates in common era (BCE) & before present (BP)
CGG	Catalogue of Global Geoscience (Seismic Image Store amongst other catalogues for subscription)
DEM	Digital Elevation Model – pixelated model of a 3D surface
ELF	Europe's Lost Frontiers Project
ERC	European Research Council
HRVC	Humber REC (cf) Vibrocore
(k)Hz	(kilo)Hertz – cycles per second measure of wave frequency
GEUS	Geological Survey of Denmark (and Greenland)
GIS	A Geographic Information System – Spatial database and analysis tool
kya	Thousand years before present (kilo-years ago)
LGM	Last Glacial Maximum (Approx. 24kya)
LIDAR	Light Detection And Ranging uses lasers to remote image
MARTA	Danish Institute for Marine Material Studies
MASLF	Marine Aggregate Levy Sustainability Fund
MLP	Multi-layer Perceptron Neural Network
NOAA	National Oceanic and Atmospheric Administration
NSPP	North Sea Palaeolandscape Project
OSL	Optically Stimulated Luminescence (dating technique)
Pa	Pascal (measurement of pressure)
PES	Parametric Echosounder – Seismic source.
PGS	Petroleum Geo-Services Group
P/S - Wave	Compressional (P) and Shear (S) Waveforms of seismic amplitude.
REC	Regional Environmental Characterisation
ResNet	Resident Networks – specialised AI routines for specific purposes.
RVO.NL	Netherlands Enterprise Agency
Seda DNA	Sedimental ancient DNA research
SEG-Y	Society of Exploration Geophysics Exchange
SLIP	Sea Level Rise Index Points
SO(P)M	Self-Organising (Pattern-Match) Map, an AI neural network variant
SPSS	Statistical Package for the Social Sciences – computer software
TIN	Triangulated Irregular Network. A vector model of a 3D surface.
TNO	Netherlands Organisation for Research in Applied Natural Science
UKOGA\CDL	UK Oil & Gas Authority \ Central Data Licensing
UNESCO NPL	United Nations Educational, Scientific and Cultural Organization National Physics Laboratory
UTM	Universal Transverse Mercator coordinate system of equal spatial zones
UVQ	Unsupervised Vector Quantiser – OpendTect's version of SOM (cf)
VGG	Visual Geometry Group part of the Deep Convolutional Network Research team at Oxford University
VLIZ	Flanders Institute of Marine Research
WGS84/EPSG	co-ordinate reference transformation systems with inbuilt datum.

List of Appendices

APPENDIX 1 … Sediment Classification Systems

APPENDIX 2 … Velocity Model Computations

APPENDIX 3 … PYTHON Script for KERAS Image Recognition

APPENDIX 4 … Legislation Surrounding Marine Archaeology

APPENDIX 5 … Digital Expanded Versions of Key Images.

APPENDIX 6 … New Calibrated Dates for Offshore Archaeological Finds

1 INTRODUCTION

1.1 Introduction to Thesis

'The Answer is in the Peat'

– Doctor Benjamin Gearey
(Gaffney et al. 2017b)

Whilst the introductory quote may appear unduly assertive, in a submarine archaeological context this observation may be substantially correct. Peat is an accumulation of dead and predominantly (>30%) decomposed organic plant material in saturated conditions and has been key in providing terrestrial archaeology with well-preserved evidence. In a submarine context, peat provides the environmental and dating proxies that allow researchers to investigate the submerged landscape, environment and cultural context for human settlement we frequently presume but have so little in the way of evidence for. It provides access to areas of high potential archaeology of human habitation that may be explored beneath the waves. Peat gives environmentalists their best available guides to localised sea level rise across the continental shelf of the UK by looking back through the last ten thousand years. It also preserves organic, archaeological material in excellent condition, in context, and in situ.

However, locating, mapping and extracting that peat from a particular chronological horizon, sometimes many metres beneath the seabed under often storm-tossed seas, is not a simple task. It is not like auguring a peat moor on land. A wealth of different resources, technologies and new disciplines are required to pursue this avenue of research.

This thesis sets out to show how the undersea landscape of the pre-inundated terrestrial land surfaces of the southern North Sea may be mapped and modelled. It demonstrates how these land surfaces may be interrogated to discover the potential for human habitation and cultural context in the late Mesolithic to early Neolithic. As part of a project team of multi-disciplinary archaeological experts, this research focuses on the investigation of marine geophysical surveys and by the interpretation of

these data, provides advice on a coring programme to gather environmental proxy evidence for the larger project (Gaffney et al. 2017a). The evidence provided is then utilised to access peat deposits within reach by means of a 4m core from the seabed.

Taking the peat question further, this thesis also specifically looks at ways in which organic signals detected in seismic surveys may be detected, analysed and classified by material type at the material boundaries. It examines and ground observes these seismic signals to make predictions on the likelihood of peat locations by means of maps and models.

1.2 The Aims of the ERC Europe's Lost Frontiers Project

The Europe's Lost Frontiers Project is a European Research Council (ERC) funded investigation into the Mesolithic / Neolithic boundary in the inundated lands of the North Sea. This involves a multi-disciplinary approach investigating existing archaeological, geophysical and environmental data as well as collecting and collating new, specifically focused, data to further our knowledge on these submerged landscapes. These new data are predominantly in the form of seismic surveys (and sub-bottom profiles) and a new programme of sedimental coring. This coring provides environmental proxies for use in dating, sedimental ancient DNA (seda DNA) investigation, coleoptera, diatom, pollen and chemical analysis (Gaffney et al. 2017a).

The research pertinent to this thesis, which played a role in the project, is around seismic interpretation and mapping. Using the latest technology to investigate seismic data, it is possible to analyse the geomorphological changes in landscapes beneath the sea and, using these data, undertake the following:

- Model the changes in land use from that of potential terrestrial occupation to that of abandonment under marine inundation.
- Identification and interpretation of features within the early Holocene terrestrial landscape based on seismic data
- Map the terrestrial extents and coverage of this landscape
- Predict sites of high potential for core locations for both ground observation and archaeological resource
- Reconstruct and spatially model the predicted palaeolandscapes derived from such core analysis

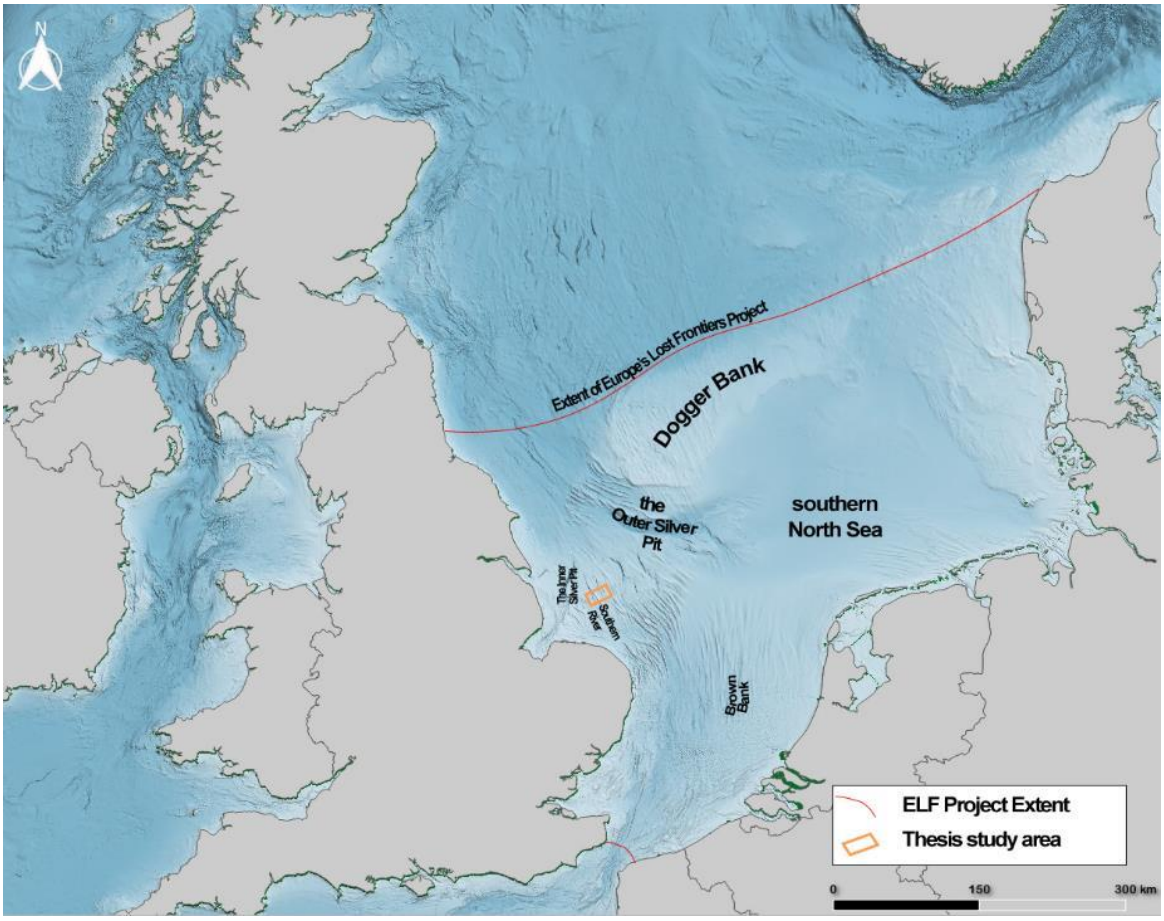

Figure 1.1 Scope of Europe's Lost Frontiers Project and this Thesis

The overall study area for the Europe's Lost Frontiers Project is the North Sea, from the north of England across to the tip of Denmark in the North and the Dover Strait in the south; approximately 210,000 km^2 in area (Figure 1.1). The seismic surveys for the project were gathered under contract or from commercially available open licence data sources. Further seismic surveys of particular areas were undertaken by the ELF project or made possible via a collaborative project with the Flanders Institute of Marine Research (VLIZ). These bespoke missions also allowed for a focused archaeological coring programme driven by the interpretation of the seismic surveys from these and previous projects.

The role of the project within this research was in the availability of data, both seismic surveys and core evidence. The mapping, modelling, interpretation and analysis within this research was pursued entirely independently. The project provided the opportunity to investigate a specialist case-study with specific focus on the link between seismic interpretation of acknowledged 'bright organic' reflectors and the

ground observation of core evidence. The research had its own set of aims and objectives, separate from the project. These were to examine the survey data and core evidence to assess whether such bright reflectors:

- could be directly attributed to a particular type of organic material e.g. free gas, generalised organic sediment or peat?
- Could denote a distinct material interface or a particular difference in abruptness of contact at these interfaces?
- Demonstrated a consistency with materials of similar densities, porosities, humification and if so, could a reliable velocity model be created that included shallow organic sediments?
- Would it be possible to develop a test to auto-detect the organic signature of submerged peat beds using a neural network?

1.3 Aim of Research

The aim of this research was to utilise open access and contractually accessible seismic marine geophysics data to analyse, interpret, map and visualise the submerged palaeolandscapes of the southern North Sea basin. These data were collected on behalf of the Europe's Lost Frontiers ERC funded Project. The focus of the research was the terrestrial landscape of the early Holocene – a pre-inundated, post-glacial landscape occupied by hunter-gatherer societies on the cusp between the Mesolithic and the Neolithic. The research involved the integration of multiple disciplines and software packages. It required the development of new skillsets to interpret a landscape transitioning from a terrestrial to marine environment and understand what that may have meant for the people living through this time of huge climatic, landscape and cultural change.

These changes may have been most evident in the low-lying plains of the southern North Sea. Fenlands, marshes, coastal and estuarine peats may bias the surviving evidence (Garton 2017), though it could be argued that these areas were preferred by prehistoric man (Leary 2014). Palynological indicators suggest a diversity of open canopy plants and micro charcoals with possible inferences to human activity (Krüger et al. 2017). Extant archaeological peatland sites discovered at Mesolithic coastal locations such as Star Carr, Howick and, possibly closest to this current research, the Somerset Levels provide vital supporting evidence for the value of peat in these contexts (Milner et al. 2018). The preservation of the archaeology

and the environmental proxies in each of these sites was improved by the anoxic environment provided by the peat (Gearey et al. 2010). Therefore, areas of submerged peats are an important focus for submarine coring. The identification and location of such peats are potentially of great archaeological significance.

1.4 Objectives (6)

The stated objectives for this research and the thesis were six-fold as follows:

> Objective 1 – To collate, collect and analyse available geophysical survey data in the project area and to interpret the results for a focused coring programme.

The first objective was to establish what data were available, at what scale, resolution, and using which technologies. Once these had been gathered, interpretations of the available geophysical data could be made to advise an archaeologically focused coring programme. Once extracted, these cores were then be sampled for environmental proxies, archaeometric and Seda DNA testing.

The interpretation of terrestrial features within the geophysical data was also vital for the understanding of geomorphological changes in the landscape. Examination of interface boundaries between differing materials and between major terrestrial and marine periods allowed the building of relative chronologies. The infilling clinoforms of each inundation event could potentially inform the interpretation on how and at what rate transgression occurred. This in turn led to a wider understanding of mapped environments and the creation of more robust models.

> Objective 2 – To identify, source and learn new software packages necessary for research purposes.

The analyses of marine geophysics and the modelling of the data required specialist knowledge and applications. Therefore, it was crucial to source and master the appropriate software needed to process these data. To

this end a suite of software applications needed to be identified. This would include the processing of SEG-Y seismic survey geophysical data, spatial analyses and georeferencing. Specialist and general neural networking solutions were investigated, and coding options pursued. Some were selected because they were industry standard, others because they were well established already within the University of Bradford. Other solutions were more niche or specialised. Each package required an element of learning to attain a competent level of usability.

> Objective 3 – Interpret seismic data, pick terrestrial horizons for topographic grids, model depths and export 2.5d surfaces (DEMs) for use in GIS maps and models. Detail palaeo features in shapefiles for use in spatial models and scenarios.

The mapping and modelling of features and landscapes for the purposes of creating a depth corrected export of a Holocene land surface required interpretation of seismic data. This was an advanced skillset to develop and put into practice, but it underpinned the work throughout this thesis and individual research. Understanding the process of sediment deposition enabled the identification and picking of appropriate seismic interfaces for gridding, modelling depths and creation of topographic surfaces of an early Holocene terrestrial landscape.

Palaeo features such as rivers were identified and then traced by hand from the survey data. These were saved as shapefiles and then digitally georeferenced with a Global Information System (GIS). Using spatial toolkits and landscape surfaces alongside these shapefiles, a palimpsest of data could be developed on which to base predictive models.

> Objective 4 – Construct a velocity model based on environmental core reports and statistical analyses and apply these to seismic data to predict peat contact locations and depth.

To differentiate organic material sediment from free gas by seismic signal, it was necessary to construct a precise set of velocity models. These velocity models correlated the peat collected from the core evidence to that demonstrated by the high intensity reflectors in the seismic data. This could be achieved by combining the precise measurements from the lithostratigraphical reports and environmental analysis with calculations based on the classification of sediment deposition, density and porosity.

The interpretations of seismic responses tied closely to the unit classifications and made possible the inclusion of a calculation for the attenuation of peat sediment specifically for a peat / clay or a peat / silt boundary.

> Objective 5 – Investigate 'bright' organic seismic reflectors and using velocity model attempt to construct a signature for detecting peat in seismic data.

DHI or Direct Hydrocarbon Indicators are used by the energy industries to refer to the four signifiers of potential gas reservoirs (Müller et al. 2018). One of these is the 'bright' reflector. Such a material contact has been identified in previous research as organic sediment, peat or even organic artefacts such as wood (Bull et al. 1998). To clarify this, a new velocity model was created to investigate these seismic reflectors and ground observe them against core evidence. The signals could be analysed under a variety of test criteria such as bandpass filters, Q-Factor analysis, Spectral Analysis, Attenuation and Scatter, Phase Function and Trace Analysis. The outcomes would be a set of criteria or a 'signature' that determined the presence of peat at a boundary with another specified material, such as silt or clay or sand.

> Objective 6 – Construct a neural networking solution for automation of peat boundary detection and classification based on the tools built from the 'seismic signature' developed in the research.

Taking the working criteria of a peat boundary signature from Objective 5, the final step would be to automate the detection by means of a neural network. Three options were pursued in the research. A Self Organising Pattern Map and a Multilayer Perceptron both in the software package OpendTect utilised full seismic survey line traces and processed event-based parameters for their analyses. The third was a coded solution in Python and was intended to replicate a Keras image recognition Artificial Neural Network of seismic facies.

For Specific Analysis in line with the PhD, the thesis therefore concentrated on answering two questions:

1) Is it possible to use ground observation techniques of core analyses based on environmental reports to build up working velocity models for peat detection and depth analysis in seismic data?
2) If so, could a verifiable signature be identified for potential clay / peat or silt / peat interfaces? Could such a signature be used in an automated routine, such as a neural network data analysing cluster method, e.g. a self-organising pattern map (SOPM)?

2 LITERATURE REVIEW OF CURRENT RESEARCH

2.1 Introduction

The North Sea occupies an area between the rocky landscapes of Scandinavia to the north east and Scotland to the north west. To the west are the eroding cliffs of England, to the east and south the sea is bordered by the flatter low-lying beaches of continental Europe. It lies between 55 degrees and the 51 degrees latitude north (Alexander 2020). Within this, the British sector of the southern North Sea alone covers some 62,000 km^2 (Fitch 2011), with water depths ranging from 18 m at the top of the Dogger Bank moraine to over 80 m in the Outer Silver Pit (Paramor et al. 2009). The most prominent feature within the southern North Sea, geologically, is Dogger Bank; a large elevated moraine of clastic deposits overlain with modern sands (Veenstra 1965). Over the last century, it has proved an important site of palaeontological and archaeological significance (Coles 1998; Flemming 2003; Mol et al. 2003; Van de Noort 2011; Fraser 2016).

2.2 Significance of Doggerland and its Archaeology

The North Sea is perhaps one of the most significant areas of submerged prehistoric archaeology in the world. Evidence for interrupted occupation can be found dating from 900 kya with Europe's earliest evidence of hominin activity at Happisburgh, eastern UK (Parfitt et al. 2010). Homo neanderthalensis skull fragments were discovered on the Zealand Ridges, off the coast of the Netherlands (Hublin et al. 2009), and other hominin species including numerous *Homo sapiens* remains have been found beneath the sea bed (De Groote et al. 2018). This is in addition to the countless palaeontological faunal finds that surface regularly in fishing nets and trawling dredges, including *Mammuthus primigenius, Bos taurus primigenius, Cervus elaphus* and other exotic large mammals (Bynoe et al. 2016). As well as purely faunal remains, the sea boasts a rich archaeological record of worked organic tools - bone, antler and wood (Louwe Kooijmans 1970; Sier et al. 2014; Bailey et al. 2020) and abundant lithics including an assemblage of 102 Palaeolithic hand axes from the sea bed off East Anglia, UK (Tizzard et al. 2011).

Archaeologists and geologists as far back as the turn of the Twentieth Century understood the significance of fossilised trees on the foreshore and the presence of moorlog caught in fishermen's trawls (Reid 1913; Clark 1932). Attempts, such as Clement Reid's hypothetical river systems (Reid 1913) have been made to postulate and map the extent of these lost lands. Despite this, archaeological interest in submerged landscapes remained low for many years. This may have been due to the perception of the North Sea as merely a 'land bridge' between the continent and the UK (Jacobi 1976). It may have been a combination of issues to do with accessibility, territorial bureaucracy, commercial restrictions and the resources needed to undertake investigations in such hostile environments. These are discussed in greater depth in the Marine Framework Document – NSPRMF (Peeters et al. 2019). Whatever the reason for neglect, it was Bryony Coles' Speculative Survey of 1998 that popularly reignited archaeological interest in Doggerland.

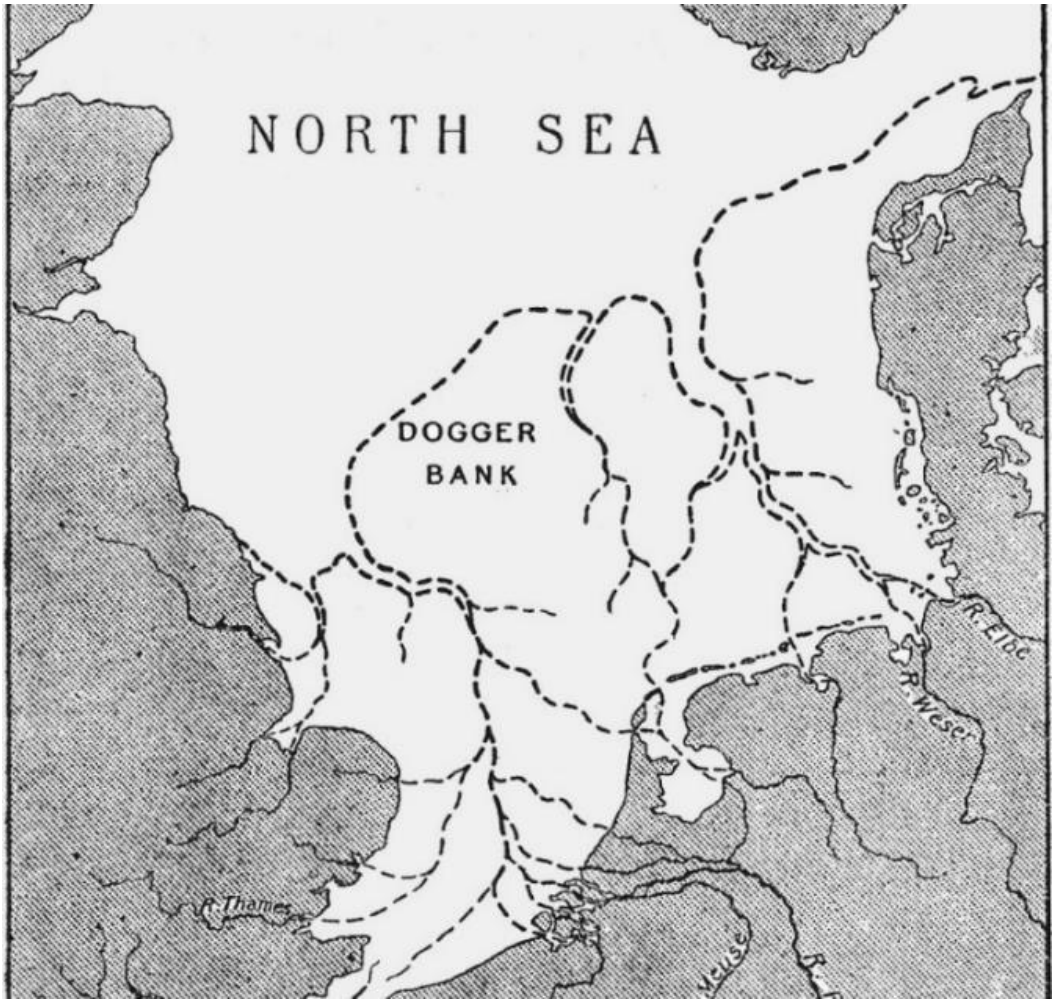

Figure 2.1 Reid's proposed representation of Mesolithic lands and riverine routes (Reid 1913: p.40)

Coles, a specialist in wetland archaeology, drew together existing data from the southern North Sea and postulated an intriguing landscape filled with plants and animals and peopled with Mesolithic hunter-gatherers. She called this '*Doggerland*' after this supposed focal point of the southern North Sea (Coles 1998).

Coles' work sparked an upsurge of interest in submerged landscapes off shore and in the intertidal regions of the UK (Coles 2000; Wenban-Smith 2002), around the coastlines of Denmark, Germany (Fischer 2004) and in the Netherlands (Duin et al. 2006). This in turn led to wider interest in continental shelf research and multi-country project participation. Excavation, curation and unified classification by dedicated projects such as SplashCOS (Bailey et al. 2020). EU-funded projects could bring together the combined knowledge of marine archaeology to work on ventures such as the mapping of submerged river valleys and major landscape features for archaeological potential (Gaffney et al. 2009). Further awareness has led to greater involvement both in Industry and government. Energy and extraction companies began to routinely engage archaeological advice and assessment in the planning stages of the bid process (Balson and Harrison 1988; Thal et al. 2018). Likewise infrastructure development such as the Storebælt in Denmark or Maasvlakte Yangtze Harbour learned to prize the cultural heritage of the projects at the centre of their planning (Aaby et al. 1997; Sier et al. 2014).

Before the Twentieth Century, the very concept of the North Sea as a terrestrial land mass was rarely, if at all, considered beyond the curiosity of tree remains rooted under coastal waters at low tides, or the bones of land animals caught in fishing nets. Geologist and interested botanist, Clement Reid, released his book *Submerged Forests* in 1913. He recognised that fossilised trees, submerged off the British coast could only have grown on dry land and that a rising sea-level in the past must have submerged them.

Using geological stratigraphy and peat analysis, he concluded that following the last glaciation, large areas of the southern North Sea could have existed as dry land with areas such as the Dogger Bank standing some 30m above an otherwise flat alluvial plain (Reid 1913: 40). His map (Figure 2.1) attempted to show the potential extent of submerged land and suggested that the area of Dogger Bank could have existed as an

island long after the rest of the land had been inundated. What Reid was missing were any dates in evidence of this prehistoric land.

In 1931, Pilgrim E Lockwood, skipper of the trawler *Colinda*, night-fishing off the Ower and Leman sand banks, hauled up his nets and found a piece of moorlog - floating peat - had become lodged in his net (Mithen 2003). Upon breaking it, he discovered a pointed implement that would become known as the Leman and Ower 'Harpoon'. Such tools had already been found on land, and the point shared similarities to those found in both the UK and Denmark (Clark 1954). However, this was the first to be discovered in an entirely marine environment and the first recorded evidence of human occupation of terrestrial land beneath the waves. Existing points helped tie the Leman and Ower 'Harpoon' to a specific culture, the Maglemose from Denmark, and to suggest a date of use within the Mesolithic period, between 12 kya and 6 kya (Clark 1932).

This discovery led archaeologist Graham Clark to examine the Maglemose cultural source of the Ower and Leman 'Harpoon' in closer depth. He was able to synthesise the cultural, environmental and palynological data together to build a picture of the Mesolithic hunter. In the appendix to his book *The Mesolithic Age in Britain* (Clark 1932: Appendix 1) he stated '*the southern part of the North Sea was dry land supporting … forest and affording a far easier passage to early settlers than is now the case.'* This was to prove a turning point in Clark's career. Soon after, he formed the Fenland Research Committee which excavated the Mesolithic site at Peacock Farm in East Anglia and then Star Carr in the Vale of Pickering.

Star Carr provided a number of well-preserved Mesolithic artefacts (Clark 1954). As well as a large number of faunal remains, ceremonial items and other tools, further Maglemose-style implements, like the one discovered by the *Colinda*, were discovered (Clark 1954; Conneller et al. 2012; Milner et al. 2018). Radiocarbon dating of the Ower and Leman point in 1988 confirmed Clark's initial research, with a range of dates contemporaneous to those of Star Carr and similar Maglemose-style points catalogued subsequently on the Netherland coastlines (Louwe Kooijmans 1970; Bronk-Ramsey et al. 1990: (Clark, 1954; Megaw 2007). Such points are still found regularly on the beaches of northern Netherlands. They are dredged from below the modern sea floor when clearing major shipping lanes and then sprayed or 'rainbowed' onto the beaches for reinforcement from the rising sea levels (Amkreutz and Spithoven 2019).

Understanding of prehistoric submerged landscapes and how to discover them via technology advanced greatly in the late 1990s and into the millennium. Geographical agencies such as the BGS began to investigate and map buried formations by means of marine geophysics (Brew 1996), the *North Sea Palaeolandscapes Project* used oil and gas industry seismic reflection data to visualise the first views of fully mapped terrestrial landscapes that did not rely on modern bathymetry for topographic data (Gaffney et al. 2007; Gaffney et al. 2009). Such work has continued in both UK and Dutch territorial waters (Duin et al. 2006); Gaffney et al. (2009); Gaffney et al. (2017a), but remains unfinished and despite some useful environmental modelling (Fitch 2011) suggesting potential faunal and floral distributions, the large scale picture remains incomplete and uncertain.

Focused archaeological work within the southern North Sea has been forthcoming during recent years. Large scale programs led by national geological agencies – TNO in the Netherlands, BGS in the UK, BGR in Germany have been careful to include archaeology into their marine assessments and reporting. Publications such as the Strategic Environmental Assessment Reports - SEA Part 3 Central and Southern North Sea – produced for the UK government (DTI 2002), the Regional environmental Characterisations (Balson and Harrison 1988; Tappin et al. 2011), and Hans Peeter's North Sea Framework research have done much to advise governments on the state of cultural heritage beneath the ocean (Peeters et al. 2019). International co-operative partnerships, especially within the European Union have enabled cultural agreements and research projects such as the COST SplashCOS database of marine archaeology to be developed and curated (http://splashcos.maris2.nl/).

Such valid concern from government and industry for the preservation of the cultural prehistory within their care is commendable, and these directives, initiatives and watching briefs have provided important data. However, focused archaeology still struggles to deliver contextual evidence for occupation in a modern offshore environment (Bynoe 2018). Direct evidence is still restricted to non-contextual finds, provided, in the majority, by serendipitous discovery. This is unsurprising due to the inaccessibility of the landscape to provide potential sites or the ability to conduct any form of excavation. It would require the removal of up to forty metres of modern sediment to uncover the Mesolithic sub-

surface(Cotterill et al. 2017). This would prove exorbitant both financially and of resources. It must remain the case that the discoveries that make up the archaeological record do not come directly from archaeological missions but from disturbed sea sediments; from beam trawling & dredge fishing (Figure 2.2), aggregate collection, or more recently from the deep channel sand dredgers that regularly clear shipping lanes at busy ports such as Rotterdam and then spray the dredged material onto the coastal levees.

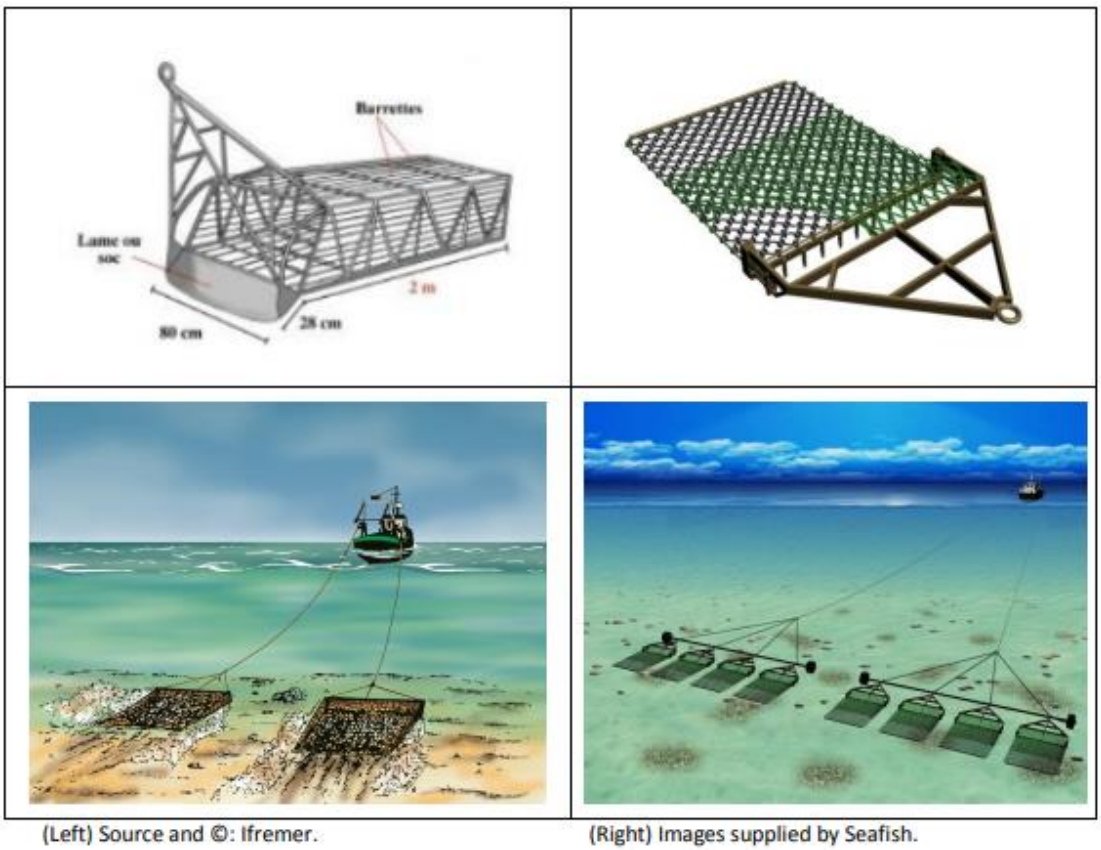

Figure 2.2 Examples of Dredges and Beam Trawling. Note the lip (left) and spikes (right) which can expose potentially eroded archaeology (Dixon 2015 p.27)

This is not to say that interest in such marine archaeology and especially the submerged landscapes of the North Sea Mesolithic is not growing. The excellent excavation at Yangtze Harbour (Sier et al. 2014) and at the Storebælt Fixed Link in Denmark (Aaby et al. 1997) demonstrate that policy frameworks are being developed for the management of marine cultural heritage (Flemming et al. 2014) and the influential COST funded research group SPLASHCOS whose interdisciplinary group's database brought together the combined knowledge of continental shelf and

submerged landscape archaeology in north western Europe (Bailey and Flemming 2008; Benjamin et al. 2011).

As further land-based archaeological discoveries are made around the coasts of Denmark, England and the Netherlands, further knowledge of human occupation of and expanded pre-inundated Europe also grows (Bailey et al. 2008; Groenendijk 2015; Hansen et al. 2017; Waddington and Wicks 2017; Milner et al. 2018). The terminology traditionally used to describe the boundary between the hunter-gatherer peoples of a pre-inundation culture and a settled, farming Neolithic culture of post transgressive sea-level rise is much hazier than first imagined. Modern near-coast discoveries such as potential crop cultivation (Smith et al. 2015) demonstrate it is, perhaps, time to move away from misleading references of supra-regional cultures and superficial tool typologies and find a new dictionary that looks to localised physical and environmental connections that link these people.

2.3 The Geology of the North Sea

The complex geological history of the North Sea is well recorded due to many years of research carried out by the hydrocarbon industries. The region is rated as the 8th largest oil and gas field in the world, with a potential of up to 25 billion barrels of recoverable oil and 75 trillion cubic feet of gas (Gautier 2005). This is a double-edged sword for research in that it both aids understanding of the underlying geology and provides data that may be outside of the financial resources usually available to academic institutions. At the same time the commercial sensitivities involved in new development may restrict such data from archaeological and academic access (Peeters et al. 2019).

The region owes its current shape and form largely due to glacial erosion during the Pleistocene and deposition during the Holocene period which created the Mesolithic landscape (Balson et al. 2001). However, a longer geological history has exerted an influence on the formation of the landscape of the area through periods of repeated tectonic activity and glacial encroachment not merely the most recent glacial episode.

Tectonic activity due to continental collision created the North Sea area from the colliding fault lines of the Baltica and Avalonia plates (Mazur et al. 2018). From the Precambrian through to the Devonian Period basement rock beds were both extruded in the form of metamorphic rock and depressed along moving plate lines to form the continental shelf. Formations created during the later Carboniferous period (360 – 300 mya) shared much in common with those of the terrestrial record of eastern England. However, while the terrestrial unconformities produced seams of coal in the north of England and North Sea, the extremely folded formations in the southern North Sea area demonstrated little of the same compression within the metamorphic beds. Such early formations played little part in final tectonic structure or hydrocarbon energy capture of the North Sea and they did not directly instruct our understanding of the region, archaeologically (Cameron 1992).

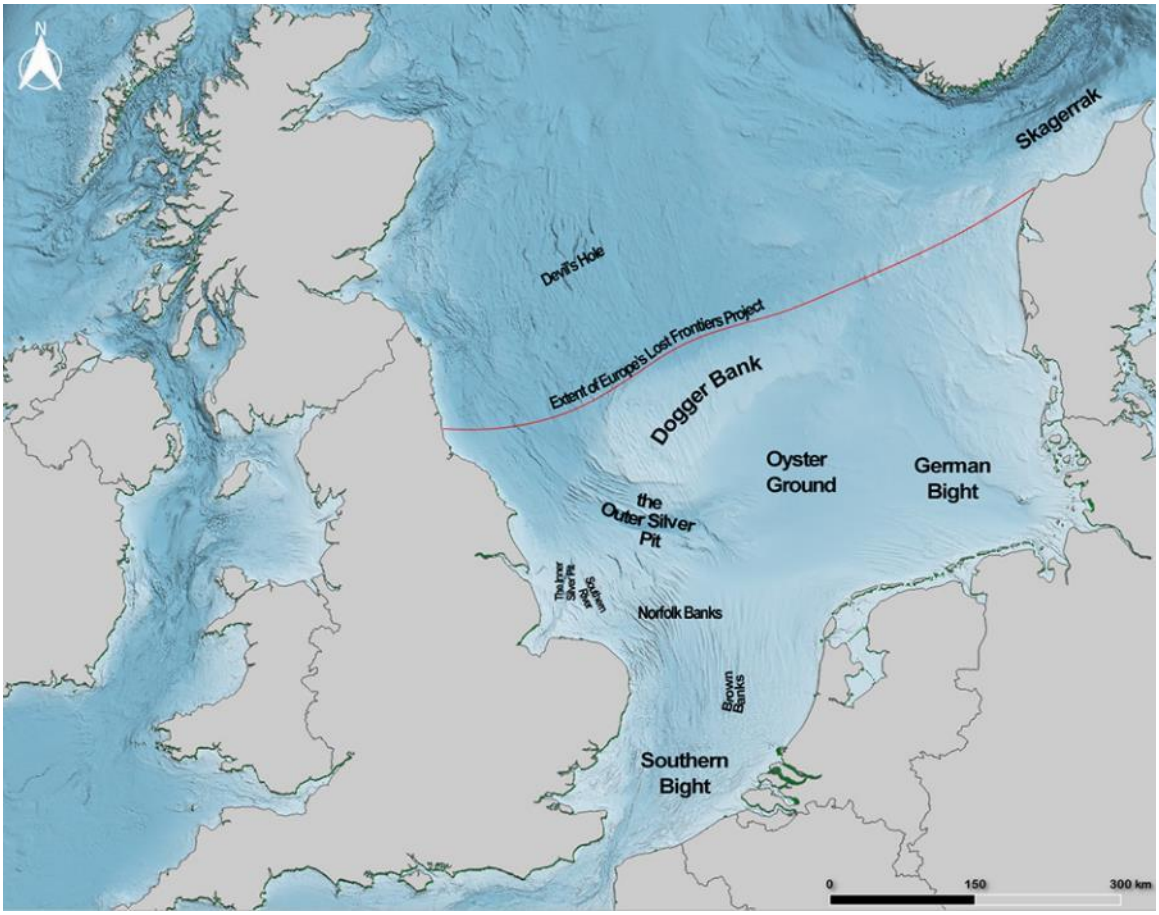

Figure 2.3 Important areas of the southern North Sea as referenced in this thesis

The Permian period (300 – 250 mya) was the opposite of the Carboniferous. The folding of the base beds due to tectonic activity, created unconformities that continue to affect the warp of the southern basin (Müller et al. 2018). The Rotliegend Group was created at this time

and it was within this sandstone deposition that the larger reservoirs sought by the hydrocarbon industry are to be found (Gautier 2005). Other features of interest, such as the Silverpit Claystone and Leman Formations were also created within this group (Figure 2.3). The sequence was then sealed by a layer of finer carbonate-evaporite sediment over a series of progradation and denudation cycles to form the Zechstein Cap of dolomitic carbonate. In some areas of the North Sea, this layer was up to 2km thick (Veenstra 1965).

Whereas the Rotliegend basin demonstrated evidence of a continued marine environment throughout its formation, the Zechstein deposits which marked the transition from the Permian to the Triassic period (250 – 200 mya), showed a terrestrial deposition sequence (Cameron 1992). A decrease in the sedimental supply at the end of the Permian era suggested a desertification and increasing arid conditions, producing evaporite deposits across the region. In the west, the England Salt basins of diapiric salt pillows were able to rise as independent domes through later sequential layers, by means of halokinesis, resulting in deformation of younger layers. In the east, the German salt basin created a linear diapiric structure that acted like a halokinetic faultline, reaching up through far younger sequences. In both cases the deformation of younger layers could be traced throughout the geological record to the quaternary landscape.

Halokinesis occurs because salt compacts less than sediment under saturation. Therefore, more compressed, dense overlying sediments create overburden. The less dense salt layer is able to rise as a dome or wall, by means of buoyancy, through the denser material surrounding it (Clapham 2014; Esestime et al. 2015). Once the process of Halokinesis is underway and a salt plug begins to rise, the weight of the overburden will push down around the moving salt, pushing it further upwards. This results in a peripheral sinking of overlying depositional surfaces, subsidence of the contemporary sea floor, and possible faults through which free gas may rise (Fig. 2.4). Such structures were active throughout the North Sea throughout its geological history and are still active today (Thomson 2004). They can cause issues with interpretation and with reflector signals (Müller et al. 2018).

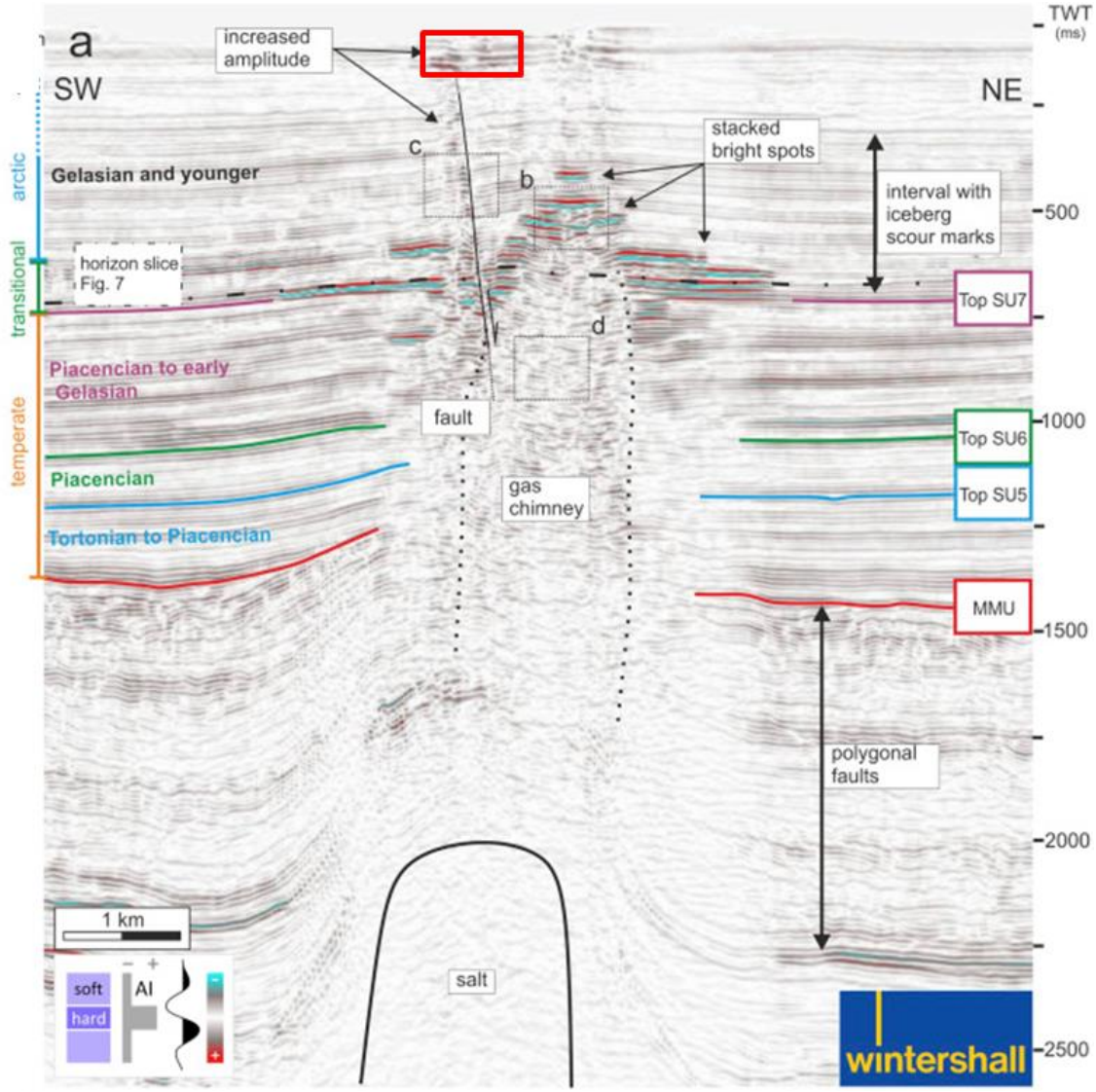

Figure 2.4 Salt Dome causing gas chimney which has repercussions to the shallowest levels (Müller et al. 2018 p.145)

The Triassic began with a glacial retreat and a subsequent world-wide rise in sea levels. During this period the Zechstein sea transgressed the region and flooded the previously arid lands (Taylor 1990). A retrogradational sequence of fluvial sandstones made up the Bunter Formation. With the exception of a single 47m sea stack on the island of Heligoland, called Lange Anna (Tall Anna), no Triassic rock formation currently outcrops within the North Sea (Kent 1967).

Similarly, none of the limestone sequences of the Jurassic period (200 – 150 mya) occurred in the North Sea region. However, this geological era demonstrated major tectonic movement and evidenced vulcanism throughout the North Sea (Balson et al. 2001). The first evidence of

outcropping rock formations are visible in the clays, mudstone and chalk of the subsequent Cretaceous period (150 – 66 mya). This was possibly as a result of an increase in tectonic subsidence and faulting as well as continuing halokinetic processes of older diapiric layers (Underhill 2009).

The start of the Palaeogene period (66 – 56 mya) marked the beginning of the Cenozoic Era (the current geological Era). It was notable in Europe for the start of the Alpine orogenic process which continues today, raising the Alps (and other Eurasian mountain ranges) while depressing the coastlines of north western Europe and the southern North Sea by approximately 0.5mm annually (Matte 2001). The previous tectonic activity within the North Sea however, meant that this depression was never applied evenly across the basin and the southern North Sea was twisted into three distinct rift-prone basins (Veenstra 1965).

The Eocene epoch (56 – 33 mya) saw these basins merge into one cratonic sedimental sea floor. This overlayed an older chalk group and developed into the Yarmouth Roads Formation (Garrison 2012). Throughout the area, subsidence and slip-strike faults (movement laterally as well as vertically) coincided with synclines following the main west-northwest / east-southeast axis of the new basin (Schroot et al. 2005). These have been proposed as due to halokinetic salt movement as at the same time a syncline at the Silverpit Crater caused the collapse of a previously significant salt dome (Thomson 2004; Underhill 2009). The main formations created over the Eocene and Oligocene were that of Balder mudstones that were overlain by London Clays. In turn these were overlain with Branden Clays (Cameron 1992).

During the Neogene period (23 – 2.5 mya) diatomic planktonic evidence suggested cooler conditions and higher sea level ranges during the creation of the Kattendijk Formation (Coetsiers and Walraevens 2006). Rasmussen postulated a single deep opening to the Atlantic at this time, fed by deltaic sediment from rivers along either side of a central aquifer as in Figure 2.5 (Rasmussen et al. 2010). This deep marine aquifer was later overlain in the Pliocene epoch with clays.

Figure 2.5 The North Sea during the Neogene was a deep marine channel fed by rivers on either side (after Rasmussen et al. 2010 p.20)

The Quaternary Period featured three glaciation events, all within the latter part of the Pleistocene epoch (2.5 mya – 11.7 kya). The Weichselian glaciations formed much of the topography in evidence today (Graham et al. 2011). Features such as the Outer Silver Pit were older, deep rock features eroded and then overlain by glacial till. Long incised tunnel valleys were created beneath extensive ice sheets due to outwashed debris. Glacial movement tore into older sedimental stratigraphy which later filled with clastic deposits, both lacustrine and marine (Cameron 1992). This was evident in the sub-glacial sediments of clays forming the Yarmouth Roads and Swarte Bank Formations in the Elsterian Glaciation, the Eem Formation in the Saalian Glaciation and the Brown Bank, Dogger Bank and Bolder's Bank Formations in the Weichselian Glaciation events (Behre 2007); Graham, 2011).

Era	Formation	MIS	Depositional environment	Description
Holocene	Bligh Banks & Indefatigable Grounds	1	Open Marine derived from re-worked glacial	Gravelly sands and sandy gravel forming a veneer of variable thickness over glacial till
	Nieuw Zeeland Gronden Terschellinger Bank Member		Open Marine - Proposed as the first fully marine deposit following transition from glacial to interglacial. Found extensively across Dogger Bank of variable thickness	Muddy, fine grained sand, re-worked periglacial and glacial deposits. Contains sparse numbers of marine molluscs.
	Well Hole Western Mud Hole Member		Shallow Marine - unconformably overlies late glacial. Infill depressions.	laminated fine grained sands and muds. Variable thickness, laterally discontinuous.
	Elbow Formation Naaldwijk Formation (Includes Wormer Member) Nieuwkoop Formation (coast) Southern Bight	1-2	Marine Intertidal - Between the end of the LGM ~18,000 years BP and final flooding of Dogger Bank at ~6000 years BP transitional deposits were laid down encompassing a fluvially incised tundra plain estuarine, brackish intertidal to shallow marine deposition	Extensive in the Dutch sector, analogous to Naaldwijk Formation. Laterally discontinuous across Dogger Bank. Upper - fine grained muddy sands and interbedded clays; middle - brackish marine clays representing early stages of marine inundation; lower - basal peats - representing fluvially incised environments.

Table 2.1 Holocene Primary Unit Descriptions (Cotterill et al. 2017)

The final glaciation event of the Weichselian and the last glacial event before our present Holocene Epoch, was known as the Last Glacial Maximum (LGM). Records show at its height, between 31 and 18 kya, the ice sheets covering north western Europe were over 2km thick. This resulted in compression of the clays at the northern end of the North Sea basin and an upthrust of the southern North Sea by approximately 40m above its present height (Peltier 2004). This glacial forebulge caused major re-routing of the riverine systems of the Thames, Rhine, Schelde, Meuse and Humber forcing the outflow down to the southern basin, altering the composition of depositional material (Andrews et al. 2000).

The geological processes of the Holocene were highly depositional and driven by changes in climate – See Table 2.1 (Stoker et al. 2011). The receding ice, post 21 kya allowed the lands of the late Palaeolithic and early Mesolithic northern Europe to begin the process of regional isostacy, that is ongoing today (Peltier 2004). The process of reversion was gradual. Sedimental build-up developed over major riverine channels and older infilled tunnel valleys overtopped and flooded to wider, shallower lacustrine areas. Across the southern North Sea basin palaeo features such as the glacial valleys surrounding the Dogger Bank, began to fill with sediment and were able to develop peat in the prograding accommodation space (Cameron 1992). The slow rising sea levels and brackish estuarine, coastal environment of the southern North Sea basin proved excellent for this build up (Cotterill et al. 2017). Finally, the shallow dendritic rivers gave way to salt marsh as the water tables rose and the inexorable transgression of the terrestrial lands became complete. (Fitch et al. 2005).

Holocene sediments of differing grain size were deposited over earlier primary unit formations, infilling sequences throughout the southern North Sea as shown in Table 2.1. Such sediments were sourced primarily from relict glacial deposits, coastal erosion and from terrestrial river and deltaic systems, the last of which is still the primary driver today (Stoker et al. 2011). From the Central Graben northwards, the North Sea was both deeper and the terrestrial coastlines continually rising, relative to mean sea-level. This and the late retreat of ice meant much less clastic infilling of the seabed and less mobile sediment movement (Graham et al. 2011). The result was that sub-glacial bedrock outcropping and glacial scouring was common and can be seen on seafloor bathymetry in the northern North Sea.

The southern North Sea maintained a depositional environment. Sand banks and relict waves formed throughout wide areas of the basin, oriented on a northwest - southwest axis at thicknesses ranging from a few metres to 40m and these could be notoriously mobile and difficult to read geologically (Shennan and Coulthard 2003). While glacial deposition still formed part of the landscape of the basin, and was itself the reason for erosion and scour, later Holocene deposition throughout the basin was more pertinent to the analysis of this research. Such Holocene sediments were, in places, vast; silts and clastic muds infilled the Pleistocene Botney Cut formation down to fine and medium unconformable sands (table 2.1). At the coastlines and estuaries where the lower lying terrestrial wetlands

existed, the muds and marshes may extended for miles, containing woody peats or unconsolidated organic muds in rising water tables (Barlow et al. 2014).

Any discussion of Quaternary features within the southern North Sea, must mention the Naaldwijk and Elbow Formations. According to the Netherlands Enterprise Agency and the Netherlands Organisation for Applied Scientific Research (TNO), the Elbow Formation is now classified as part of the Naaldwijk Formation and the basal peats found at the base of the Elbow Formation are now classified as the Nieuwkoop Formation (Rijsdijk et al. 2005; Thal et al. 2018). However, this terminology has yet to be adopted universally and in the UK it is difficult to find reference to such an agreement, though Stoker acknowledges they are the same formation in certain locations (Stoker et al. 2011). For the sake of clarity, Naaldwijk and Nieuwkoop Formations will be used throughout this thesis.

The Naaldwijk Formation is ubiquitous throughout the southern North Sea basin. It reaches from the Dogger Bank in the north far into the Dover Strait to the south, making up part of the California Glaciogenic Group (Balson et al. 2001). It has often been characterised as the 'base Holocene' as it appears as a distinct high-amplitude, strong reflector on seismic surveys due to the interbedded clays and the propensity for basal peat at the Nieuwkoop Formation (Bos et al. 2012).

The unit comprises of deposited sands and silts within palaeochannels and often features distinct layers of blue or green clay laminates called the Wormer Member. The Naaldwijk formation varies in thickness from less than 10cm which is difficult to detect on any given seismic survey, to a depth of more than 8m (Cameron 1992). The deposition into palaeochannels and the high potential for peat accommodation within the Naaldwijk formation mean that, where this erodes near the modern seabed, or within coring depth, it makes a good target for archaeological coring (Bailey et al. 2020).

The large-scale, almost regional sized low-lying plains, coastal marshlands and estuarine fluvial systems exposed at the end of the LGM already had potential for a high water Table and good accommodation space. During the prolonged inundation environment of the early Holocene, peat formation was an early development in the stratigraphical chronologies

of infilling depositional units. This is why the Nieuwkoop Formation was also known as the Holocene 'basal peat' (Bos et al. 2012).

As the region became subjected to marine inundation, depositional clays and silts were intercalated with successive peat formations between 9 kya and 6 kya, often thickening with multiple layers of organic sediment infilling the accommodation space of palaeovalley formations making these an ideal place for archaeological investigation. Once all accommodation space was filled, peat no longer formed and sediment supply developed above, often gradually in solid, tidal-clay Wormer Member layers that were impermeable, low in porosity, inert to chemical change and finally overlain with modern mobile sediments.

2.4 Evolution of the Holocene Landscape: Sea Level Change

Sea-level rise and fall is a continually occurring process reflecting climatic change (Petit et al. 1999). The complex relationship between marine temperature and climate throughout glacial and interglacial periods has been measured in oxygen-18 isotope abundance from 57 globally aligned benthic core records (Lisiecki and Raymo 2005). While there is discussion on a global level concerning hemisphere variability (Raynaud et al. 2003; Guo et al. 2009; Buiron et al. 2012), it does not concern the focus of this research. Suffice it to say that over 100 glacial and interglacial periods have been calculated, spanning over 850 kya (Lisiecki and Raymo 2005). Further, $\delta^{18}O$ measurements denoting changes in sea level and temperature have been noted as far back as 560 million years, though these have not been linked to a Marine Isotopic Stage (MIS) of glaciation or interglaciation (Miller et al. 2005).

Figure 2.6 shows the variability over time of global sea level rise and fall. Over 200 kya and the last 7 MIS, Stevens shows that sea level has been predominantly below the current level, often by as much as 120 m. Odd numbered MIS represent interglacial (warmer) periods and even numbered MIS represent glacial periods. The periods are differentiated by means of their $\delta^{18}O$ values. Ice-locked pollen and foraminifera return lower $\delta^{18}O$ values than their marine counterparts (Miller et al. 2005).

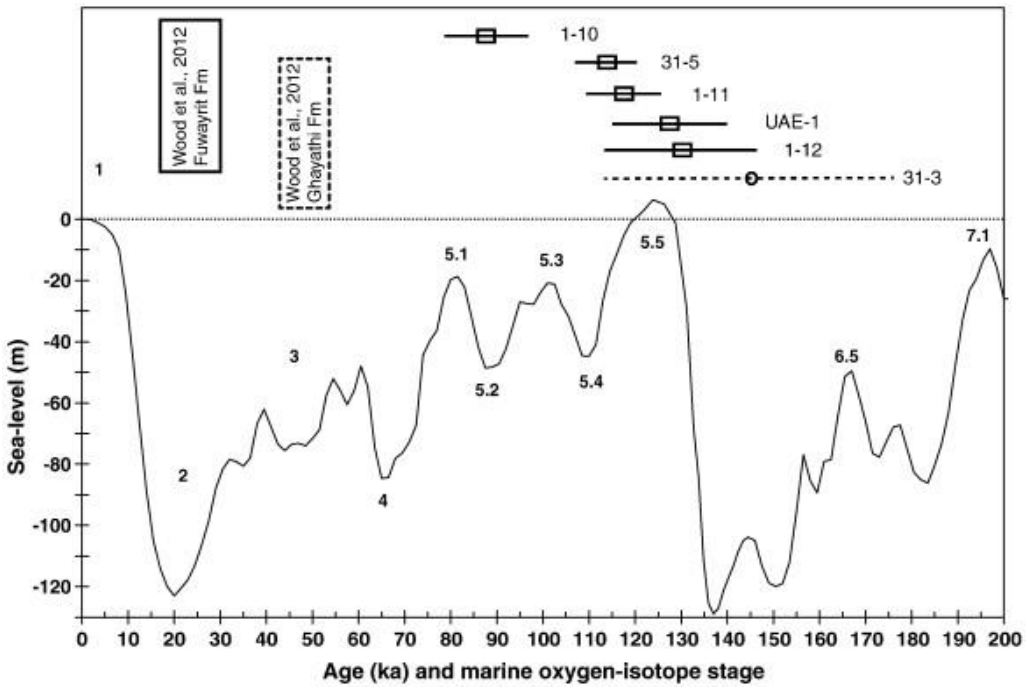

Figure 2.6 Global sea levels as measured over stratified deposits from the last 7 marine oxygen isotope stages from two sites in Persian Gulf (Stevens et al. 2014 p.182)

Global eustatic sea level measurements are a broad brush and work best a distance from regional ice effects. In order to focus on the southern North Sea and in particular the glaciation and interglaciation MIS 2 and 1, this thesis must investigate isostatic effects in play. The last glacial maximum reached its peak in the UK and the southern North Sea around 24 kya at which time glaciers up to 2km thick sat over northern Britain and Scandinavia compressing the lands to the north and thrusting the lands to the south up in a forebulge before the ice (Bradley et al. 2011). However, by 11.7 kya the glaciers had all but receded from the UK, the lands were in the process of rebound and sea-levels were rising. In most cases, inundation follows a pattern of 5 phased events (Sier et al. 2014):

i) Terrestrial Landscape – Lowest lying land and plains are above the water table, except for floodplains.

ii) Deltaic Landscape – Land above the water Table but with extended waterlogging of floodplains and low-lying ground. Peat growth along river valleys

iii) Tidal Landscape – higher land such as dunes above water but low-lying land submerged except for low tide. Reeds dominate tidal fringe and mudflats develop on submerged plains. Rivers become marine with increased sediment and salinity.

iv) Estuarine Landscape – Higher land such as dunes waterlogged and \ or submerged at high tide. Open water dominates landscape.

v) Submerged Landscape – Open water remains, high land below water Table even at extreme low tide.

The process usually occurs gradually, often over hundreds if not thousands of years from a fully terrestrial landscape to one that is entirely submerged. However, in the southern North Sea, with its many wide flat plains and low-lying shallow riverine environment it may have been predisposed to rapid pulse transgression in storm surges or repeated transgression (Waddington and Wicks 2017). Some areas may have transgressed much faster than others due to wind and tidal currents.

Of specific interest to this research is section ii) above. The phase between terrestrial landscape and a tidally inundated landscape with marine deposition is one in which peat develops along river valleys. In theory, the dating of that peat could be used as an indicator to suggest a time during the inundation process before the land is classified as tidal (Behre 2007).

The localised measurement of sea-level rise in the North Sea was first proposed as a sea-level rise curve for the southern North Sea by Saskia Jelgersma in 1961 and refined in 1979 (Jelgersma 1961; Jelgersma and Tooley 1995). By means of palynological analysis of first moorlog and then cored peat from the Nieuwkoop Formation, Jelgersma was able to plot a line of terrestrial vs marine biota (in orange in Figure 2.7 below). Many academics have since joined in the regional Holocene sea-level curve debate utilising differing techniques to date the inundation (Mörner 1980; Lambeck and Chappell 2001; Vink et al. 2007). The most convincing and large scale of these took 118 samples from a wide variety of sources and proxies including peat and phragmite 14C dates, sedimental Optically Stimulated Luminescence dating and pollen analysis to build up a supra-regional sea-level curve based on the Calais-Dunkirk system of peat horizons (Behre 2007; Baeteman et al. 2012). Many of the dates from this and Behre's curve are also represented in Figure 2.7 which demonstrates a regional curve for the southern North Sea rising steeply between 10 and 8 kya before slowing. To balance these rising curves, it is worth noting that in Scandinavia and Scotland the sea level curve is reversed and can be

measured in the uplifted stratigraphy on the isostatically rebounded shoreline (Smith et al. 1992).

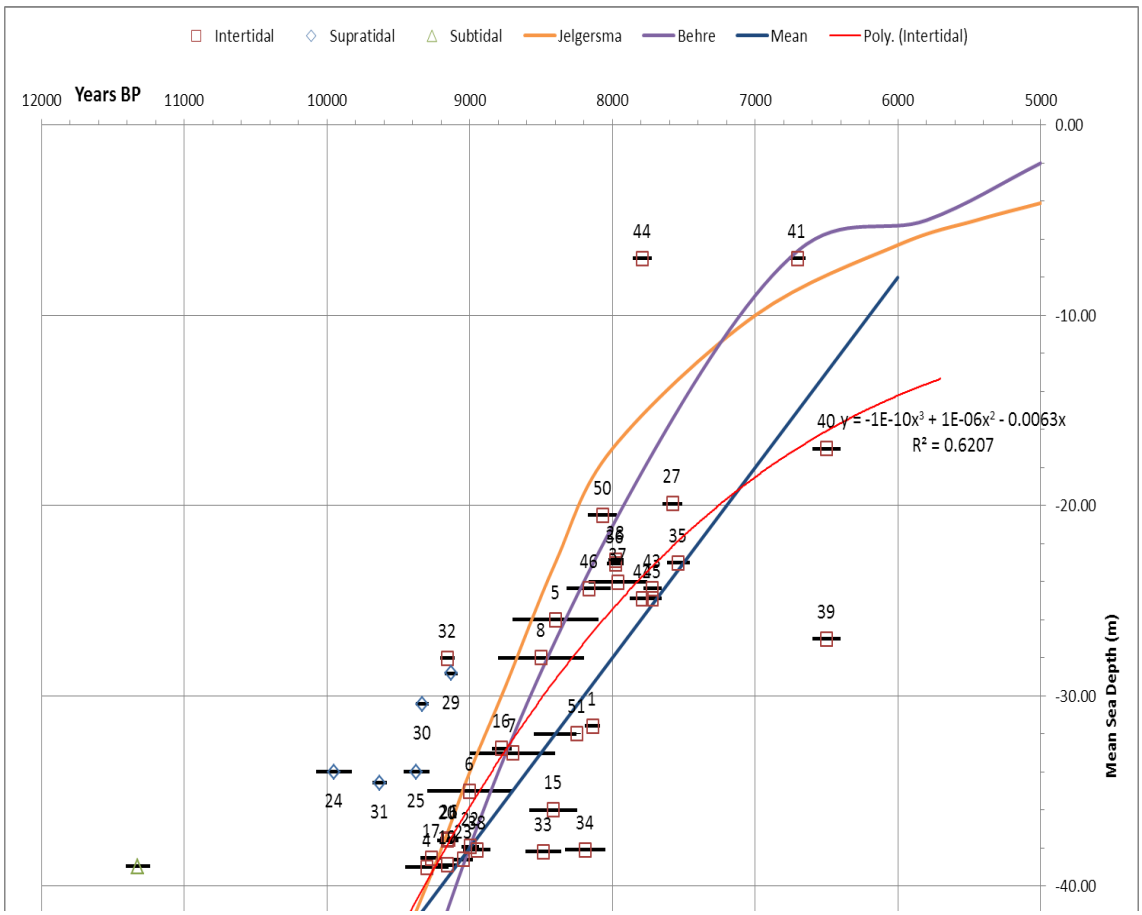

Figure 2.7 Early Holocene Sea-Level Curves as represented by Jelgersma and Behre, (Jelgersma 1979; Behre 2007) with mean line of all intertidal dates by the author. Including data from Ward (Ward et al. 2006) from previous work by the author.

Table 2.2 below shows a selection of sea level indicators and the chronological methods they employ. It gives a rough estimate of the time scale they can be reliably expected to report upon and the resolution of the dates that can be expected within that range (Milne et al. 2009). Not all indicators are available at all locations.

At the top of Table 2.2 are the basal peats of the Nieuwkoop Formation and sedimental facies both of which are obtained via coring. The widespread nature of the Naaldwijk Formation and therefore the underlying Nieuwkoop, make this an ideal focus for regional sea-level rise investigation (Stoker et al. 2011). The coring of such peat also grants additional sea level indicators in respect of a core of Holocene sediments and the potential of well-preserved palynological proxies and

microfossils within the peat (Jelgersma and Tooley 1995).

Sea Level Indicator	Chronological Methods	Time Scale	Resolution (yrs.)
Basal Peats	^{14}C	0 – 12 kya	50 – 200
Sediment facies	OSL, varve palaeomagnetism	0 – 20 kya	50 – 200
Microfossils	^{14}C, palynology	0 – 20 kya	50 – 200
Corals ('fossil sunshine')	U/Th	0 – 30 kya	200 – 400
Shoreline stratigraphical markers	Sediment sequences	10 – 500 kya	Approx. 500
Oxygen Isotopes ($\delta^{18}O$)	^{14}C, varve, OSL palaeomagnetism,	0 – 470 kya	50 – 200

Table 2.2 Regional sea level indicators used around the world (Milne et al. 2009)

Therefore, the use of a peat as a basis for the cataloguing of a database of regional Sea Level Indicator Points (SLIPs) has allowed the building of complex models of the inundation over time. From Coles' seminal Doggerland: A Speculative Survey (Coles 1998) through Shennan's calibrated regional inundation model (Shennan et al. 2015) to the latest glacio-isostatic adjustment models (Ferrier et al. 2017) the curves are being finessed as the dates become more refined.

There are still questions to be answered concerning exact chronologies, sediment loading, gravitational levering and a host of other complexities that are expertly covered elsewhere (Whitehouse 2018). Yet on a regional scale, the curves for the early Holocene, 12 kya to 5 kya are now in agreement and models built from these, while not locally consistent, all adhere to a fundamental timespan (Baeteman et al. 2012).

Comparing Sturt's GIA modelling of sea-Level Rise from 2013 (Figure 2.8) to Europe's Lost Frontier's Project map in 2020 (Figure 2.9); both show the southern North Sea at approximately 10 kya and 9 kya, both utilise modern topology and geographic outlines in their reconstruction, the methods and data employed to reach these conclusions however were very different. Sturt bases his model on Bradley's (Bradley et al. 2011) GIA model while Europe's Lost Frontier's Project is based on the 2018 BritICE data (Roberts et al. 2019) and their own coring proxy results (Gaffney et al. 2020).

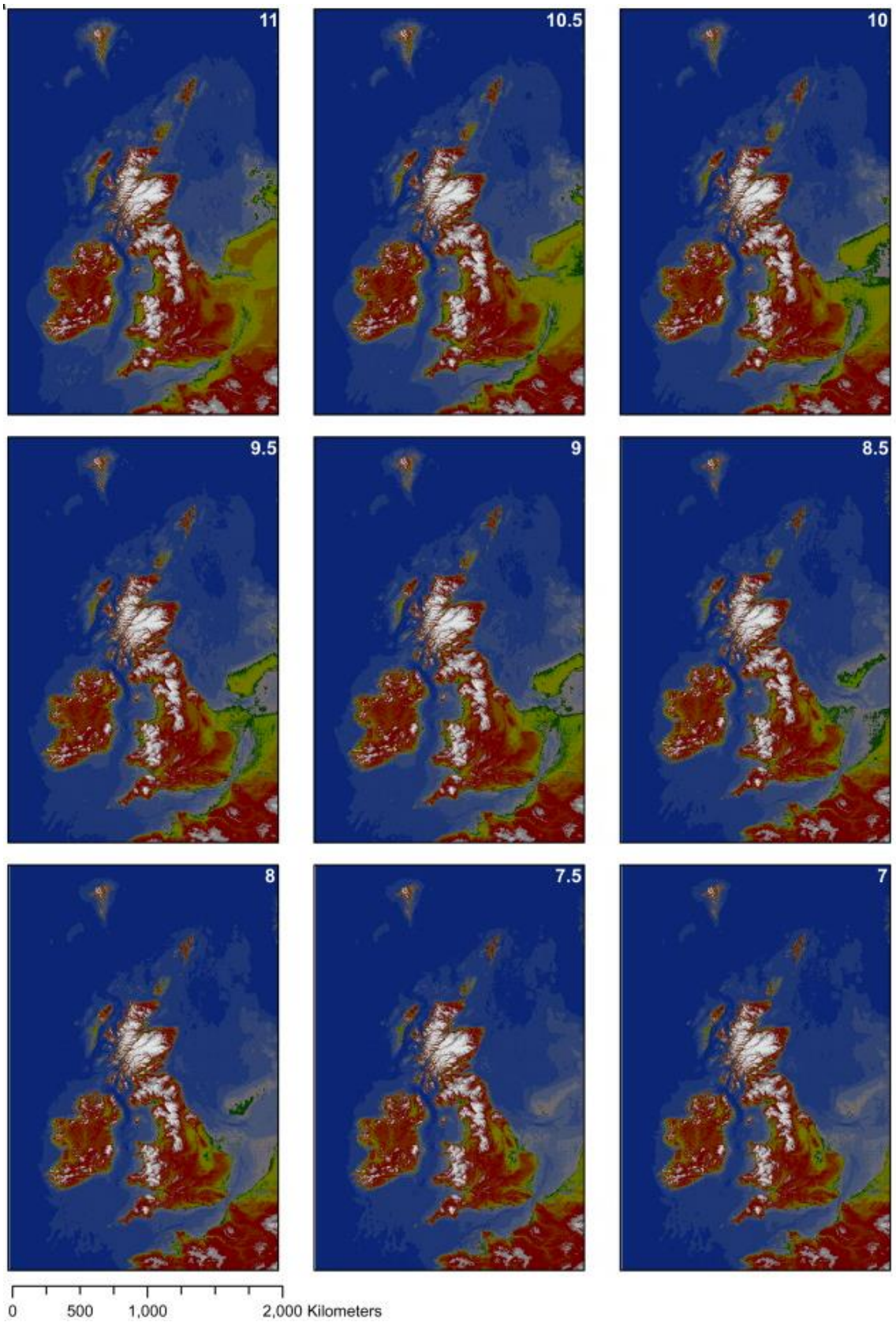

Figure 2.8 GIA Model of sea level rise in years BP at 500 year intervals from (Sturt et al. 2013)

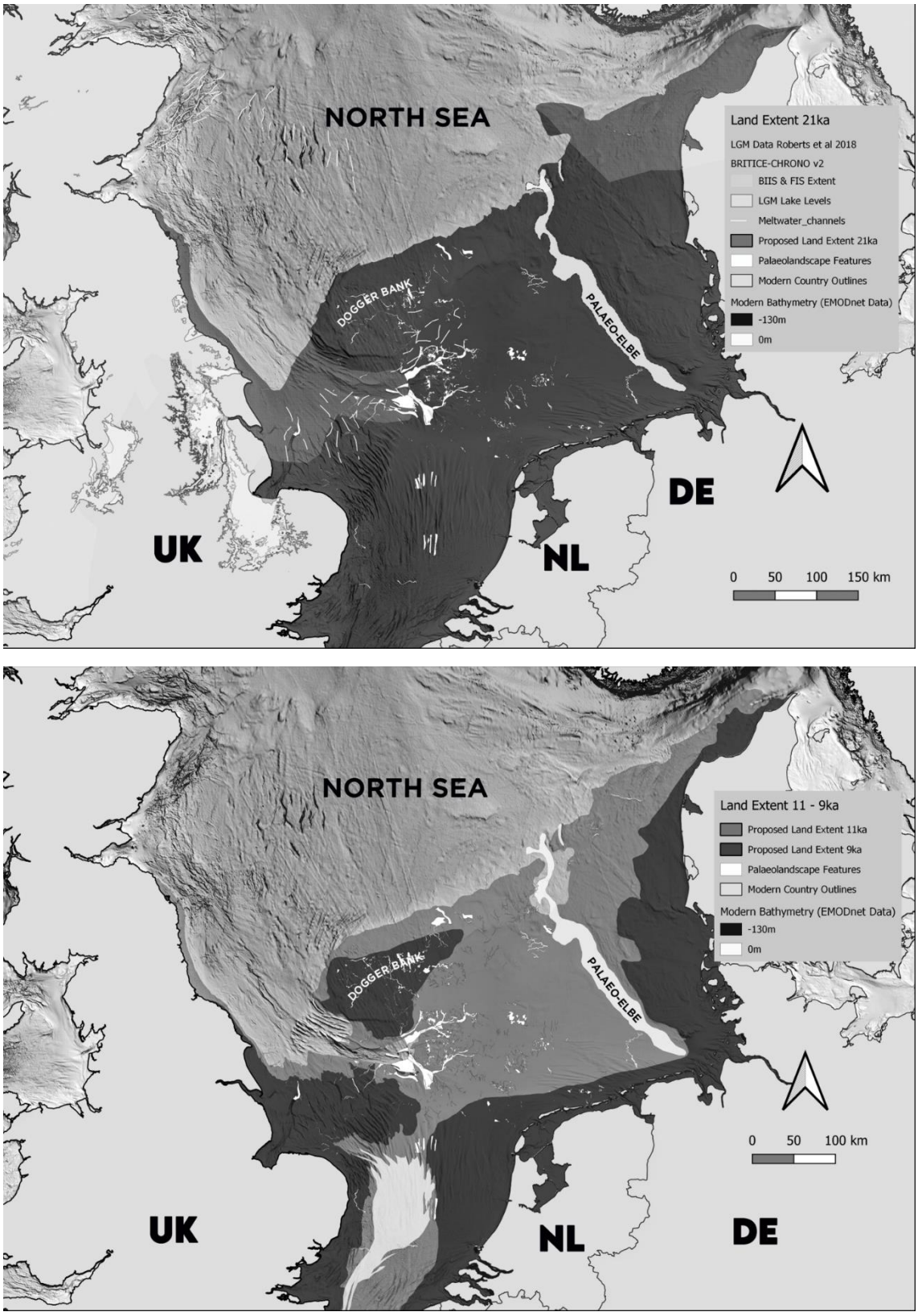

Figure 2.9 Europe's Lost Frontiers mapping of land extent 2020 (Walker et al., 2021 in press)

Bradley's model of the glacio-hydro-isostatic rebound, in collaboration with Lambeck (Bradley et al. 2011), and Sturt (Sturt et al. 2013) have produced an impressive analytical narrative to the changing landscape (Figure 2.8). However, their basis in satellite bathymetry, makes them both susceptible, as Sturt himself pointed out, to the same issues of erosion and deposition that effected Jelgersma's model from 1969 (Sturt et al. 2013). Shennan et al, stated in 2003 "At the present stage in the analysis we ignore sediment erosion and deposition" (Shennan et al. 2003) and while an acknowledgment of the greater complexity of sedimental transport now exists (Ferrier et al. 2017; Wal and IJpelaar 2017; Ferrier et al. 2018), there is still debate on the priorities regionally (Whitehouse 2018). Models of deposition, erosion and deglaciation are furthering our understanding of sea level rise on a macro landscape basis which can be extrapolated to the larger landscapes (García-Artola et al. 2018; Roberts et al. 2019)

Sea-level rise, as observed through the lens of environmental core data will be vital to the understanding of the case study aspect of this thesis - in particular the tying of inundation markers within modern geophysical survey data to core proxy evidence that can be georeferenced. As discussed above, the Nieuwkoop Formation of basal peats would be just such a commonality. Already used as an established, if contentious, sea-level index point (Shennan et al. 2015), basal peat is extensive across the southern North Sea (Balson et al. 2001). The reason for this – low lying marshlands, slow moving waters and coastal, estuarine plains with a gradually rising water Table creating bog-like anoxic conditions – may have also proved beneficial open hunting grounds (Andrews et al. 2000; Barlow et al. 2014). The organic nature of peat, and its acidity against an alkali seawater make it an excellent microbial-killing preserver (Hazell 2013) and the inundation sediments that overly the peat have capped the transgression within a stratigraphic context that can be referenced from the Norfolk Broads to Friedrichskoog (Rijsdijk et al. 2005; Stoker et al. 2011).

The final aspect, focusing on peat as an indicator of sea level rise is the importance to archaeology. Aside from the debate surrounding compaction and the resolution of dating which is expertly discussed elsewhere (Behre 2007; Bradley et al. 2011; Baeteman et al. 2012; Whitehouse 2018), peat development is important to the understanding of inundation chronologies of surrounding landscape inundations.

The fact that peat develops in accommodation space at the base of shallow palaeo channels (Stoker et al. 2011; Coughlan et al. 2018) strongly suggests it was a post LGM occurrence and not present in the height of glaciation. Rising water tables in the low lying lands of the early Holocene would have meant that peat development from salt marsh areas occurred at a similar time to the occupation of the lands by humans (Shennan et al. 2000; Larsson 2013). Over a few thousand years, North Sea transgression occurred throughout the basin dispersing humans (Turney and Brown 2007) leaving the peat to humify. However due to the sedimental loading of the overlying fill, this rarely proved entirely possible which is why much of these peat layers still contain undecomposed plant remains and other organic detritus (Grover and Baldock 2013). So long as the context remains undisturbed, any archaeological evidence found in the relevant peat layers has the potential to be well preserved and constrained to within a set of environmental dateable proxies.

It is also worth noting that the process of inundation continues. The water Table is still rising throughout the southern North Sea coastal areas and peat still forms in the Netherlands and in Norfolk today (Milne et al. 2009; Barlow et al. 2014). In fact the entire Broads canal system was originally an interconnected peat-works (French 1993). Just as global warming had a fundamental impact on the people who occupied the low-lying plains of the southern North Sea basin after the LGM at the last interglacial, it will have a massive impact on life today. By furthering our understanding of the landscapes and environments of the past, we can hope to model ways to look at our future.

2.5 The Archaeology of the southern North Sea

To understand the archaeology of the southern North Sea it is necessary to understand the people within their cultural landscape. Before any discussions and debate however, it is important to set down the facts, which fall into three broad categories:

1) direct archaeological evidence – here split into offshore, intertidal and terrestrial and how these have influenced archaeological thought over the years.

2) environmental proxy evidence and how this has allowed the reconstruction of landscapes.

3) climate and how discoveries about changes to the environment can be seen to reflect on the movement of people and arguably visa-versa.

2.5.1 Archaeological Evidence – Offshore and Intertidal

To introduce offshore archaeological finds, the best example is possibly the Leman and Ower 'Harpoon' (Figure 2.10) often called the Colinda Point after the trawler that discovered it in 1931 (Burkitt 1932). This barbed point, possibly from a fishing spear or leister, measured over 20cm, and was made of red deer antler. It is presented here for three reasons: First, in 1931, it was notable for representing a recognisable, Maglemosian type tool – encased in peat – yet discovered many miles from terrestrial land with some provenance of origin, if not context. This allowed archaeologists to consider the submerged landscape of the North Sea as a potential Mesolithic terra-incognita (Clark 1936).

Figure 2.10 The Leman and Ower Point Photograph: Anthony Kelly Norfolk Museum Services

Second, the peat itself -so pertinent to this research, both in the preservation of archaeology and the extent of its bedding– was critical to the survival and discovery of the Colinda Point. The scale of serendipitous evidence that has come to the surface from eroded and outcropping peat at the sea bed has been one of the main guides to archaeological heritage management in the North Sea (Peeters et al. 2019). Admittedly, in the case of the Colinda Point, previous dating of the peat to the Late Mesolithic (8.5kya) misled research until the point itself was radiocarbon dated in 1988 and revised the date to 11.7kya (Bronk-Ramsey et al. 1990). This leads to the third reason for the Colinda point being of interest as an introduction to the archaeology of the southern North Sea. This is because the dates mark a major transition from the late Upper Palaeolithic to the early Mesolithic (Table 2.3). It is the Mesolithic that will provide the hunting ground for this research.

The precise dates for the transition from Upper Palaeolithic to Early Mesolithic are continually discussed and one region's Mesolithic will not

occur at the same time as another region's (Dolukhanov 1996). For instance, in the UK, historically, the Mesolithic started at 10 kya (Barton and Roberts 2004; Jacobi et al. 1976) while in Europe the agreement is to adhere to the geological Holocene date of 11.65 kya as set by the International Commission on Stratigraphy (Head 2018). Outside of Europe, the period is called the Epi-Palaeolithic, and in some regions can be all but ignored as the transition from Palaeolithic to Neolithic is so smooth and fast. Recently a move away from lithic typology toward a more site specific and palaeoenvironmental chronology has begun to gain in popularity (Bayliss and Woodman 2009; Benjamin and Hale 2012). As this research is based on a regional European landscape and is not bound by lithic evidence, it will comply with the 11.65 kya schema, as per Table 2.3 below (Bicket and Tizzard 2015).

The Mesolithic Period from 11.65 kya until the beginning of the Neolithic at 6.1 kya is when archaeological industry in the southern North Sea was active. Prior to this date, evidence of occupation is limited. Early hominin footprints and flint remains dating back 800,000 years (Ashton et al. 2014). Peaks of faunal assemblages occur between 48 and 43 kya and then a paucity during the LGM until 11.7 kya when evidence once more appears (Peeters and Momber 2014). The finds are then well established until the Neolithic period when the southern North Sea basin finally succumbs to rising sea levels and archaeological evidence dries up.

Archaeological Divisions		**Date range (c. kya)**	**Equivalent MIS**	**Approx Years BCE**
Lower Palaeolithic		1000–325	27–9	
Middle Palaeolithic	Early Middle Late	330–180 120–80 60–42	9–6 4/5 3/2	
Upper Palaeolithic	Early Late	35–24 14.7–12.6	3/2 2/1	 12,750 – 10,650
Mesolithic	Early Late	11.6–8.2 8.2–6.1	1 1	9,650–6,250 6,250–4,150
Neolithic		6.1–4.5	1	4,150–2,550

Table 2.3 Archaeological Dating Divisions for North Western Europe with Mesolithic and Neolithic focus in bold (Bicket and Tizzard 2015)

That is not to say that other fortuitous archaeological finds have not been made that fall outside of this date range. There is certainly sufficient evidence to suggest that the southern North Sea basin was occupied by hunter-gatherer people at least by 13 kya of a culture similar in nature to

that of the Magdalenian or Cresswellian cultures (Verhagen et al. 2013). However, the evidence for this period is scant and usually found washed up on coasts with no provenance or clue to their origin. Securely dated finds originating from the Late Palaeolithic are absent. The Colinda harpoon above, dated to 11,740±150 BP (Hedges et al. 1990) places it on the very cusp of the Late Palaeolithic and Early Mesolithic, though even this date is contentious due to possible calibration issues for radiocarbon dates between 12 kya and 10.5 kya (Blockley et al. 2007). A worked flint known as the Viking Bergen Flint, discovered in apparently intact stratigraphic core off the Norwegian coast, was dated using the contextualising sands and was found to be of Late Palaeolithic age (Long et al. 1986). However, these sands were possibly reworked so it is difficult to fix these dates with any confidence (Peeters et al. 2019). Of worked Mesolithic stone tools, notably a collection of Mesolithic flint was discovered alongside earlier Palaeolithic flint assemblages in UK waters, as part of the MASLF dredging agreement with Wessex Archaeology between December 2007 and February 2008 (Tizzard et al. 2014).

The presence of Neolithic activity is equally surprising post inundation, 6.1 kya. Controversy surrounds a set of Neolithic style core axes discovered in fishing nets originally said to be over the Dogger Bank (Glimmerveen et al. 2006; Van de Noort 2011; Maarleveld 2020). These finds were typologically assigned a date of between 5.5 and 4 kya (Flemming et al. 2012; Bailey et al. 2020). These later researchers also acknowledge that the location of the finds was less likely to have been the Dogger Bank itself and more likely to have been closer to an area known as the Brown Bank (Figure 2.11). It is certainly true that the Brown Bank area has been known of for many years as an area rich in palaeontological and archaeological remains, especially by the fishermen who trawl the area.

Fig 2.11 shows a number of colloquial terms used for the erosion pits rich in outcroppings of early Holocene peat or earlier. These are believed to be where the best faunal remains and archaeological finds originate (Post and Reumer 2016). However, this is hugely biased towards organic evidence. Apart from the previously mentioned flint finds, the evidence for stone working in the southern North Sea is extremely poor. As Maarleveld suggests, the paucity of stone tool discoveries may not be one of period but of modern method and visibility. The bone barbed and pointed tools of the Mesolithic may come away from the sea floor easier in the fishing nets. More to the point, these items may be more

immediately recognisable to the untrained eye than a small worked flint or microlith (Bailey et al. 2020).

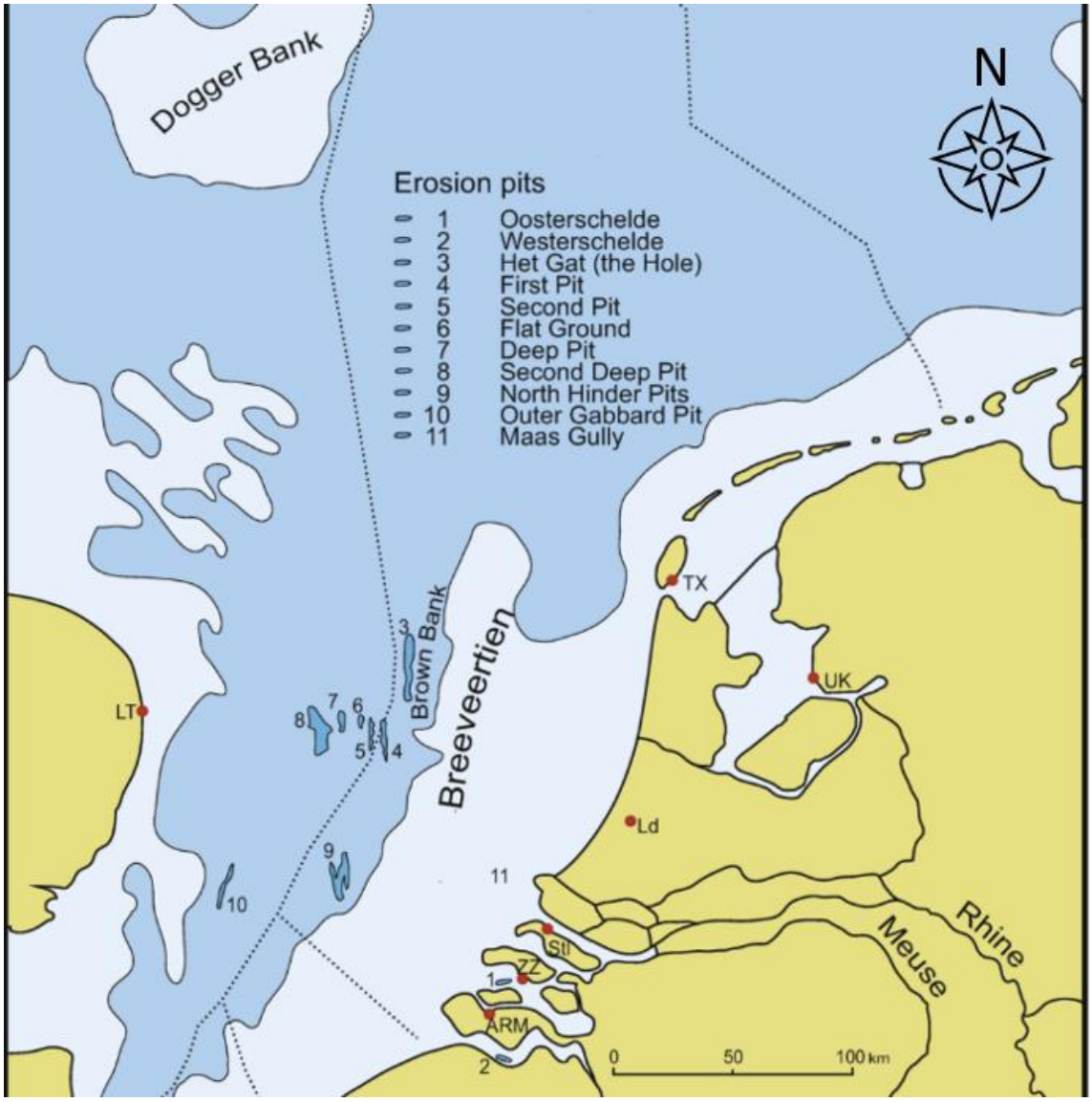

Figure 2.11 After (Maarleveld 2020) in The Archaeology of Europe's Drowned Landscapes (pp. 521-535)Drawing by Thijs Maarleveld

Of the bone and antler tools and evidence discovered in providential intertidal and offshore locations (though often lacking precise co-ordinates due to dredging run lengths) these can be summarised as per Table 2.4 below.

Location	Species	Faunal Element	Lab No	C14 BP	Cal BCE (>90%)	Cite
Leman & Owen	*C elaphus*	antler 'harpoon'	OxA-1950	11750±200	11287	(4)
SW Brown Bank[1]	*Bos primigenius*	worked metapodial	GrAÐ28364	11560±180	11166	(1)
SW Brown Bank[1]	*A alces*	worked antler	GrA-27206	11350±190	10934	(3)
SW Brown Bank[1]	*H sapiens*	mandibular	GrA-23205	11330±100	11140	(2)
52°10' N, 02° 49' E	*H sapiens*	cranium	UtC-3750	11110±620	9330	(1)
SW Brown Bank[1]	*A alces*	worked antler	GrA-37004	10880±150	10668	(1)
SW Brown Bank[1]	*Sus scrofa*	humerus	UtC-7886	10790±180	10486	(2)
SW Brown Bank[1]	*H sapiens*	humerus	GrA-27188	10320±70	9927	(3)
SW Brown Bank[1]	*H sapiens*	humerus	GrA-30733	10250±40	9864	(3)
SW Brown Bank[1]	*H sapiens*	humerus	GrA-31287	10210±30	9861	(3)
SW Brown Bank[1]	*H sapiens*	humerus	GrA-35949	10140±90	9367	(3)
52° 22' N, 03° 06' E	*C elaphus*	1st phalanx	GrA-20256	9920±160	9117	(2)
Eurogeul	*C capreolus*	worked antler	GrA-33949	9420±60	8547	(3)
53° 0' N, 02° 54' E	*H sapiens*	mandible	GrA-11642	9390±70	8431	(2)
52° 27' N, 02° 55' E	*C elaphus*	2nd phalanx	GrA-20353	9370±70	8419	(2)
SW Brown Bank[1]	*H sapiens*	cranium	UtC-624	9300±150	8246	(2)
SW Brown Bank[1]	*A alces*	worked antler	GrA-30731	9220±80	8286	(3)
NE Brown Bank	*H sapiens*	humerus	GrA-27205	9140±90	8225	(3)
Eurogeul	*C elaphus*	modified antler	GrA-22999	8950±110	7717	(2)
Eurogeul	*A alces*	antler	GrA-23201	8830±120	7606	(2)

Table 2.4 Upper Palaeolithic and Mesolithic radiocarbon calibrated dates on human and worked faunal remains dredged from the North Sea (Weninger et al. 2008). Collation and new calibrated dates of all finds by author.

Sources: 1 - Amkreutz, 2019; *2* - Glimmerveen et al. 2004; *3* - Mol et al. 2008; *4* - Gillespie et al. 1984. Calibration BCE results were carried out using OxCal v4.4 and are presented in Appendix 6 of this thesis.

[1] precise location data for items attributed to SW of Brown Bank is unavailable. Suggested area is within 5km of 52° 34' N, 02° 35' E

2.5.2 Archaeological Evidence – Coastal Sites

If these offshore and intertidal finds are combined with Mesolithic archaeological finds from modern coastal sites as in Figure 2.12 below, what do they tell us? To Graham Clarke, the Colinda Point proved a focal point for a Mesolithic culture in the North Sea (Mesolithic) and allowed him to draw parallels between the Maglemose culture of modern-day Denmark and the newly discovered Star Carr in modern-day UK (Clark 1936; Clark 1954). The fundamental similarities to bone and antler barbed spearheads from across the southern North Sea basin is striking.

However, the time frame that Clarke strove to match – especially that of the parallel lakeside Duvensee culture (Clark and Clark 1975) - did not, in reality, exist. The Star Carr industries were from an earlier period, around 11 kya to 10 kya, while those of the southern Maglemose in Denmark, and German Duvensee around 10.5 to 9.5 kya (Groß et al. 2019). Lithically, the cultures were not aligned either, with the UK developing a uniquely broad trapezoidal flint type not seen anywhere else in Europe (Reynier 2005). Whether there was a specifically UK 'culture' with internal division of upland and lowland Mesolithic flint typologies derived from Star Carr type and Deep Carr type is a discussion that is ongoing (Reynier 2005; Tolan-Smith 2008; Conneller et al. 2016). However, there is an acceptance that while different cultures developed, rather than being independent silos, the archaeological cultures of north-western Europe were inextricably linked throughout the Mesolithic. Is it therefore too far a stretch to suggest that what remains is merely the littoral evidence for a more connected central hub of Mesolithic culture within the southern North Sea? Certainly, the offshore evidence is unavailable at present. However, the submerged evidence from modern intertidal and coastal zones can provide clues (Figure 2.12).

In the UK, submerged coastal Mesolithic sites have recently given great insights into settlement activity. However, the best-preserved evidence is not to be found on the North Sea. Bouldnor Cliff in the Solent, was discovered at the start of the millennium and consists of in situ wooden remains of a Mesolithic settlement with a high degree of preservation in the cold salt water (Smith et al. 2015). The environmental proxy evidence from the site, including preserved DNA hint at clues to palaeodiet and cultural industries at such sites. They also reveal much about how taphonomic processes may be affected by seawater and sediments on archaeological finds (Smith et al. 2015).

Also, in the UK, Goldcliff, a site in the Severn Estuary, made famous for the Mesolithic footprints in the mudstone was then revisited by the TV show Time Team (2003). The site presented researchers with an intact submerged peat shelf containing potential heat-cracked hearth-stones and evidence of butchery and fish bones dating from the mid to late Mesolithic – 8.5 to 6.8 kya (Bell et al. 2000). In Orkney, a series of potential shelter structures have been discovered in the shallow sediments along with numerous lithic assemblages dating from around 9 kya (Parfitt et al. 2005), suggesting seasonal return with onsite knapping.

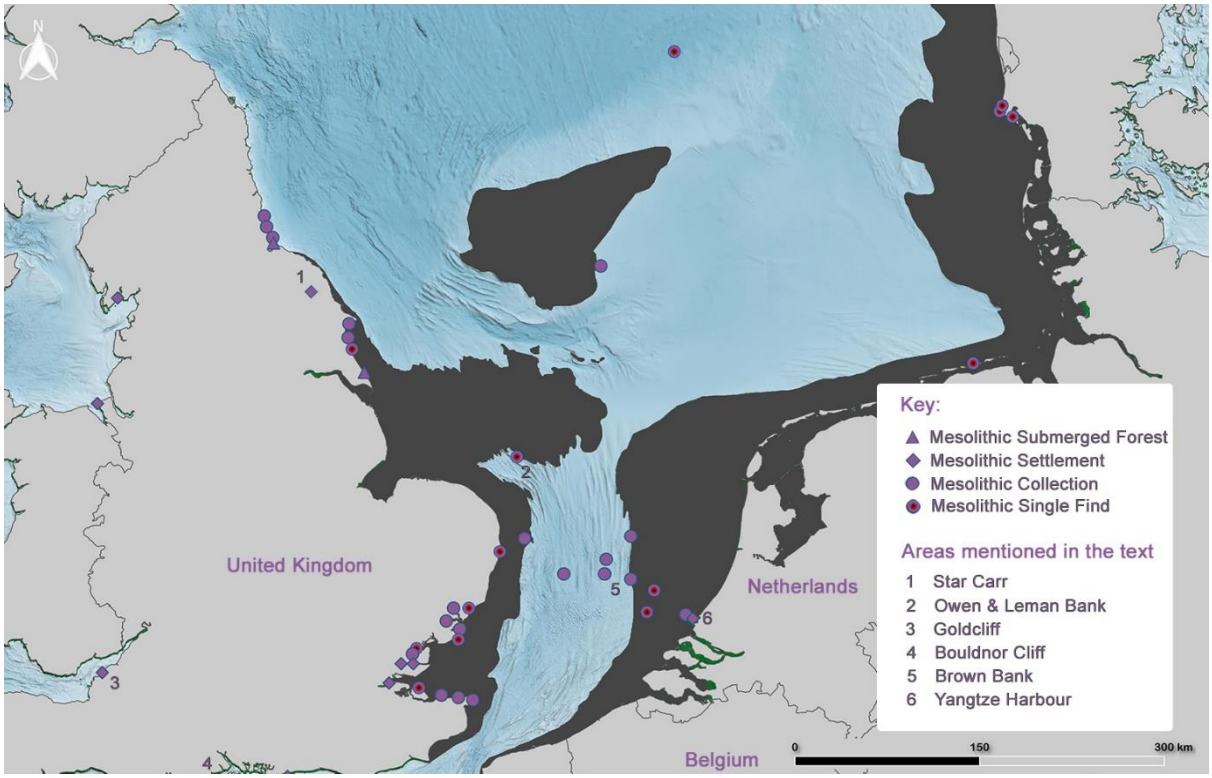

Figure 2.12 Sites of Mesolithic significance taken from the SplashCOS database (splashcosviewer.net). Black outline shows approximate coastline at 8.2ky

Continuous occupational sites have also been uncovered in submerged archaeology off the coast of the Netherlands. The excavations at Yangtze Harbour development in Rotterdam (Sier et al. 2014) revealed a multi-layered Mesolithic settlement site that spanned many generations and, from the diversity of remains discovered, was in all probability a continually occupied base of activity throughout the year. It is important to note that while the Netherlands Yangtze Harbour site provided years of research, this is the only submerged Mesolithic site known to exist in the lowlands.

Belgium has no submerged marine Mesolithic sites at present, only inland terrestrial sites.

When it comes to research into submerged Mesolithic settlements however, the rest of North-West Europe falls far behind Denmark and Germany. Between these two countries they have excavated twelve principle submerged sites with approximately 160 potential Mesolithic sites to be fully developed (Bailey et al. 2020). Unfortunately, these all lie within either the Baltic Littorina or the Limfjord areas of inland Jutland as opposed to the North Sea, so are not directly within the focus of this thesis. Despite this, these settlement sites range in date from the middle Mesolithic onwards, reflecting the marine transgression of this basin from around 8.4 kya (Aaby et al. 1997; Astrup 2018). Following the Maglemose Culture in southern Denmark, the marine inundation of the area and the economic changes brought about by the Kongemose and Ertebølle cultures spreading from this extensive Baltic area had a decided impact on the wider region.

There is evidence throughout north-western Europe of a larger exploitation of marine resources and the toolset to acquire them including microlith arrowheads with traverse barbs and stationary fish traps (Philippsen and Meadows 2014). The evidence for such industry has been argued to originate with the Kongemose and later, the Ertebølle cultures – with the evidence of raised shell middens both at submerged and later at inland sites begin to show a widening diversity of resource base (Davison et al. 2006). Stable isotope analysis shows larger game begin to account for a smaller percentage of the diet, alongside fish and shellfish (Richards and Schulting 2006). Easily foraged staples such as hazelnuts, acorns, blackberries and juniper make up the rest, supplemented with root vegetables and sea grasses to account for a proposed 14% of the hunter-gatherer diet (Cordain et al. 2000). This must be an assumption however as very little evidence survives for the vegetarian aspect of the palaeodiet from extant Mesolithic sites with the exception of hazelnuts (Waddington and Pedersen 2007). This is not a reflection on the favoured nature of hazelnuts. It is rather that the comparative preservation of hazelnuts, especially in terrestrial settings where preservation of all organic matter is poor, generally tends to be superior (López-Dóriga 2015).

Inland Mesolithic sites vary in preservation and detail and with what they are able to tell us about offshore cultural connections. In the UK, sites are

often characterised by little more than lithic scatters with post holes, hearths and the occasional midden (Waddington 2007; Waddington and Wicks 2017). Obvious variations to this rule have been found, such as Star Carr where peat formed around on the banks of the post glacial Lake Flixton. The thick peat that covered the lake has preserved organic remains including bones and midden evidence that tell us more about the palaeodiet to suggest a more nuanced seasonal settlement structure (Milner et al. 2018). While the lithic assemblages at Star Carr and Deep Carr nearby have their own characteristic typology, there is definite sign of cultural import with diversification of resource including evidence for fish trapping and processing (Robson et al. 2018).

Human remains from continuously occupied Mesolithic sites have a lot to tell us about the hunter-gatherer palaeodiet and thus about the landscape in which they lived. Stable isotopic signatures taken at an inland site in Belgium were analysed and revealed a gradual change from large game hunting in the early Mesolithic period to a majority vegetarian diet come the Neolithic period, supplemented with occasional freshwater meats and with terrestrial meat making up only a small percentage (Bocherens et al. 2007). Meanwhile, remains in Sweden and Norway demonstrated extremely high δ15N percentages in comparison to other Mesolithic mammals indicating a majority marine-based protein palaeodiet, most likely involving sea predators such as seals (Schoeninger and DeNiro 1984). Such variations may show local environmental or landscape changes such as heavier forestation making hunting more difficult or water levels changing the floral makeup, making it less appealing to larger game, altering water courses and therefore game routes. Over-population and over-hunting may force a change in economies; however, this is all purely conjecture.

What can be noted by archaeologists is a gradual change in the activity of long-standing settlement sites during the Mesolithic period. These are guided by discoveries made at inland sites for which we have many more examples. Some, such as Star Carr and Howick however, are close enough to the coastline (or over it in the case of the now part-eroded Howick), as to be important markers as examples of potential permanent settlements in the early Mesolithic (Waddington 2007). They would have been in continuous occupation over a long period of time with little or no stratigraphical evidence of abandonment. It does not say anything about whether these sites were occupied all year round. In fact, of the following

three postulated scenarios for occupational base settlements, there is little compelling evidence anywhere in Europe for identifying which interpretation can be assigned to which Mesolithic site:

1) Seasonal occupation – The entire group follow large game migration to a summer hunting ground, leaving the winter base for an entire season. The entire group return to base out of season to forage and fish off-coast alongside limited terrestrial local hunting.

2) Mixed Occupation – Smaller hunting groups follow game migration and return throughout the season with regular supplies from hunt. Meanwhile the majority remain in the permanent base, supplementing hunting with year-round foraging and fishing.

3) Continuous occupation – Small hunting groups on short range missions with more emphasis on localised industry, possibly with a marine focus with terrestrial hunting and forage as supplement.

Such interpretations do allow archaeologists to predict potential settlement sites based on resource centres and gathering methodologies as demonstrated successfully in Danish waters by Anders Fischer whose fishing site prediction model (Fischer 1995) has uncovered over a dozen potential sites. A variant of this model has been proposed for use in UK waters but results remain inconclusive (Hall 2014). The move from purely economic led archaeological industry to one that is more experiential in outlook during the last decade (Leary 2009; Gaffney et al. 2017a) has also forced a move to regard the landscape – and its loss – as intrinsic to the Mesolithic people.

2.5.3 Palaeolandscape Modelling

Mapping of the North Sea for archaeological purpose has been touched on in the introduction but it is worth pointing out that the discovery of the Colinda point came at a crucial moment. The Mesolithic period, which had been regarded as regarded as the 'impoverished cousin' of the Palaeolithic and Neolithic (Childe 1925), comprising of a 'huddle of march-ridden food gatherers' (Wheeler 1954). It was thought to offer little to the archaeological understanding of our cultural ancestry. Reid, in his book *Submerged Forests* had speculated about the terrestrial origin of submerged landscapes beneath the North Sea (Reid 1913) and Gordon Childe had postulated an early map, though it was little more than an attempt to join the UK to the Baltic (Childe 1925).

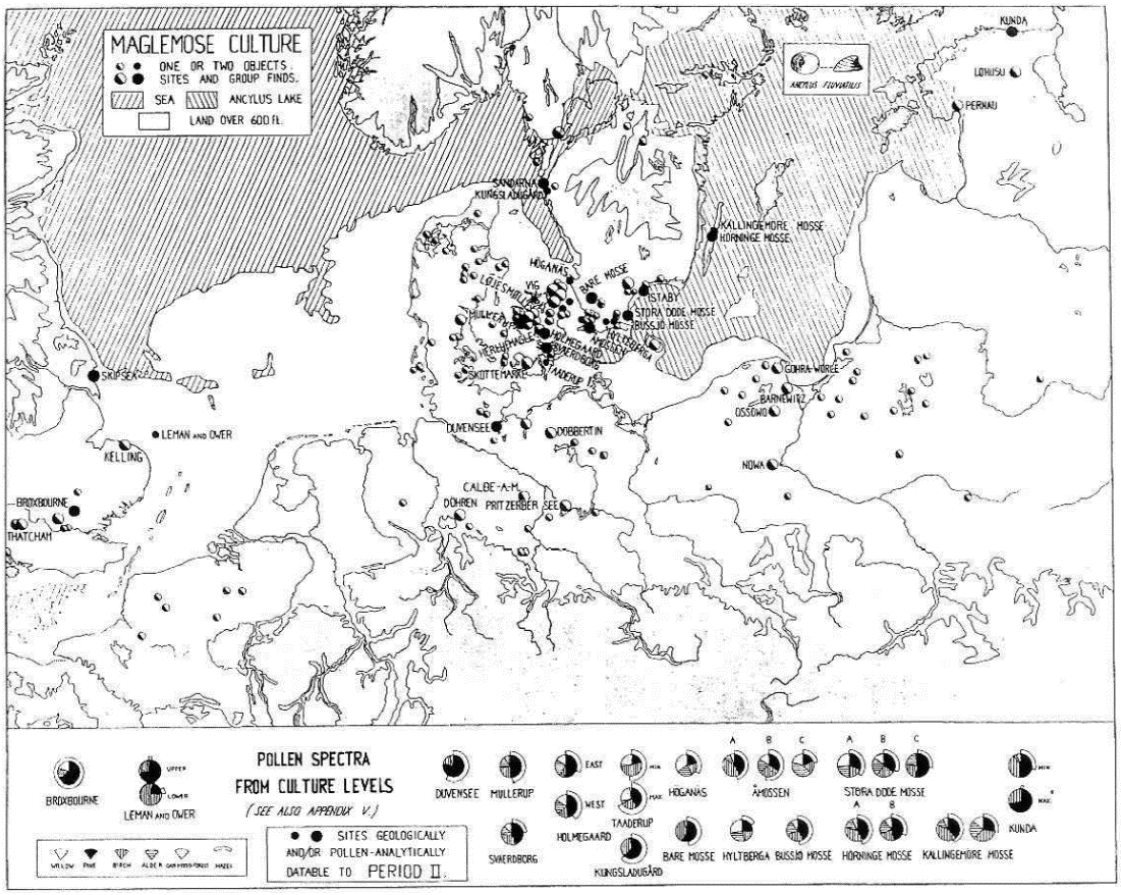

Figure 2.13 Clark's map of northern Europe shows Doggerland closely resembling the extent we propose today (Clark 1936: insert.)

Graham Clark felt differently, specialising in Mesolithic Europe and drawing analogies from contemporary hunter-gatherer peoples from North America and Greenland, he was able to stir an archaeological awakening that Reid and Childe had been unable to achieve (Clark 1954). His use of pollen analysis across the North Sea basin, linked with tool typology such as the Colinda Point, and later from the excavations at Star Carr, allowed him to create maps such as Figure 2.13 featuring a Mesolithic terrestrial landscape under the southern North Sea which proved highly influential, refocusing archaeological minds on potential landscapes.

Clark reasoned that if two geographically distinct cultures could develop with shared lithic and bone assemblages, it may be possible that some central cultural hub lay between them and the scarcity of evidence was potentially just an absence of evidence (Clark 1936).

This idea was met by a paucity of imagination. Rather than see a European landscape stretching from the West Coast of England to the East of Denmark, archaeological maps still portrayed cultural and economic exchange between peripheral, modern-day territories – areas where terrestrial sites were preserved with little concern for what lay between. The land beneath the North Sea was little more than a land bridge between modern coastlines (Jacobi 1976). The first archaeologist to deviate from this idea was Morrison (Figure 2.14) who retained a full land mass below the Dogger Bank and even suggested river courses and the placement of lakes within the landscape (Morrison 1980). Morrison was sadly overlooked and the trend to view the archaeology of the southern North Sea as a peripheral industry that pollinated across the divide remained almost until the millennium.

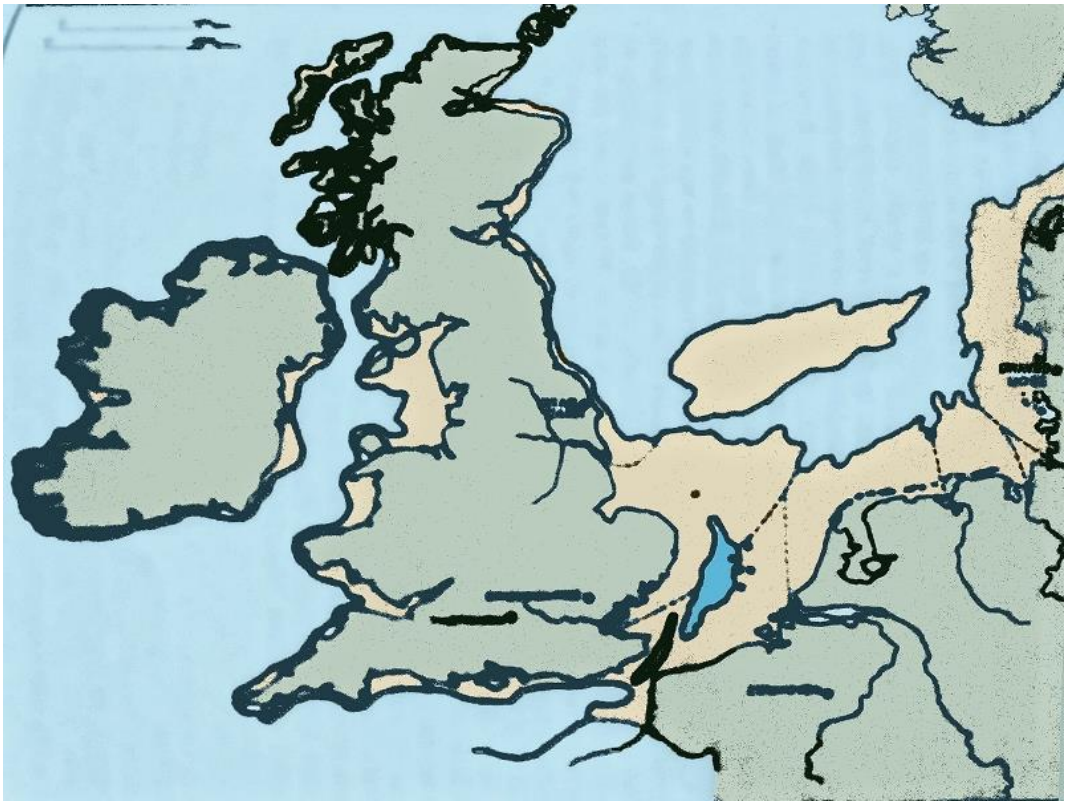

Figure 2.14 Morrison's Mesolithic UK coastline with lakes and rivers reproduced by author (Morrison 1980 p.85)

Bryony Coles' Speculative Survey (Coles 1998) allowed the focus to shift once again to consider broader cultural phenomena propagating outward to these littoral sites from a central area. This work and her follow up, Doggerland: the *cultural dynamics of a shifting coastline* (Coles 2000) took the opportunity to synthesise all the previous research of finds,

theories, models and mapping from Reid to Morrison alongside an awareness of (but not adherence to) sea-level rise to formulate her own conclusions and mapping of the region (Coles 1998). By placing the 'speculative Doggerland' as the central component of a Mesolithic cultural landscape, Coles brought a dynamism that had been missing from the static representations of earlier maps. As well as popularising the name 'Doggerland', Coles also brought a realisation that archaeological investigation in the southern North Sea would always remain speculative until it could undergo the same scientific analysis to which terrestrial sites were subjected. So, while Coles' research recognised the paradigm shift in landscape archaeology that the North Sea required, it was still merely a palaeoenvironmental narrative based on speculation. In some ways this was exactly the point at which Reid arrived when he saw the fossilised trees and postulated the submerged lands in 1913. All the environmental speculators since (Reid 1913; Clark 1936; Louwe Kooijmans 1970; Jelgersma 1979; Smith et al. 1992; Coles 1998; Lambeck and Chappell 2001) have in fact merely been reconfirming the need for further data and analysis.

The real move from static speculative maps to reconstructions and models of submerged terrestrial landscapes has only been possible with the introduction of a temporal aspect to the mapping. The coastlines of northwest Europe at the beginning of the Mesolithic period and the end were so different that a single snapshot was of little aid to the archaeologist searching for potential settlement sites. Coles understood this in her Speculative Survey (Coles 1998) and since then, models have attempted to accommodate sea-level rise and the ever-changing environment in their parameters.

The North Sea Palaeolandscape Project at the University of Birmingham, published in 2007 (Gaffney et al. 2009) utilised seismic geophysics alongside core environmental data and bathymetry to build its models and while the technology had been utilised in other industries, it provided a new path for archaeologists; foundations upon which new palaeoenvironmental understanding could be built (van Heteren et al. 2014b; Verhegge et al. 2016). The Europe's Lost Frontiers Project took the submerged landscape mapping of the Mesolithic southern North Sea Basin another step with a fully funded archaeological coring programme, ship time and access to the widest range of industry seismic data available for analysis (Gaffney et al. 2017a).

Such models are still able to create maps but also have the potential for much more. They source data from multiple scientific disciplines in order to build up environmental models. For, to understand the behaviour of Mesolithic people in north-western Europe, with a focal point of the North Sea, archaeological evidence alone will not suffice. The people and the landscapes within which they lived were interconnected. As such, reconstruction must now include topological mapping and landscape features, modern bathymetry, isostatic rebound modelling and seismic interpretation (Sturt et al. 2013; Verhegge et al. 2016; Gaffney et al. 2017a). It must combine this with environmental proxies from cores to populate the naked surfaces with flora and fauna, to understand the climate that supported different economic resources. Offshore coring of the North Sea has been extensively performed for both geological and petrochemical use but until recently these provided little in the way of archaeological environmental proxies (Peeters et al. 2019). Pollen analysis across the southern North Sea has been carried out at both supra-regional and macro levels (Clark 1936; Jelgersma 1979; Smith et al. 1992; Berglund et al. 1994). This has led to a good broad impression of climatic condition for the region. The addition of the Greenland Ice Sheet Project coring correlation of oxygen isotopes in 1997 allowed the tying in of larger, global climate trends from the LGM through to the late Holocene (Meese et al. 1997: 1997).

At this point, core analyses may be utilised. National geoscience organisations have taken core samples at over 6,000 logged locations throughout the southern North Sea and entered details into more than sixteen incompatible databases, eight of which are available online (EMODnet, NorthSeaCore Online). The archaeological detail contained within these databases is extremely limited. Therefore, archaeological focused coring programmes are essential to the production of quality proxy data. Such cores are analysed under strict sets of archaeological procedures to ensure the maximum efficiency of usage, considering the non-destructive vs destructive nature of differing proxy sampling techniques (Bates M, pers comm). From these analyses, it is not only possible to obtain multiple dating sources but also lithography, pollen, diatoms, macrofossils, foraminifer, coleoptera, chemical analysis, DNA and molluscs. These can be combined to build a landscape with a history, populated by plants and animals and a date for inundation. It gives the archaeologist a record of the climate and the environment throughout the Mesolithic period.

2.5.4 Climatic Change

From analyses of global and local proxy evidence it has been possible to determine that prior to the Mesolithic period (13 kya to 11.6 kya), the southern North Sea basin was a landscape of open tundra and low-lying floral coverage (Berglund et al. 1994). The fact, that there is little in the way of archaeological evidence of the Late Palaeolithic Ahrensburgian reindeer hunters must be due to an absence of evidence as this landscape of shallow valleys, low-lying hills, plenty of easily navigable, and relatively slow-moving waterways would have been attractive for hunting (Peeters and Momber 2014).

During this period – at around 12 kya - the retreating ice, created a melt-water pulse that flooded the Baltic region at Mt Billingen, cutting Denmark off from northern Scandinavia by the Yoldia Sea (Rasmussen et al. 2014). The Storebælt remained dry but this sudden change in water load may be linked to a localised climatic change across north-western Europe, from a cold but dry late-Palaeolithic Younger Dryas to a warmer but wetter Holocene (Harrison et al. 2019). This wide-scale and relatively sudden inundation has also been seen as the first diversification in Denmark of Maglemosian material culture (Sørensen 2003; Crombé 2018) though a millennia passed before the culture began to assert itself in the archaeological record and for this to impact on the southern North Sea basin as a whole (Philippsen and Meadows 2014; Astrup 2018).

A warming and wetting climate promoted a gradual vegetation expansion alongside an increased deposition of mineral and organic-rich matter throughout the region (Wymer and King 1962; PAUS 1988). Pollen, coleopteran, micro-fossil and geochemical analyses from both sides of the North Sea basin show a rise in *corylus* (Hazell 2013) and *pinus* (pine) (Birchenough et al. 2011) while *betula* (Birchenough et al. 2011) is shown to decline briefly after 12 kya. This is less noticeable in the western regions than the east (Kristiansen et al. 1988).

By 11.6 kya and the dawn of the Mesolithic period, pollen assemblages showed widespread woodland of *betula, pinus* and *corylus* (Hazell 2013) with an increase over time of *alnus* (alder) (Wiltshire and Edwards 1993). These covered uplands and slopes while the lower lands featured shallow, slow moving and braided river systems and marshlands.

Between 9 kya and 6 kya a more mixed woodland canopy prevailed, except on the coastlines. *Quercus* (Deegan et al. 2004) (Deegan et al. 2004) and *alnus* became more common alongside less common but widespread *fraxinus* (ash) and *tilia* (lime). The low-lying fertile soils of the Baltic and southern North Sea basins and ex-glacial lakes such as the Vale of Pickering demonstrated evidence of wider, open landscapes. These exhibited a varied mosaic of woodland species co-existing with shrub-like *crataegus* (hawthorn), *sorbus* (rowan) and *prunus* (wild cherry) (Innes et al. 2011). While there is little evidence for an anthropogenic Mesolithic plant economy, the burning of woodland, for the management of land and the animals thereon became systemic after 8.2 kya (Lewis et al. 2016). In fact, Tolan-Smith et al. (Tolan-Smith 2008) argue for a pronounced managed Mesolithic impact on woodland throughout the late Mesolithic, claiming that the pollen record is profoundly affected by such burn-back events.

As illustrated in Figure 2.15, sea level rise during the Mesolithic period was more rapid than at any time in our existence. Two Rapidly Rising Phases (RRPIII and RRPIV) occurred, during which global sea level mean rise was calculated to have been 1.7cm and 1.1cm per year respectively (Li et al. 2014). This rapidity would have been noticeable within a generational timespan and forced adaptation and dispersal in fauna, flora and people.

Significantly, the Rapidly Rising Phases RRPII and III fall at points where a melt-water pulse was detected with a corresponding peak in the ice core oxygen isotope record. The first of these occurred too early for the jurisdiction of this research. The second however, at 11.3 kya corresponded to a short-lived (150 year) cold snap of between 1° and 2°C (Rasmussen et al. 2014). While studies in the Rhine-Meuse area of the Netherlands identified cultural and environmental changes including increased levels of wildfires and decreased freshwater activity (Crombé 2018), no firm causality or chronological links could be made with any assurity. The cultural changes may have preceded the climatic changes and have been ongoing throughout.

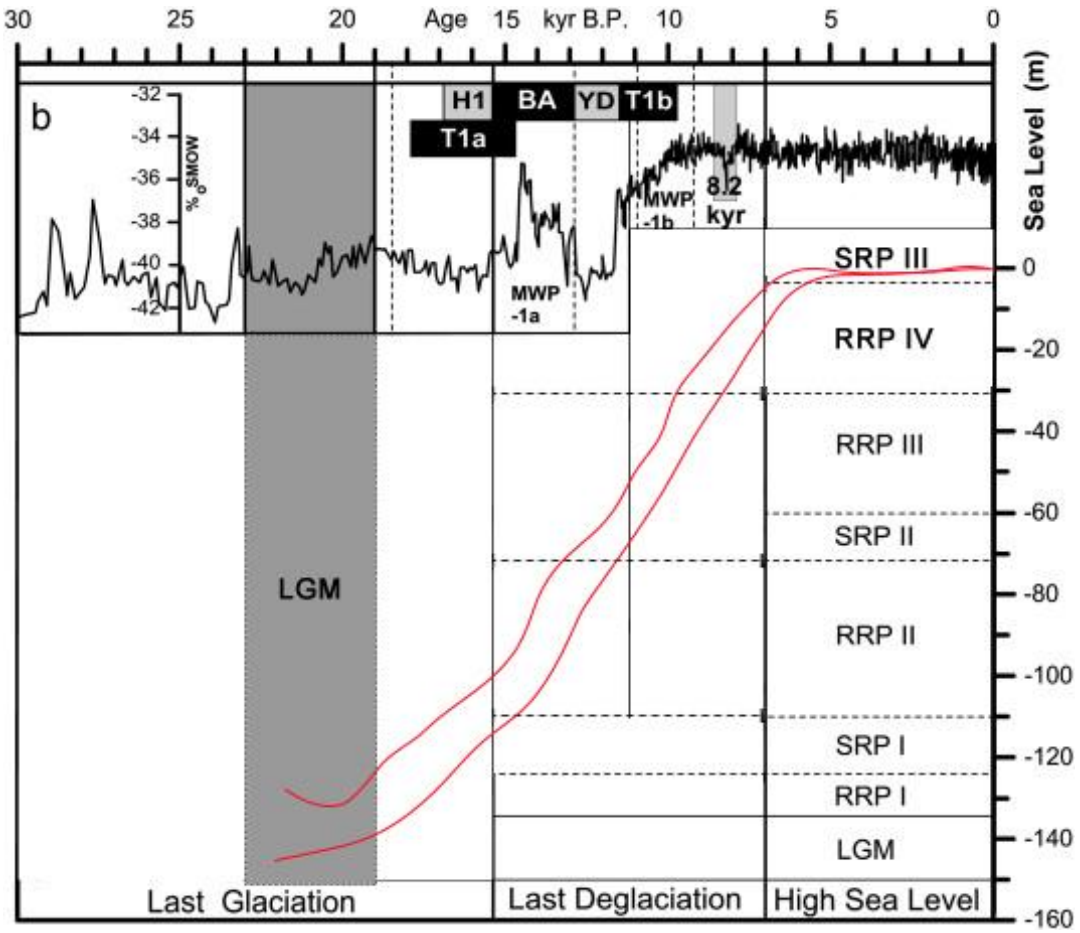

Figure 2.15 Global Sea-Level Rise in phased responses (from Li et al. 2014). Red lines mark the range of interpreted sea-level data (from Lambeck and Chappell 2001).

It was suggested that around this time, on a global scale, the retreat of the Laurentide glacier from Hudson Bay created an outburst flood of meltwater from the newly conjoined proglacial lakes; Agassiz and Ojibway (Barber et al. 1999; Clarke et al. 2004). The rise in water level and pressure that overwhelmed the narrow ice-dam, delivered an estimated 163,000 km^3 of glacial water into the northern Atlantic. This influx would have disrupted the thermohaline circulation of the ocean and reduced the coastal temperature around Greenland by 3°C and around north-western Europe by 1°C (Matero et al. 2017). The dates for this are hotly debated due to other significant releases of water from these lakes throughout the post-glacial period from 12 kya through to 7.7kya, though it is often referred to as an 8.2 kya event (Broecker 2006).

RRPIV shows the opposite to the melt-water pulses. A rapid rise in sea level and a drop in oxygen isotope percentage at the 8.2 kya point. This may be confused with an 8.2 kya event, the Storegga Slide (Bryn et al. 2005).

This submarine landslide off the coast of Norway, was most probably caused by post-glacial rebound which resulted in either a slumping faultline or earthquake. Some have chosen to see the tsunami resulting from this slide as the 'final flooding of Doggerland' and the catastrophic extinction of entire North Sea cultures (Weninger et al. 2008). Core samples taken in Scotland and Jutland show depositional layers attributed to the Storegga Slide and related modelling of the subsequent tsunami show wave heights between 10 – 12m extending out into the northern Atlantic (Bondevik et al. 2005). However, similar deposits in the southern North Sea demonstrate only 2 – 3m rise (Weninger et al. 2008). Therefore, populations in the coastal regions of Scotland, the Orkneys and Jutland would have experienced sudden, impactful environment change. To Doggerland and the southern North Sea, however, which were already largely transgressed with minimal populations, the tsunami would have been short-lived and was unlikely to have made a significant long-term impact on this localised area (Walker et al. 2020).

Of course, the ranges in Figure 2.15, above, are calculated using a eustatic, global mean sea level range. Local isostatic variations are dependent on a range of factors – land subsidence and uplift due to unloading of glacial ice, tectonic movement and glacial hydro-isostatic adjustment as well as topographic factors such as high and low gradient barriers of land (Flemming et al. 2014). For regional and more macro spatial models of the southern North Sea, such eustatic mean figures are insufficient. Localised index points and core evidence are needed to build up specific sea level curves that can explain where the coastline may potentially have been located at specific point in time.

Time and resources have been engaged in looking into exact rates of sea-level rise around the region, using localised sea-level curves derived from core samples (Shennan and Andrews 2000; Lambeck and Chappell 2001; Peltier 2004) and these provide an accurate record of the rates of transgression. In addition to general sea-level rise, specific localised markers for events on a global scale can be noted and used to join together 'rafts' of index point dates to the global curve. Such is the case with the Storegga Slide which has been measured in the uplifted coastlines of Scotland, the Hebrides, Scandinavia and now, in archaeological cores from the southern North Sea (Walker et al. 2020).

After the last islands of Dogger Bank and much of the low-lying European coastlines had been inundated, the population move toward higher, more insular lands, further inside the continent. As Tolan-Smith points out (Tolan-Smith 2008), this may be more a result of a lack of evidence for the submerged coastal sites and not a change in landscape usage at the time. We do however see a change in material culture as becoming more isolated and divergent in nature as communities develop independently, suggesting less movement and cross-over of knowledge as Neolithization occurs. Though this does not necessitate a lack of trade and exchange with other communities, it does suggest more localised self-reliance, sufficiency and a sedentism. Territoriality increases, often with land beginning to be marked and social interaction becomes complex (Momber 2000; Waddington 2007).

The traditional archaeological view of the one-way path from the hunter-gatherer toward sedentary farming, however, now seems over-simplified. Recent research by, amongst others, Waddington and Wicks (2017) and Astrup (2018), suggest that landscape, resource, climate and cultural isolation may all have played a role in the direction and speed of change. Therefore it is still pertinent to map and understand the environments in which this took place.

2.6 An Overview of Marine Geophysics

While the research undertaken for this thesis employed a great amount of computing resource and software application power and was almost entirely desk-based, it also embarked on survey missions in the southern North Sea. These multi-disciplinary missions from the UK, Belgium and the Netherlands carried out focused archaeological coring, dredging and marine geophysics. Shallow sediment seismic interpretations were used to focus on archaeological potential and guide the coring program. The cores recovered then underwent processing and analyses by multi-disciplinary elements of the larger project and affiliated partners and the reports processed. As part of the later peat analysis, used in this thesis, core environmental and lithological data were employed.

Archaeology at sea is expensive in comparison to land. Underwater archaeology is also a lot more difficult, especially at depth. To investigate archaeology within warm, clear seas to a depth of 5m, especially within reach of a Mediterranean town is no punishment, but as Flemming points out, the number of discovered submerged sites drop off steeply at depths over 5m as the difficulty in accessibility and lack of available technologies rise at inverse rates (Flemming et al. 2014). When shallow dives are a concern, then archaeological excavation becomes a logistical and financial undertaking in and of itself. Therefore excavation becomes exceedingly rare and watching briefs, cultural heritage frameworks and best practice guidelines become commonplace (Peeters et al. 2019). The archaeological utilisation of remote sensing marine geophysics is still under-developed but focused methodologies already for shallow interpretation as shown in Table 2.5 (Bates et al. 2007; Verhegge et al. 2016).

METHOD	TECHNIQUE	DATA FOCUS	TECHNOLOGY	RES.	FREQUENCY	MAX DEPTH	USED FOR
REMOTE SENSING	Acoustic	Seafloor mapping	Side-Scan Sonar	High	100 - 500kHz	<2,000m	Wreck / Feature Investigation
			Multibeam echosounder	High	multiple	4 x water depth	Wreck / Feature Investigation
	Light	Coastal Mapping	Green laser LIDAR	High		Shallow water	Wreck / Feature Investigation
	Acoustic	Sub-seafloor mapping (2D)	sub-bottom profiler - chirp/ping	High	2kHz - 16kHz	50m	Shallow environmental
			multi-channel chirp & boomer	High	200Hz - 15kH:	150m	Detailed Palaeolandscapes
		Sub-seafloor mapping (3D)	sub-bottom profiler - Sparker	Low	0.2kHz - 3kHz	750m	Deep water geology
			sub-bottom profiler - Boomer	Medium	0.3kHz - 6kHz	150m	Continental shelf mapping
			sub-bottom profiler - chirp	High	3kHz - 10kHz	60m	Shallow morphological detail
DIRECT INVESTIGATION	Sampling	Modern Sediment analysis	Grabs / Box cores			3m	Shallow Holocene strata
	Coring	Environmental sedimentological	Piston core, Vibrocore, gravity core			9m	LGM to bedrock
	Dive	archaeological / environmental	Photographic recording			20m	Wreck / Feature Investigation
	Excavation	archaeological	Dredge Hose			5m	coastal site specific
AUTONOMOUS UNDERWATER VEHICLE (AUV)	Acoustic	seafloor mapping	side-scan Sonar (as above)				Wreck / Feature investigation
	Photographic	archaeological	recording				Wreck / Feature investigation
	sampling	archaeological / environmental	grabs				Shallow Holocene Strata

Table 2.5 Techniques in Marine Geophysics (after Bates et al., 2007; Verhegge et al. 2016)

Due to the inaccessibility of the seabed subsurface and the sheer scale of continental shelf mapping, almost all geophysical techniques are rendered inapplicable for the focus of this research. Site level investigation within shallow coastal regions have used electro-magnetic induction techniques with great success to locate palaeo-wetlands in terrestrial environments. However, these techniques cannot be used in any depth of water (Missiaen et al. 2018). Green-laser LIDAR has also proved popular in near-coastline landscape mapping as it has the ability to penetrate shallow waters and back-strip the water column. However, good results are heavily reliant on an outcropping palaeolandscape with little or no sediment overburden and suspension of silts and sediment in the water will eliminate all visibility (Lecours et al. 2016).

Case studies on acoustic remote sensing such as multi-beam echosounders have demonstrated that the resolution of imagery i.e. the detection and identification of ever smaller objects and structures, is improving at an exponential rate to the point at which wrecks may be confidently pin-pointed beneath a consistent modern sea floor, so long as the presence is already known (Missiaen et al. 2008). A resolution cap still exists for unknown sites that prevents confidence in analysis. No computer software yet exists that can utilise pattern recognition to predict and identify previously unknown archaeological sites. Neural networking solutions that run such auto-location sweeps are currently being undertaken and this early work has great implications for submerged wreck archaeology in the future (Brown and Poulton 1996).

2.6.1 Non-Acoustic Methods

Although acoustic methods are predominantly favoured in sub-sea imaging and mapping, they are by no means the only ones. In shallow, clear waters green-light LIDAR is a very useful tool at fast, high precision mapping of large areas of the sea bed from the air as it is able to processionally remove the water column and any flora from the surface image. This allows features to be readily identified. Electromagnetic (EM) and magnetic (or gradiometric) tools have also been developed for shallow water sediment research using two or more spatially independent sensors. While the gradiometrics can be performed from smaller vessels, the EM equipment is large and requires a large boat. In both cases data

capture is slow and the resolution poor in comparison to seismic acquisition (Missiaen and Feller 2008).

Site identification and survey requires resolutions at a scale of 1-2m while the mapping of landscapes has historically relied on resolutions in the tens of metres, even for High definition landscape work (Table 2.5). This discrepancy of resolution must be a barrier to archaeological prospection. A number of significant archaeological sites have been discovered at <5m depth below sea level (Bailey and Flemming 2008). It is likely that a similar number of archaeologically important sites exist at depths of 5-50m, but the spatial scale between site exploration and submerged landscape mapping has, up until current times, been incompatible (Bailey et al. 2020). Recent upscaling in resolution however means that bin grid sizes, coverage and a high resolution can be married together to make topographical detail at sufficient site level detail, where needed.

Before any investigation into potential sites can be performed in high resolution, it is important to understand the geological and topographical layout of the submerged lands, reconstructing shorelines, deltas, river systems, hills and valleys in order to propose potential areas for investigation. Table 2.5 above shows the average resolution and coverage capabilities of various remote sensing technologies. It demonstrates that the only practical option for mapping a wide area must be acoustic surveys.

2.6.2 Acoustic Mapping

Seafloor mapping of surface or shallow buried sub-surfaces and sediment can be performed relatively quickly with side-scan sonar. These have the advantage of having excellent resolution to sub-metre scales. They can be towed at relatively fast speeds, attached to streamers behind larger vessels or on external craft such as AUVs and ROVs. They can be used in alignment with multiple streamers to provide a wide enough swath to cover square kilometres in a few hours (Bates et al. 2007). However, even taken at such relatively high speeds, this process is still too slow to cover the vast distances required for this project. Depth is also an issue, with the Holocene palaeolandscapes of this research located deeper than the initial few metres accessible to side-scan sonar, seafloor mapping is not the solution.

Sub-bottom profiling is a further acoustic technique that can penetrate further into the submerged landscapes using seismic reflections at the boundaries between two material types. Differing sources of signal are used to send out pulses at different frequencies. Higher frequency sources such as chirp give better resolution but suffer from greater attenuation than lower frequency sources such as boomer which have much greater penetration. Multichannel profiling combines multiple frequencies while parametric echosounders (PES) use a combined pulse of low and high frequencies. Such seismic techniques have been used for decades and technologies have improved over time to provide resolutions of between 1 m to 25 cm. While new surveys are expensive to commission on a scale required by the project, they are relatively quick to perform and there is already a wealth of available data to use (Wunderlich and Muller 2003).

The seismic reflection method relies on inducing an acoustic wave from a source directed into the seabed and recording the waves that are reflected from each sub-surface layer by means of hydrophones strung behind a vessel on streamers (Figure 2.16). Historically, this acoustic pulse has been generated and received at the surface of the water through which they travel regardless of the depth of water that needs to be penetrated. New technologies allow both source and receiver to be set at depths within the water, to try and eliminate shallow mirroring from the water itself or fish shoals beneath the vessel for better definition.

Geological interfaces may be mapped through sediment and rock layers to great depths. The seismic energy generated by the source passes through the substrates and, as it does, part of the energy wave bounces back from each new surface contact. This reflection coefficient is caused by differences in the acoustic impedance between various strata through which the acoustic wave passes. The amplitude of the reflected wave is recorded by the receiving hydrophone(s) (Parkes and Hatton 2013). The final product is a dataset of seismic reflectors, measuring different amplitudes dependent on the attenuation of the signal at given frequencies. The resulting peaks and troughs can then be interpreted to specific geological interfaces.

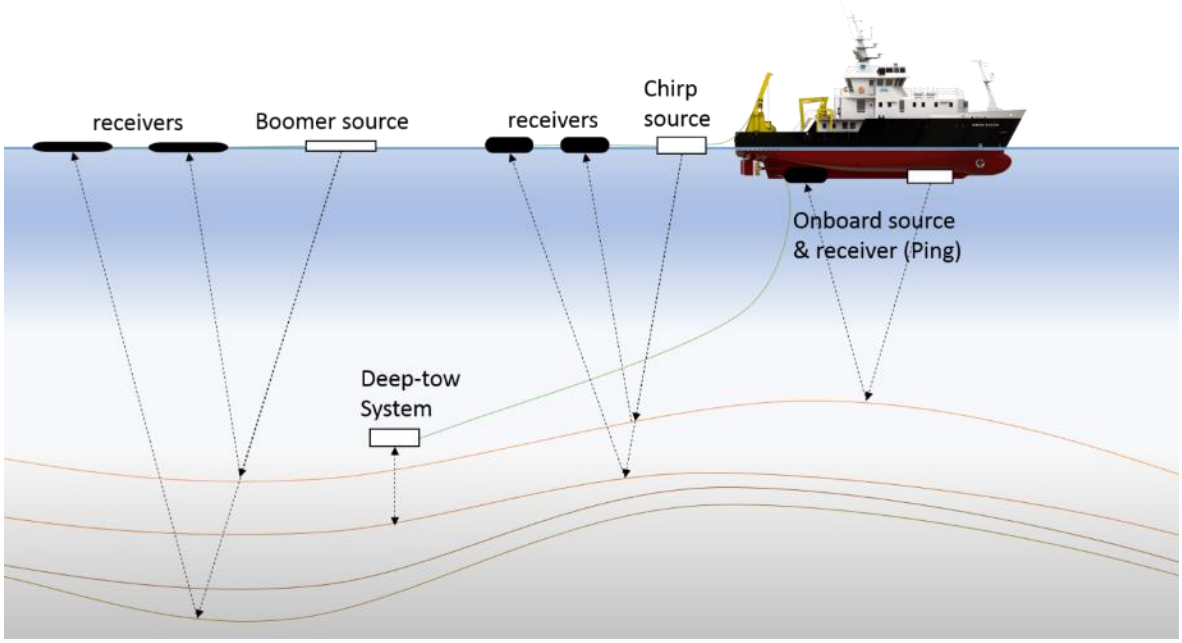

Figure 2.16 Differing acoustic technologies that can be employed. After Stoker et al. 1997

Depending on the technology and date, these surveys provide an ideal scale requiring a resolution of between 10 to 100 m and at the higher, HD end, can even reveal sequences of sea-level transgression and regression over the terrestrial landscape at sub metre resolution. It can reveal erosional outcropping or channel infill and relevant depths so that interpretations about landscape retreat, riverine routes and flow may be made. However, such resolution may dictate how clear an image can be determined on a horizontal x-y axis for the sake of landscape mapping. It does not necessarily improve the amplitude quality or z axis resolution (depth) to the data. This relies on three factors:

- Number of hydrophone streamers – the more streamers pulled by the vessels allows more hydrophone receivers and therefore better spatial interpolation of the processed data.

- Amplitude Frequency of acoustic source – High frequency acoustic sources give better detail at shallow depths but suffer more easily from diffraction in the water column and false reflections on many sedimental interfaces. This is especially the case with modern, mobile sand banks such as those covering much of the lower southern North Sea (Van Lancker et al. 2009). These can leave gaps in the data or even show false data (false positives). Lower frequency acoustic sources alleviate much of the problems associated with water diffraction and mirroring, due to their superior penetration. As a result they provide much worse detail at shallow depths and a lack of distinction between sedimental sequences and

interfaces. Energy industries favour lower frequency acoustic sources in their surveys because of this superior penetration as the data they wish to investigate are located hundreds, sometimes thousands of metres below the surface. However, the archaeological focus – i.e. encompassing the geomorphological units through to the LGM, are all contained within the first 2 – 40 m sediment or 0.7 s of two-way acoustic signal.

- Frequency of shots fired – horizontal smearing and vertical resolution can be linked to how many sparks, shots of air etc are produced per metre travelled. Lower shot rates, or faster boat travel per shot rates may result in varying bin grid resolutions and can cause discrepancies due to misinterpreted features within the data.

Since the majority of available data are low frequency 2D surveys provided by the energy industries whose focus is deep geology, this thesis utilises commercially available low frequency survey data and high frequency 3D data. Alongside this, high-frequency geophysical data commissioned with an archaeological focus as part of the ELF Project is used. Where possible, these are combined. Where the two datasets overlap, in areas of double coverage, useful interpolation of the two may then be possible.

The main disadvantages of 2D seismic, notwithstanding the technology involved are concerned with spatial accuracy. As a single streamer is used, the receivers do not receive any reference to their lateral position behind the source, as they would in a multi-streamer situation. Therefore, the streamer must be assumed to be straight, with an equally spaced bin size and the source firing directly down, beneath the vessel which is not necessarily the case.

2.7 An Overview of the Archaeological uses of a Geographical Information System

The use of Geographical Information Systems (GIS) in archaeology has revolutionised the spatial based components of academic research and site-based investigation. It is not only a data management tool that allows collaboration and shared datasets but, with the pursuance of landscape characterisations, GIS has become an archaeological methodology in its own right. The earliest uses were in archaeological management projects

in the United States (Kohler and Parker 1986). In the UK at the time, GIS was used primarily to present data in spatially significant ways for use in research and planning (Wheatley and Gillings 2013).

The consideration of both spatial and temporal scale in the reconstruction of landscapes has allowed archaeologists to understand site in the context of the larger environment characterisation. This has allowed for predictive modelling, not just in respect to the specific context of site stratigraphy and dispersal, though there is no doubting the impact GIS has made to this field (Marchand et al. 2018; Trizio et al. 2018). It has allowed the visualisation of the palimpsests of landscapes that palaeoenvironmental data and geophysics describe, allowing a new scheme of theories and suggest new interpretations of these reconstructed landscapes. Toolsets can integrate layers of data and slice them, cross-reference them and present the data in ways that not only map a palaeolandscape but manage, analyse and visualise it in a spatially useful, contextually meaningful way (Conolly and Lake 2006).

A geographical information system such as ArcGIS has become a staple of the archaeological process from small scale, site specific uses to large scale supra-regional characterisation and mapping. The flexibility of both the views and toolsets allows a GIS to become more than an illustration. It is therefore the obvious candidate for bringing together the component datasets for this thesis. It is the capability of ArcGIS' spatial handling technology that allows the importing of datasets from multiple IHS Kingdom projects that would otherwise remain isolated due to their projection limitations.

In this thesis a GIS was relied upon. In the first instance to give a spatial and contextual representation of potential coring locations. For instance, in the second round of project coring it was evident from bathymetric mapping that a palaeochannel ran north-north west to-south-south east, parallel to the Norfolk coast. New interpretations of existing seismic survey lines from the Humber Region Environmental Characterisation Project as well as 3D survey data from PGS, led the research to a new interpretation that the channel represented a river, extant in the early Holocene which opened directly onto a coastal estuary at the time of the proposed inundation. This 'Southern River' would become a primary coring target due to research results made possible in this paper. Further research and spatial analysis would also identify this area as a potential experimental

archaeological recovery area. Dredging was attempted across the mouth of the 'Southern River' with some considerable success (Missiaen et al. 2020).

In such ways, interpretation of data via geophysical software can be interpolated from small survey line features across a much wider canvas in a GIS. Localised areas of research such as the peat investigation from this research, the Humber and East Coast RECs, the Brown Banks research, new Windfarm reports and supporting research papers across the southern North Sea can all be brought together within a GIS and tested under the parameters of a single model.

The software packages that were sourced for this work were ESRI ArcGIS 10.6 and 10.8 primarily employing ArcMap. This is the industry standard GIS package for use in archaeology and the leading GIS package for spatial analysis in many scientific fields. It was also already under site licence at the University of Bradford and therefore accessible.

The second piece of geographical information system software is an open source developed system called QGIS. Versions 3.6, 3.8 and 3.10 Coruna were all used in the research of this thesis. While there is much cross-over between the two GIS packages, they each have their strengths and weaknesses and together they proved able to perform all the tasks necessary.

3 SEISMIC INTERPRETATION METHOD

3.1 The Acquisition and Usage of Data: 2D Seismic Data

Location	Data	Resolution	Data	source
Northern North Sea (multiple country)	Megamerge PGS North Sea 3D	12.5m (grid) 25m	Block 3D	PGS
Southern North Sea (multiple country)	Megamerge PGS S North Sea 3D	12.5m (grid) 25m	Block 3D	PGS
UK East Anglia Waters	East Coast REC	10 – 30m	Multi 2D & 3D	UKOGA \ CDL
West Coast, Bristol Channel UK	West Coast Project SGY & Kingdom	15 – 25m	Multi 2D	MASLF
Wash, Humber, UK waters to O.S.P.	Humber 2D Mainline & Kingdom	10 – 30m	Multi 2D	MASLF \ Humber REC
UK Waters and Central Graben	Mid High North Sea	15 – 75m	Multi 2D	OGA \ CDA
UK & Dutch Waters	Birmingham NSPP Megamerge	12.5m (grid) 25m	Multi 3D	PGS \ NOAA \ TNO
UK & Dutch Waters (Brandt et al. 1992)	Brown Bank, SR Belgica	10 – 15m	Multi 2D	VLIZ & ELF
UK Waters Northern	Government Mid-North Sea 2015	10 – 20m	Multi 2D	UKOGA \ CDL \ OG
UK Waters nearshore (Howick)	UK Coal Authority - Amble Northumberland	25m	Multi 2D	UKOGA
Assorted Dutch Water 2D lines	TNO 2 Southern North Sea 2D Gauss Lines	15 – 75m	Multi 2D	dGB Earth Sciences B.V.
S North Sea general	Dutch SMT Legacy Birmingham	12.5 – 75m	Multi 2D	NOAA \ TNO
S North Sea Windfarm Projects	Hollandze Kust (Noord & Zuid)	10 – 20m	Multi 2D	Fugro \ RVO.NL
German Bight 2D mainlines	BGR Stacked Geological Survey Data	30m	Multi 2D	BGR - Geoviewer
German Bight 2D assorted	AURO surveys for BGR	30 – 75m	Multi 2D	AUR02 and AUR03 BGR
Danish near shore low frequency 2D	GEUS Geological Survey near shore	35 – 75m	Multi 2D	GEUS
Danish North Sea high frequency	MARTA boomer \ Chirper data	35m	Multi 2D	MARTA

Table 3.1 Source data acquired for the Europe's Lost Frontiers Project. Shot at differing resolutions and bin size ratios.

Coverage is an important factor for the project. Seismic surveying is an expensive process which, is unavailable to most archaeological research. This research was fortunate to be able to carry out some focused survey work but the vast bulk of the data used for the purposes of interpretation, mapping and analyses relied on commercially free, available or contractual data from the organisations in Table 3.1.

A wide range of sources from sparker and chirp to the ubiquitous boomer, single and multi-channel streamers have been employed in the North Sea since the 1960s. The technologies behind these have improved over time and the curation, international cooperation and standardisation of many data sharing aspects has improved. However, there remain varying levels of knowledge and proprietorial standards, navigational and projection protocols and resolution criteria when working with said data. Despite these issues, common scientific standards such as SEG-Y have ensured that there is conformity of data and, over time, resolution has improved allowing better interpretation (Hagelund and Stewart 2017). The frequency of these sources and the resolution of the receivers can vary a great deal from 75m to less than a metre in the case of HD Surveying techniques.

Surface or sub-surface-towed boomers are the most commonly acquired source data sets available due to their suitability for depth penetration in oil and gas hydrocarbon geological surveying. Boomer surveys were also employed in both the East Coast and Humber Regional Environmental Characterisation Report surveys (Birchenough et al. 2011). These applied an acoustic plate source and a number of hydrophone receivers in line. Each line was tuned for offshore or near-shore responses incorporating a low-pass cut between 100 Hz – 1 kHz, a high cut of 1.5 – 2 kHz and an anti-aliasing filter to avoid engine interference set to 4.5 MHz Line spacing was generally 30 x 30m as is common for all modern boomer surveys, though high resolution surveys are also available which can set this as high as 10 x 10m.

2D Chirp and Ping surveys are much less commonly used for large scale mapping of landscape features. These are more often found for wreck and shallow inter-tidal zone investigation so are not owned by governmental or research-based institutions. The MARTA lines for near shores surveys in Denmark use 35m x 35m (Table 3.1).

All data are pre-processed to International SEG-Y standard, though this does not extend to the headers which can vary in the presence of survey start and end co-ordinates and the shotpoint multipliers. Where this is the case, the data may require some creative trial and error to geo-locate the survey lines and the importing of GIS shapefiles to demonstrate the precise geo-spatial locations of the surveys. This is also an issue when it comes to navigation files as there is no global standard set as to which co-ordinate system or geodesic projection system to use when taking a survey. If this is not recorded in the header, then it can be difficult to identify whether a survey has been taken in decimal degree arc-seconds, metres from meridian or in a country's local co-ordinate system e.g. Ordnance Survey OSGB.

2D seismic survey data were here used in addition to the 3D grids to give greater coverage and were used in comparative interpolations where cross-over existed. Recent studies in Belgium have demonstrated a multi-channel approach combined with a shallow focus post-processing returned a much better focus for archaeological surveying than a reliance on a single data source alone (Zurita Hurtado 2014). The 2D survey lines used in this thesis originated primarily from industry and government sources and did not have an archaeological focus, being concerned with oil and gas or deep geological study. However, it is important to note that further multichannel surveys have been undertaken as part of the project in the area of the Brown Bank to be used in future work. They have been shot with an archaeological focus, for shallow sediment and give far superior results.

3.2 Interpretation of 2D survey data

Seismic Interpretation refers to the process of bringing out selected information from a seismic survey to ascertain an understanding of the geological and geomorphological processes. This can be performed in many ways and be focused to answer many different questions, but for this research the most immediate and most important concerns were split into two distinct functions:

1) The identification of potential archaeologically-focused core locations – specifically, areas of palaeoenvironmental interest in the early transgressive landscape. These locations were picked out for

the preservation potential and accessibility of the deposits. Such deposits may contain high potential of settlement activity.

2) The identification and marking of features for the purposes of mapping and modelling the transgressive palaeolandscape. This was accomplished by interpretation of potential terrestrial surfaces, channels, landscape features and their associated seismic reflectors.

Vital to this thesis and implicit in both investigations was the investigation of potential peat beds – especially those of the Nieuwkoop Formation. For these outputs, the interpretations needed to examine complex geophysics and present the results in as simple a format as possible. The diagrammatic style needed to contain all relevant data to enable both the above outcomes to achieve their goals while only displaying the features necessary for the understanding of the scene. In Figure 3.1 the seabed was shown alongside a Holocene channel and a number of strong reflectors beneath a set of laminated layers. Further information was also contained within the seismic survey but as the intention was to focus on the strong reflectors to assess coring potential, only the major depositional layers were required in this diagram. The presence of free gases and the erosional surface were of potential interest for further proxy activities such as potential dredging, and therefore marked.

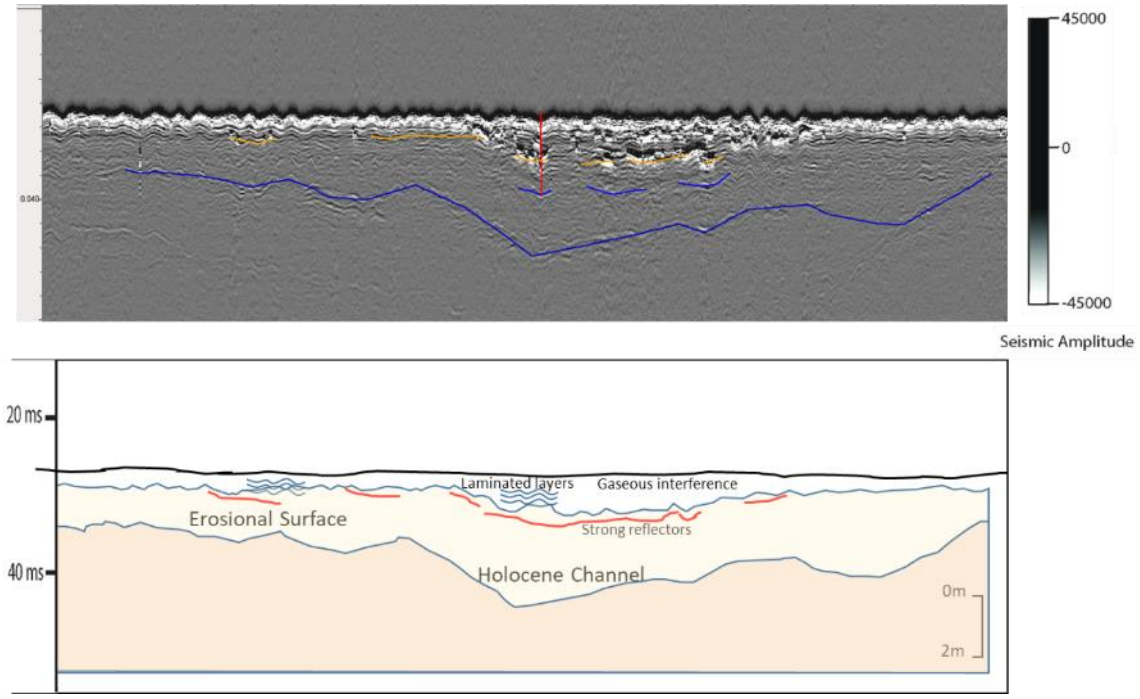

Figure 3.1 Feature overlay from Humber REC marked on seismic above (including suggested core location in red) and sequence interpretation below (after Fitch 2011).

To interpret sites for potential coring programmes it was useful to note depth and ensure the targeted layers were not beyond the reach of the coring device. The seabed needed to also be relatively level for the corestand to rest upon to prevent the corer toppling or drilling at an angle. For archaeological context, an interpreted landscape feature were a benefit. Riverine or coastal features such as a river valley, delta, coastal embayment, flood plain etc. were indicators for higher archaeological preservation potential (Bruck and Goodman 2012).

When examining shallow depositional formations in any seismic data. The primary target was a strong 'Holocene' reflector, i.e. a baseline unconformity above which transgressive sequences occurred and below which it was likely that the palaeolandscape was terrestrial. Visible depositional sequences, such as clinoforms that built up could then be plotted to show accommodation, aggradation and direction of sedimental deposition. This was vital in determining the rate and direction of transgression and the environmental conditions under which it took place.

Such sequences would ideally be marked or 'picked' along the zero polarity – i.e., where the reflective coefficient was zero (or the wave was at zero amplitude). However, this was often difficult to see as the default seismic interpretation colour scheme was graduated from black (positive amplitude) to white (negative amplitude) or visa-versa. The obvious solution to this was to change the colour bar and insert a bright contrasting colour for zero. However, this could have the effect of bleaching important features.

Throughout the seismic line, the peak signal (positive amplitude) was displayed as bolder and less 'fuzzy' that the trough (negative amplitude). However, the bright reflectors that were considered organic in nature were always negative (Bull et al. 1998; Plets et al. 2007). Therefore, if changing the zero colour had no effect, one solution was to select the most obvious of the peaks or troughs and always pick against that line. This enabled consistency to be retained at the expense of a few centimetres of vertical accuracy.

Using the software package IHS Kingdom (versions 2017, 2018, and 2019), which have been designed specifically for the analysis and interpretation

of geophysical seismic products, the interpretation could be carried out following a set checklist (Cojan and Renard 2002):

1) Identify and mark unconformities, preferably along the zero amplitude:
    a. Unconformities are continuous surfaces or surfaces where reflectors meet (convergence)
    b. Zero amplitude will generally lie between the peak and trough lines
    c. Attempt to perform an automated 'hunt' before manually picking. The software will seek the zero amplitude.
2) Extend unconformity over a complete feature filling in any conformable sections.
3) Identify the unconformity type:
    a. Does it have onlap above and a truncation below?
        i. Then it is a Sequence Boundary
    b. Does it have downlap with no truncation?
        i. Then it is a downlap surface
4) Mark the relevant clinoform sequences for progradation.
5) Mark strong and relevant reflectors (non-multiples).

For the mapping aspects of the seismic data, it was important to remember that the acoustic reflections were not representing actual land surfaces. What they represented were the variances in attenuation at the interface between two different materials. The more abrupt that contact, the greater the definition in the wave amplitude. The 'Holocene' baseline unconformity was used because the differentiation between the terrestrial land surface (soil, river sands and boulder clay) and the marine unconsolidated sediments of sands and muds was distinct during the saltwater transgression. This contact presented a stark difference in attenuation which was clearly seen reflected in the data.

By examining the 2D seismic data, the strong reflected unconformities could be picked where extensive or unbroken sequence boundaries occurred, commonly at major geomorphological events like inundations. These strong reflections also occurred between major lithological unit divisions that signified a known geological formation. These were likewise marked as horizons for any given interpretation. A minimum of three horizon boundaries were picked for interpretations connected to this study, often many more. These three were a) the seabed; b) a

palaeolandscape feature and, between the two, c) a Holocene base horizon which represented the terrestrial surface.

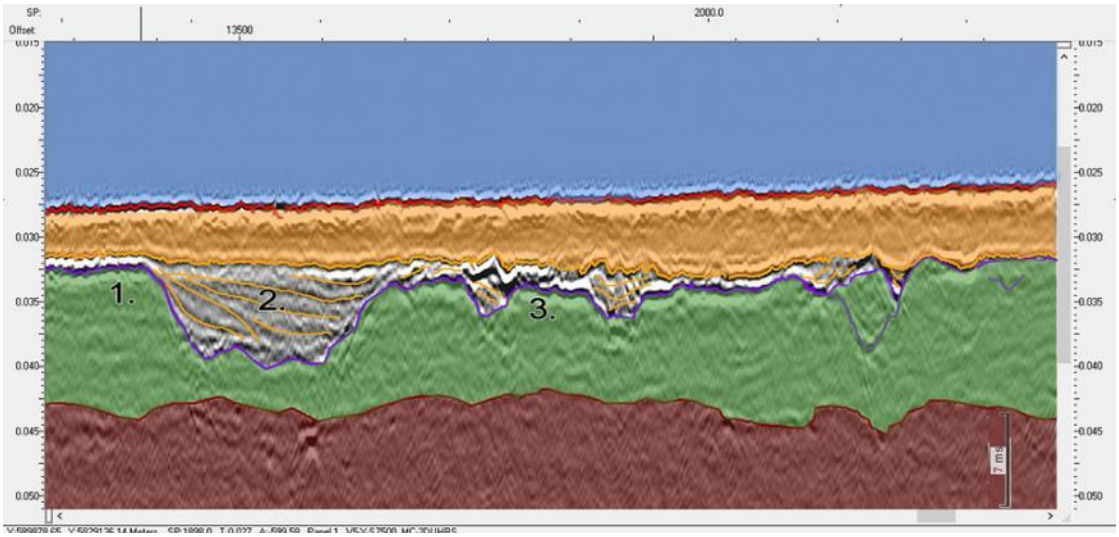

Figure 3.2 Coloured Interpretation showing clinoform sequences of fill deposition. Green - horizon of final terrestrial landscape, gold - modern Holocene sands. Between these are clinoforms demonstrating the inundation deposition. Data from FUGRO\RVO.nl (Thal et al. 2018)

Further depositional reflectors were picked as horizons pertinent to the study. For instance, Figure 3.2 shows several boundaries, two of which were strong enough for IHS Kingdom to have auto-picked the zero amplitude lines. These were glacial unconformity (brown) and Holocene base surface unconformity (1. purple line) delineating a last terrestrial surface before depositional sequences appeared. There was an obvious truncated clinoform (2. gold) that capped the small valley bottom at the left-hand side. The clinoform was itself capped by onlap deposition before the modern Holocene sediment layer overlay it (orange). The seabed in red was marked as a final individual horizon for the purposes of velocity modelling to calculate depth. Of significance to this research were repeated bright reflectors between the Holocene surface and later deposition, marked at (3.) in Figure 3.2 above. These were thought to represent potential peat deposits.

It is important to note that the interpretation does not give an absolute date for transgression. Absolute ages cannot be known until some form of dating is performed on a sample, e.g. a core. Rather, by using the positions of known geological units only a relative age can be ascribed. This moment may not be the same at different locations, depending on sea-level rise and topological height. Once sample dates from cores have been collated and modelled as spatial events within a GIS package, the

temporal aspect of the inundation may become clearer. Until then, the interpretations remain isolated snapshots.

To locate and create this Holocene Horizon the following checklist was devised by this research:

1) Mark 000 as sea-level datum (the data should already have been tidally corrected).
2) First main reflector was set as the seabed. This was picked for later use in the depth conversion.
3) Below the seabed were varying thicknesses of negative amplitude without sequence features. These, often chaotic modern, mobile sands were ignored.
4) Below the modern sediment, signals for any multiples reflected from the seabed were eliminated.
5) The first sequences of depositional fill appeared. Questions regarding single or multiple transgressions and the direction were considered including:
    i. Were clinoforms present?
        1. how were they formed?
        2. were they angled?
        3. did they bulge?
        4. were they capped by a uniform top layer?
        5. mark major formations.
6) Have these sequences been interrupted or cut short and truncated from above or below? If so, then erosion may have occurred.
7) Below these will be the latest land formations – the terrestrial horizon that we wish to map. Look for the unbroken unconformity and pick it.
8) Below this horizon there may be palaeolandscape features, valleys, channels, rivers, scours etc. These should also be picked.

3.3 Depth Conversion

The final stage of interpretation was to convert the two-way time of the acoustic sound wave (from source to target and from target to receiver) into depth. This allowed a determination of whether the coring devices (generally 3 to 6m maximum) would reach the identified horizons. It also

allowed for an interpolation of the horizon depths for creating mapped surfaces.

Multiple conversion criterion could be utilised at this point and refining a conversion routine would be one of the outcomes of this research. However, for mapping large areas, simplification was necessary. Where horizontal resolution was measured in tens of metres, errors within centimetre ranges for depth were acceptable, therefore a single velocity conversion algorithm such as below, could justifiably be employed:

$$Z = \frac{((W_t * W_v) + (S_t * S_v))}{2}$$

(Emery and Myers 2009)

Where: -

Depth (Z) was a combination of time spent through water (W_t) and speed of sound in water(W_v) plus time spent through sediment (S_t) and speed of sound through sediment(S_v) divided by two.

The first step in the above equation was to calculate the depth of water. Conjecture over the best algorithm to use for speed of sound through seawater has been discussed in depth on the UNESCO website (UNESCO 2020). Due to the shallow depths, small pressure values and large areas in this study, the difference in these equations was insignificant. This study used Del Grosso's Whong & Zhu (Wong and Zhu 1995) equation which took into account temperature and salinity to calculate speed of sound using the Vcalc calculator.

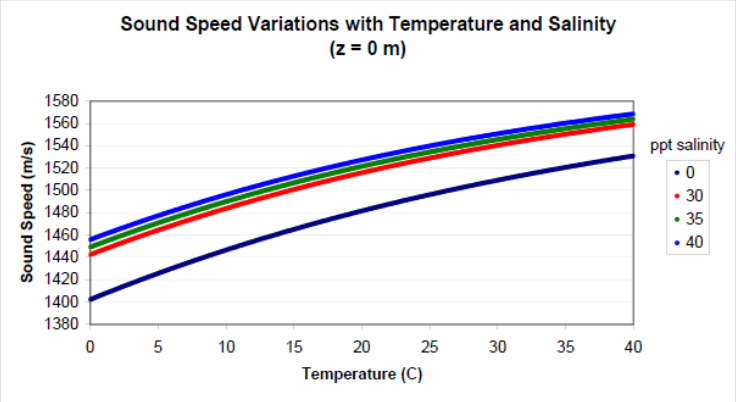

Figure 3.3 Sound Speed Curve based on salinity over temperature (Lurton 2002)

The speed of sound through water is measured dependent on temperature, salinity and depth as in Figure 3.3. above (Lurton 2002) or pressure (Kinsler et al. 1999). Variation on salinity and temperature throughout the year in the North Sea could be high and many of the survey data do not capture the exact time of the survey. Some surveys such as the PGS Megamerge take place over many years and cannot employ this level of detailed analysis. Therefore, the salinity and temperature figures were estimated based on yearly averages. This methodology was expanded in Chapter 5, but for the purposes of surface mapping and interpretation, an average salinity and temperature point set such as in Figure 3.4 was used.

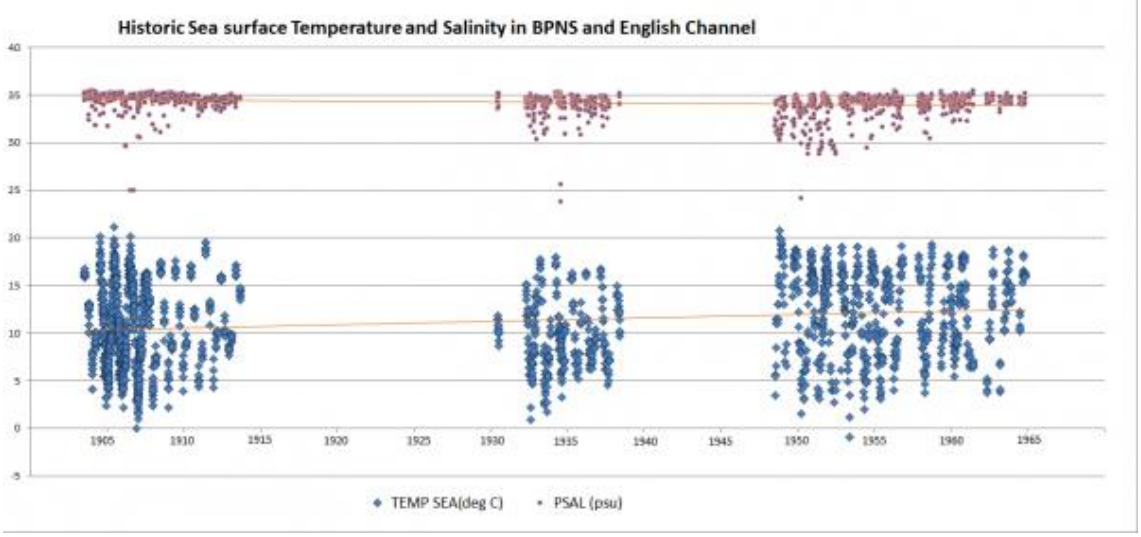

Figure 3.4 Figure 3.4 Historical surface salinity (‰ in red) and temperature (°C in blue) of Southern Bight and English Channel in the 20th Century. Data provided by VLIZ (L van Meel 1975)

Because the seabed as a horizon, required a depth reading through the water column, there was a need to measure depth from the sea surface as if from a static point and call this zero – a datum. In reality, sea level rises and falls by metres during a single survey. Therefore, surveys had to be set to a geographical datum before they could be interpreted. As it suggested, this arbitrary zero-level constant, was not perfect but constituted the closest to an independently verifiable constant that could be found in a moving marine environment. As long as all surveys were set using the same datum and all the horizons were depth converted using the same algorithm, the surfaces and depths remained accurate in relation to themselves.

Once the velocity through the water column had been calculated, the second part of the equation could be processed; that of the velocity

through sediment. This was concerned with the penetration from the sea floor and beyond.

Speed through sediment is more difficult to measure without ground observation from cores. While Folk models (Folk 1954) and wide-area sediment maps for the North Sea give an overall impression of the undersea composition, they are of a highly general nature (Balson et al. 2001). They do not take into account unconsolidated sediments, suspended particles or low-porosity solids in composition such as sands and clays of varying particle size. These can radically change the physical properties of an acoustic signal (Nafe and Drake 1961). Thickness of stratigraphic layer and the abruptness of reflector strength is also a strong indicator of stratigraphic facies, but not necessarily of its composition. Determining the reflection coefficient to obtain information about a sediment's porosity can be complicated by other factors. These include the angle used by the source or interference in the signal strength which may never be known - especially for legacy or older single streamer 2D seismic data.

This does not mean that there is no way of calculating the velocity of sound through differing sediment. Laboratory controlled work (Billette and Brandsberg-Dahl 2005) and evolving models such as Biot-Stoll (Chotiros and Isakson 2004) have enabled ever increasing accuracy. However, without core evidence to reference, the materials at such measured interfaces and the calculations needed to resolve velocities are only estimations. Good reference data such as produced by the Office of Naval Research do exist (Lewis 1967). This maintained a set of unconformable shallow water depositional sediment velocity speeds by depth which could be employed in most shallow water marine situations, though the values can only be considered mean. The results fall between 1460 and 1580 m/s (Buckingham 2005). This allows many geophysicists to apply a sediment model of 1500 m/s as a safe average.

3.4 The Acquisition and Usage of Data: 3D Seismic Data

The 3D data used in the Project which provided the backbone to the mapping of the North Sea came from a data source provided to the Europe's Lost Frontiers Project for scientific research under contract from

Petroleum GeoServices (PGS). The data the PGS supplied had been post-processed into merged 3D blocks comprising of 2 'MEGAMERGE' areas:

- MC3D_NSEA_MEGA – Covered the Central Graben and Northern North Sea to the Norwegian Trench (Parts 2 and 3 in yellow and Orange Figure 3.5)
- MC3D_SNS_MEGA – Covered the southern North Sea from the Wash to the Netherlands (in green Figure 3.5).

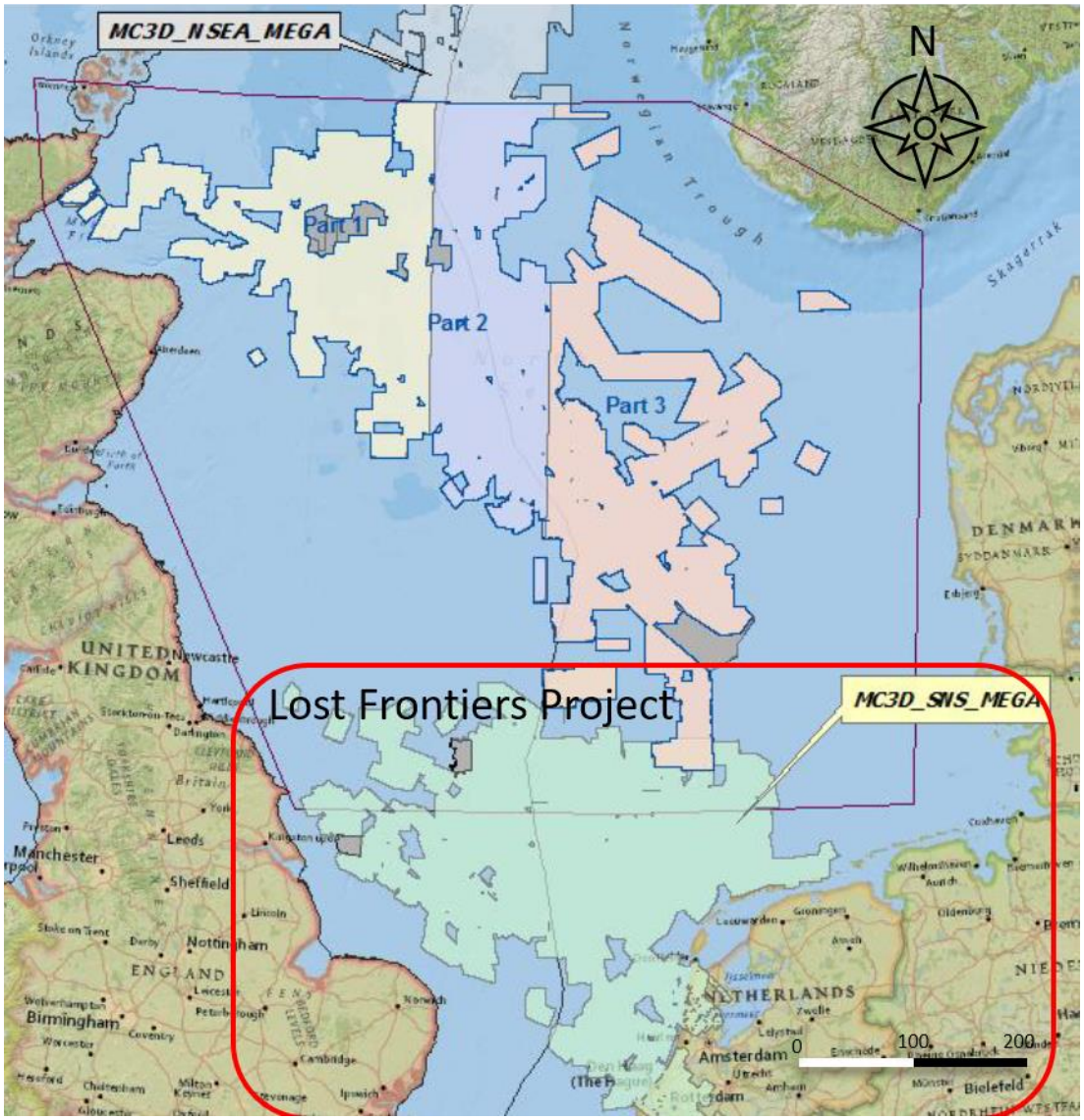

Figure 3.5 The extent of the PGS 3D MEGA MERGE Blocks (geo-referenced from PGS data)

The PGS Megamerge 3D data had a pre-rendered resolution of 25m x 25m grid bin. This fit well with the 30m x 30m line spacing of the boomer data and was exactly half the 12.5m x 12.5m of the highest resolution 2D surveys used in this research.

The PGS data was limited in three distinct ways which had to be considered as part of this study. Firstly, the megamerge blocks were pre-rendered so splitting the survey data into smaller distinct packages was impossible. The data needed to be loaded and processed as one, though the results could be split into manageable sizes.

Secondly, the data were pre-merged and migrated to projection ED50 UTM Zone 31N. To accommodate this, any surveys used in conjunction with the PGS Megamerge needed to be re-projected to ED50 UTM Zone 31N, or a common project projection adopted for all surveys. This had the potential to be problematic surveys, especially of older, legacy data, whose SEG-Y headers had not been categorised with standard navigational projection files and did not include sufficient details on how their projection might be transformed and geo-located.

Finally, the data were limited in depth to 500 ms two-way response time to protect commercial interests. This was considered to have no effect on archaeological research as this two-way time window gave enough range to explore the geomorphology of the North Sea back through the Holocene and into the Pleistocene.

This thesis utilised the PGS MC3D_SNS_MEGA data as the 'backbone' for many of the maps and models of the southern North Sea area, Much of the cultural detail, the river outlines, the coastal interpretations and surface features were picked using this 3D dataset. No use of the more northerly MC3D_NSEA_MEGA was made in this thesis.

The PGS 3D datasets were imported to IHS Kingdom 2018 and timesliced down through millisecond thick layers of top-down horizontal (Z) planes of the inline and crossline X and Y data. Drilling down through the timeslices revealed landscape features, depositional sequences and glacial land deformation in a more obvious and understandable way than a vertical 2D survey. The top-down image immediately resembled the more familiar aspect of spatial landscape mapping as could be seen in Figure 3.6.

Such timeslices were the initial steps to any 3D interpretation and were used before vertical interpretations of the crossline and inline 2D data. This

was because 3D surveying suffered from poor resolution at the shallowest of sedimental layers and the 30 m x 30 m resolution allowed for a large amount of horizontal smear.

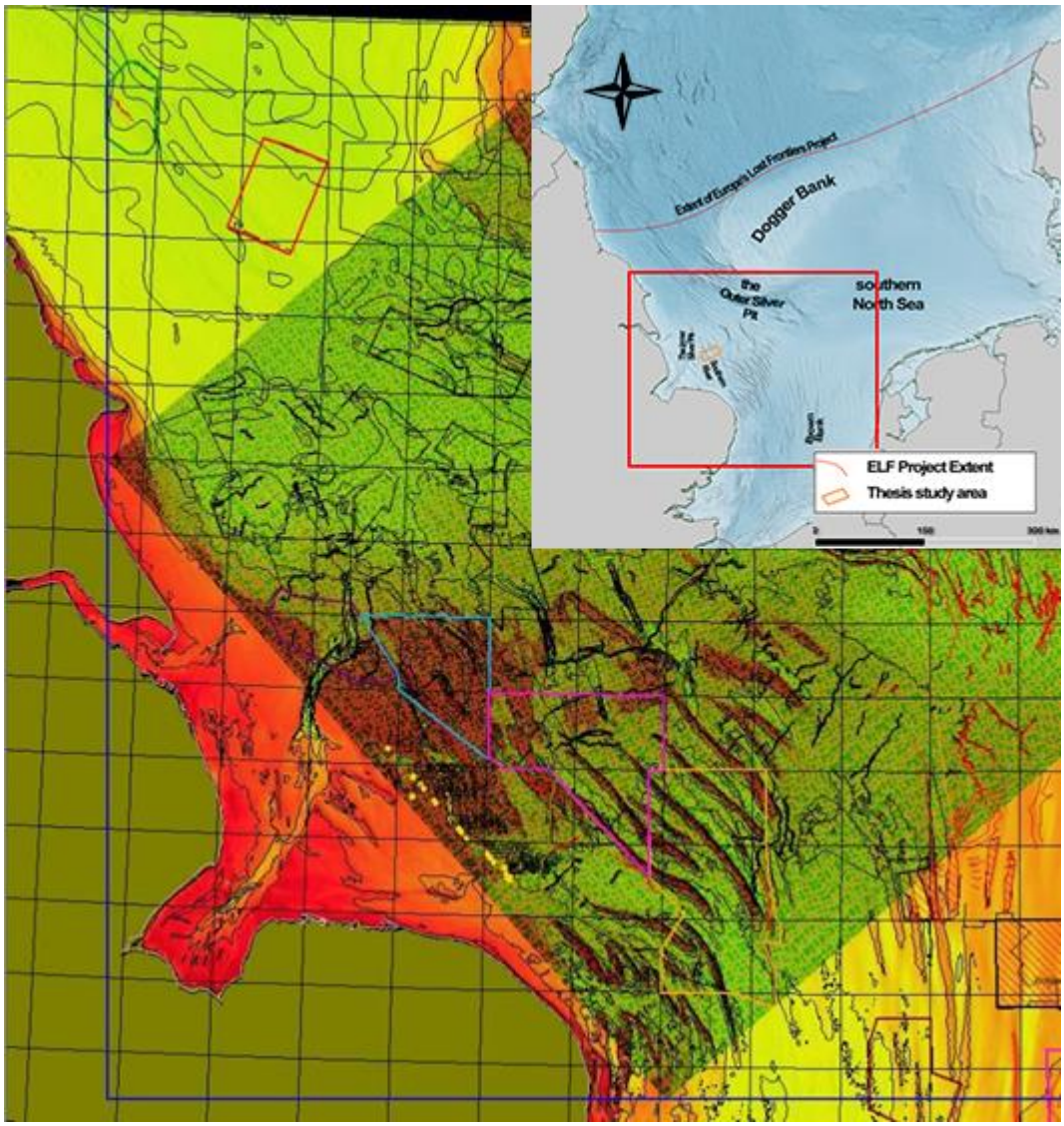

Figure 3.6 Bathymetry, palaeochannels, glacial and geological features may be highlighted and overlaid as cultural layers in IHS Kingdom.

Timeslices were taken of horizontal planes at 0.004s intervals from 0.04s to 0.1s below the current seafloor. This window comfortably covered the chronological period of the modern Holocene seabed, through the marine inundation back to the end of the LGM throughout the North Sea. It also allowed for variations in water depth, thickness of modern sediment and the warping of the sea basin during this time. For areas of missing or poor resolution data, where possible, a root mean square of the amplitudes of two significant timeslices was employed to build a coherency cube as successfully demonstrated to smooth vertical density issues between timeslices (Paramor et al. 2009).

Using a progression of such timeslices, features that may not have been noticeable on a vertical 2D survey appeared and subsided as though via the passage of time. All such features could be highlighted and marked up in IHS Kingdom as 'culture layers' (Figure 3.5). These hand-picked features and anomalies in the top-down data were then viewed in the vertical 2D data (Figure 3.6). The same feature cross-referenced both on the inline and crossline 2D surveys were then confirmed or denied by ascertaining the relevant features in respect of the proximity to the early Holocene transgression as discussed in the 2D interpretation section (above). Without fixed dating techniques it was sometimes problematic to place such features precisely at a geomorphological period as landscapes tend to be palimpsests and deeper sequences may have co-exist alongside shallower ones but by slicing through 'time' to see the signals appear and then correlate those with the Holocene horizons allowed the affirmation of extant landscape features.

Each category of feature was saved as a 'culture file' in Kingdom. In this way, hand drawn features such as entire river systems, coastlines and lakes, could be followed in their entirety and exported into a GIS as shapefiles for further analysis. It is important to note that these vector files were not intended to represent dateable features. As with the horizon picking above, the shapefiles were not depth converted at this stage, merely representative of visible depositional and / or lithic boundaries.

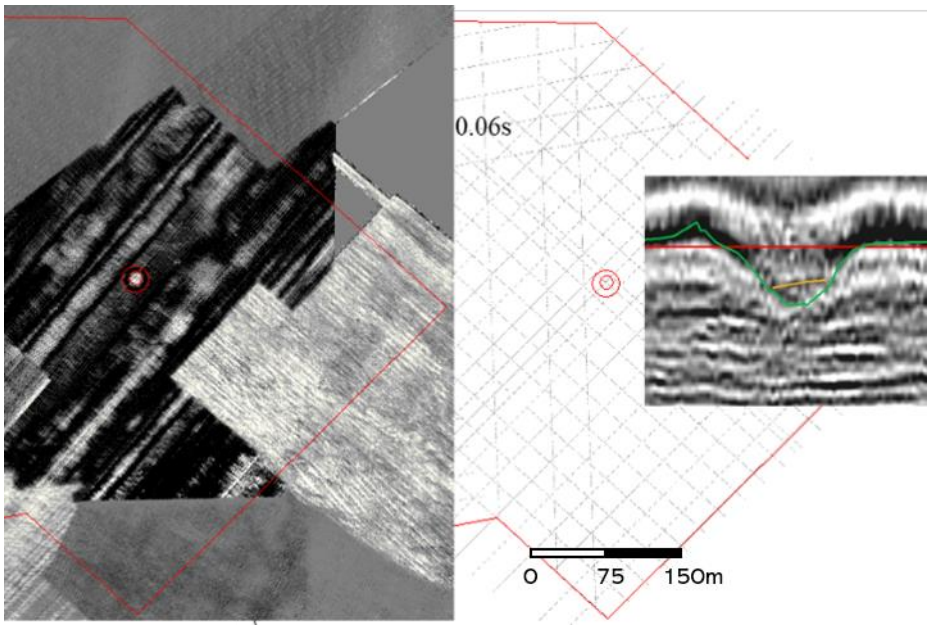

Figure 3.7 Timeslicing and Gridding of 3D Blocks and highlighting of features allows correlation of 2D vertical data associated with even small features.

3.5 3D Geomorphological Interpretation

As with 2D interpretation above, each of the inline and crossline aspects of the 3D survey had to be interpreted with the same horizon picking process. Where possible, these were marked with the entire clinoform shape and type. Truncated sequences that could have been interpreted as the result of successive transgressive and regressive behaviour were also recorded. Unconformities were identified and marked between onlapping and downlapping reflectors. If possible, these were extended over the entire section. Where the boundaries became conformable this needed to be marked manually.

Major sequence boundaries were plotted on the 3D inline and crossline vertical surveys as on the 2D. These were the same Holocene horizon picks as were marked out on the 2D to bring out the discontinuity between surfaces and therefore the interfaces between units of dissimilar materials. Depending on the resolution of the imagery much of this could be auto-picked within Kingdom and manually corrected. However, where the shallow data is less defined all of the horizon picking needed to be completed manually, using the interpretation data marked in previous steps. Horizons were picked at intervals corresponding to the resolution of the 3D surveys. In the case of the PGS Megamerge data this is natively 25m x 25m. However, due to the immense size of the terrain area, a grid of this resolution would be highly resource intensive and topographically more detailed than required. It would also make the resolution of our topographic map higher for the 3D blocks than we might accomplish with the resolution of some of the less technically sophisticated 2D surveys (30 x 30m). Therefore, stepped intervals of 50m x 50m make more sense. This resolution is also closer to many of the 2D survey lines at our disposal, making the interpolation more consistent over the whole.

Features such as coastlines, embayments, deltaic systems, river valleys and flood plains have been noted to have high potential as archaeological interest sites (Flemming et al. 2017). As such, strong sequential stratigraphy in these areas were flagged for future core sampling. Whilst there was not the opportunity to core every site, it was important to log and describe as many sites as possible that show potential to be logged and described.

This research was in the fortunate situation of being able to investigate a number of survey lines and interpret many high potential sites and then to follow up on the interpretations with a focused coring programme to investigate further. This allowed the testing of methods developed in this study.

3.6 Creating terrain surfaces from 3D seismic data

Due to the Megamerge survey being one monolithic file, dividing it into sections was not governed by a set logical rule. This research decided upon an existing, external division system devised by the International Council for the Exploration of the Seas (ICES). It divided the PGS data into a grid system (Figure 3.7) with the following benefits:

a) ICES already provided a GIS layer file of the divisions which was easily overlain onto existing maps.
b) Each square was supposedly equal in size (though this was found to be true only in certain projections and not in ED50 UTM 31N).

Each individual section was then measured into stepped intervals of 50m x 50m as above and a grid was calculated for each horizon based on X, Y and Z co-ordinates. At this stage X and Y in the current projection were measured in metres but Z was still measured in milliseconds of two-way time. A depth conversion was required before all 3 axes could use the same metric. Dead space – the area between the crosslines and inlines was interpolated using a mathematical method. IHS Kingdom offered a selection, and after experimentation, a simple Hilbert's Curve was employed for efficiency and performance. However, for final mapping an integrated solution of using Hilbert's Curve alongside modern bathymetry was used. This gave a more consistent topographic feel to an area and alleviated issues of dead space and lack of data bins. The issue with this method was finding a convincing solution that could strip back the mobile modern sands while retaining the base bathymetry level relative to the datum.

The depth conversion was then performed, following the process as with the 2D depth conversion in Section 3.3 above. Once complete, an estimation of the modern sediment was made by hand for the data block and removed across the depth modelled surface. Future models may involve the use of specialised, multi-step velocity models based on the

picked seabed and Holocene horizons that will calculate a more precise depth for this removal process (see Chapter 5).

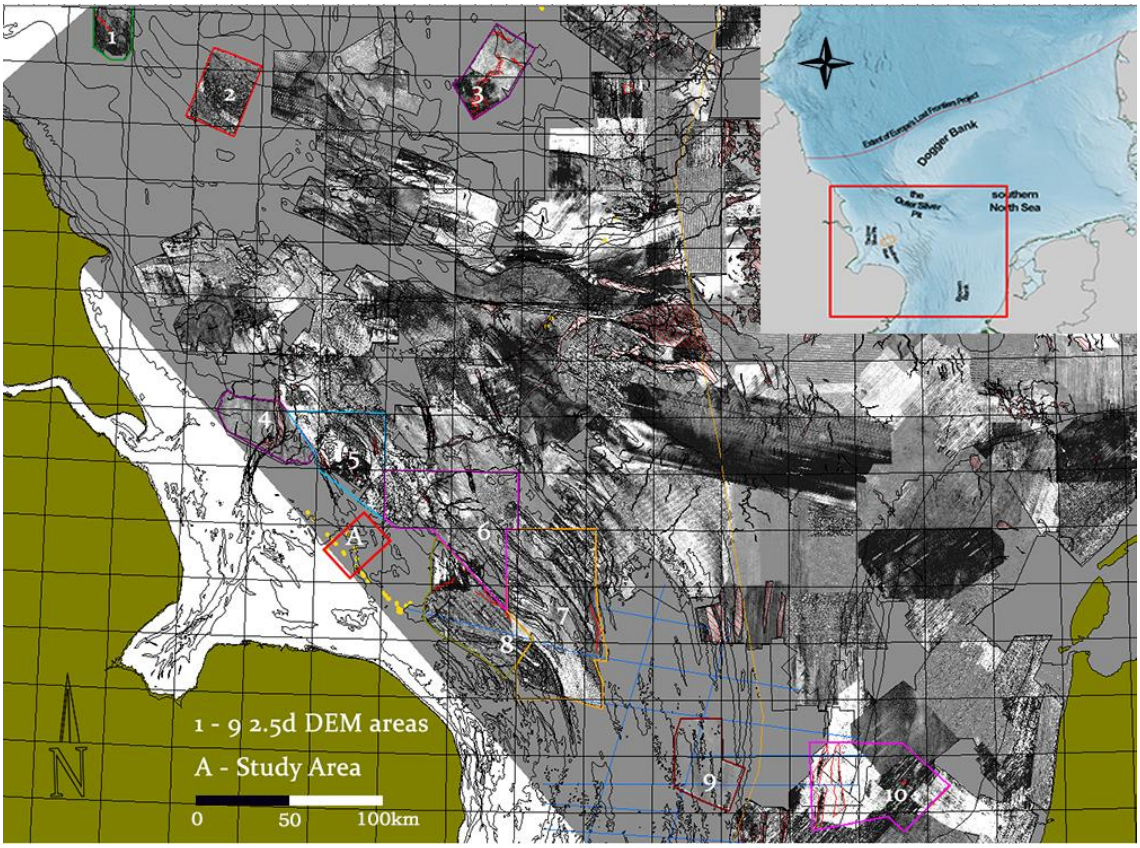

Figure 3.8 The ICES grid overlying PGS southern North Sea data blocks.

Finally, a second grid was created, taking the interpolated data from the Kingdom surveys and surface terrain files built for input into a GIS. These surface files could have been either Digital Elevation Model (DEM) raster files, or – if the number of vector x, y and z data points were not too great for on the fly interpolation – Triangular Irregular Network (TIN) vector files (Delefortrie et al. 2014). A patchwork or mosaic of these surface files within ArcGIS could then be further interpolation using spline or Krige models alongside the existing bathymetry to smooth out data loss and height differentiation.

A DEM is a 2D cell-based model of 3D topographical data. Large scale resolutions create problems in interpolation of the data within the DEM, so features may be misrepresented or even entirely missed. TINs suffer less from this as they are vector based and not cell-based in their models. Each x, y and z co-ordinate is constructed into a triangle using Delaunay Triangulation (Okabe 2016). Because TINs are computed on the fly, they

can be set to match the x, y and z points of their neighbours and eradicate many of the interpolative barriers that might trouble a DEM, however, because of this process, TINs are also heavily resource intensive. On small sites, this would not have been an issue. Over such a vast area as the southern North Sea, such considerations became important. Using the same resolution as the gridding model used in Kingdom (50m x 50m), the number of data points rapidly rose into the millions which proved computationally exhaustive. The decision was made to use DEMs, but to keep the same grid resolution.

It is important to note that computational analysis using both DEM and TIN are based on a terrestrial based surface mapping terminology (Li et al. 2004). There are aspects of this that may be open to confusion in a marine context. For the purposes of this research Li's specific terminology was applied as follows:

Ground: "the solid surface of the earth" – This was a baseline against which the interpreted DEM was measured. In terrestrial surface mapping this was set as a datum of 0 or sea level as the lowest baseline point. In the context of submerged landscape this made no sense and the baseline must be set to the seabed horizon as the datum of 0.

Height: "measurement from base to top" – For calculations of marine data, the opposite was held to be true. Instead of from base to top, depth from the top to the base would be measured from datum 0 to the lowest point.

Elevation: "height above a given level, especially that of sea" – It made sense to retain elevation as the height (in this case depth below) the sea level datum, not ground level datum. The effect of this was to record an overall depth including the water column.

Terrain: "tract of landscape considered with regard to its natural features" – This would constitute the extent of the model. For much of the mapping this was regarded as the entire southern North Sea basin. For other, small scale, or regional research studies, including the ones specific to the peat investigation of successive chapters in this thesis, smaller logical extents were utilised. The detail of landscape accuracy was dependent on the scale of the model built and the purpose of the investigation.

Resolution: "Scale and detail of region" – Most DEMs are created using a single set of acquisition points and a single resolution. The surfaces created in this research were acquired from a wide range of survey types, in a variety of point sizes and resolutions. Despite the best attempts at

normalisation of such data, no one-size fits all resolution would work for every grid. The compromise resolution of 50m x 50m resulted in a downscaling of some survey detail and an upscaling of others, resulting in some pixel blurring and misalignment.

DEM creation was output from IHS Kingdom in the form of text-based ASCII files and imported into GIS in raster ASCII format. This is a simple 3-column format with only x, y and z data in meters contained in a comma separated file. Despite their simplicity, each of the ICES grid DEM files ran into many GB of data.

3.7 Discussion – issues with interpolating to bathymetry

Despite collating a large amount of survey data over the southern North Sea basin, there were still many areas that had no seismic survey coverage. A few of these gaps were solved by sending vessels to survey the areas and data for these will be available for future research. However, for the purposes of this thesis and the mapping of the southern North Sea, a solution was still required to interpolate large areas of landscape for which there were no Holocene horizons.

The solution to this problem was to interpolate the seismic data to a depth aligned bathymetry. Therefore, once the seismic depth conversion had been completed and a surface DEM created, this was aligned at an appropriate elevation below the datum on the Z axis. Modern bathymetry from above this elevation was then stripped away leaving only the deeper channels. This was not a foolproof solution as it did not mean that the sediment that remained was any older than the layers removed. In fact, all that had been removed was information, it did not add clarity to the data. However, as a representation it accomplished two things. First, it allowed the gridded interpolation of a plotted DEM surface alongside the bathymetry at the same z depths and second, it preserved the channels and cuts that were visible in modern bathymetry while cutting away the sand banks and mobile sands that obfuscated the detail that was important to display.

The steps in processing seismic 2D and 3D data as laid out in this chapter enabled logical interpretation of the contrasting wave intensities into lithostratigraphical layers. These horizons could then be used to calculate

feature depth and potential surfaces which could be usefully mapped. Although the creation of DEMs could only provide a rough estimation of the picked Holocene horizon due to the lack of coverage and need for interpolated results, it did give an overall impression of the landscape. Palaeo features that are inundated, could then be overlain to aid in the understanding of a landscape through time. These were crucial to the development of landscape models and in the spatial analysis of the pre-inundated southern North Sea.

4 SPATIAL MAPPING & MODELLING

4.1 Introduction

While the project employed a specialist arm in agent-based modelling for focused modelling of individual processes, there was opportunity for larger regional models based on spatial analyses. Such models could focus on environmental resource distribution and landscape change due to sea-level rise. The main technology behind these would be mapping and analysis packages such as a GIS.

The focus of any map is not to present every aspect of the data about a geographical location. Each map is rather a focused representation designed to answer a specific question. So, a modern OS walking map serves a different purpose to a bathymetric navigation chart or an electoral map categorised by county. The International Cartographic Association (Engler et al. 2013) categorises maps into five basic types:

1) Reference, which include useful, possibly eye-catching, but generally unrealistic representations such as political borders, road maps, tourist relief maps, etc.
2) Thematic, which may be even more unrealistic but are designed to answer specific questions such as population density, virus spread, electoral breakdown and so forth.
3) Specialised maps such as navigational charts for seafarers
4) Cadastral maps such as floorplans for architects which require accuracy.
5) Topographic map which aim to represent the elevation (or depth) of a 3D terrain using a 2D surface. Often such maps may attempt to layer multiple levels of data onto the same 2D surface (for instance geology and overlying vegetation).

When modelling the palaeolandscapes of the southern North Sea, the focus of the mapping within the GIS had to be both topographic in form while addressing specialist archaeological concerns. It needed to represent details at both regional and site level scales. Modern seabed bathymetry, depositional sediment fill, the transgressive interpretations

and underlying palaeo features all made up the palimpsest of data that created the submerged landscape. Further, the landscape did not exist at a single moment in time but changed dramatically and spatially over a temporal range that all required capture.

The first question to ask was why model palaeolandscapes in the first place? There have been many models proposed for determining hunter-gatherer behaviour and population density; they have sought to predict supportable population size based on the parameterisation of resource intensities such as faunal, floral, climate and environmental elements. Of these, a good grounding in the theory and discussions were made in Jochim's *Hunter-Gatherer Subsistence and Settlement* (Jochim 1976) and Zorn's later paper (Zorn 1994). More recent models worthy of discussion included the mapping potential for predicting prehistoric settlement (Kuiper and Wescott 1999), catchment analysis (Hunt 1992) specific land use dynamics (Peeters 2007) and even woodland distribution and disturbance modelling based on fungal spore assemblages (Innes and Blackford 2003).

Another very useful model to investigate via spatial analysis would be that of sea-level rise during the Mesolithic. There are a number of global eustatic, regional curves (Jelgersma 1979) and localised isostatic models of Shennan, Behre and Baetemann (Shennan et al. 2000; Behre 2007; Baeteman et al. 2012). This research was unlikely to change the interpretation of these models. However, focused coring, in part led by interpretations developed by this study, would impact the investigation of sea-level rise and sediment deposition in the southern North Sea (Walker et al. 2020).

As above, the specific questions asked were dependent on the environmental reports returned from multi-disciplinary archaeologists working on the cores. These in turn were dependent on a focused coring programme which depended on the interpretations of the seismic surveys produced initially by this research. The potential of spatial modelling for the discovery of settlement and economic probability in the southern North Sea had been demonstrated based on marine resource (Fitch 2011) and fishing models from Denmark (Fischer 2004). These models were used as a building block for development of a new model to spatially model potential archaeology over regional scales.

Before any analyses could be undertaken, the 'fit' of the model had to be considered under a number of criterion to ensure the appropriate results could be produced.

4.2 Comparison of Differing data types, scales, projections and geo-spatial references.

4.2.1 Temporality:

Geo-spatial mapping, in and of itself, is a static solution. It does not have a native mechanism for chronological movement. Each mapped solution can be set as a 'timeslice' and show progression at intervals but is not dynamic. There are computer modelling packages that can be used to interpolate from ArcGIS to enable such dynamic models to be created but this is not the primary driver of the spatial mapping software itself. To address this, it is important to focus on important boundaries to map, whether these are physical within the landscape, or at specific chronological moments throughout a wider regional scale.

4.2.2 Scale:

The scale of the investigation is of primary importance when deciding on the focus of the spatial mapping process. An ArcGIS database can store data for an entire project study area, but each mapping operation does not need to utilize the whole of the supra-regional scale. Some questions may require only a focused landscape feature, for other questions however, it may be entirely valid. Cultural exchange patterns for instance may require a pan European scope, while an examination of hydrology runoffs into a particular river may need a much tighter, local detail.

4.2.3 Projection:

The basic property of a geo-spatial map is its use of referenced positions on the earth's surface and the ability to then use these positions for analyses. To do this, the GIS must store and maintain a consistent set of data to be employed in the maps and models based on the geodatabase. Geophysical surveys will use a geographical co-ordinate system relative to a known geodetic datum e.g. WGS84 to collect and process their data and this must be transformed into a consistent geographical co-ordinate system for the GIS to display. Individual surveys may use their own geographical co-ordinate systems and it is very

common for national bodies to undertake surveys using their individual national grid systems. Such data must be transformed into a consistent system prior to import into a GIS. In addition to this, the GIS must display real-world data in a representative format. However, as Gauss stated, it is impossible to accurately represent spherical bodies on 2-dimensional surfaces (Gauss 1828). The translation of real-world longitude and latitude measurements onto a projected 2D surface is by no means a trivial matter. Each mode of representation will, by necessity, only accurately reflect one 2-dimensional plane (a single x and y) of a 3-dimensional sphere. This ultimately results in a flattened surface, be it traverse or slice as in Figure 4.1.

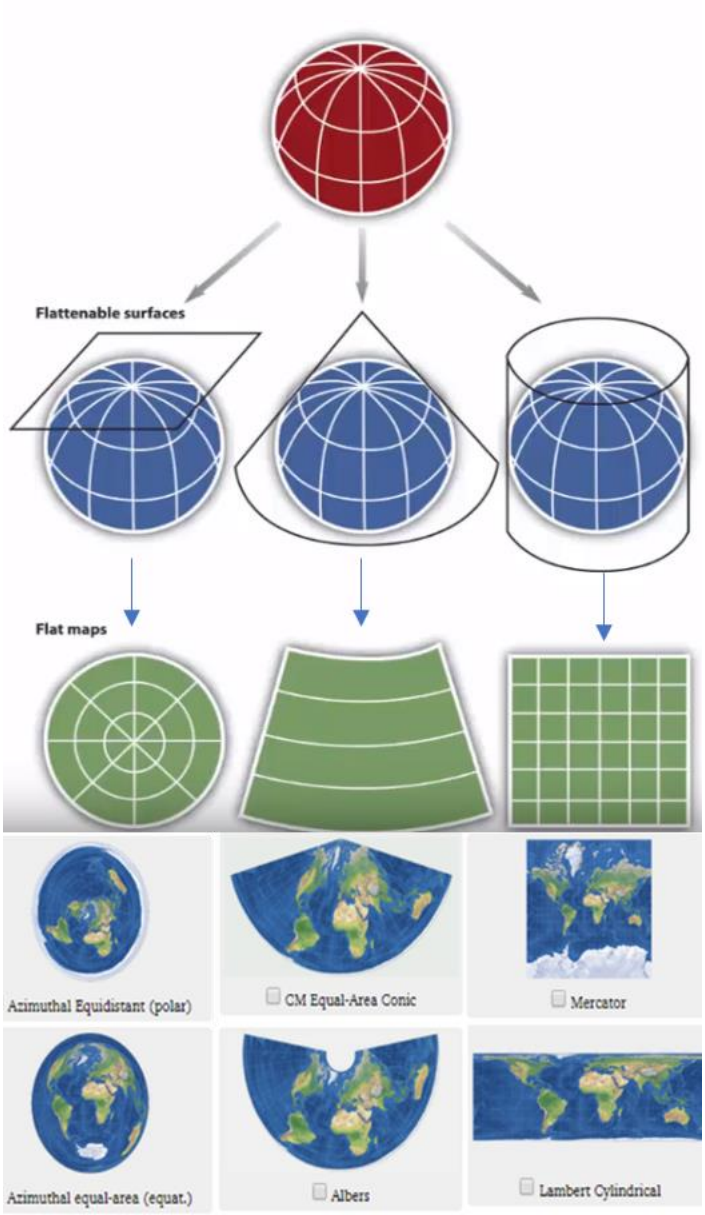

Figure 4.1 Above, the 3 representations of a sphere on a flat surface; Azimuthal, Conical and Cylindrical and below, examples of these projections and how they distort (source: MapProjections.net)

The use of a flattened surface within a projected co-ordinate system is based on a geoid. There are three basic models as in Figure 4.1; planar or azimuth which traverses on a flat circular plane, a conical model which maps concentric circles onto a cone, beginning at an apex (generally a pole) and flattening out to a plane at the furthest point and finally the cylindrical model where the features are flattened out as if the globe were a cylinder and then unrolled. This makes the point at which the globe touches the cylinder (generally the equator) very accurate, but the further from the cylinder, toward the poles, the more distorted and inaccurate the model becomes. For each of these basic models there are many variations, with new, complex, and often surprising, additions regularly added.

Fig 4.1 shows a small selection of the more popular projections in each category. There are dozens, and not one of them will give an entirely satisfactory solution for every question or for every location in the world. As projections, they must focus on one area and distort another. Therefore it is important to establish a) which area to focus on; b) what size of area to focus on and c) what implications this may have on the localised / regional / surpra-regional measurements of any mapping carried out.

For example, Mercator and, by development, Web Mercator, as used by media giants such as the BBC and Google, are popular due to the clarity and the familiarity of their images. The bias on Europe and North America is almost taken for granted such is the ubiquitous nature of this projection. However, the projection forsakes the geoidal aspect of the planet in favour of a flat earth which results in a bias of up to fourteen times in size and area towards the poles in comparison to the equator. The result is that Greenland, a country measuring 2.1million km^2 appears as big as the entirety of Africa measuring 30.37million km^2.

This research required a far greater level of detail than a single world projection can deliver, while at the same time not limiting the study to purely localised national grid mapping regions such as UK-OS. To examine the southern North Sea, required a projection co-ordinate system designed to work on a geodetic datum that could maintain accuracy over supra-regional scale such as the hundreds of kilometres of north-western Europe. It had to also have the capability to display detailed analysis of individual landscape features such as the thesis study area for

peat analysis. This required spatial identification on a microcosm level down to mere metres.

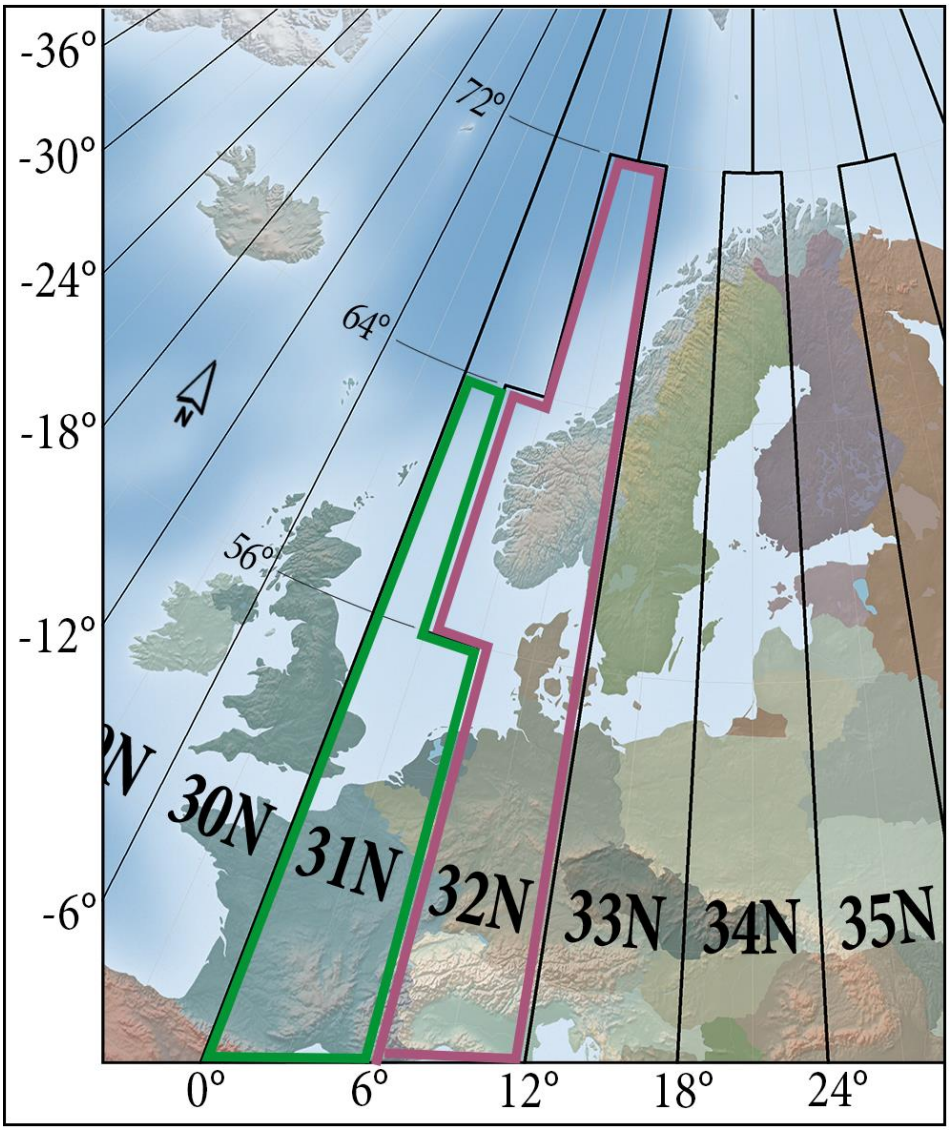

Figure 4.2 European UTM North Zones 29 – 35 shown in longitude. (Source: K Bellis, Creative Commons Wikimedia).

The best fit projection for this range was found to be Universal Trans Mercator (UTM), which was based on a cylindrical Trans Mercator ellipsoidal model. However, the projection was divided east-west into 60 independently calculated, equirectangular zones of 6° longitude. UTM +31N covered the vast majority of the North Sea and was commonly employed, with reference to datum WGS84 or EPSG (marked green in Figure 4.2). The eastern North Sea and Baltic Sea areas were covered in UTM +32N (in pink, Figure 4.2), while the coastlines of northern England and Scotland fell into +30N. Because each UTM zone was calculated independently from the ellipsoid, the projection remained extremely

accurate and in proportion when mapped. However, the obverse of this was that because each UTM zone was calculated independently, aligning them required a small amount of geo-reference rectification of data to stitch GIS components together when items from two overlapped zones were to be displayed.

4.2.4 Resolution:

Due to the research requirements, models needed to be constructed using data originating from many sources and gathered over a long period of time. The resolution of these data, at the time of survey (the method used, variation in source and receiver arrays) and at the time of data processing had an effect on quality and consistency of data. As the main spine of the research dataset for the southern North Sea, the 3D Megamerge provided by PGS, had an array bin size of 30m which could have been used natively. However, the decision was made to normalise the data at a resolution of 50m x 50m. This was done in order that the grids would be spaced more evenly for the majority of legacy data and to give the best resolution to data handling size compromise. The surface DEMs would still retain enough detail per pixel while not becoming overly intensive on data storage. The palaeo features noted within the 3D timeslices were classified within IHS Kingdom as culture items and exported as vector shapefiles (or converted to vector shapefiles within GIS) therefore these retained their original resolution and due to their nature as vector graphics were able to scale to the desired size required by the spatial model with no loss of definition.

A small amount of older legacy survey data needed to be upscale from lower resolution such as 75m. This was achieved during the interpolation process and resulted in 'smearing' of pixels. Upscale and downscaled data are perfectly valid for the purposes of producing DEMs as these DEMs were to be surfaces modelled as investigative interpretations, not as accurate one-to-one representations of exactly how the landscape looked at any one moment.

4.3 An Overview of Qualitative and Predictive Modelling

Of the many different types of model designed to represent and study the world, this research would investigate two that were pertinent to the study of submerged landscape via a GIS. It did not attempt to represent the southern North Sea as a 100% accurate depiction of the early Holocene landscape. Instead, the focus was on spatial qualitative and predictive modelling that attempted to answer specific questions. Due to absence of definitive environmental and control data for statistical and mathematical analysis, the modelling was not intended to present quantitative analysis.

One of the strongest weapons in the GIS arsenal is the ability to demonstrate the palimpsest nature of a palaeolandscape, one that would otherwise be confusing, if not misleading, were it all to be viewed as one annotated data dump. The ability to gradually employ logical layers, some data driven, others speculative, illustrative and predictive are not only used to make better cartographic representations but can add real scientific value to archaeological modelling. Data already available to GIS include current bathymetric features, water tables, geological classifications and terrestrial geographical boundaries. To these were added data specific to the project as follows:

- topological raster datasets taken from geophysical surveys as set out in Chapter 3.
- palaeolandscape features such as rivers channels, lake beds, and coastal embayments.
- Areas of low lying and high rising land contours.
- Positions of cores and survey lines.
- Areas of interpreted potential – organic sediment, erosional surfaces etc.

While each individual layer held important data, it was in combination that the layers demonstrate true qualitative and predictive power. The simplest of these was the combination of topological rasters with river channels and a watershed analysis. By plotting the visible palaeo river channels from the survey data alongside the topological data it was possible to compute slope orientation and therefore a watershed analysis could be built to indicate directions and therefore a water source within the topography and the likely direction of flow of extinct riverine systems.

Once watersheds had been established, slopes could be analysed. This played a potentially important role in the changing environmental dataset (Dunn and Hickey 1998). The angle and steepness of slopes was directly linked to the likelihood of wind erosion, soil loss and pollen distribution across the landscape. Protected lees would have experienced different climates to windward slopes, therefore performing slope orientation mapping gave potentially important distribution sets.

This in turn could have implications for the modelling of sea-level rise. If wind direction could be demonstrated in a particular direction, or channelled through a particular route, transgression in these areas may have appeared earlier than in other locations. This, model, irrespective of dating evidence presented via coring proxies, may show reason for altering the regional sea-level indicator curves. However, it is the proxy material evidence gathered from cores that presented the most important layer analysis for modelling sea-level rise. By overlying carbon-14 dated evidence of the inundation onto topological raster surfaces, it was possible to correlate the depth analyses to the transgression. In this way it was possible to map potential coastlines at points in a chronological context.

This spatial analysis modelling of the sea level rise could extrapolate causal links and perform comparisons with Shennan's sea level curve based on SLIPs (Bradley et al. 2011). It also had potential to feed into agent based models as part of an integrated toolbox for the specialised investigation of individual study areas.

To take a wider look at the theory behind models of predictive and qualitative nature, especially those specific to an archaeological use in a Mesolithic landscape context such as site density / distribution and optimal foraging models, it is important to break these down further to focus on their component theories:

4.3.1 Predictive Modelling

A predictive model is built on a set of known criteria, and unknown variables with the goal of predicting the likelihood of a given outcome (Price and Brown 1985). In the above example this would be settlement density / distribution within a given area. Barceló states that the dispersal activities of a species, i.e. the movement of the creatures themselves, can

be inferred from the dispersion of material observation related to that action (Barcelo et al. 2016). So, further distribution of materials on the basis of social, economic or, in an archaeological context, cultural parameters, equals further dispersal of the species. Although these terms were first coined by Pielou (1974), he in turn cited Gordon Willey's development of settlement prediction in Peru as the earliest in the field (Willey 1953). Specific focus on Mesolithic application and seasonal sedentism were factored in during the 1980s (Brandt et al. 1992). By applying parameters individually and in combination to layers containing additive multi-economic and environmental datasets, complicated local area analyses may be developed (Carleton et al. 2012). Layers of modelled analyses such as distance to water, slope, susceptibility to erosion and the soil type allows the building of floral and faunal predictive modelling where no such site information is available and even in blind test scenarios (Brandt et al. 1992; Verhagen and Whitley 2012).

4.3.2 Deductive & Inductive Modelling

How one tests the results of a given predictive model comes down to a decision between deductive – Approaching the test with a knowledge based on the outcome and inductive – Approaching the test blind and creating new causal hypotheses. Within archaeology this means the former are based on general theories of human behaviour and are considered more qualitative. They can, as pointed out by Sebastian and Judge in their editorial (Sebastian and Judge 1988) be difficult to validate. The latter tend, in general to be mechanically rigorous and often quantitative and have been subject to much debate (Deravignone et al. 2015).

4.3.3 Qualitative vs Quantitative Modelling

'A qualitative model does not require a mathematical value but is used to visually represent an idea, a pattern or a relationship that attempts to describe causality at points of time and space' (Byrne 2002)

The debate within archaeology concerning data-led quantitative predictive modelling and post processual qualitative modelling is not one to be entered here now. It is well covered elsewhere (Gaffney and Van Leusen 1995; Brück 2005). Only, to note that the former claim that the data to correctly predict human nature is not available and the models

archaeologists should attempt therefore should be based in empirical scientific process. The latter, argue for a more experiential exploration of the variables and claim this may be achieved via qualitative methods.

There are no existing extant Mesolithic sites within the southern North Sea and currently no models exist to predict locations with which to find one. There is a Danish fishing model (Fischer 1995) that has successfully been tested on submerged Mesolithic settlement sites around northern Denmark. However, variants of the model have met with inconclusive results in UK waters (Hall 2014). More experiential models that move away from a purely economic or archaeological industry focus have developed over the last decade or so (Leary 2009; Gaffney et al. 2017a). It is in the mould of these qualitative models that any spatial analysis GIS landscape models would be developed in this research. For quantitative modelling, Chapter 8, on Neural Networking features cluster maps which are data led purely logical maps that are excellent examples of this model type.

4.4 Methods of integrating Seismic Interpretation into ArcGIS

The majority of GIS work undertaken on the project was performed using ESRI's ArcGIS version 10.4 and 10.6 with supplemental work carried out on versions 10.8. This package was chosen due to its being the industry standard for archaeological geo-mapping and having the most widely supported integration with other packages including that of IHS Kingdom, though, interesting, not visa-versa. While Esri's ArcGIS does have a 3D visualisation extension (ArcScene) this was not used within the project. QGIS3 was also used (versions 3.4 Madeira, 3.6 Noosa and 3.8 Coruna). This was primarily for specific toolsets that ArcGIS was not as inherently capable (e.g. the import of .DAT data files and conversion of .DAT to X,Y,Z ASCII DEM or TIF geotiff formats). Files thus converted were then added to maps and models created in ArcGIS. By using both software packages to their strengths, more robust analysis could be accomplished more efficiently.

The simplest method of bringing in the largest portion of the North Sea data, that of the PGS Mega Merge, into ArcGIS would have been to directly import generated timeslices as ASCII X, Y files. These would have been easily generated and exported from IHS Kingdom. They could have

been appropriately geo-referenced and overlain on the bathymetry in the GIS. The X, Y files would have contained their own co-ordinates but only as raster pixelated files. The major drawback would have been the lack of Z, or depth, co-ordinates. The timeslices would not have acted as surfaces and would not have acted as topological layers. Therefore, they would have relied on the hand-drawn shapefile features exported for any archaeological definition. These shapefiles were vector formats and contained both co-ordinates and the ability to scale to any resolution.

A number of time slices could have been imported, each at a stepped two-way time. By doing so, it would have been possible to create a layer for each interval from deeper Pleistocene features, through the Naaldwijk formation and into the modern sediment, thus creating a model over time, despite no definitive depth being present. This was dismissed for the following reasons:

a) Each timeslice would be very large (one for the southern North Sea alone took over ten minutes to refresh) and to divide into smaller areas needed expert handling.
b) The file would be flat and contain no topographic data. This would prove sub-optimal for landscape modelling
c) The file would not integrate with other survey data from other sources
d) The file could not be used for later 3D visualisations
e) The ASCII files proved difficult to import directly into ArcGIS, especially at such large size. It proved better to depth grid the data and import into GIS in geotiff format.

For these reasons, it was agreed to break up the PGS data into smaller, self-contained areas. These would then be geo-referenced, gridded, interpolated and a depth conversion performed (see the mapping method, Chapter 3.6). From these X, Y, Z, ASCII DEM files could be created for a picked Holocene horizon. This gridding meshed together all the available 3D and 2D data surveys at a resolution of 50m x 50m in grid formation equating roughly to the ICES international grid divisions and named appropriately. The result was a number of independently geo-referenced, topographically aligned raster surface files. It must be noted that this use of ICES grid referencing was only used for the southern section of the North Sea and was not employed by the Europe's Lost Frontiers Project for any purpose other than this research The result was a combination of depth gridded surfaces and shapefile vector features that

could be combined for a deeper analysis of the palimpsest landscape as in Figure 4.3 below.

4.4.1 Use of Digital Elevation Models in GIS:

Terrain surface information as previously discussed is delivered to a GIS in the form of a flat file matrix containing entries for x, y and z data within a geo-referenced bounding area. This can be in the form of a triangulated network of vertices (TIN) or as cell-based raster grids called Altitude Matrices or more commonly DEMS – Digital Elevation Models (Delefortrie et al. 2014). Due to the resolution, the grid-cell format of the surface model, its suitability for the largest selection of practical applications within ArcGIS and the ease of exporting from IHS Kingdom, the Raster DEM format was the chosen model for this process. Once imported into ArcGIS these surfaces could be utilised by a number of tools to model different environments and outcomes (as per Table 4.1). These could be performed individually upon each raster DEM or, in combination, if the DEMs were tiled together using a specific GIS tool called a 'raster mosaic'. This tiling geo-referenced the DEMs together into one continuous extent, triangulating the co-ordinates of cells to their neighbours. Single models can be built for the entire project area, though this may be highly computer resource intensive.

Toolset	Definition	Practical Application
Slope	Max rate of change in elevation	Steepness of terrain: difficulty in movement; land capability classification
Aspect	Bearing of steepest downhill slopes	Solar irradiance; vegetation modelling; site predictive modelling
Profile Curvature	Rate of slope change	Erosion modelling; vegetation modelling
Relief \ Shade	Terrain relief	Visual assessment; Terrain Variability;
Irradiance	Amount of solar energy reaching land	Vegetation modelling; land capability classification
Viewshed	Visible landscape from given point	Site & settlement predictive modelling
Watershed	Regional drainage	Site & settlement predictive modelling

Table 4.1 GIS DEM toolkit (Conolly and Lake 2006)

4.4.2 Raster Grid Definition:

Each raster grid was built upon a bounding area which was geo-referenced to a datum and a projection. Within this area each cell within the grid was of a uniform size and assigned its own unique location ID and

attributes, the absolute minimum of which was a Z number signifying height (or depth). However, any number of other attributes could be assigned to this Table in order to add further levels of classification, though for surfaces, this was not deemed necessary. While these DEMs gave a wide scale palaeolandscape, with broad brushstrokes, they missed the detail on a macro scale. Certainly, on the site-level scale that was part of the criteria for investigation of settlement potential mapping, this detail was important. Therefore, it was vital to also introduce the shapefile features that were brought from the seismic interpretations. These added in the features that were necessary to aid the predictive models.

These features were recorded in IHS Kingdom and exported in one of two ways. First, 'Culture' lines or polygons hand-drawn directly on the base map or timeslice were exported as shapefile vector features. The second were the stratigraphic sequences, reflectors and clinoforms picked within the seismic data. These were picked, gridded and exported in the same manner as the Holocene horizon with their projection and co-ordinates packaged as part of the vertices.

Once imported to ArcGIS these lines and polygons needed transforming into polyline features to a) visually represent linear features on the map and b) allow further analysis. At this point they could be grouped into logical polygonal joins such as 'rivers' to make one cogent layer for analysis in modelling.

Straightforward shapefiles (.shp) were imported for each survey for visualisation purposes as the gridded topographies were all set to square polygons and not to the actual survey lines themselves. Shapefiles, polylines and polygons could all be grouped together and stored in the geodatabase under a referenced naming system in preparation for use in spatial queries.

4.5 Spatial Analysis and Mapping of Seismic Data within ArcGIS

The mapping of the 3D seismic data from PGS required both the integration of exported X,Y,Z gridded DEMs for use as surfaces, which could be imported as rasters with depth co-ordinates, as well as vector

shapefiles from the picked out 'culture' features detected in the timeslice data. When these were added together as seen in Figure 4.3, we start to see a large amount of information building up. While at this regional scale the surfaces and timeslice imagery show little detail there is useful analysis to be undertaken in the overlying of palaeo features layers on the extant time amplitudes in the 0.07s timeslice. Though the detail is not clear, the very presence is indicative of depositional change activity. The fact that the features lie over this so neatly in almost every situation suggests that what is mapped is, in almost all cases, of terrestrial origin, which does seem likely given their riverine appearance. The features, timeslices and even the surface DEMs fit well onto the bathymetry in many places. This suggested that where there were multiple large palaeo features, they could inform us of large-scale landscape formations such as estuaries, coastlines and erosional sea cliffs extant at the time of the 0.07s timeslice. The fact that the seismics did not demonstrate terrestrial surfaces above this timeslice and because modern bathymetry disguised these surfaces, such palimpsest mapping was a very useful tool.

The use of layered GIS analysis enabled the investigation of potential landscapes below the visible bathymetry. In this way, pre-inundated coastlines could be proposed and tracked. The direction of flow for numerous river channels throughout the area was investigated, giving a wider understanding of the riverine connectivity throughout the area. Where these rivers broadened to meet the coast in estuary environments could be plotted with heightened confidence and these areas focused for further coring. As can be seen however, the brush strokes at this regional level are very broad and cannot reveal site level data. Therefore, in order to investigate potential settlement area and habitable environment, it was necessary to carry out analyses on a much smaller area. To establish the presence and potential of peat beds, a case study area was required.

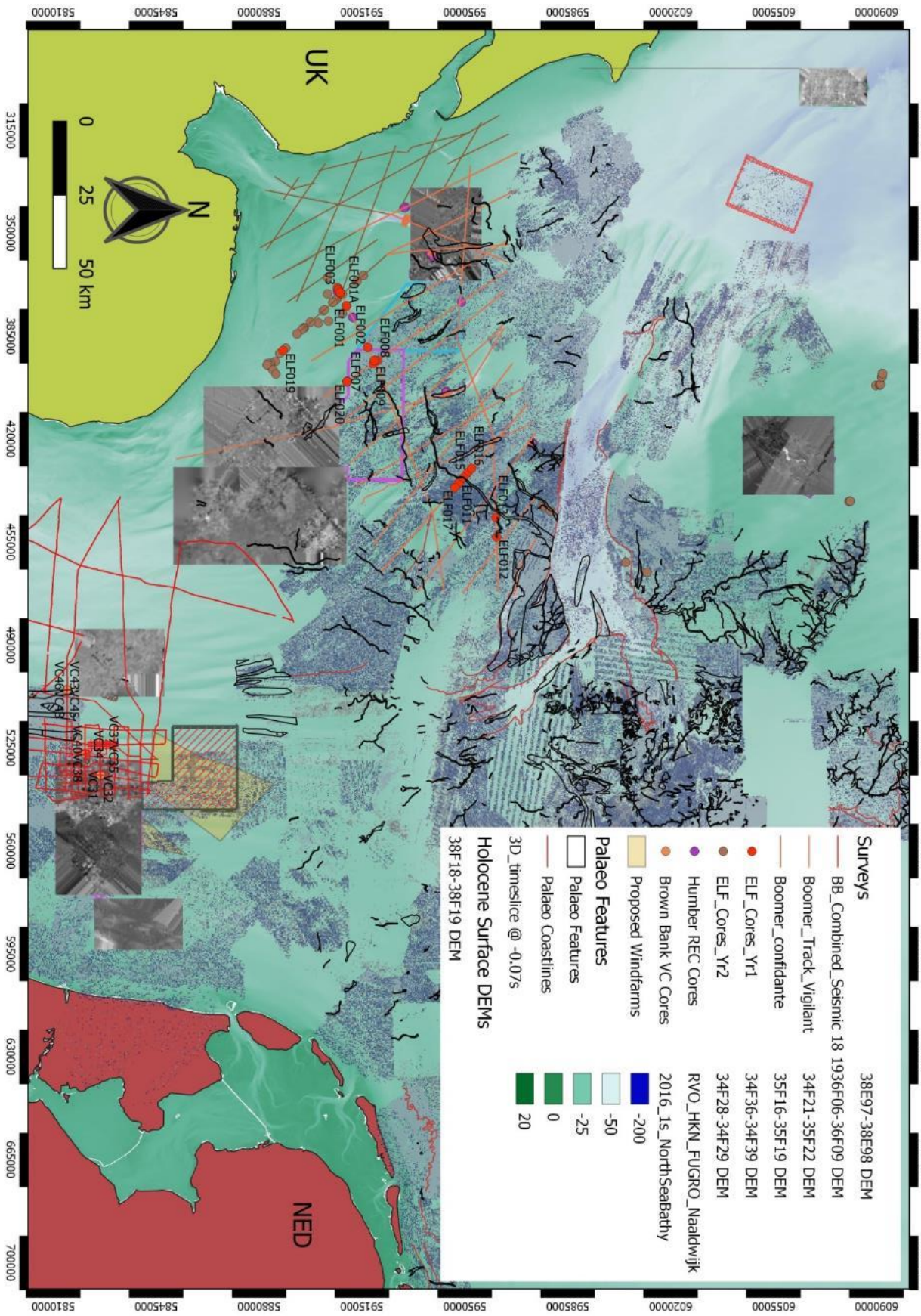

Figure 4.3 DEM, Culture and Timeslice (0.07s) data in a palimpsest layered GIS. Also included as Digital Appendix 13.5 Section 5

5 CASE STUDY - PEAT IDENTIFICATION IN GROUND OBSERVED SEISMIC SURVEYS

5.1 An Introduction to Submerged Peat and its Formation

Peat is an accumulation of dead and predominantly (>30%) decomposed organic plant material in saturated conditions. Peat has been key in providing terrestrial archaeology with well-preserved evidence, of headline-grabbing discoveries such as bog-bodies (Chapman 2015) and abandoned foodstuffs still extant in cooking pots at Must Farm (Malim et al. 2015). It has also played a vital role in the understanding of numerous archaeological processes associated with contextual preservation of both artefacts and organic – thus dateable – environmental proxies.

Terrestrial Peatland excavations in the UK at sites such as the Thatcham Reed Beds at Kennet Valley (Wymer and King 1962), the Somerset Levels (Bell et al. 2016)and Star Carr (Conneller et al. 2012) demonstrate these wetland areas were also favourable occupation sites from early prehistory, possibly due to their catchment of fresh-water and \ or marine resources including fish, birds and vegetation, especially reeds and grasses (Leary 2009; Crombé 2018).

Submarine peat is valued for this same favourable occupation potential, and also benefits from the fact that it has remained at constant low temperature, in waterlogged conditions (no drying out periods) and without human interference since inundation. Finally, it also benefits from the preservative effects of an anoxic environment.

Decomposition and waterlogging give peat beds an acidic and anaerobic character which then retards further decay, at low temperatures such as those under the North Sea, maybe indefinitely (Glob and Bruce-Mitford 1975). This preservation aspect is only relevant to organic matter but can be used to analyse the composition of peat itself at the time of formation by using a technique known as peat humification

analysis (Blackford 2000). This is possible because peat is formed in two distinct layers. The top 0.2 – 0.7m acrotelm breaks down biomass rapidly which descends to the deeper catotelm (Botch et al. 1995). At this deeper, anaerobic layer, humic acids are formed which mineralise the resultant organic and inorganic mass while drying (frying) the peat (Klavins et al. 2008).

Examination of the decomposition of the organic matter in the acrotelm compared to that of the anoxic catotelm will reveal whether the surface environment was wetter (less humified) or drier at the time of formation (more humified). More humified organic matter suggests drier conditions at the time of formation. The process would have taken longer and a greater degree of decomposition would have set in between the matter passing from the acrotelm to the catotelm (Blackford 2000). While this technique is not foolproof and there are issues with complex humic processes (Zaccone et al. 2011), it is applicable to marine and terrestrial peats of all types and has been shown to be replicable as a palaeoclimate indicator (Charman et al. 2009).

Peat develops in anoxic, anaerobic conditions below water level, whether fresh water or saltmarsh. It may be present in multiple forms such as moss or wood peat and inhabit more than one trophic state (Figure 5.1). This in itself can, in the right circumstances, such as at the Mesolithic inundation, be utilised as localised sea level indicator points (SLIP) to date isostatic variability and rates of progression or transgression (Bradley et al. 2011). However, it must be borne in mind that due to a variability in its porosity (void space) and capacity for waterlogging, peat is prone to compression which can impact the precise dating of sea-level 'curves' and pose contextual problems (Behre 2007).

Therefore, in environments where excavation is not possible yet and where landscape reconstruction is predicated by such organic proxies and dating techniques, peat is a prime source of contextual environmental evidence when cored.

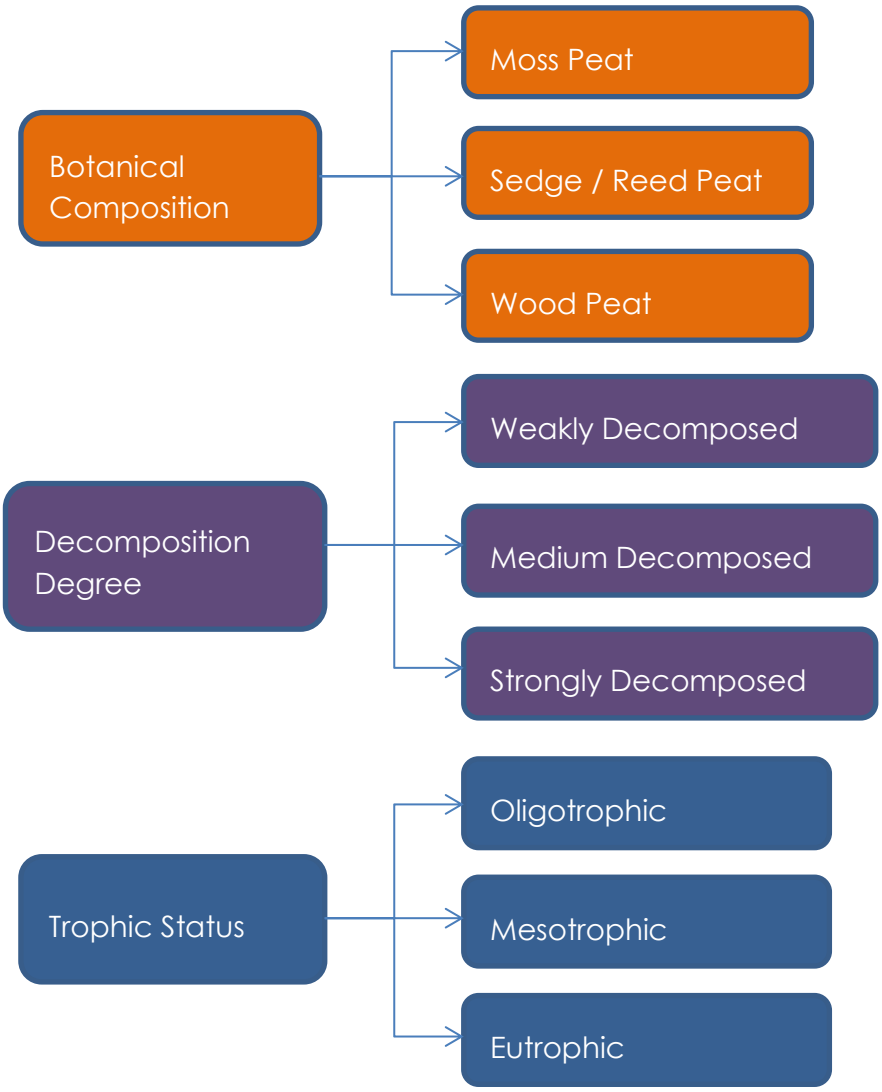

Figure 5.1 Kivenen's general classification scheme for peat (Kivinen 1980)

Preservation of organic remains such as wood, pollens, beetles and other useful environmental proxies in submerged peats is highly likely where temperature, salinity are stable. The contextual stratigraphy of the southern North Sea has proved an ideal combination of taphonomic factors within a single anoxic environment.

The preservative qualities of peat have been demonstrated profoundly during activity at the Star Carr site. In-situ finds of recent years are of a noticeably deleterious nature compared to those discovered at the beginning of the excavations in the 1930s (Milner et al. 2018).

The preservation issue is of specific interest to marine organic material, especially where it is overlain by cemented clastic silts (grain sizes between 0.06 – 0.02mm) or clays (grain sizes of <0.02mm) or other fine impermeable sediments as may occur in the event of an inundation. These overlying layers not only provide organic material with the accommodation space to infill, but they also protect the layers from erosion and seemingly from chemical interactions with the modern Holocene sands (Smith et al. 2015). Ideally, for archaeological purposes, these clay or thick silt layers accumulate gradually over many years, creating a non-porous (i.e. watertight) and impermeable (gas-sealed) laminated layer which effectively 'caps' the accommodation space of the organic layer beneath. Therefore, compression issues aside, the taphonomic provenance of organic matter within such layers, not to mention the radiocarbon dating of the inundated peat layers themselves remains a superb target. Abrupt clay-peat boundaries are thought to be a good predictor for the preservation of another environmental proxy of increasing importance within archaeology, sedimental ancient DNA, due to the combination of low temperature, water salinity and the above-mentioned contextualised stratigraphy that allows its isolation and identification (Kistler et al. 2017).

The stratigraphic context of sharp boundary locations between laminated clays, silts and peat would therefore be of great interest for evidential and environmental proxy purposes (Gearey et al. 2010). As such, a method of identifying such contacts via remote sensing would be of importance to archaeology and beyond. Research carried out on inundated peats using marine seismic data show correlation between organic interfaces and strong (bright) negative reflector signals. These have been noted and analysed in more than one paper (Plets et al., 2007: Kelley et al., 2018; Coughlan et al., 2018). However, studies to examine the nature of these signals, analysing precisely which interfacial boundary these signals are to correlate against and the building of a predictive model to interpret such signals has, until now, not been attempted.

It is important to state at this point that throughout this research the terms 'organic' and 'peat' are not interchangeable. Peat is a specific material type (Sh) and is only be used when discussing the evidence in core analysis, ground observations or in the discussions of the research as to the difference between specific material types. Investigation of seismic surveys and the 'identification signature' of bright reflectors against

organic layers in cores use the term organic sediment and organic layers when precise nature of the material cannot be determined. This could refer to silts, clays, sands, peats and even gases (though see below).

It was important to determine a nomenclature for classifying these organic reflector types by material and composition. Therefore, a necessary first step was to first adopt the Troels-Smith classification of organic sediments (Troels-Smith 1955) to allow the differentiation between material composition. (For a more robust breakdown of Troels-Smith classification, see Appendix 1 – Sediment Classification Systems).

Free phase gas could be treated as an entity in its own right and was not classified as a sediment type (Kontorovich et al. 2019). Minerogenic organic sediments classified included silts (Ag), clays (As) and sands (gMin). Non conformable sediment such as limus, gyffa or organic muds (L) or '*substantia humosa*' - peat (Sh) could contain any amount of water and organic detritus such as plant fragments, bark, seeds, leaves and grasses. The conformability and grain size determine the sediment type and therefore would govern the analyses undertaken. Straight minerogenic or clastic sediment would be identifiable primarily by the Wentworth Scale of sedimentary grain size (Wentworth 1922) and the organic element secondarily was processed via a simplified Von Post humification classification (Table 5.1 below).

By doing so, this thesis was able to analyse specific bright negative reflectors within the seismic record in the context of differing organic signals and classify particular boundary signatures for specific organic facies. In particular the research was attempting to determine a particular boundary signature for peat (Sh) at the contact with silts or clay boundary signals in the seismic record. To do this the research required a study area which could provide access to both core data from existing core reports as well as decent quality seismic data which demonstrated bright reflectors. Specifically, this thesis required an archaeologically focused coring programme led by interpreted seismic work performed in an area of organic sediment such as could be found across the southern North Sea basin (see Chapter 2.3 on the geology of the southern North Sea).

The identification of submerged peat and subsequent location and coring is of high intrinsic value to archaeology, so this tied the thesis into the

objectives of the larger Europe's Lost Frontiers Project and provided the study area required for the research (see Section 5.3 below). Such a geophysical investigation would require an interpretation of the submerged Holocene landscapes as seen in the seismic surveys. It would also need to correlate these with observable unit lithography within the cores.

The features and formations that could be interpreted as identifiable peat formations such as those described in Figure 5.2 were to be used to refine a more focused seismic model of 'bright' reflectors and their unit boundaries. A more precisely defined velocity model for peat, based on porosity, humic nature and bulk density was required to better judge depth and penetration and reduce the error variance imposed by current resolutions. To do this in a consistent manner, a method which involved ground observation of the geophysics alongside core evidence was employed.

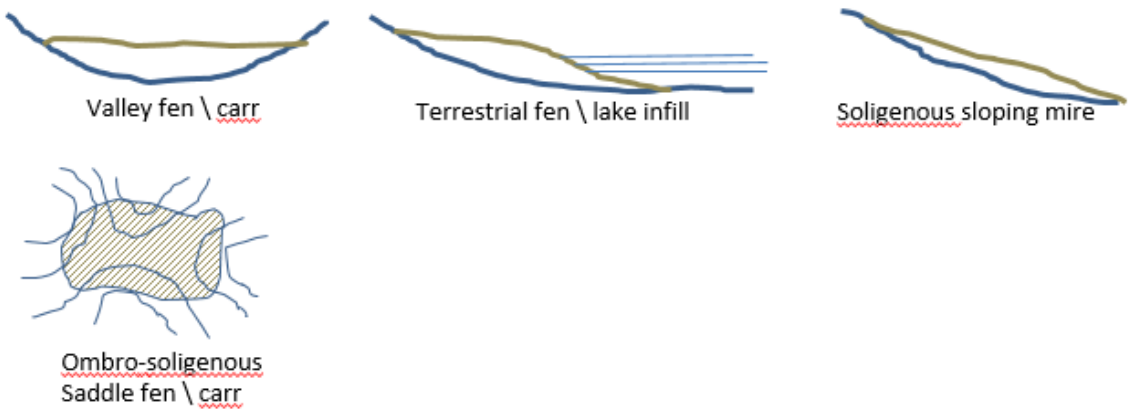

Figure 5.2 Types of Peat development. First 3 images show cross-sectional development, Final image is top-down view of saddle fen (Kivinen 1980).

5.2 Knowledge and Skillsets

Knowledge of seismic interpretation was of priority in this field and the research necessitated an undertaking of self-learning as discussed in Chapter 3. The manual picking of palaeo features was an important part of the mapping stage and would also prove to be of importance to the location of an organic seismic signal. Bright reflectors may appear almost anywhere in shallow seismic data, but peat development is very specific. As Figure 5.2 shows, there are a number of ways in which peat may develop in a small valley feature. Of these valley fen and terrestrial fen development in estuarine or shallow braided swamp environments are

most likely to produce the accommodation space for peat to infill (Blackford 2000). Bright reflectors in deposition without a landscape feature or, as commonly appears for gas deposits, projecting out from a feature unsupported, are highly unlikely to be peat and can be eliminated from investigation.

Using a seismic interpretation software package, namely, IHS Kingdom (versions 2017, 2018 and 2019) it was possible to investigate the available marine surveys to identify seismic lines with strong negative reflective signals and match those to existing core environmental and lithological reports to establish material types. There were also a number of tools available within the geophysical software to allow investigation of the bright reflectors themselves - isolate the p-wave amplitudes within the negative reflective index to gauge the range of frequencies represented by these negative peaks. Initial analyses would include:

- Applying bandpass filters, to eliminate frequencies ranges that do not apply to the organic reflector responses would have the effect of emphasising other amplitudes ranges, boosting particular positive or negative signals, but at the expense of resolution.
- Looking at attenuation and Q-Factor for organic material in sediment (using grain shearing static modelling) would suggest material types in unit boundaries
- Trace analysis could differentiate particulates from gas pockets
- Cosine phase functionality could look at the phase polarity and the amplitude spectrum to show the wavelet shape and direction.

To ensure the signals relate to the correct organic sedimental layers, it was important to ground observe the seismic data, therefore cores from the seismic lines under investigation were required. Each of these needed to include precise lithographic descriptors, measurements and location data as well as classifications of sediment types using the Troels-Smith scale. In utilising these environmental reports and the precise measurements of the cores themselves, a new shallow sediment velocity model could be created that could, for the first time, include organic 'peat' layers to compliment the already existing silts, sands and clays. This was only made possible based on an existing model using the synthesis of the Wentworth Scale of sedimentary grain size (Wentworth 1922) and adding a simplified version of the current Von Post Humification Scale descriptors of peat types (Table 5.1) already used in humification analysis for environmental reports (Blackford 2000).

Symbol	Description
H1	Completely undecomposed peat which, when squeezed, releases almost clear water. Plant remains easily identifiable. No amorphous material present.
H2	Almost entirely undecomposed peat which, when squeezed, releases clear or yellowish water. Plant remains still easily identifiable. No amorphous material present.
H3	Very slightly decomposed peat which, when squeezed, releases muddy brown water, but from which no peat passes between the fingers. Plant remains still identifiable and no amorphous material present.
H4	Slightly decomposed peat which, when squeezed, releases very muddy dark water. No peat is passed between the fingers but the plant remains are slightly pasty and have lost some of their identifiable features.
H5	Moderately decomposed peat which, when squeezed, releases very "muddy" water with a very small amount of amorphous granular peat escaping between the fingers. The structure of the plant remains is quite indistinct although it is still possible to recognize certain features. The residue is very pasty.
H6	Moderately highly decomposed peat with a very indistinct plant structure. When squeezed, about one-third of the peat escapes between the fingers. The residue is very pasty but shows the plant structure more distinctly than before squeezing.
H7	Highly decomposed peat. Contains a lot of amorphous material with very faintly recognizable plant structure. When squeezed, about one-half of the peat escapes between the fingers. The water, if any is released, is very dark and almost pasty.
H8	Very highly decomposed peat with a large quantity of amorphous material and very indistinct plant structure. When squeezed, about two-thirds of the peat escapes between the fingers. A small quantity of pasty water may be released. The plant material remaining in the hand consists of residues such as roots and fibres that resist decomposition.
H9	Practically fully decomposed peat in which there is hardly any recognizable plant structure. When squeezed it is a fairly uniform paste.
H10	Completely decomposed peat with no discernible plant structure. When squeezed, all the wet peat escapes between the fingers.
B1	Dry peat
B2	Low moisture content
B3	Moderate moisture content
B4	High moisture content
B5	Very high moisture content

Table 5.1 The Von Post Scale of Humification (Ekono 1981)

5.3 Methods

Selection of a study area was made so that it comprised of both available seismic survey data and core evidence. For uniformity, this research used

recent cores from three programmes of known providence located within this study area:

1) the Humber Regional Environmental Characterisation Project 2007 – 2011(Tappin et al. 2011). Data for these were taken from environmental reports.
2) The Lost Frontiers Project Coring Programme 1 (2016) containing cores numbered ELF001 – ELF020 utilising primary data and reports (Gaffney et al. 2017a)
3) The Lost Frontiers Project Coring Programme 2 (2017) containing cores numbered ELF021 – ELF059 utilising primary data and reports

From these core reports, 25 were found to contain peat or other organic rich material for investigation.

Core Name	Description (from environmental reports)	Survey Line
ELF002	Weakly laminated clay silts – organic materials	Route 18
ELF005B	Two thin layers of peat and silts	Route 18
ELF009	Peat present in lithostratigraphy	Line 11A
ELF019	Organically rich silts but no peat present	Not applicable
ELF027	Well humified peat and organic rich material	Not applicable
ELF031A	Organic material in till, charcoal present	Line 5 BM_1A
ELF033A	Reeds present at base of core	Line 5 BM_1A
ELF034	Organic material, peat present in erosional surface	Not applicable
ELF034A	Mud / peat – recorded as particularly smelly	Not applicable
ELF035	Peat found at top but not sealed and eroded	Not applicable
ELF036	Peat at bottom, mostly lost due to lack of catcher	Not applicable
ELF037A	Single peat pebble	Not applicable
ELF039	Very small amount of very wet peat	Line 5 BM_1A
ELF053	Organic rich sands, no peat	Line 5 BM_1A
ELF054	Deep peat layers, dry, friable	Line 5 BM_1A
HRVC01	Well humified organic material with shell fragments	Line 16
HRVC16	Rare humified – well humified silty peat / clays	Route 18
HRVC25	No peat but humified wood	Route 18_100N
HRVC26	Organic clays & humified organic detritus, charcoal	Route 18_100N
HRVC29	Abrupt clay to brown peat with woody fragments	Line 11A
HRVC29A	Clay with thin organic layer back to clays	Line 11A
HRVC29B	Clay weakly laminated. Peat will humified, wood	Line 11A
HRVC48	Clay weakly laminated to mottled peaty silts	Route 18_100N
HRVC49	Abrupt silt to black humified peat boundary	Route 18
HRVC50	Laminated silts to dark brown humified peats	Not applicable

Table 5.2 Brief description of all cores containing organic material within study area

The next step was to look at the location of these cores in relation to available survey data. The area had been chosen due to a number of 2D boomer survey lines from the Humber REC project that were made available for study. These were taken several weeks apart in 2008 and 2009 using two Gardline vessels towing seismic Boomer units and single streamer

receivers (Tappin et al. 2011). Table 5.2 shows that of 25 cores containing peat or organic material for investigation, 5 survey lines could be correlated and were required for interpretation in the study (Figure 5.3 below). Of these, weather was an impacting factor, especially on Line 11A, but less so on Line 5 BM_1A and Route_18_100_N).

The surveys were shot at a frequency of 3.5 kHz at 4λ for a vertical resolution of between 0.08m and 0.12m dependent on velocity (Tappin et al. 2011).

Examination of the data throughout the area revealed which cores contained verifiable peat according to the lithological reports and was able to separate these from other sediments which were organic matter - but not peats - such as organic silts, sands and clays. Cores that were not located on a survey line were eliminated from the investigation, as were those without organic sediment material. The thesis was not concerned, at this juncture, in the investigation of the reflective properties of actual organic detritus (woods, reeds etc.), that Troels-Smith would classify as LD. For initial interpretation and modelling purposes, only the peat cores were used. Further spatial analyses mapped which of these cores fell within geomorphological catchments – or within an area of definable error tolerance - to an accessible seismic survey line (table 5.3).

For this reason, HRVC01 was also eliminated from the investigation. For although it had potential peat ('silty clay with rare organics … but no assessment work was carried out on this core' – Tappin et al 2011), the location of survey Line 16 was an outlier in relation to the other cores and surveys marked in Figure 5.3.

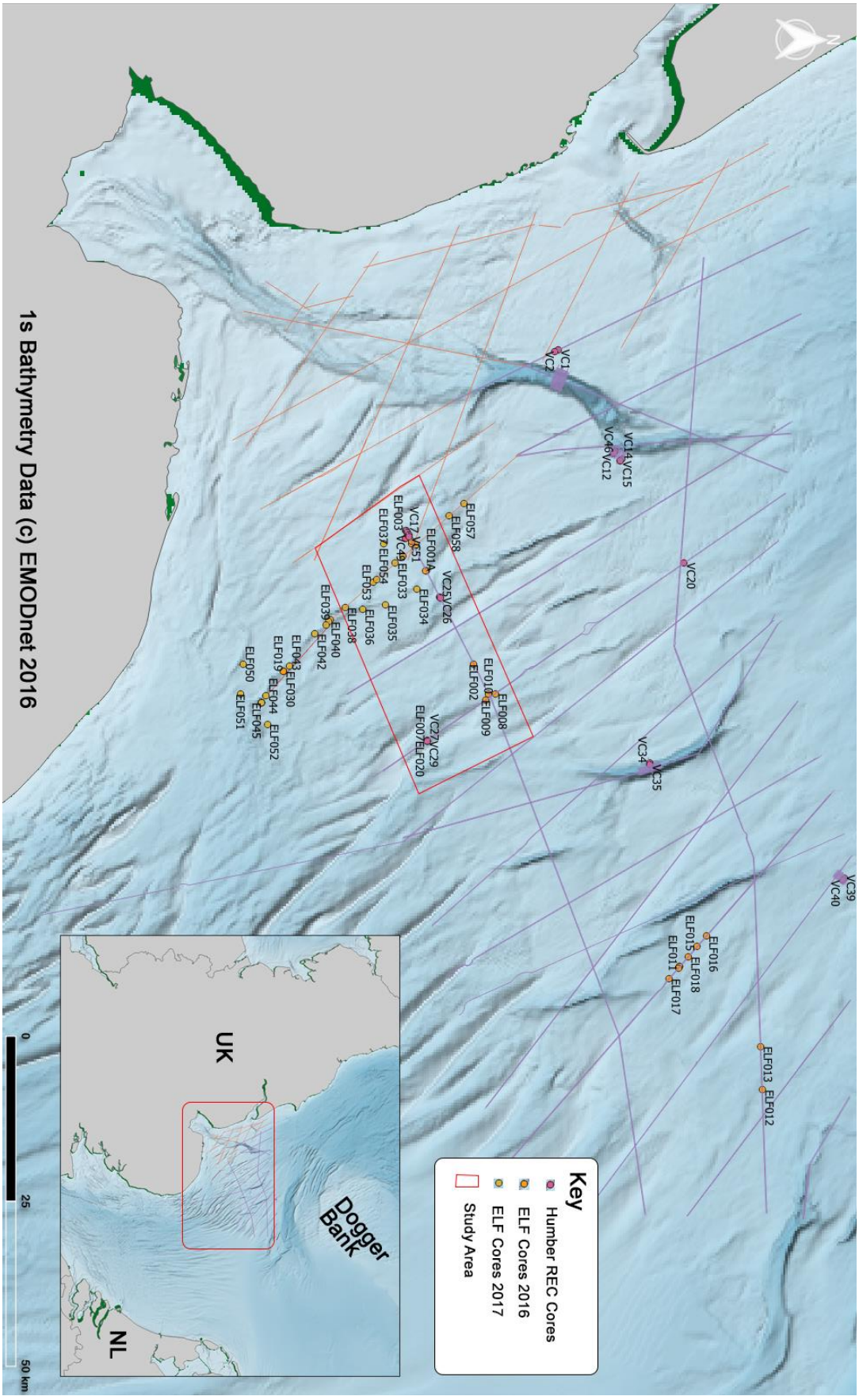

Figure 5.3 Spatial representation of cores to survey lines to establish a study area

The Vibrocores were employed by means of a boat anchored at either end to stop drift as much as possible (R. Tappin et al. 2011). This would not prevent all motion however and movement of anywhere up to 10m from the intended core location must be anticipated. The was also the accuracy of the global navigation satellite system (Systems 2020) to take into account. No receiver information was provided by the vibrocore teams for either the 2011 survey or the 2016/17 surveys, though both state the use of DGPS equipment (Tappin et al 2011; M Bates pers comm). If the GNSS receiver used was the United States GPS, the accuracy of that system is stated to be an average of 1.89m horizontal and 3.87m vertically + 1ppm RMS (Renfro et al. 2018). However, other satellite receivers, such as NVS, GLONASS and uBlox have horizontal accuracy more in the range of 2.5m + 1ppm RMS (Junipersys GNSS Accuracy - website Updated April 2020). For statistical safety a measurement of 2m horizontal accuracy tolerance was assigned. Vertical accuracy is less of an issue as the vibrocore sits atop the seabed and drills as near to vertical as is achievable in the conditions.

The results of this analysis reduced the initial list of cores presented down to the following cores all lying within the central study area and within a 10m tolerance of a survey line:

Survey Line	Core Name	Distance from survey line
Route_18		
	ELF002	<1.9m
	ELF005B	8.2m
	HRVC49	<0.2m
Line_11A		
	ELF009	<2.1m
	ELF020	4.63m
	HRVC29	6.44m
	ELF007	<0.8m
Line 5 BM_1A		
	ELF054	<1.1m

Table 5.3 Cores containing organic material and proximity to verifiable seismic survey data

The lithostratigraphical data were compiled with sequence depth, Troels-Smith colour descriptions (Troels-Smith 1955) and simplified terrestrial, freshwater, marine environmental proxy indicators.

Each core was measured and described by lithological unit type, organic classification and abruptness of boundary. Locations of the cores were plotted onto the seismic surveys and a brief interpretation based on material type created to include features, extant Holocene and erosional surfaces and subsequent progressive, transgressive and regressive activity indicative of sea-level rise.

When analysing the physical cores and the seismic surveys and how these parallel data could be used to determine the existence of peat alongside the geophysical context; it is worth noting that the core depth measurements come from three different missions using three different survey datum. Therefore, to ensure consistency throughout this research and beyond, a new velocity model was required. This would start anew with a new sea level datum. The internal measurements of conformable units and their lithostratigraphical descriptors still retain their precision and were independently verifiable.

The surface temperature of the southern North Sea in numerous station locations has been collated historically along with salinity and these have remained relatively static over the years (Figure 5.4 Cefas, SeaDataNET 2019). Obviously, these records do not extend back to the early to mid-Holocene when the peat beds were initially inundated. There is evidence from ice cores for climatic conditions being cooler and wetter than those of today (Lisiecki and Raymo 2005). Though cooler periods on land do not necessarily equate to a similar level of impact on oceans and sea level surface temperature appears to have remained an average of 11 to 13° Celsius throughout the early Holocene (Calvo et al. 2002).

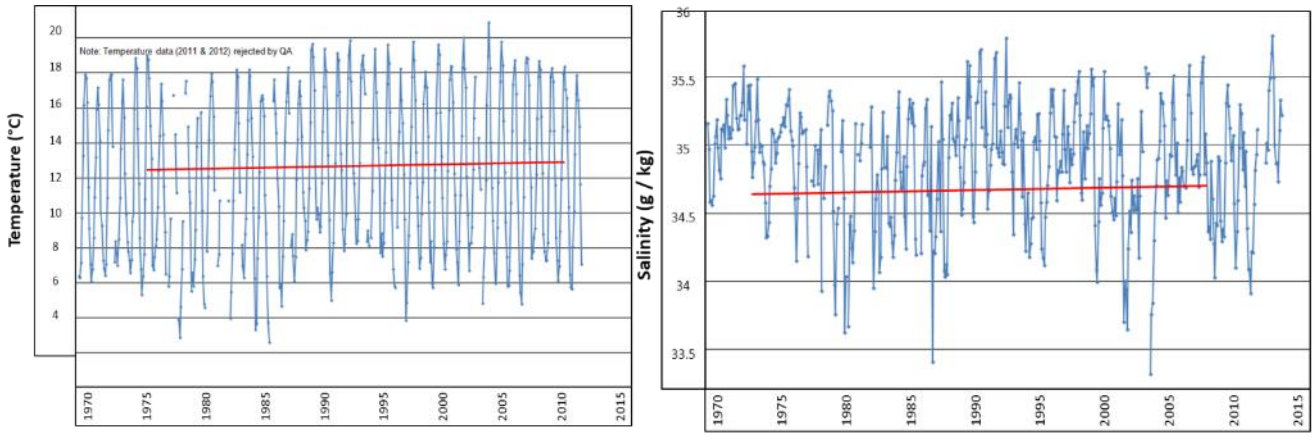

Figure 5.4 Surface temperature & salinity of southern North Sea over 40 years (data source: Cefas 2019)

Archaeologists have analysed salinity levels from diatoms dating from earliest inundation events of brackish to marine water species in the Holocene and have concluded that except for a dip of around 3g between 9.25 and 7.25kya salinity has remained relatively static around 35g/kg or 3.5% (Frenzel and Boomer 2005).

For the purposes of this research, modern temperature and salinity ranges correspond to the water column when the surveys were taken. Bulk density and pressure, the other parameters, were also unlikely to change between surveys or over the last decade. Therefore, mean values, taking into account seasonal peaks and troughs and averaging out depth changes for the study area of around 35m would give balanced parameters. This resulted in an average annual temperature of 13° Celsius for shallow water and a salinity of 34.6g / kg.

The next step was to calculate the speed of sound the sediment medium. To do this the Wentworth Scale was used as a comparator for the core environmental assessments in order to estimate grain size and bulk density in line with Hamilton's 1970 North Atlantic continental shelf data assessment for shallow marine sediment (Hamilton 1970). At this stage, such an assessment must only be an estimate but may give sufficient parameters to discover a bulk density and porosity valuation as follows:

$$c = f\lambda$$

(Sheriff 2012)

Where speed of sound = c

Frequency = f

Wavelength = λ

And the speed of sound was affected by medium it passed through by both density (p) and compression(k). When either is increased, the speed of sound decreased by a product of the square root:

$$c = \frac{1}{\sqrt{pk}}$$

(Hamilton 1970)

Compressibility was either very important to the research, or totally irrelevant. Different materials compress differently; Gas – as in free phase gas is highly compressible but does not feature in core evidence as it is

released during the coring process and cannot be counted in the environmental report (on site notes M Bates 2017). This does not mean it may not account for many of the bright reflectors in seismic surveys.

Liquid, such as seawater, is entirely incompressible (Barus 1892) and therefore irrelevant to Hamilton's equation. Therefore, the only medium through which submarine acoustic signals may pass and that may undergo compression is solid sediment. It is this bulk density and its ratio to void space that can be bulked by seawater content that requires investigation. It has already been stated in Chapter 2.3 that the Naaldwijk Formation was often characterised by the basal Nieuwkoop formation beds of peat found at its lower layers (Cotterill et al. 2017). These have been found to be highly compressed with little void space (porosity) and a high bulk density (Baeteman et al. 2012).

Density of marine sediment is not merely a single entity. The bulk density is a composite measurement of structure. It ranges from a consolidated mass of microscopic fine grains between which there is little to no void space. At the other end of the scale are poorly sorted and unconsolidated, large grained materials with a high ratio of void spaces filled with seawater. The differing mass between the bulk density (p_b) and the grain size (p_g) gives the porosity(n) as a percentage of the material mass:

$$n = \frac{(p_g - p_w)}{(p_g - p_b)}$$

(Athy 1930).

Where p_w is the density of water at 13 degrees Celsius and 34g / kg Salinity = 1.025 g/cc

The impact of this equation was that bulk density and porosity were seen to be inversely reciprocal i.e., as bulk density increases, pore space decreases which meant that this equation may also be used to express the bulk density in terms of weighted mean of the pore water and grain density.

$$p_b = np_w + (1 - n)p_g$$

(Schlitzer 1989)

energy usage can be shown as in Figure 5.5 below. Acoustic energy travelling through a medium, such as water is slowed by a coefficient specific to that medium (W_E). When it arrives at an interface between two material types, part of the signal reflects back. This energy can be recorded by a waiting receiver (W_R). Part of the energy continues on through the material to the next interface (Wrona et al. 2018) but a third part gets absorbed or attenuated (W_A). The amount reflected (the reflection coefficient) for any boundary at normal incidence is calculated by means of the following equation as demonstrated in Figure 5.6.

$$\propto = \frac{Z_2 - Z_1}{Z_2 + Z_1}$$

(Wrona et al. 2018)

Attenuation is therefore the absorption of energy through material and is not to be confused with impedance. Acoustic Impedance (Z) is a value computed from the velocity (ν) and sediment bulk density with the following criteria:

$$Z = \nu p_b$$

(Sheriff 2012)

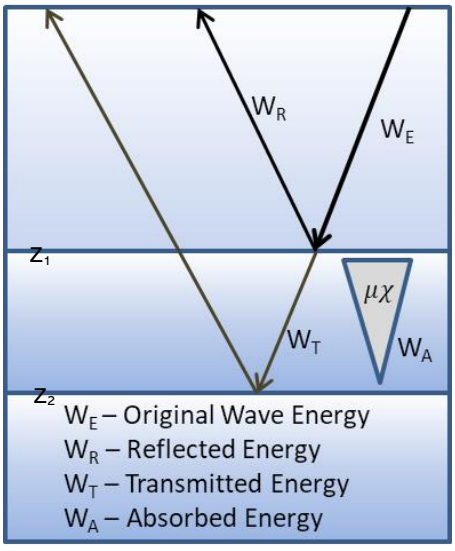

Figure 5.5 Process of acoustic attenuation (WA) and the attenuation coefficient μ through material χ (after Kearey et al. 2013)

Acoustic attenuation is the process of energy loss and requires a calculation on the estimate of impedance under pressure (ρ) for the energy rate (J):

$$J = \frac{1}{2Z}\Delta\rho^2 \max$$

(Chopra and Alexeev 2006)

This can then be used in the calculation of the attenuation process:

$$J_1 = J_0\, e^{-\mu\chi}$$

(Chopra and Alexeev 2006)

Where $J_1$is the attenuated energy, while J_0 is the source energy rate through which the estimate product of the attenuation coefficient (μ) through the material depth (χ). The attenuation coefficient is based upon the medium's Quality Factor (Q) and the frequency (Pinson 2008). The parallel therefore is straight-forward. Higher frequency has a direct correlation to higher absorption and certain boundary factors, porosity levels, grain sizes etc. may play parts in this. The Q-Factor is calculated via spectral analysis which will be addressed later in this chapter. Before these calculations can be rigorously tested, a further aspect must first be in place to ensure consistency in results.

5.4 A New Velocity Model

To calculate accurate depths for seismic reflections, the current use of an average single velocity model based on shallow depth sediment has been relatively reliable e.g. by the Office of US Naval Research (Lewis 1967) and in coastal Atlantic waters (Buckingham 2005). This averaged sound velocities through sediment materials at shallow depths and reflectivity coefficients between 1460 and 1580m/s. It did not take into account porosity, moisture content, compaction, bulk density, obstacles within the material, degrees of humification or levels of free phase gas within individual pockets of peat (Slater and Reeve 2002). Hamilton (Hamilton 1970) considered the above attributes for marine surveys, investigating the behaviour of continental shelf deposits and provided data for such in-situ environments. However, along with the majority geophysicists, he did not differentiate between organic sediments and non-organic. He made no separate sediment classification for peat as opposed to any other unconsolidated submarine sediment (Hamilton 1970).

To fully understand the environmental cores therefore, it was necessary to take Hamilton's 1970 continental shelf dataset and consider it within a multi-layer velocity model that could account for:

a) Sea water column velocity
b) unconsolidated sediment (Hamilton 1970)
c) additional peat boundaries with specific classification criteria.

To this end a three-level calibrated velocity model was built and measured against an average single velocity model for example that of Lowry (Lowry et al. 2009) as a control. As outlined above the three-level model consisted of:

a) one consistent velocity model for the water Table to seabed horizon using the Whong & Zhu (Wong and Zhu 1995) Unesco Guidelines:

$$c(STp)=cw(Tp)+a((Tp)S)+\beta((Tp)S\frac{3}{2})+\gamma((T\rho)S^2$$

where

c = speed of sound,

T = Surface temperature in Celsius = Averaged at 13°C

S = salinity in grams per one thousand units = Averaged at 34.6g / kg

ρ= pressure in Pascal = 0.0Pa at surface to Pascal reading at deepest seabed level in the study area (35m below datum) and averaged for each core using Kurt Heckman's Vcalc Underwater pressure calculator (2018). This gives velocity averages based on the following ranges:

At 0m sea level datum and 0.0 kPa = speed of sound at 1481.8 m/s

At 35m below sea level datum and 351.8 kPa = speed of sound at 1500.183 m/s

b) A single velocity model used for all units up to the peat boundary based upon the environmental report classification. This in turn was based on interpretation of the Wentworth phi Scale of grain size (Wentworth 1922; where grain size in phi = $-\log_2$ x grain size in mm). Where evidence was available appertaining to the organic nature of the material, this grain sorting was then categorised further against Troels-Smith classifications (Troels-Smith 1955). At this point, a rationalisation of the core material was made alongside Hamilton's 1970 model of porosity and grain size versus bulk density and weighted for their individual unit depths through the consolidated layers. Without specific volume measurements the

estimation of material makeup and relationship of porosity versus bulk density provided a solid empirical basis for the computational model.

	Humic State	Porosity	Composition	Expected Boundary
1	Organic. May contain plant remains	Open voids prone to Waterlogging	Organic Matter	Very bright
2	Undecomposed peat, less plant material. Wet.	Variable	Organic, Dark	Bright
3	Decomposed peat, little plant material,	Compressed. Medium to Dry	May be friable but dark	Still distinct against clay, less against sand
4	Highly decomposed peat. Contains much amorphous material with little recognizable plant structure. When squeezed, about one-half escapes between fingers. Water, if any, is very dark and almost pasty.	No void space. High density	Silty or sandy peat mix	Poor context
5	Little to no organic content remains.	Dry. High density	Mineralic or silty, not peaty	Poor context

Table 5.4 Breakdown of descriptive classifications for velocity models (Ekono 1981)

c) A velocity model created for a lower boundary contact bright reflector (from base of the zero RC on the seismic survey) for the weighted internal depth of the core measured peat to the next interface below. This was developed to establish a velocity model purely for peat. The intention was two-fold: 1) to identify a reproduceable signature for peat in other seismic surveys and 2) to ascertain the depth of existing peat beds. The classification of peat was based on the Von Post Scale (Table 5.1, page 105) and simplified for marine submerged peat. The humic states were aligned with Hamilton's 1970 porosity model but were adapted to work with weighted silts, clays and a mix of organic sediments including peat (Table 5.4).

The velocity models of categories 4 and 5 above closely followed the models in part b) above while categories 1, 2 and 3 required new calculations velocity model. This includes porosity against bulk density which used an index based on descriptive text as per the Troels-Smith index aligned with the Von Post porosity and humic state descriptors.

These were placed on a suitable scalar on the bulk density vs porosity vs grain size graph (Figure 5.6). Hamilton maintained such a scalar of inverse proportional data in his North Atlantic Continental Shelf analysis (Hamilton 1970).

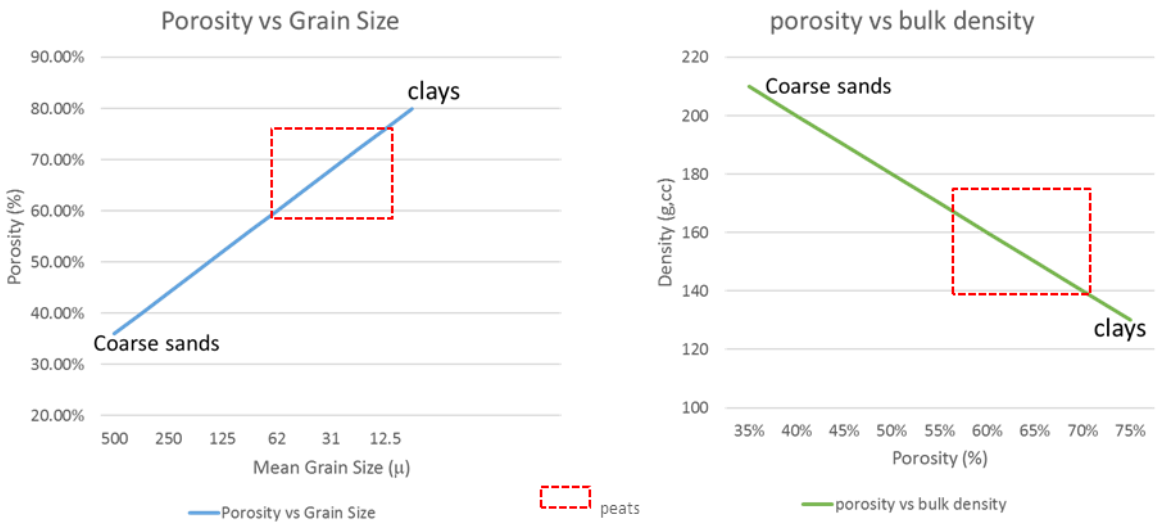

Figure 5.6 Simplification of Hamilton's continental shelf min-max variability of porosity vs grain size and porosity vs bulk density in material type with added potential peat ranges.

As Hamilton pointed out, bulk grain size and porosity were the most important factors in the calculation of this model, (Hamilton 1970). While more precise computational models employing shear wave or elasticity framework moduli have been used in recent computational models (Buckingham 2005) and may add finesse in future work, the focus of this research was to identify patterns and determine classifications in material boundary contacts. By building upon the simpler sedimental model of Hamilton's porosity vs grain size vs bulk density model, this research was able to create a basis for verifiable, repeatable velocity analysis of core data.

The addition of the Wentworth 1922 classification scale and bulk grain size were obvious choices to calculate quantitative core data from the qualitative environmental measurements (Appendix 1). By expanding an existing model with additional classifications for organic sediments, most notably peat, more complex sediment velocity analyses. These would initially involve porosity, grain size and bulk density values but could be built upon to bring further precision to shallow water sediment velocity modelling.

The proposed solution required four velocity models to be generated independently in IHS Kingdom. The first, a single generic water-plus-sediment model as was used in the mapping section in Chapter 3 for the depth conversion gridding. This gave a single figure average velocity of 1489m/s. This would be used as a control for the new velocity model.

The new velocity model itself was generated as three independent levels of velocity computation. The first level was run solely for the water column as per the Unesco Guidelines (Wong and Zhu 1995). Next, two sediment velocity models were calculated separately by means of the core weighting and individual modelling based on bulk density / porosity. Full calculations for each core can be found in Appendix 2 – Velocity Model Calculations. The seismic reflectors were picked on interpreted horizons between the seabed at the top and a palaeochannel at the base acting as guides.

Each velocity calculation necessitated a division by two to account for the data being made up of source wave and received signal (two-way travel time) when the velocity model only required a single measurement. The results were then clipped to within the appropriate horizon stages, staggered and weighted by means of their overall percentage volume within the core analysis.

Finally, the velocity models were summed to calculate total depth and the final result in cm/s required conversion to metres for the sake of clarity and consistency with the core analysis. For the purposes of this research the survey datum and the coring datum at the sea surface were assumed to be the same 0 m above / below mean sea level. The model calculations can be viewed in Appendix 2 and an overview is presented in the following Chapter - Case Study Results (Table 6.3, page 154).

5.5 Vertical Resolution and Fresnel Zones

It was important to note that while the total energy in the wavefield changes little in the shallow depths of the study, the signal would alter (Sheriff 2012). The acoustic signal would spread, the velocity would increase with depth and the energy would experience reflection,

refraction, attenuation and scattering within the media through which it passed (White 1992). The velocity may be calculated as above, and the attenuation can be estimated as an inverse of the frequency of the survey (Wang 2016). The Quality Factor (Q) which will be used further in this section can be employed to give an approximate value for attenuation levels and spread (Aki and Richards 2002). Q_{EFF} is the effective value for attenuation and is made up of an intrinsic attenuation and a scattering value based on the equation:

$$f_s = \frac{V_\rho}{2\pi h'}$$

(Sheriff 2012)

Where f_s is the scattering frequency, V_ρ the velocity through the medium and h' is the threshold thickness of a layer before acoustic scattering occurs. In the case of the study area in this research the frequency range for each survey line, was taken directly from IHS Kingdom, and the frequency analysed by ignoring the outlying peaks and looking at the main range of cycle frequencies alongside the velocities from the above models to calculate the scatter thickness. Adapting the above equation for use on the study area surveys, it was possible to insert the known frequency of 3.5 kHz (Tappin et al. 2011):

$$2\pi h' = \frac{V_\rho}{f_s}$$

(Sheriff 2012)

$$6.28(h') = \frac{1480m/s}{3500Hz}$$

$$h' = \frac{0.423}{6.28} = 0.06m$$

Thus, the vertical threshold before acoustic scattering – and loss of vertical resolution (areas of occlusion within which waveforms could cancel out) measured at 6cm. Resolution determined the differentiation of signal between two reflective points e.g. surfaces. Low frequency, thin layered or closely laminated contacts could appear as one thick boundary or produce an unwanted multiple. In reflective seismic geophysics this could occur both vertically and laterally. At the Fresnel Zone, an area measuring a quarter wavelength from the source and a depth radii plus quarter wavelength lateral distance (Sheriff 2012). The threshold for such

resolution, at which differentiation could be maintained was calculated vertically as:

$$\frac{v}{4f}$$

(Sheriff 2012)

$$\frac{1480m/s}{24000Hz} = 0.06m$$

And laterally as:

$$A = (\frac{v}{2})\sqrt{\frac{t}{f}}$$

$$A = (\frac{1480m/s}{2})\sqrt{\frac{t}{6000Hz}}$$

(Whitewright 2015)

Where A represented the lateral Fresnel Zone A to A' in Figure 5.7 below and t = time to Z depth in seconds at frequency (f). i.e. at a depth Z at two-way time 0.1s and a velocity of 1480m/s for the above survey line, the lateral Fresnel zone calculated at:

$$A = (740m/s)\sqrt{\frac{0.1s}{6000Hz}} = 3.02m$$

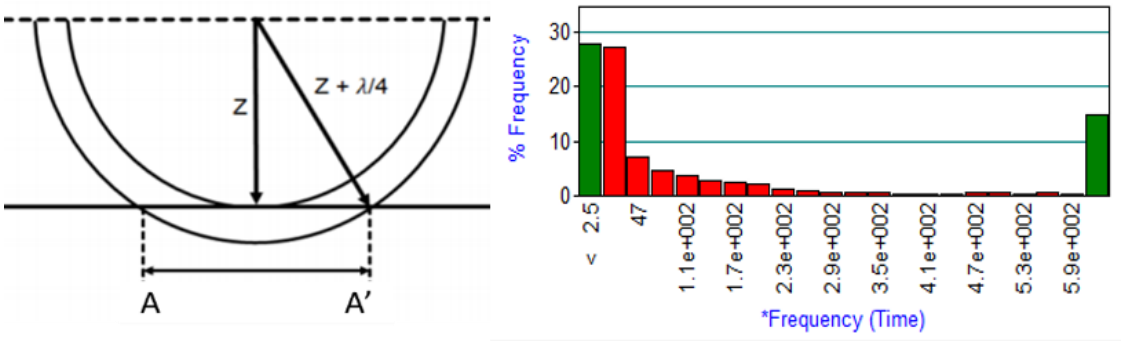

Figure 5.7 Left lateral Fresnel Zone represented by A to A' (Whitewright 2015) calculated dependent on frequency of individual survey. In the case of survey line 11A Frequency range shown right from 2.5Hz to a max of 6 kHz.

5.6 Facias and Signal Strength

While a velocity model could tie core lithography to the seismic stratigraphy, the other important role of the research was to attempt to look at the correlation between the intensity of the seismic signals and the composition of the organic matter at specific contact facies. Specifically, the thesis was to examine bright boundary interfaces observed in the seismic surveys and ground observe these to material units within environmental coring evidence.

In order to do so, the research looked to find a unifying aspect to the peat boundaries in the coring evidence with their locations on the survey data in order to create a recurring seismic 'signature'. The model needed to have clearly defined unit boundaries, depths and characterisation within the core definition and a robust, well interpreted velocity model to align the survey data against. Picked unconformities within the seismic interpretation should match unit changes within the core evidence, however further supporting evidence was required within the seismic surveys that could refine the interpretation of organic material. The otherwise 'bright' boundaries required specific analysis to differentiate between types of organic matter and makeup, to give further insight into a differentiation between gas pockets and solid materials and between clays, silts and peats from the signals they produced.

Therefore, all boundaries between pertinent units found in the cores were plotted onto the survey at the precise depths and the amplitudes re-measured at those markers. The amplitude strength was calculated, and the range of frequencies determined. The strongest reflection ranges were enhanced using bandpass filters. These were tested over a wide bracket governed by the noise frequencies of the survey (Sheriff 2012). A general setting of between 5 – 8Hz was set for the low cut pass and between 8 to 15KHz for a high pass (Wang 2016). Ranges of strong negative and positive reflective signals were then marked up manually, and basic interpretation performed independent of the core units where they did not overlie, expanding the landscape out to the surrounding area.

5.7 Q Factor and Attenuation

The Quality Factor Q is a function of depth and frequency and can be used to measure the dissipating effects of wave propagation through a given media (Dasgupta and Clark 1998). It must be pointed out that Q alone is not a scientifically robust entity. It is an estimation and without corroboration cannot be utilised in scientific calculation. However, in combination with spectral analysis and attenuation coefficients, Q can be used to measure the local correlation between increasing higher frequencies and the increase in relative acoustic impedance that is therefore related to attenuation - whether as a result of intrinsic attenuation or scatter. For instance, higher absorption rates can indicate higher liquid content than pore density alone. New research is pulling Q-Factor and attenuation coefficients directly from high frequency phase S-Wave velocities (Xia 2014). The study area for this research does not have access to such Shear-Wave data though this would be a fascinating opportunity for the future. However, by means of spectral analysis and using IHS Kingdom's Rock Solid modelling module, the Q-Factor was estimated (Figure 5.8). In doing so, it is worth considering the two main sediment models for attenuation – theoretical vs empirical.

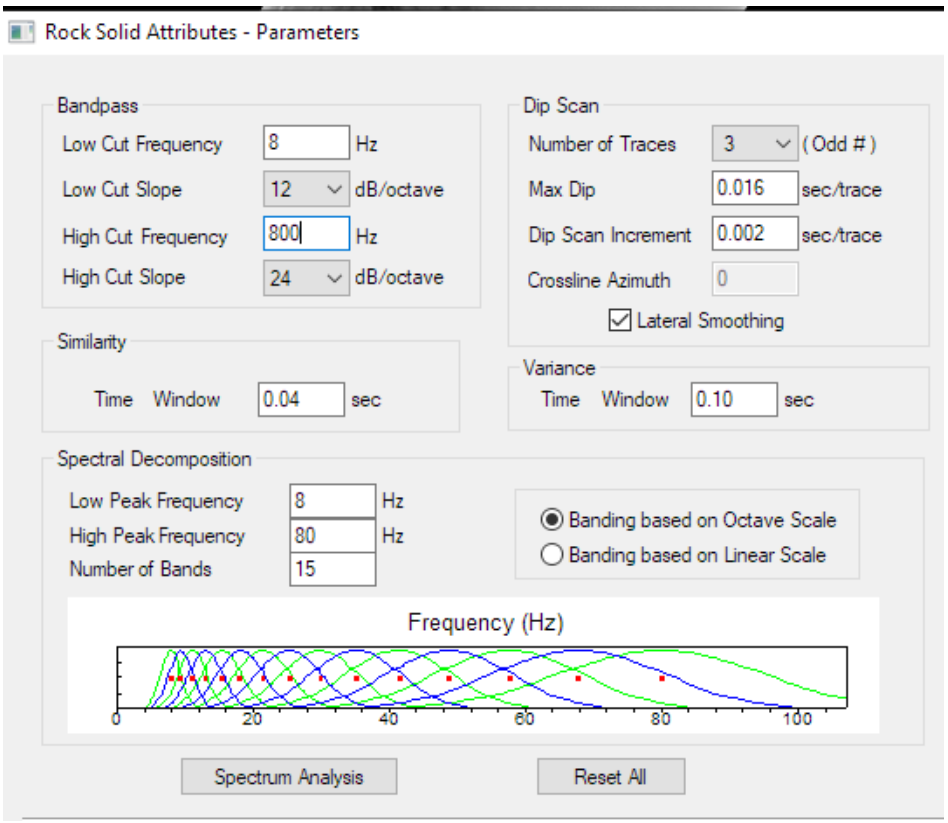

Figure 5.8 Applying spectral analysis for Q Estimation with bandpass filters in IHS Kingdom.

The Biot-Stoll model (Biot 1956) suggests that, under zero stress i.e. at the surface or sea bed, the elasticity of a moduli is also zero but that attenuation is controlled by two movements; viscous loss through pore fluid and friction loss through grain-to-grain shearing. This theoretical model works well on a non-linear scale for seismic wave frequencies between 50Hz and 10 kHz. Below this range and the Q values are too weak to interact in the model except on global mantle size regions (Morozov 2008b) and above the 10kHz range the compressional wave attenuation begins to show a distinctly near-linear logarithmic scaling that looks more in line with the second model proposed by Buckingham (Buckingham 2005) called the Grain-Sliding (Esestime et al. 2015) theory.

The G-S theory removes the need for a viscous loss and relies solely on a grain-to-grain shearing mechanism in a non-elastic modulus. This means that grain-size and porosity become the only factors that govern attenuation and allow for the calculation of a near-constant effective Q-Factor. The G-S model was updated in 2008 to become the BICSQS Model (Chotiros and Isakson 2004).

	Sandy Silt Sediment	Silty Clay Sediment	Model
Sound Speed (weak linear gradient) 25Hz to 250kHz	1638 to 1658 m/s	1548 to 1571 m/s	Closer to G-S
Attenuation coefficient on positive gradient 25Hz to 250kHz	14.2 to 51.9 dB /m	7.8 to 31.7dB/m	Closer to Biot
Quality Factor	35 to 75	30 to 40	

Table 5.5 (Wang 2016) showing primary conclusions.

Peat falls into a broad unconsolidated sediment classification covering sandy silt through to silty clays and as such has been a by-product of intense comparative research into empirical versus theoretical models of just such acoustic propagation modelling (Wang 2016, Table 5.5). The conclusions of this research were, in summary:

For the purposes of this research combining the G-S theory with a forward modelling theory such as the one employed by Pinson (Pinson 2008) and following the geometric guidelines employed by Morozov (2018), it was

possible to combine a constant Q Factor with the previous phase analysis, where Q Factor alone might be considered too general to deliver a highly focused and specific calculation of the attenuation coefficient as a value derived from the frequency of the dominant P-Wave (Morgan et al. 2012). Based on the following basic mathematical descriptions:

$$\alpha(f) = \gamma f$$

Where α, the attenuation coefficient is a linear function dependent on frequency (f) so that γ can be expressed as a constant calculated using Q Factor and velocity as follows:

$$\gamma = \frac{\pi}{Qv}$$

(Morgan et al. 2012)

Which can then plug directly into an amplitude analysis to describe the loss of intensity through depth from the source to the receiver.

$$A(x) = A_0 \left(-\frac{\pi f}{Qv} x\right)$$

Where $A(x)$ is the wave depth, A_0 the wave source, f the frequency and v the velocity. However, this does not take into account multiple material types and it is here that IHS Kingdom's spectral analysis and Q Factor prove their worth. Using logarithmic scaling to determine the attenuation between layers based on the Q Factor:

$$\ln\left|\frac{A_1(f)}{A_2(f)}\right| = \mathrm{e} - (a(f) - (a(f))$$

(Pinson 2008)

Or as Pinson (Pinson 2010) fine tuned the equation for use with velocity models 2-way seismic frequencies:

$$\alpha(f) = \frac{\pi \cdot f}{c(f) \cdot Q(f)} = \frac{\pi \cdot f \cdot \Delta t(f)}{X \cdot Q(f)}$$

Where $\alpha(f)$ is the attenuation coefficient, $Q(f)$ the quality factor as a function of the frequency f and $c(f)$ the phase velocity, Δt the total two-way recorded time and X the distance travelled through the medium. So that when applying the equation to $A_0(f)$ – the amplitude frequency as measured from source at a distance and time of zero to the seabed amplitude frequency $A_s(f)$ at seabed depth X_s so that a single material layer will read as:

$$|A_S(f)| = |A_0(f) \cdot G_S \cdot R_S| \cdot exp\,(-2 \cdot \alpha_S(f) \cdot X_S)$$

(Pinson 2010)

And a second will add a further set of values:

$$|A_R(f)| = A_0(f) \cdot G_S \cdot G_R \cdot (1 - R_S^2) \cdot R_R \cdot exp\,(-2 \cdot \alpha_R(f) \cdot X_R)$$

This can be refined as:

$$\frac{A_S}{A_R}(f) = \frac{G_S}{G_R} e^{-(\alpha S - \alpha R) f x}$$

(Pinson 2010)

Using Pinson's two-layer equation alongside the Wang 2016 Q-Factor model, it was possible to identify a selected area of survey line for which there was known core evidence, bright reflector beds, highly suggestive of peat a strong sea bed horizon and an equally strong palaeochannel base for analysis. A trace analysis was run, set in a window between the two horizons in order to cross plot the frequency against Q values for known velocity and depth of known material composition. Survey *Line 11A* was chosen as an ideal candidate having a self-contained feature as well as containing three analysed cores within close proximity (Figure 5.9 below). By looking at the specific window of 250 traces between shotpoint 42,250 and 42,500 and taking the seabed as a source point (A_S) and the Holocene palaeochannel as the lower frequency limit (A_R), it was possible to look for correlations between organic evidence in the cores, and in the Q-Factor leading to attenuation coefficients dependency on frequency.

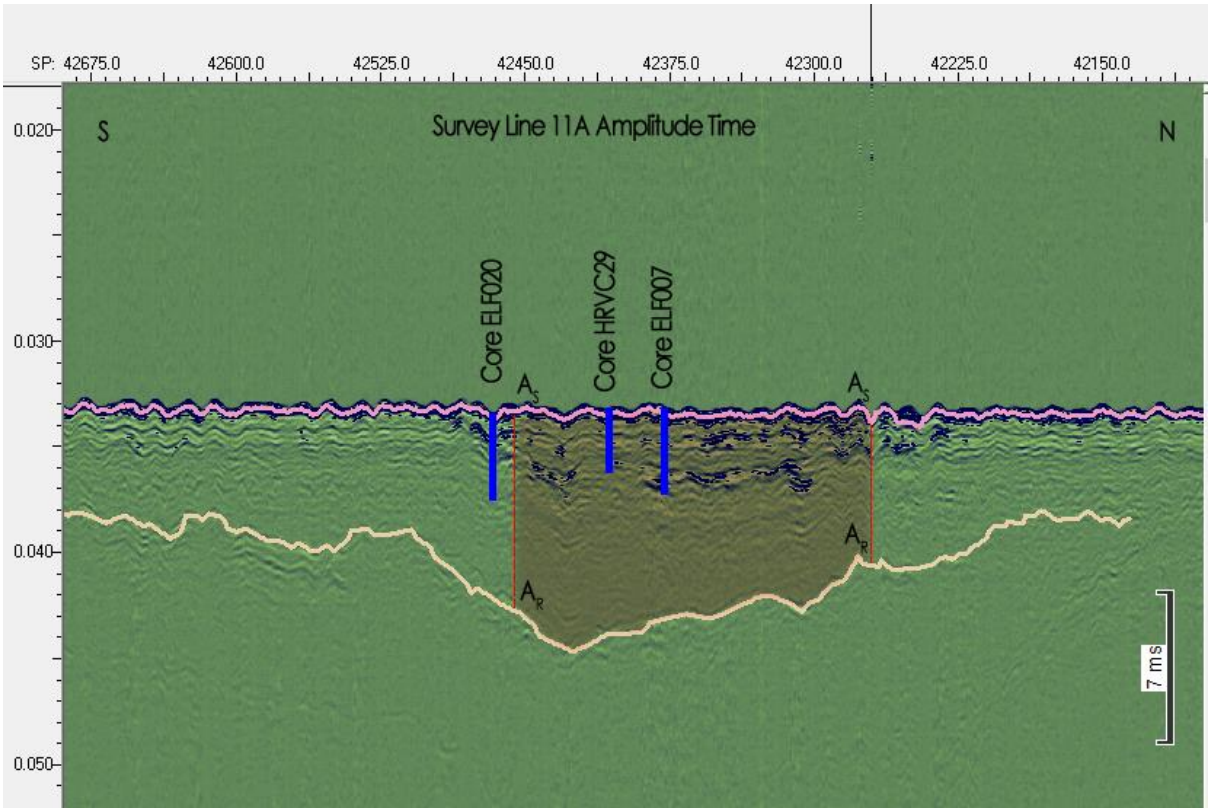

Figure 5.9 Trace Analysis from Upper Horizon As to Lower Horizon A_R

The environmental reports for Core *ELF020, CORE HRVC29* and Core *ELF007* demonstrated a predominantly sandy-silt lithography (see following chapter for full description). Therefore, it was expected that the Q-Factor ranges would fit Wang's 2016 prediction of sandy-silt sediment of 35 to 75 at -and up to- the 3.5 kHz frequency range.

5.8 Phase Analysis

Finally, as proposed in Pinson's final equation, a Phase function was identified as a calculation of velocity to measure the delay and angle of the wave against the frequency (Pinson 2010). Phase is a characterisation of a wavelet that may possess the same amplitude but represents its energy with polarity spectra that are distinct, dependent on the wavelet (Brown and Poulton 1996). Figure 5.10 below demonstrates the energy patterns of differing phase wavelets (Sheriff 2012). A minimum phase wavelet (a) energy arrives early producing a small negative polarity. A linear phase shows linear polarity b). Maximum phase c) demonstrates a lag which results in angular polarity known as a doublet (Aki and Richards 2002). The zero-phase wavelet d) falls on the zero polarity as the wavelet dissipates equal energy before and after the wavelet, cancelling the polarity.

Instantaneous Phase function has been used extensively to 'identify sequence boundaries and visualise bedding features' (SEG Wiki Resource) and can be performed in numerous ways in IHS Kingdom. More complex phase functionality such as full phase filtering or cosine phase function may have delivered more granular results but for the purposes of this research were considered excessive.

In order to identify the boundaries and test Pinson's 2012 scenario along with the equations for Q Factor analysis above, a simplified instantaneous phase function utilising a Hilbert's transform on the seismic trace with an envelope was employed. Using this phase function, the analysis could no longer rely on the amplitude peaks of the seismic p-waves. Thus, it could not directly correlate the units identified in the phase view to 'bright' organic reflectors highlighted in the interpretations. It did however utilize frequency and velocity so was able to run the full trace analysis for the

Pinson equations (Pinson 2010). These data could then be cross referenced with the depth analysis and core references.

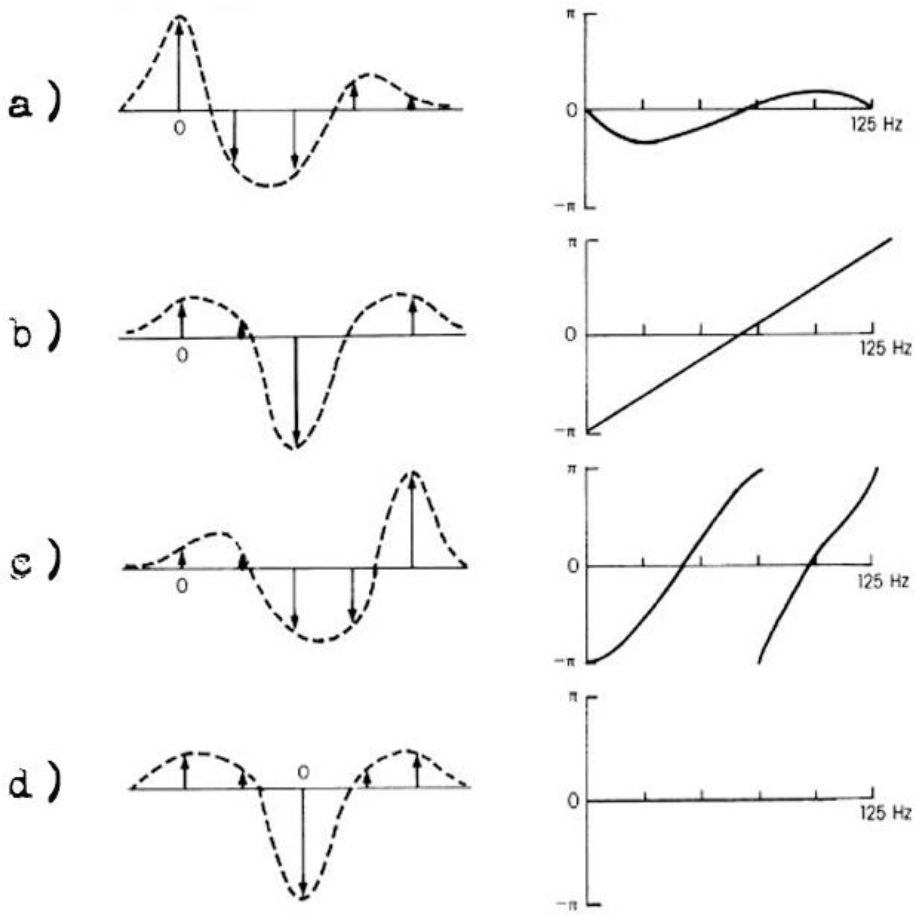

Figure 5.10 four types of phase wavelet and their corresponding polarity: a) Minimum Phase, b) Linear Phase, c) Maximum Phase, d) Zero Phase (Sheriff 2012)

These results suggested that the IHS Kingdom Phase view, when optimised for a simplified basic colour bar that displayed only extremes, could be used to display unit boundaries. By isolating the phase wavelet and delineating the neutral, positive and negative variances, it could be ascertained that at each of these boundaries, the net polarity was zero, yet directly above and below were strong negative and positive swings. This was suggestive of zero phase wavelets and needed further investigation on all coring sites.

The addition of a variable area wiggle overlay placed over the survey area also showed filled in peaks of significant variance in the phase view. These correlated with high amplitude negative reflectors picked as

'bright' reflectors. Analysis of how these variance 'wiggle kicks' related to unit boundaries in amplitude or to the zero polarity in the phase was required in the next step of research.

Therefore, frequencies and the polarity strength of the phase signals were recorded and correlated with the amplitude strengths from the original survey view and marked on the interpretation. These data were then analysed to determine if specific signals could be tied to individual unit types, classifications or even to the peat layers within the core depths. Would it be possible to isolate peat over other organic signals by utilising polarities of the phase function alongside amplitude intensity?

To summarise, cores containing peat were identified within the study area and analysed alongside interpreted seismic data. To match the lithostratigraphic unit divisions in the cores to the interpreted horizons of the seismic and new multi-step and weighted velocity model was created. Further investigation on the seismic attenuation of the interpreted organic sediments identified correlation between abrupt contacts of different sediment types in accordance with the findings of Wang (2016). This related to Q Factor. Trace analyses of the seismics were run alongside instantaneous phase to determine if the sediment classification could be determined.

6 CASE STUDY RESULTS

6.1 Environmental Core Analysis & Initial Interpretation

The lithostratigraphy and environmental reports from the focused coring programme were provided by specialist archaeologists from the Europe's Lost Frontiers Project and the Humber REC (Tappin et al 2011; M Bates pers. Comms). Figure 6.1 below shows the study area in which the survey lines and cores originate. These data were analysed line with the methods presented in chapter 5.2, to calculate precise values, or in some cases, estimate ranges for unknown classifications. This was performed on a core-by-core basis.

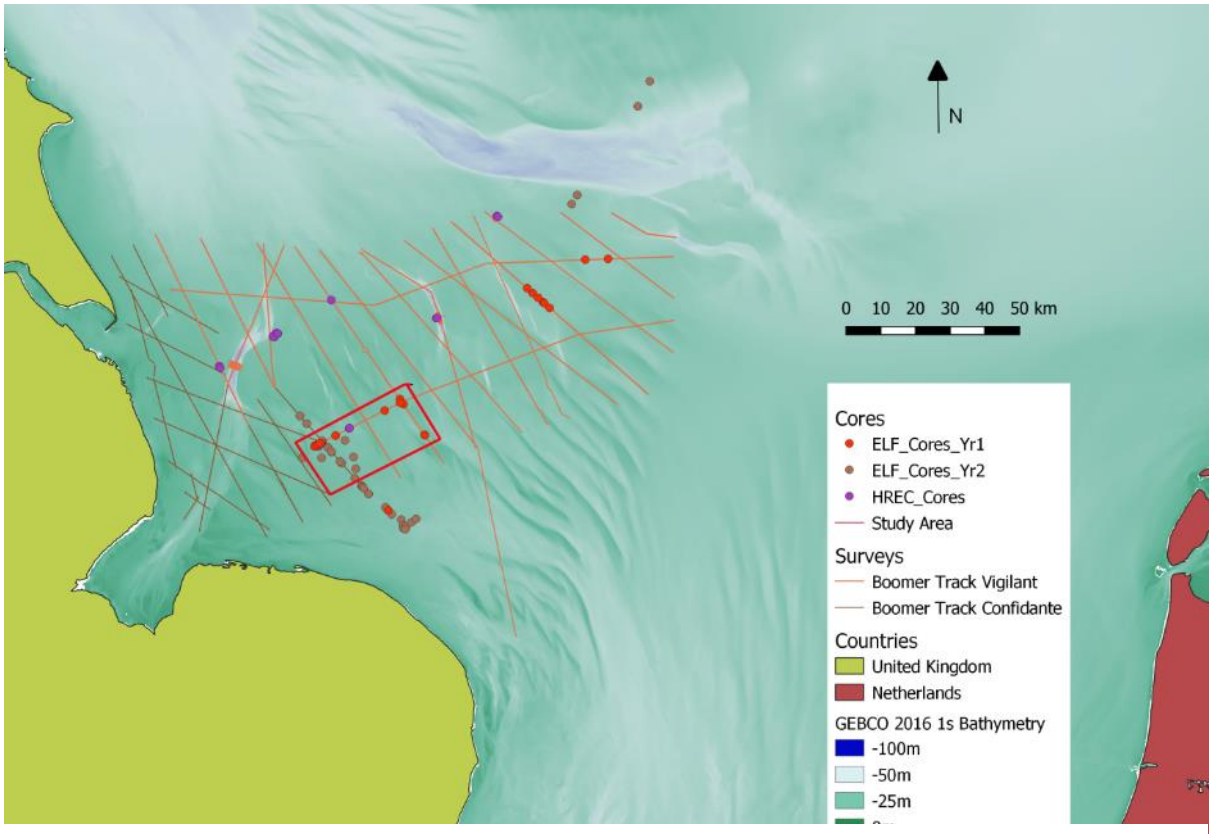

Figure 6.1 Study Area within larger coring environment

Within the study area were three coring datasets taken from three separate missions as set out in Table 5.3 in the previous chapter. As ascertained, all of the cores contained peat in varying amounts, and each were positioned on attributable survey lines and could therefore be ground observed.

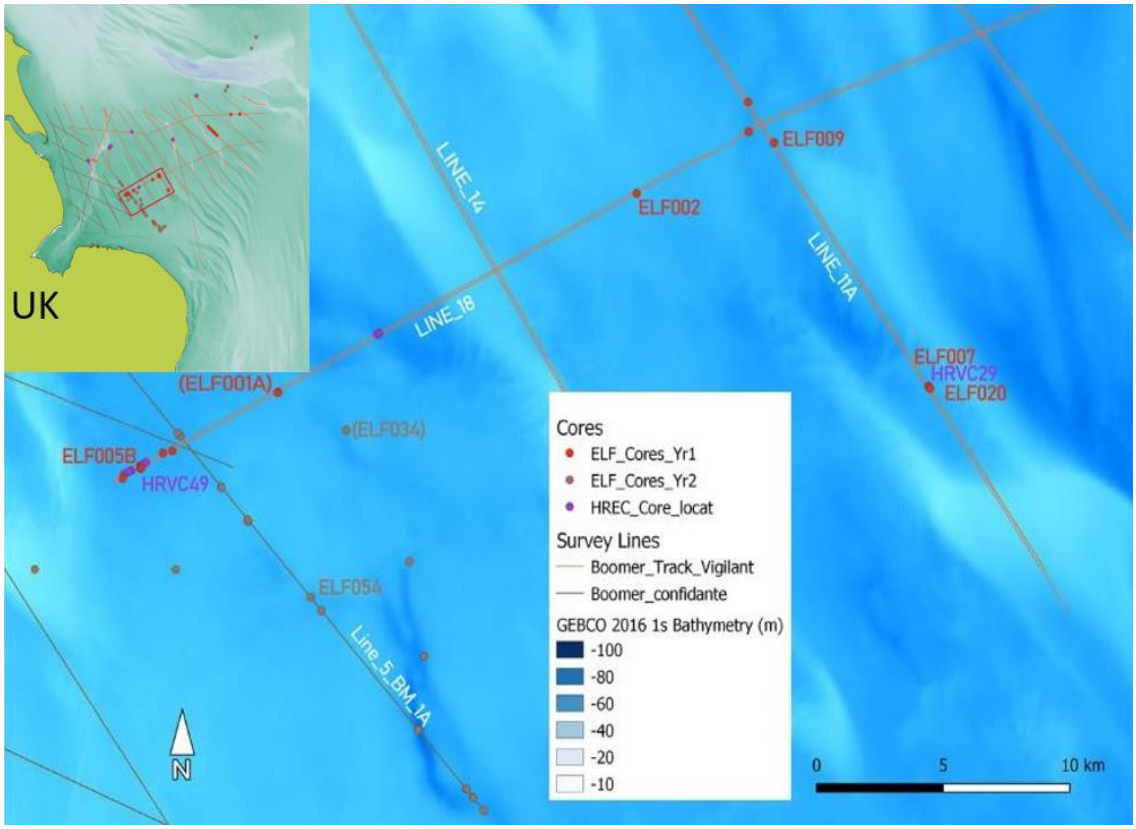

Figure 6.2 Close up of the study area with prominent cores and survey lines marked

The lines upon which they were cored (as per Figure 6.2) were:

- *Line_18* running approximately west southwest to east northeast along which *ELF005B* and *HRVC49* were located toward the western end and *ELF002* toward the eastern end. A second survey line running parallel to *Line_18* but 100m to the north named *Line_18_100N* was also referenced for interpretative and spatial analyses.
- Close to its western end, *Line_18* was bisected by *Line_5_BM_1A*. This survey line travelled north northwest to south southeast finally ending in the visible feature of the Southern River area. Here, extensive coring and dredging revealed interesting settlement potential. This survey line contained study core *ELF0054*.

- The final survey line was *Line_11A* at the eastern side of the study area. This ran north northwest to south southeast, bisecting *Line_18* at the very eastern end. On this line were four peat contextual cores. The first; *ELF009* lay close to the survey crossline. The other three coexisted in the same wide river valley feature and were drilled over two different coring missions (Tappin et al. 2011). *ELF007, ELF020* and HRVC029 were cored at either side of the shallow valley and one HRVC029 into the river sediment at the bottom.

Also illustrated in Figure 6.2 above, Core ELF001A lies very close to *Line_18*. This core proved to be very important to the furthering of archaeological knowledge about the dating of the early Holocene inundation and evidence of the Storegga Tsunami (Gaffney et al. 2020). It was not included in this study due to lack of organic sediment. Core ELF034 which did contain ample peat and suggested a saddleback mire feature, was also noteworthy. This core lay directly between *Line_18* and *Line_5_BM_1A*. Unfortunately, no survey line fell directly over this core and so could not be investigated but should be considered for future survey work. A further survey line (*Line_14*) ran north northwest to south southeast midway through the study area but contained no relevant cores and was likewise not investigated in this thesis except for wider-scale environmental implication for spatial mapping and artificial networking (see Chapters 7 and 8).

6.2 Seismic Interpretations of Horizons & Identification of Holocene Features

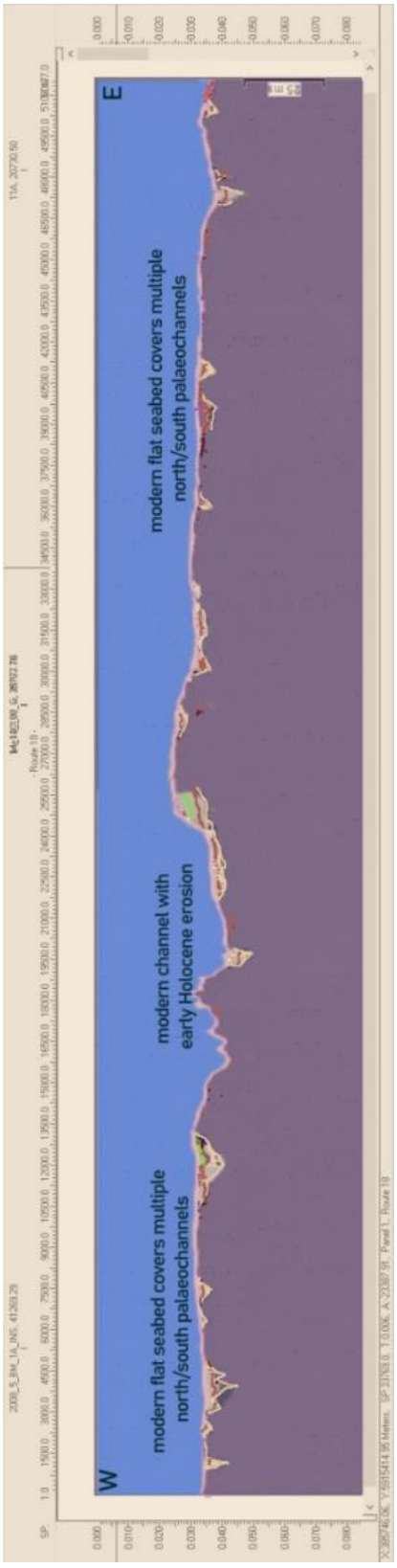

Figure 6.3 Survey Line_18 in its entirety. Vertical scales have been exaggerated for clarity

6.3 Line 18 Core Interpretations

Examination of each core revealed the lithology divided into geomorphological units. Further material classification was added which allowed a wider environmental view of the survey line to be built up (Figure 6.3). This showed an area of changing terrestrial nature during the last glacial maximum to marine in the early Holocene. The pre-inundated landscape crossed a wide flattish plain with shallow but active braided riverine features with wider gravel waterbeds and reed or marsh areas, especially to the west-south-west. A number of relict palaeochannels on a north-south alignment also crossed this survey many exhibited erosional marks that looked likely to have been caused by glacial riverine outwash channels.

6.3.1 ELF005B & HRVC49

Due to the proximity of these cores, they were examined together as part of the same submerged feature. *ELF005B* (Figure 6.5) was located 8.2m south of the survey line, still within the river feature. *HRVC49* is plotted directly on the survey line on the shallow valley side. Both cores collected approximately 2m of material. While there was no definite peat within *ELF005B*, there was 4cm of 'silt/peat' containing plant and wood fragments and salt marsh deposits. *HRVC49* (Table 6.1) contained a 6cm layer of peat and a thicker layer on either side of peaty silts and clays. Both cores demonstrate abrupt contacts and strong laminated fine overlying deposition, and several other cores were sunk in the the vicinity (though not on these survey lines) contained silty peats and peaty silts. A number of bright reflectors were present throughout the landscape feature, appearing on the shallow channel sides close to this area, a very good predictor for soligenous peat development on the valley slope. A survey line that travelled exactly parallel to *Line_18* but 100m north also displayed a similar wide shallow riverine feature in the same position (Figure 6.4). As with *Line_18*, *Line 18_100N* survey, demonstrated strong beds of organic reflectors on the shallow slopes of the riverine valleys, which also suggested widespread soligenous peat and would most likely present similar cores to those of *HRVC49* and *ELF005B*, comprising peat and organic silts were it to have been cored.

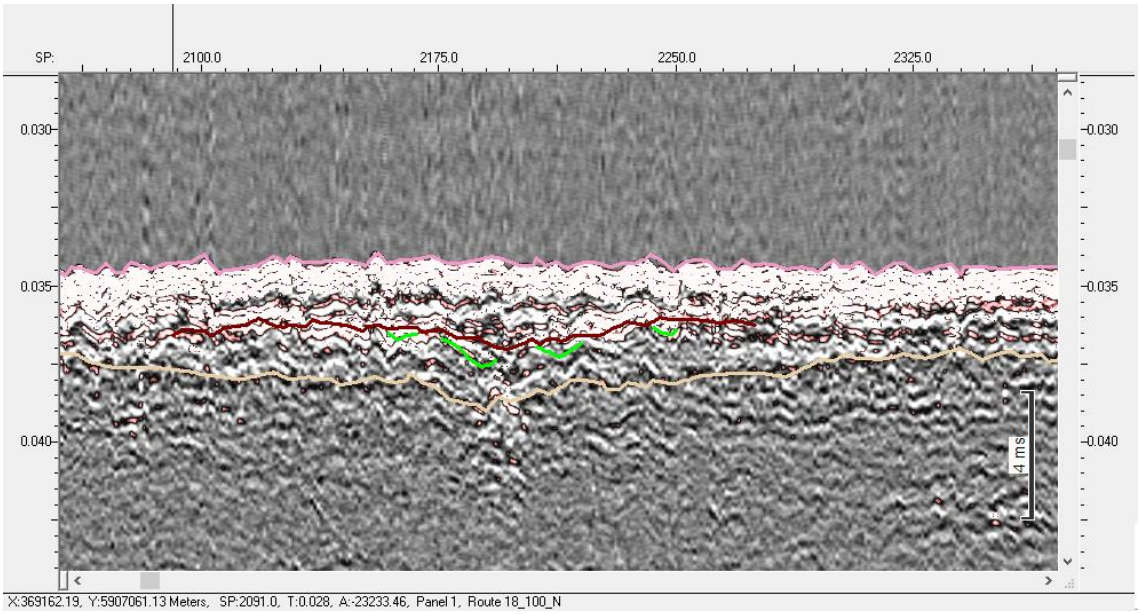

Figure 6.4 *Line 18 100N* showing similar high quantities of reflective signals on shallow slopes

Core *ELF005B* (Figure 6.5) was interpreted to originate in an environment of shallow, slow-running or even stagnant water. During the final terrestrial phases, brackish waters within a marshland or estuarine bed was suggested by the organic remains. The core was drilled from the base of a shallow valley and contained base units of riverine silts and gravels. These were overlain by what was described as a peaty silt (Ag2)/ (Sh2) with 'woody fragments' (DT)/(DG). Though not specifically peat, the Ag2 silts were not sufficient to discourage a seismic interpretation from an assumption of marsh-fen associated peat bed.

4cm of silty peat, though thin, were abrupt and fulfilled the criteria for boundary contacts needed in the research. The lack of material compared to the bright reflectors present in the seismic survey may be due to distance from the line or even the organic fragments. Depth corrolation later in the chapter would be needed to analyse the results.

ELF005B

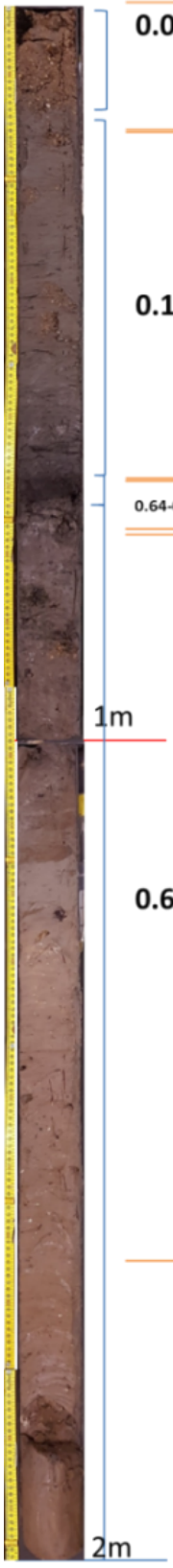

0.00-0.13m	Unit Ia Gmin2 Gmaj2	Greyish brown to brown shelly sand. Structureless. Moderately compact.
0.13-0.64m	Unit IIa Ag1	Mid to dark grey laminated silt, becoming dark grey below 0.60. Common, wavy, sub-parallel laminations 1-2mm thick, becoming more common below 0.60. Occasional brown, organic, fragments
0.64-0.68m	Unit IIb	Dark grey to brownish grey organic silt/peat with brown woody fragments. Fairly compact.
0.68-2.0m	Unit IIc Gmin2	Mid brownish grey silty fine sand with occasional stones <1cm. Structureless. Relatively loose.

Figure 6.5 ELF005B photograph and Lithography courtesy of M Bates, Lost Frontiers 2017. Adapted by author

Core *HRVC49* (Table 6.1) was located at the valley edge. The core showed evidence of chalk gravel at 1.0m which would seem likely to have been the valley feature. A further 0.83m of material was captured in the core but unreported in this instance. The palaeo feature into which both cores were drilled was very shallow, a total of 3ms response time *HRVC49* was drilled through modern coarse sands and two layers of organic rich units with abrupt contacts between them. The vertical distance would prove too small for the resolution of the surveys to differentiate between these. The clayey peat then gave onto chalk gravel base. This suggested a shallow chalk stream or aquifer and therefore immediately called to mind a source of flint or chert, making this area a valuable economic resource. *ELF005B* delves a little deeper though the survey is misleading to say it hits the river bottom. The core is 8.2m south of the survey and the vertical scale has been magnified on the seismic display.

HRVC49

Project		Humber REC	Borehole	HRVC49
Easting		590697	Northing	369207
Water Depth		24.9m	Total Recovery	1.83m
Date to laboratory			Date recorded	
Date sampled			Location of samples	
Depth below ground surface (m)	Unit	Lithological description		Troels Smith
0.0-0.14m	Ia	coarse sand with small stones		Ga2 Gg(min)1 ptm1
0.14-0.30m	IIa	organic rich silt		Sh2 Ag2
		--Abrupt Contact --		
0.30-0.36m	IIb	Well humified silty peat.		Sh3 Ag1
		--Abrupt Contact --		
0.36-0.83m	IIc	Clayey-silt with organic, decreasing to base		Ag2 Sh1 As1 Gg(min)+
0.83-1.00m	IIIa	Stiff grey brown clay with occasional chalk gravel		As3Ag1
1.0-1.83m		unreported		
		--- Base 1.83m ---		

Table 6.1 Data from the Humber REC Environment Report by Dr Benjamin R. Gearey and Emma-Jayne Hopla adapted by the author to correspond to seismic interpreted colours.

Fig 6.6 shows a basic interpretation of the shallow valley feature. Three main unit boundaries were recorded in the core reports. Despite poor resolution on the seismic survey all three were visible in the data with the palaeo feature prominent at the base. Unit Ia and IIa at the seafloor (pink) were uniformly bright with strong negative amplitude waves but little attenuation of signal. Units IIb and IIc contained the laminated silts, clays and the organic layers. It was with these units that the bright reflectors

appeared at amplitudes of -17,000 p-waves. *ELF005B* contains half a metre of parallel laminated clay silts. These laminations appear relatively uniform, demonstrating a prolonged transgressive period but do not appear on the amplitude surveys. What was pronounced in the survey was an abrupt unconformity that ran the length of the feature with brighter notes at the edges of the valley sides. This was possibly an erosional area, exhibiting stronger negative peaks at around -25,000 p-wave ranges.

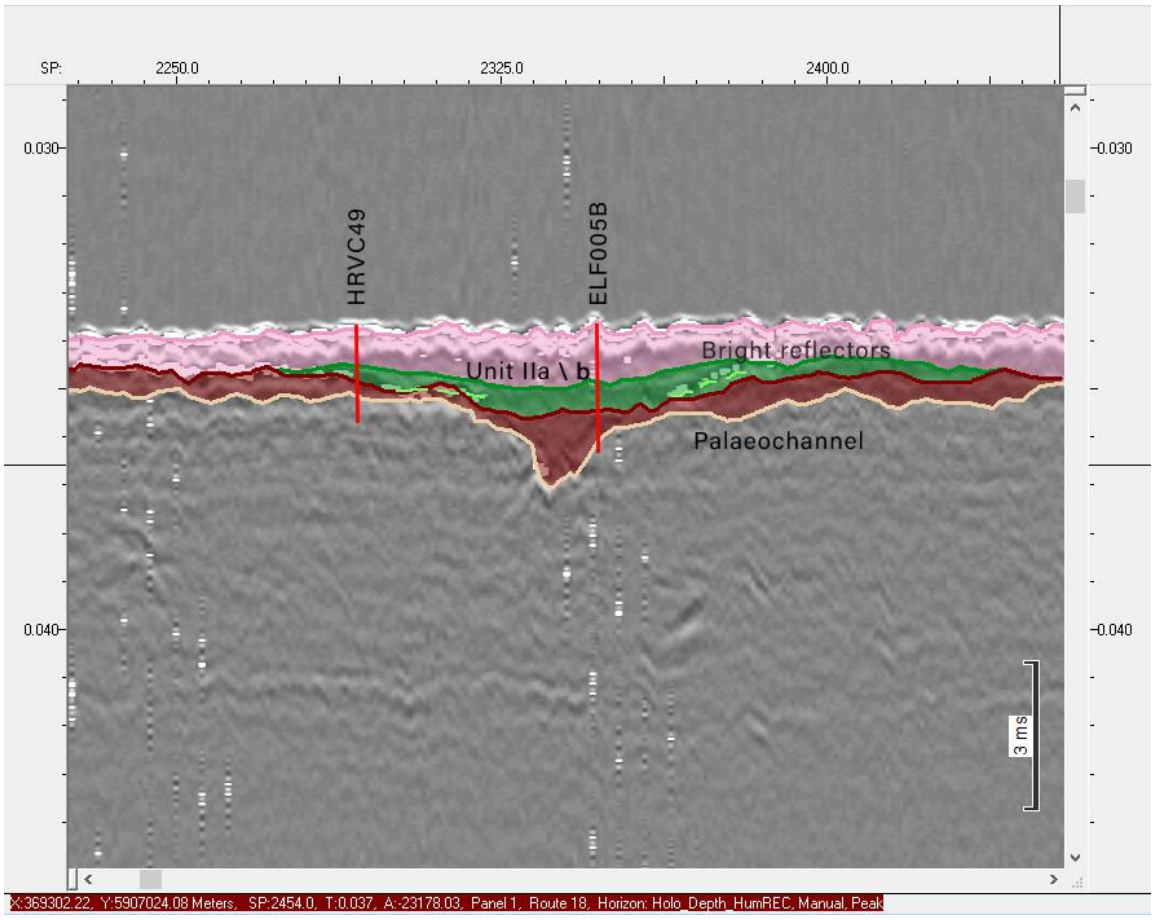

Figure 6.6 Basic Interpretation of HRVC49 and ELF005B showing unit lithology as per Table 6.1

The palaeochannel itself was possibly a shallow aquifer or chalk river bearing a source of flint and chert as hinted at by the Core *HRVC49* report, or a widespread marshland as suggested by the surrounding survey lines. The full extent of this potential marshland was unknown but as shall be demonstrated later in this chapter, this section of the study area contains the greatest mass of organic amplitude reflectors found on any of the survey lines in the study area. Spatial interpolation of the extent was performed (Chapter 7) to attempt to tie in the landscape of this marshland with the saddle fen peat found in core *ELF034*. As has been explained

previously however, no supporting survey lines existed to ground observe this interpolation.

6.3.2 Core ELF002

Towards the eastern end of the survey *Line_18* there was a similar pattern of flattish modern seabed covering shallow Holocene features and north-south glacial outflows. In the wide, shallow feature in which core *ELF002* was drilled there was evidence of riverine activity, silts and graduated infills. The lack of depth indicated the torpidity of water flow, but the bed stretched for many metres. The core itself (Figure 6.7) contained upper units of modern sands which had been repeatedly agitated. These overlay fine laminated clays. Such laminations accumulated gradually but continuously with repeated transgression events over hundreds of years. A total thickness of 0.9m of fine laminated clays made up unit IIa in Core *ELF002*. The peat layer below the clay however demonstrates an abrupt boundary and is classified as decomposed, amorphous, compact, dry and firm. This confirms that the peat developed into the accommodation space offered by the clays. A second peat layer of 1cm thickness, separated by a 6cm thick silt-sand boundary did not show on the seismic survey as an independent signature due to insufficient vertical resolution. Below, an abrupt contact and then silty sand with gravel and chalk signified the core touched upon the base of the riverine feature.

ELF002

0.20-0.62m	Unit Ia Gmin2 Gmaj2	Clast supported yellowish brown gravel. Poorly sorted, Very coarse sand matrix. Common shell fragments. Loose & structureless.
0.62-1.95m	Unit Ib Ga2Gg(min)2	Greyish brown becoming grey, shelly sand with occasional gravel & large shell fragments 5/6cm thick, Otherwise shell fragments scattered throughout. Loose & unconsolidated.
1.95-2.85m	Unit IIa Ag1	Mid grey, slightly brownish, clay silt. Finely laminated 102mm, wavy & sub parallel. Discontinuous. Occasional shells & shell fragments. Below 2.42 laminations thicker, shell fragments increase, some articulated bivalves present. Soft & pliable.
2.85 – 3.0m & 3.07-3.08	Unit IIb Sh H10	Very dark brown peat with horizontal *phragmites* remains. Very compact, firm, amorphous.
3.10 – 3.64m	Unit IIc	Fine, silty sand, gravel and chalk clasts.

Figure 6.7 Core ELF002 (Photograph and lithology courtesy of M Bates, Lost Frontiers 2018 Adapted by author.

Initial interpretations (Figure 6.8) of the surveyed feature reveal the channel and two distinct unconformities which relate to the main abrupt unit boundaries within the core. The high negative peak signal ranges of -32,000 and -29,000 p-wave amplitudes respectively demonstrate distinct change from one material type to another – sands to clay, clays to organic. The laminated clay layers suggest a gradual and continual prograding transgression with the horizons marked semi-parallel. Lack of a bright amplitude response at the organic boundary is worth noting for discussion. If this was due to compaction or desiccation, as suggested in the peat description, it may necessitate an increase to the velocity model timing above Hamilton's 1970 model to account for the density \ lack of void space.

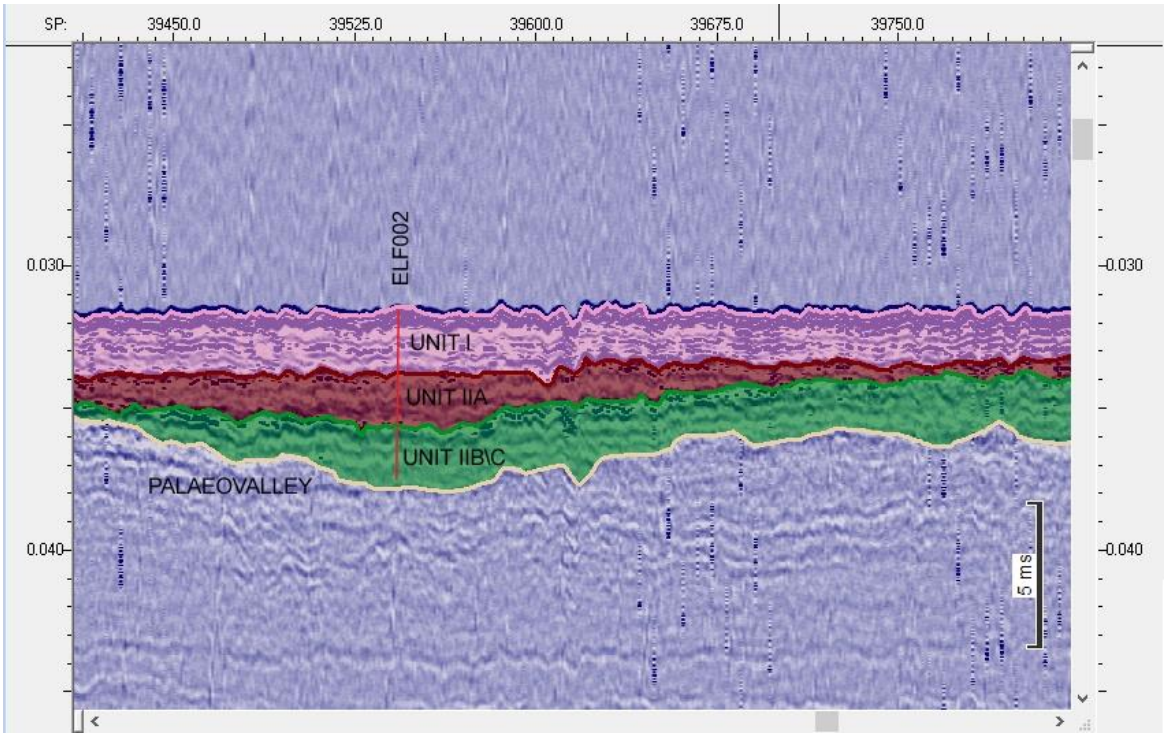

Figure 6.8 Basic Interpretation of ELF002 Core Lithography

6.4 Line 11A Core Interpretations

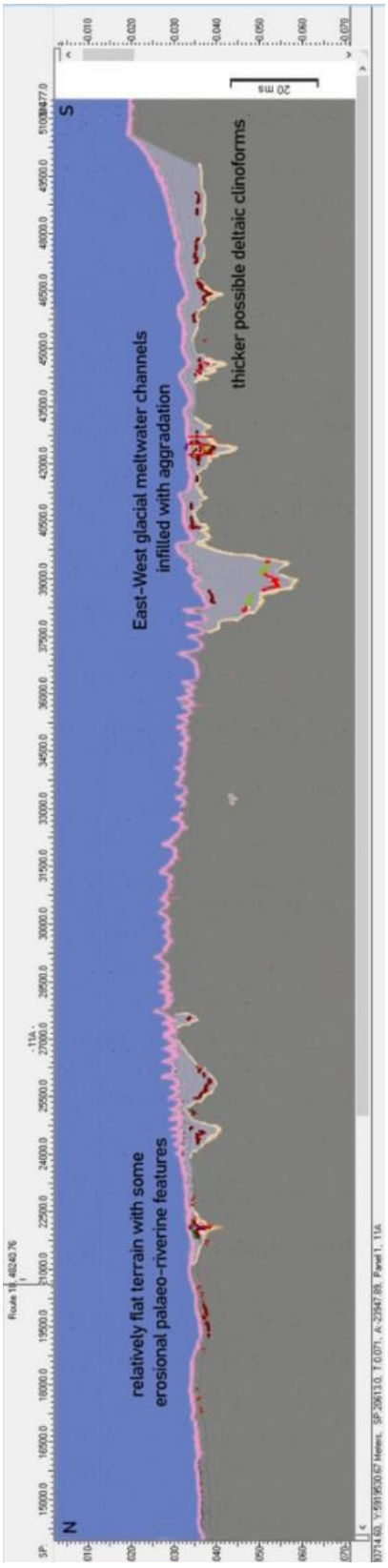

Figure 6.9 Line_11A in its entirety. Vertical scales are exaggerated for clarity

Survey *Line_11A* runs approximately north-west to south east, intersecting *Line_18* at its eastern end (Figure 6.9). The subsea topography showed a flattish landscape that ran from inland plain to coastal or possibly deltaic river outflow. Progradation occurred toward the southern end in pre-glacial times. The landscape had been terrestrial during the LGM and finally marine in the early Holocene. Along the survey length, recent sedimentology demonstrated a landscape punctuated with glacial outwash valleys and low-lying basins, infilled with uniform rising onlap clinoforms and –toward the southern end – possible prograding deltaic clinoforms. A deeper east-west channel bisected the survey two-thirds of its length south providing a major riverine artery. Four cores in two major features were employed in this study; core *ELF009* in a single narrow river feature towards the north of the survey and cores *ELF007*, *HRVC29* and *ELF020* made up a separate study in a second, wider shallow basin feature to the south of the large east-west channel.

6.4.1 Core ELF009

The upper two units within this core demonstrated much disturbance (Figure 6.10). Shells and gravel were deposited throughout and the whole may have been reworked a number of times through the recent Holocene. Below this however, unit IIb and IIc were distinct and presented almost 2m of fine clay-silt laminations with abrupt, sharp contacts with organic deposits. The bottom-most layer of peat is cut off at the base of the core and may have run much deeper than the core suggested. Certainly, there was no indication that the core had penetrated to the base of the palaeo feature. The peat deposit below the clay silt in ELF009 was dry, compacted, highly decomposed and dense. The boundary between the laminated overlying silts and peat was eroded and contained sands and shells which could have made the organic reflector display less of an organic signal than an abrupt contact against pure clays but that did not appear to be the case.

Initial interpretation of the seismic data shows in fact that the bright responses were as perturbed as the core evidence. There were obvious suggestions of soligenous peat beds and valley fen infills but other signals with equally high amplitude responses were harder to explain. These appeared throughout the survey data and appeared at depths corresponding to units IIb and IIc.

ELF009

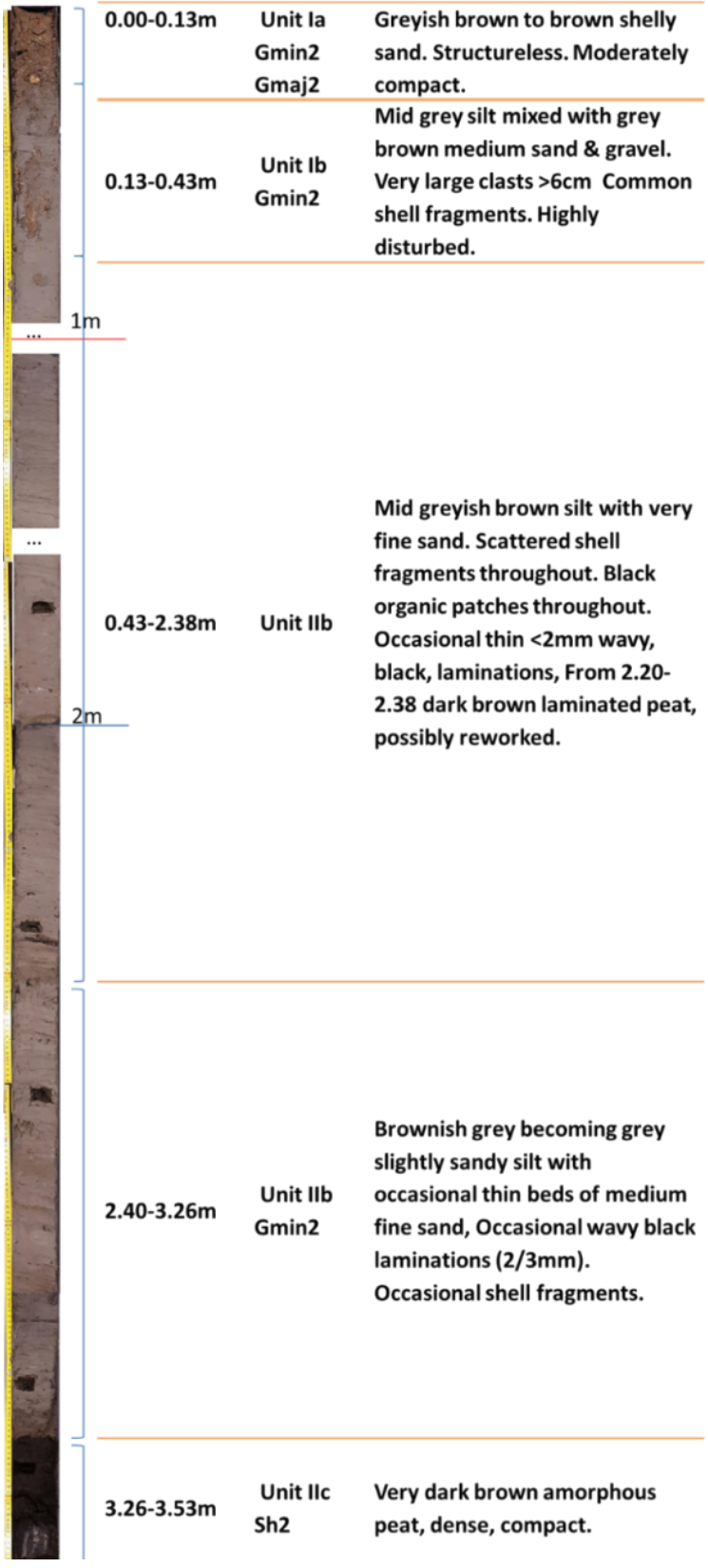

0.00-0.13m	Unit Ia Gmin2 Gmaj2	Greyish brown to brown shelly sand. Structureless. Moderately compact.
0.13-0.43m	Unit Ib Gmin2	Mid grey silt mixed with grey brown medium sand & gravel. Very large clasts >6cm Common shell fragments. Highly disturbed.
0.43-2.38m	Unit IIb	Mid greyish brown silt with very fine sand. Scattered shell fragments throughout. Black organic patches throughout. Occasional thin <2mm wavy, black, laminations, From 2.20-2.38 dark brown laminated peat, possibly reworked.
2.40-3.26m	Unit IIb Gmin2	Brownish grey becoming grey slightly sandy silt with occasional thin beds of medium fine sand, Occasional wavy black laminations (2/3mm). Occasional shell fragments.
3.26-3.53m	Unit IIc Sh2	Very dark brown amorphous peat, dense, compact.

Figure 6.10 Core ELF009 Photograph and lithology courtesy of M Bates, Lost Frontiers 2018 adapted by author

The amplitude responses included a number of strong negative reflections in the range of -18,000 to -27,000 p-waves in the vicinity of the core in Figure 6.11 below including one particularly strong reflector directly beneath the core that reflected in the negative amplitude range of -33,000 p-waves. However, there were no bright reflector signals that actually touched the core. It must be borne in mind that the core was 2.1m from the survey line and these reflector locations would change to some degree.

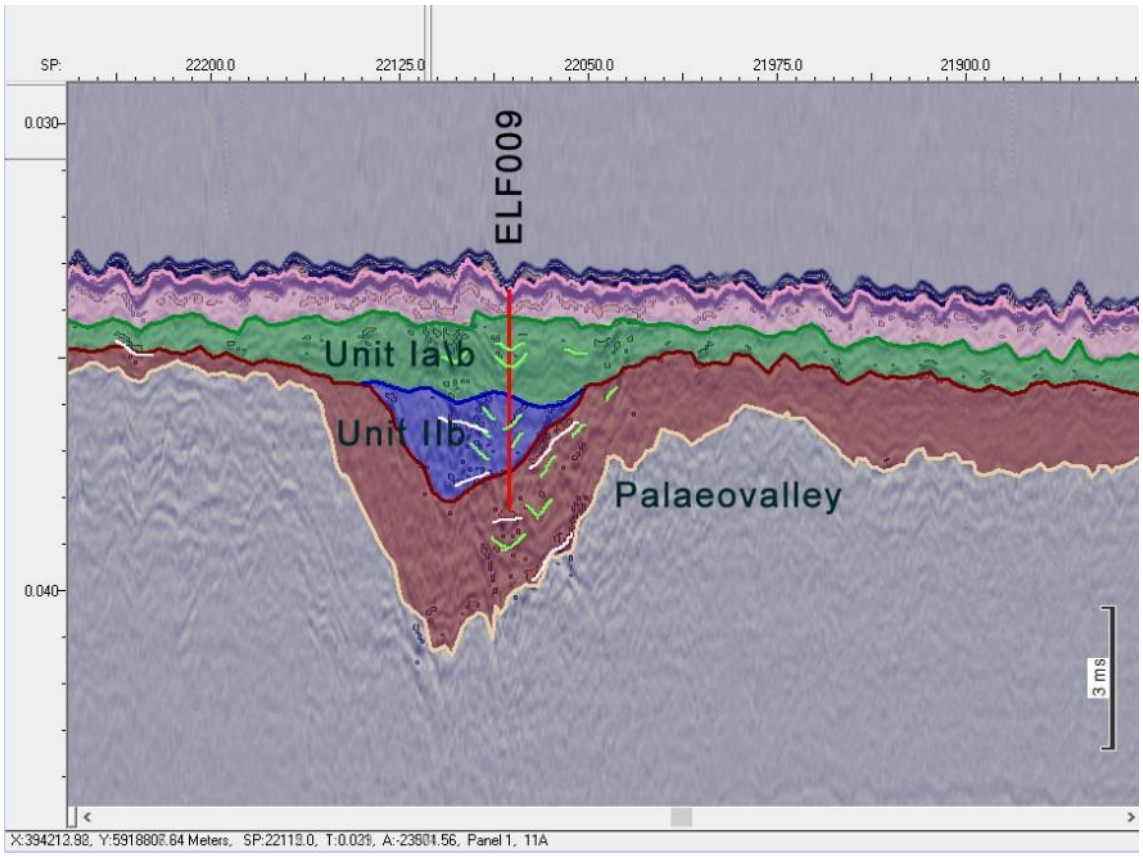

Figure 6.11 Initial interpretation of the area surrounding core ELF009 showing bright reflectors (white).

6.4.2 ELF007, HRVC29 & ELF020

The next wide but shallow valley feature shared much in common with that of the valley cored for *ELF002* but on this line, three separate cores were drilled into the bed and were best described as one feature. Each core shared common units found throughout the feature. Uppermost 75cm (Units Ia and Ib) were coarse and shelly sands crudely bedded turning to medium. These also contained raw flints and stone. By 1m in all cases these had given way to Unit IIa silts or clayey silts with wavy, horizontal or dipping laminations.

The gradual facia changes demonstrated no sharp contacts between sands and silts in the core report yet presented distinctly on the seismic survey. It was the bed of almost continuous bright reflectors below this layer that defined the boundary between unit IIa and IIb and that tied the peat depths in the three cores (Figure 6.12). Core *ELF007* (Figure 6.13) had abrupt contacts at 1.92m and 2.01m and thus marked the beginning of two distinct peat layers. However, due to the vertical resolution issues raised in Chapter 5, the 7cm gap between the two proved insufficient to differentiate within the 6.2cm vertical resolution limit. The best that could be gleaned was one larger layer. The peat in core *HRVC29* (Table 6.2) occurred much higher, at 1.36m and due to the lack of a sharp boundary the boundary between the similar material types of organic silts and organic peat had to compete with stronger boundaries such as that between the shelly sand with flint and the organic clay / silt at 0.75m to pick as the bright reflector. *ELF020* (Figure 6.14, p.148) similar to *ELF007* in the depth observations of clay laminations and the sharp contact to the peat bed marked another double thin layer, indistinguishable on the seismics. Instead, displayed as a single 26cm layer. *ELF020* also tied up with *HRVC29* in hitting the chalk base of the channel beneath the bright reflector bed. Intercalated flint deposits in chalk beds are of huge interest to archaeologists as a reference to potential settlement. Raw flint was also found in the upper unit of core HRVC29.

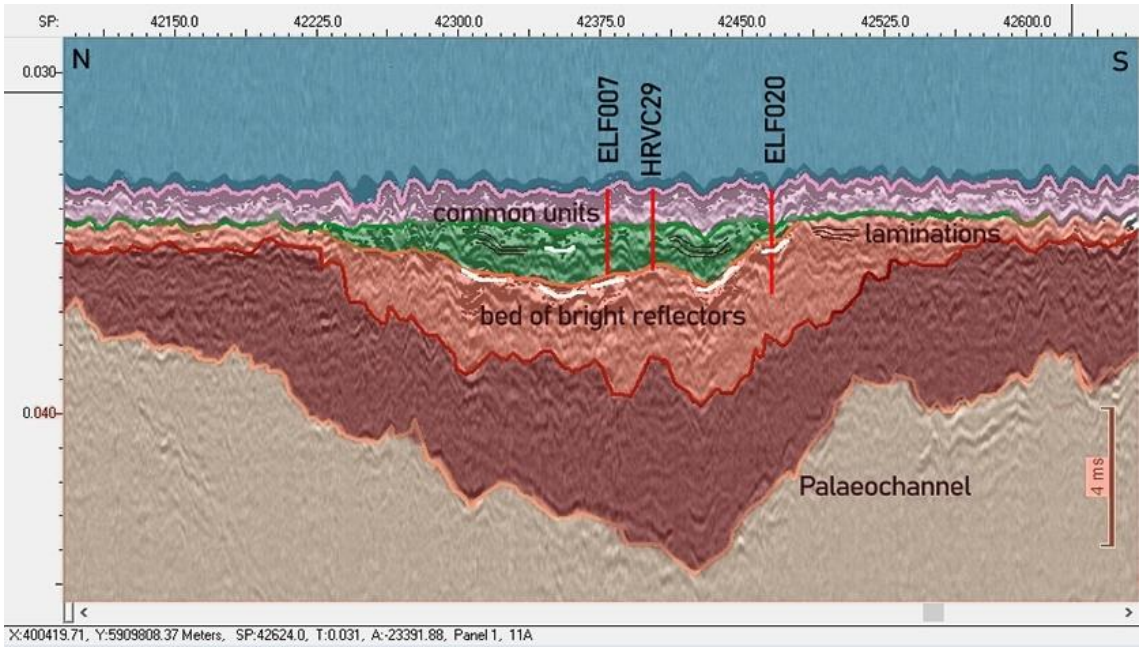

Figure 6.12 Basic Interpretation of feature containing cores ELF007, HRVC29 and ELF020 with the bed of bright reflectors below and laminated units above

The reflective amplitude response from this location proved excellent with strong signals peaking at between -27,000 and -30,000 in the p-wave range. The bright reflectors were present on the valley sides and consistently across the valley floor at the above amplitude ranges. With fine clastic laminations present throughout the unit IIa core evidence the potential of a valley fen peat bed across this feature was extremely high (Fig. 6.12). There was no requirement for bandwidth filters or use of envelopes in this interpretation. The negative reflectors were uniformly strong throughout the feature and presented an almost solid bedding of sediment unit. A higher band of equally strong negative reflectors above the laminated units, near the surface modern sands was interpreted as a layer of gaseous interference. This in itself was a good indicator of an organic presence beneath as the decomposition of organic matter produces such free gas that rises through the sediment layers.

HRVC29

Project	Humber REC	Borehole	HRVC29
Easting	5909879	Northing	400361
Water Depth	23.9m	Total Recovery	1.81m
Date sampled		Location of samples	

Depth below ground surface (m)	Unit	Lithological description	Troels Smith		
0.0-0.5m	Ia	Shell rich coarse sands and gravels	Gmin2 Gmaj2 Ptm++		
0.5 – 0.75m	Ib	Grey medium coarse shelly sands with occasional flints	Gmin3 Ag1		
0.75-1.36m	IIa	Grey clayey silt, black mottled humified organic fragments	Ag3 As1 Dg+		
		--Abrupt Contact --			
1.36-1.44m	IIb	Black brown well humified silty peat with wood fragments	Sh2 Ag1 Dg1		
1.44-1.60m	IIb	Grey brown organic silt with humified organic detritus	Ag3 Sh1 As+		
1.60-1.81	IIc	Grey medium coarse sands slightly silty with chalky gravels to base	Gmin4 Ag+		

Table 6.2 HRVC29 Data from the Humber REC Environment Report by Dr Benjamin R. Gearey and Emma-Jayne Hopla adapted by the author to correspond to seismic interpreted colours

ELF007

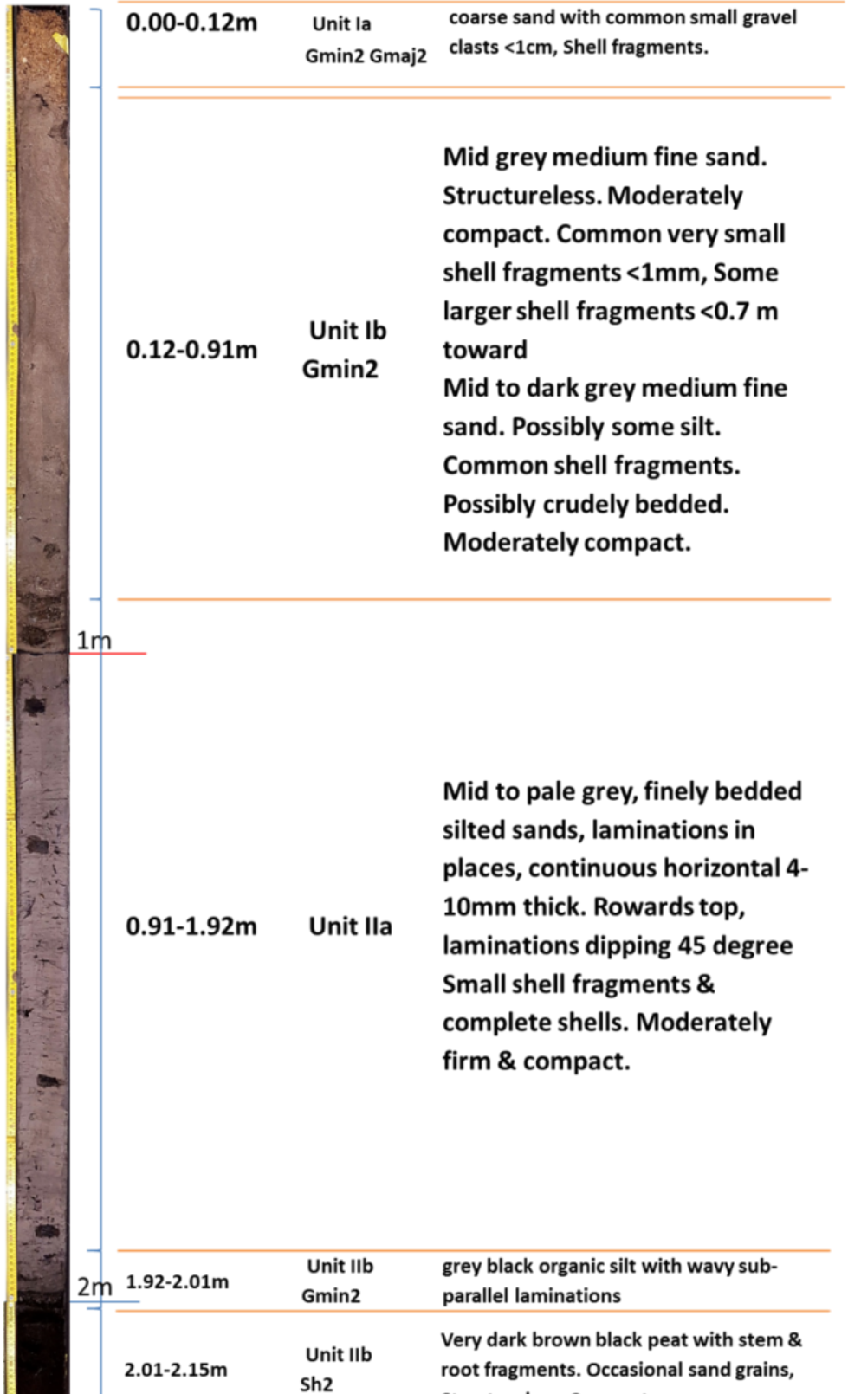

Figure 6.13 ELF007 Photograph and lithology courtesy of M Bates, Lost Frontiers 2018 adapted by author

ELF020

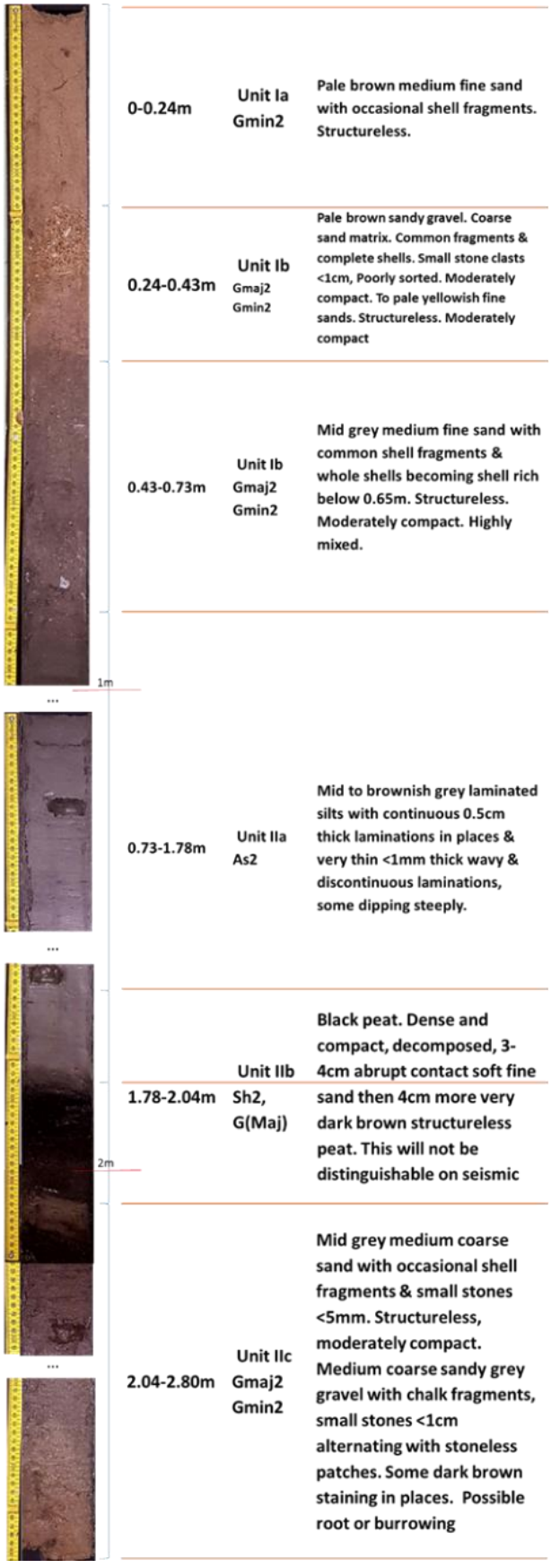

0-0.24m	Unit Ia Gmin2	Pale brown medium fine sand with occasional shell fragments. Structureless.
0.24-0.43m	Unit Ib Gmaj2 Gmin2	Pale brown sandy gravel. Coarse sand matrix. Common fragments & complete shells. Small stone clasts <1cm, Poorly sorted. Moderately compact. To pale yellowish fine sands. Structureless. Moderately compact
0.43-0.73m	Unit Ib Gmaj2 Gmin2	Mid grey medium fine sand with common shell fragments & whole shells becoming shell rich below 0.65m. Structureless. Moderately compact. Highly mixed.
0.73-1.78m	Unit IIa As2	Mid to brownish grey laminated silts with continuous 0.5cm thick laminations in places & very thin <1mm thick wavy & discontinuous laminations, some dipping steeply.
1.78-2.04m	Unit IIb Sh2, G(Maj)	Black peat. Dense and compact, decomposed, 3-4cm abrupt contact soft fine sand then 4cm more very dark brown structureless peat. This will not be distinguishable on seismic
2.04-2.80m	Unit IIc Gmaj2 Gmin2	Mid grey medium coarse sand with occasional shell fragments & small stones <5mm. Structureless, moderately compact. Medium coarse sandy grey gravel with chalk fragments, small stones <1cm alternating with stoneless patches. Some dark brown staining in places. Possible root or burrowing

Figure 6.14 ELF020 photograph and Lithography courtesy of M Bates, Lost Frontiers 2017 adapted by author

6.5 Line 5 BM_1A Interpretations

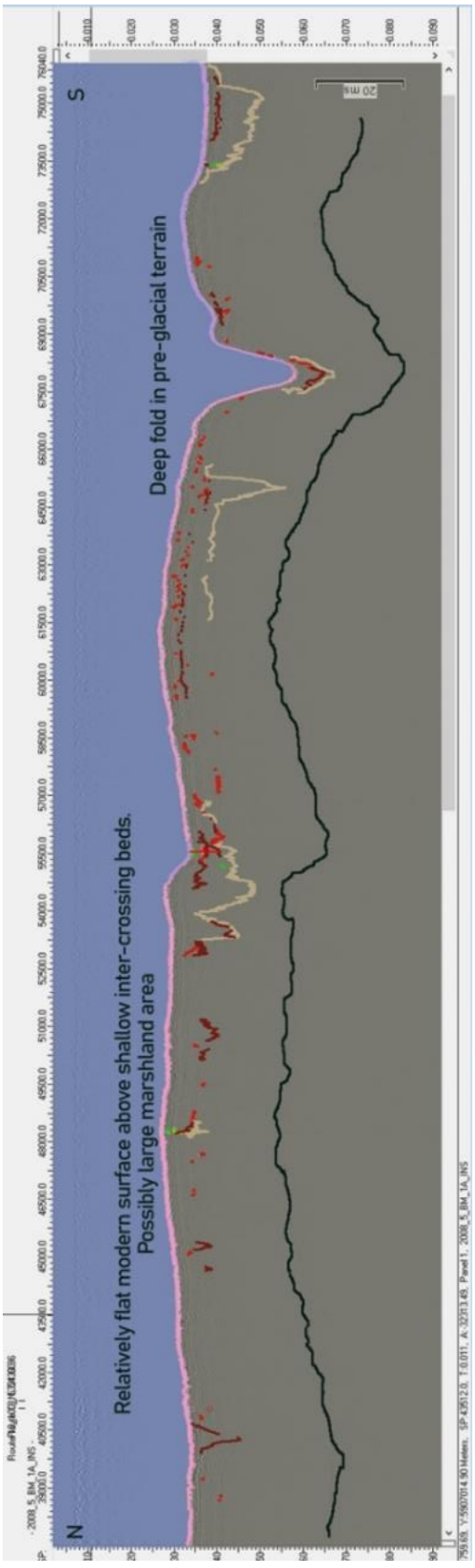

Figure 6.15 Line 5 BM_1A with Core ELF054 approx. midway. Vertical scales exaggerated for clarity

Line 5 BM_1A (Figure 6.15) ran northwest to southeast crossing *Route_18* 2km to the east of core *ELF005B*. At this point the inundated terrestrial landscape was shallow and thin and contained a multitude of small, possibly braided rivers or marshy wetland environments. This seemed a natural extension of the marshland territory prevalent in the surveys of *Line 18* and *Line 18_100N* and suggested a possible extensive peat-based reed fen. From here the land rose gently as it progressed south before descending to a northwest-southeast river valley below which lay deeper glacial erosion below the Holocene surface. The survey line followed the upper valley as it led into the top of a deeper riverine system finally widening to a broad coastline to the south. A deep fold in the terrain toward the southern end of the survey pre-dated the glacial period and appeared tectonic in nature.

6.5.1 ELF054

Of the 3 cores taken along this seismic line only one contained peat; that of *ELF054* (Figure 6.16). This core contained estuarine deposits 3.8m deep penetrating the sea floor at a depth of 36m. Unfortunately, the weather on the day of the survey was particularly poor which resulted in attenuated signals throughout. Clarity of resolution within the phase signals were especially impacted. However, the overall frequencies remained relatively high and the polarities retained zero wave ranges of +/- 175.

The core contained a very coarse but thin modern surface layer overlying a deep Holocene formation of clay silt units, some 2.5m thick (Unit IIa). The seismic survey showed this was cut into by a possible erosional surface (Figure 6.17) but no presence of such a surface was found in the core itself. Unit IIa, while a continuous member within the core, appeared discontinuous in the survey. The interpretation divided this unit into two distinct boundaries which were not present within the core.

ELF054

0-0.11m	Unit Ia Gmin2	Very coarse yellowish brown, becoming grey, sand, with very common shell fragments. Occasional stones.
0.11-2.84m	Unit IIa As2	Grey clay silt, contains thin, dark brown, undulating laminations that are 2-3 mm thick, discontinuous. Becomes slightly lighter grey below 1.5m with occasionally tiny shell fragments. coarse sand. Soft and pliable. To Dark brownish grey clay silt with some dark brown laminations about 4mm thick, continuous, slightly undulating.
2.84-3.25m	Unit IIb Sh2	Dark brown fibrous peat with wood fragments below 3m. Quite friable and dry.
3.25-3.30m	Unit ? As2	Mid grey clay silt with occasional dark brown, discontinuous, laminations.
3.30-3.80m	Unit IIb Sh2	Greyish brown, becoming brown, fibrous peat with occasional sand flecks. Amorphous. Some wood fragments below 3.7m.

Figure 6.16 ELF054 photograph and Lithography courtesy of M Bates, Lost Frontiers 2017

The core boundary between Unit IIa and IIb – the peat layer – was reported as gradational and amorphous. There was no abrupt material change from clay silt to dark, thick, fibrous peat. This upper contact was not detected in the seismic interpretation (Figure 6.17). The peat layer within the core measured almost 50cm thick and then closed with an abrupt contact to clay silt. A further abrupt and sharp contact on the lower boundary of the wedge of laminated silt delineated a break between two separate peat layers. However, due to the poor weather interfering with the frequencies on the day of the survey, vertical resolution were much reduced on this line and the ability to differentiate the relatively thin clay-silt unit between the thicker peat layers at only 5cm was impossible. For the rest of the study area the average vertical resolution was around 6cm. *Line 5 BM_1A* suffered from reduced frequency time in the range of 0.01Hz to 3.1MHz, thus using an average of velocity through sediment of 1500ms the vertical resolution was reduced to 8.8 cm and using the new velocity model for *ELF054* in this research, the vertical

resolution was reduced still further to an average tolerance of ±9.2cm in which individual signals may not be differentiated.

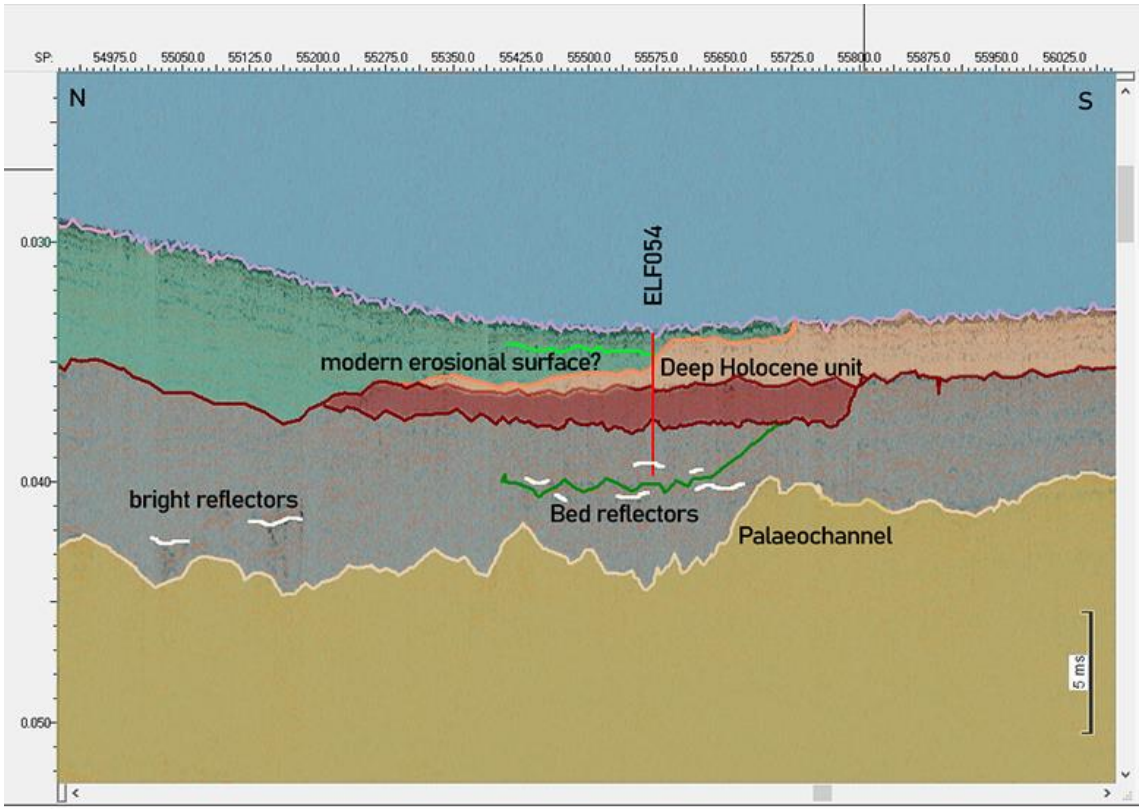

Figure 6.17 Basic Interpretation around core ELF054. The poor imaging is due to interference from weather

6.6 Results for the New Velocity Model

By utilizing Hamilton's sedimental model (Hamilton 1970) and introducing organic aspects as per the methods set out in Chapter 5, the research was able to look specifically at building a velocity model for each core in turn. This was based on grain size classification and fluid density by unit material, a porosity fraction could then be assessed and used in combination with the frequency ranges of the surveys to calculate individual sedimental velocity models. The results of these calculations are shown in Table 6.3. These figures were then weighted for the thickness of sediment passed through. They were added to the water depth average for a precise total per core. All calculations can be found in the Appendix 2 – Method Data.xls.

The lithological description and grain size were assigned a phi classification as per the Udden-Wentworth scale (Wentworth 1922). The grain density was then adjusted for salinity, temperature and water pressure to give a combined bulk density. This was used to calculate the porosity as an inverse fractionate and the velocity worked out as per the Hamilton equations set out in Chapter 5.

The unweighted unit velocities for the cores within the study area fell within three relatively tight bands (Figure 6.18). The first, sands and gravels, generally from the uppermost units or those nearer clastic chalk base deposits, fell within around 1630m/s sedimental velocity ±10m/s. A larger than anticipated gap opened between the sands and silts which banded around 1555m/s ±10m/s and clayey silts and silty clays which occurred at a velocity band of 1525m/s ±10m/s. As expected, the finer granularity and the higher porosity fractionate demonstrated lower velocities while larger grain, greater bulk densities enabled higher velocities. Also, the deeper the penetration, the slower the velocity. The organic quality of the silt or clay played less of an impactful role as initially thought. Rather, the wet or dryness of the material played a greater part in the response time between 1560 m/s and 1530 m/s. Organic silts did lower the responses marginally for silts while organic presence tended to increase the responses marginally for clays, but not consistently. Responses between 1520 and 1565 m/s that contained organic components remained complicated and could not necessarily be differentiated in the velocity model via material classification alone. Coarser sands, shelly sands and gravels however did stand out distinctly in this analysis.

Descriptive				Fluid Dens	Grain Dens	Por'sity	Bulk Density		Calc Velocity
φ	Udden-Wentworth		Organic	ρ(kg /m³)	g/cc	Fract'n	g / cc	adj	V (m/s)
-1.5		very fine sandy pebbles		2	2.05	0.28	2.3	2.321142	1737.554
-1	Sand	very coarse pebbly sand		2	2.04	0.36	2.2	2.212821	1701.598
-0.5		very coarse pebbly sand		2	2.03	0.38	2.1	2.107901	1662.855
0		coarse granular sand		2	2.02	0.386	2	2.019365	1628.726
0.5		medium sand		2	2.01	0.392	1.9	2.002293	1622.554
1		medium sand		2	2	0.398	1.8	2.015792	1628.533
1.5		medium sand		2	1.99	0.402	1.8	2.027028	1633.455
2		fine sand		1.95	1.98	0.439	1.8	2.002419	1627.021
2.5		fine sand		1.9	1.96	0.457	1.7	1.932721	1601.244
3		very fine sand		1.9	1.91	0.474	1.7	1.820151	1558.22
3.5		very fine sand		1.8	1.87	0.48	1.6	1.849795	1572.211
3.75		Unconsolidated sediment		1.8	1.85	0.495	1.6	1.742605	1530
4		very fine silty sand	sandy organic	1.8	1.83	0.528	1.6	1.73121	1530.109
4.5	Silt	coarse sandy silt		1.7	1.65	0.573	1.6	1.689098	1528.101
5		coarse silt		1.7	1.58	0.683	1.5	1.625114	1529.064
5.25		medium organic silt	dry comp silty peat	1.7	1.57	0.624	1.5	1.650331	1527.511
5.5		medium silt	silty organic	1.6	1.57	0.697	1.5	1.615314	1529.244
6		medium sand-silt-clay		1.6	1.56	0.675	1.4	1.705008	1562.558
6.25		fine silt with organic	variable peat	1.5	1.52	0.684	1.4	1.608313	1528.572
6.5		fine silt	peat	1.5	1.5	0.725	1.4	1.638645	1554.289
7		fine silt	peat	1.5	1.4	0.75	1.4	1.522193	1527.884
7.25			decomp peat mix	1.5	1.43	0.675	1.3	1.573616	1522.488
7.5		very fine silt		1.5	1.42	0.751	1.3	1.520866	1524.244
8		very fine clayey silt		1.4	1.42	0.758	1.3	1.50556	1519.977
8.25			dark, wet organic peat	1.3	1.41	0.688	1.3	1.539734	1514.584
8.5	Clay	silty clay		1.3	1.41	0.765	1.3	1.513069	1527.145
9		Clay Silt Boundary	Clay Peat open void	1.2	1.4	0.782	1.3	1.45777	1511.151
9.5		fine	clay organic	1.2	1.4	0.784	1.2	1.471416	1517.645
10		clay very fine		1.1	1.4	0.8	1.2	1.467662	1476.139

Table 6.3 Velocities based on Hamilton's porosity and bulk density calculations (Hamilton 1970) classified by grain size based on the Udden-Wentworth Scale (Wentworth 1922).

Material differentiation became clearer when the model was assigned appropriate weighting (Figure 6.19 below). This took into account individual units by volume of material (not purely by the bulk density of each material used in the calculation of the velocity model). The units were broken down into their component layer thicknesses and it was noticeable that the sub-1550 m/s velocities – which included the organic clays and silts – in general made up a much smaller proportion of the overall volume of sediment material. It demonstrated that to define material boundary division, the need for a three stepped weighted velocity model approach based on unit classification was the correct way forward.

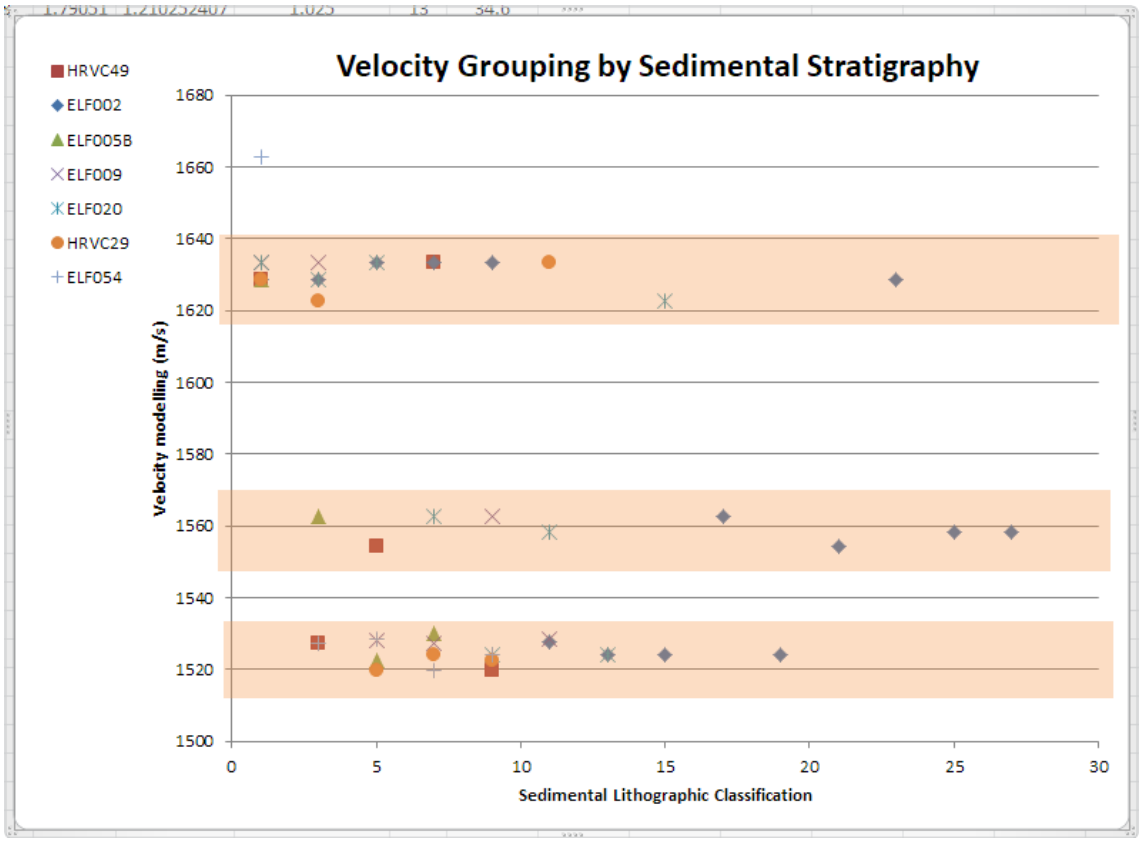

Figure 6.18 Three distinct bands of unweighted velocities grouped from new sedimental models

Cores such as *ELF002* which were comprised of a number of units of differing material types and contact boundaries, gave a more even distribution of weighting to the average velocity model. Cores which had few units, such as *ELF054* which had only five or *ELF005B* which, in essence, had only 3 separate units, heavily skewed their weighting toward one particular material classification. To ensure the depth analysis of these cores hit the correct interface contacts the weighting of faster and slower

sediments was crucial to avoid a bias toward a single unit in the lithostratigraphy.

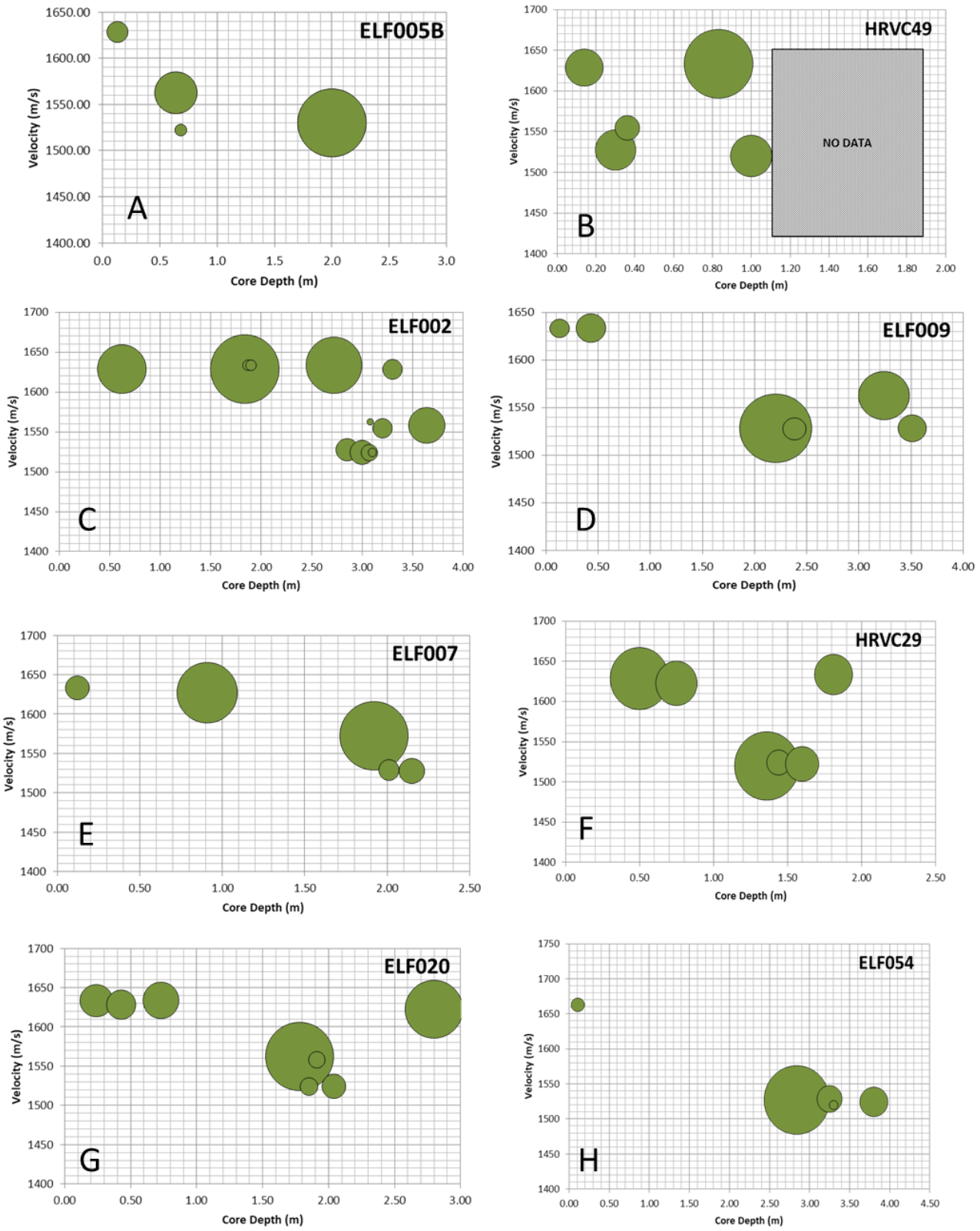

Figure 6.19 Velocities weighted by material volume within the core evidence. Average velocities favoured sandy shallower sediment obscuring deeper organic and silty / clayey sediments thus required weighting

Therefore, the velocity model was predicated on unit boundaries and stepped accordingly, adding proportional weighting according to the volume of material passed through as per the cores. This allowed the creation of precise time-depth analysis models from which we could ground-observe the core units to our seismic surveys, the amplitude peaks and reflector signals. The importance of creating separate sediment velocity speeds calculations was borne out when looking at the variation from the average velocity (Figure 6.19). Creating a model that weighted these velocity calculations by the amount of material passed through enabled the final model to avoid the sand heavy average velocities that would have skewed the results toward modern mobile sands. This was the first time such a stepped velocity model had been attempted that integrated organic sediments.

Before interpreting the results of the new velocity model however, it is important to examine the results of the Q Factor and Phase analysis methods to these observations.

6.7 Q Factor and Phase Analysis Results

Before looking at the depth analysis of the velocity models it is useful at this point to look at the Quality Factor analysis of the traces taken between two reflector indexes after Pinson (Pinson 2010) and the method set up in Chapter 5. The analysis was to cross plot the frequency and acoustic impedance by means of effective Q-Factor. This was performed with the addition of bandpass filters and instantaneous phase functionality to distinguish unit and bedding classification.

The results of the cross plot did not prove conclusive in determining any separation between organic and inorganic material volumes. Nor did they show any correlation between higher frequency ranges and increasing acoustic impedance. As can be shown in Figure 6.20 (A) below, the Q-Factor (time) on the Y-Axis against the Frequency (time) on the X-Axis demonstrated a predominance of traces around the 45-65 Q-Factor range and across the frequencies from 700Hz up to 6.3kHz where all traces tail away. This would, as described in Chapter 5.3, according to Wang's prediction and Morozov's equation (Morozov 2008a), place the Q-Factor traces firmly in the Q range of 35 and 75 Q for organic sandy silt (Wang

2016). A look at *ELF007* and *ELF020* Unit classification for Unit IIb described the sediment type as 'finely bedded silted sands' directly above unit IIc 'black organic silt' and peat. *HRVC29* did not follow this trend, describing the IIb unit as 'silty clay', a material Wang proposed a Q-Factor measurement of between 30 – 40 on the organic range (Wang 2016). This research found all three cores returned strong trace signals in the 45 – 65 Q-Factor range associated with organic sandy silts.

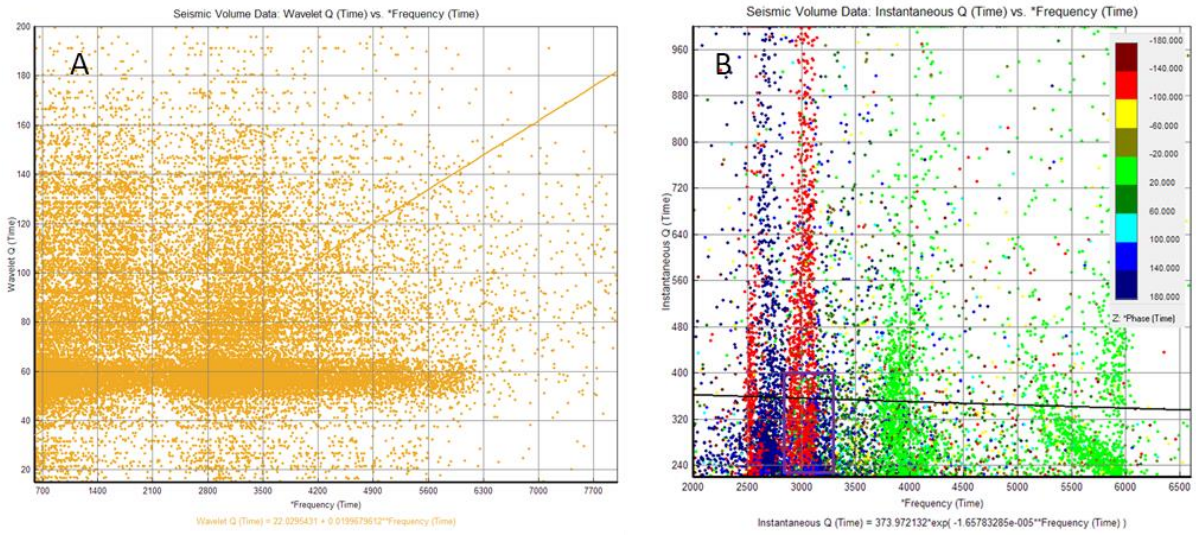

Figure 6.20 A (left) Q Time banding between 45 and 65, while in Q against Frequency B (Whitewright 2015) a strong correlation between negative and positive phase is evident

There were two issues with these results, however. The first was the number of traces calculated. In this single window over 12,000 traces were calculated and in repeated tests on this and other survey lines, such cross plots failed due to time out problems or memory excesses with the calculations. The suggestion is that the traces per shotpoint included in the initial gather were too ambitious and either the window should have been reduced, or the survey trace file simplified. The second problem was that despite tweaking the frequency using bandpass filters, it proved impossible to eradicate the noise in the Q-Factor wavelets above the 65 Q level. This made identifying any trend except the single obvious grouping problematic. Any analysis of more granular activity was lost.

A second cross plot using the same traces and instantaneous Q (for the entire window but not for individual wavelets) was plotted against frequency, and colour matched for the zero wave phase peak (Figure 6.20 B) In this there was a fascinating and unexpected correlation. As was

pointed out in the previous chapter, Q-Factor estimation alone was not robust enough to be a legitimate scientific dependent for calculation. However, as an indicator of other, calculable trends, it was highly effective. In B, the Q Factor peaks were spread across all frequencies from 2 kHz up to 6 kHz.

At 2.5 kHz and 3.0 kHz the peak were twice those at any other frequency and more interestingly, the phase signals for both peaks were highly negative (-150). They were then followed immediately at 2.75 kHz and 3.2 kHz by equal Q-Factor peaks with a phase polarity of +150 this signal is not then repeated outside of this frequency range. Not only were the Q-Factor peaks more extreme but they polarised the phase functionality to the same extent. Therefore, individually, Q may not have the power to define the presence of organic sediments in the seismic survey lines but as a confirmatory tool it was able to unlock a new process of understanding the bright reflectors as phase functions within the depth converted data. The appearance of the negative followed immediately by the positive in equal polarity was suggestive of a zero-phase wave form and if the organic reflectors were zero wave forms they would have a negative polarity lead in and equal positive polarity lead out as the Q-Factor peaks in the figure above demonstrate.

6.8 Core Analysis by Depth and Phase Polarity

6.8.1 HRVC49 & ELF005B

Using the new velocity model, the depth analysis achieved proved extremely precise in many of the cores. Figure 6.21 shows error bars of only 6.2cm either side of the contact measurement. These were hit in all four unit divisions for core *HRVC49* supporting the evidence that the velocity model worked well at both the upper units and further within the volume. The interface marked as an abrupt contact between silt and peat at 0.30m (unit IIa to IIb) and a similarly abrupt contact between the peat and clay silt boundary at 0.36m was – at 6cm – below the 6.2cm limit of the vertical resolution. However, it showed strongly in the seismic data as a single entity. The -27,800 negative peak in the p-wave amplitude demonstrated at the boundary of unit IIc to IIIa at 0.83m was the strongest signal in the seismic amplitude even before running any envelope or bandpass filters. This interface between clay-silt and stiff clay was reported

as gradated and the material types similar; silt clays to clays, thus less of a fundamental difference in their density or porosity. Therefore, the presence of the chalk gravel must have accounted for the high amplitude response, not the unit boundary. It can be said however that the boundary measurements validated the velocity modelling on this core.

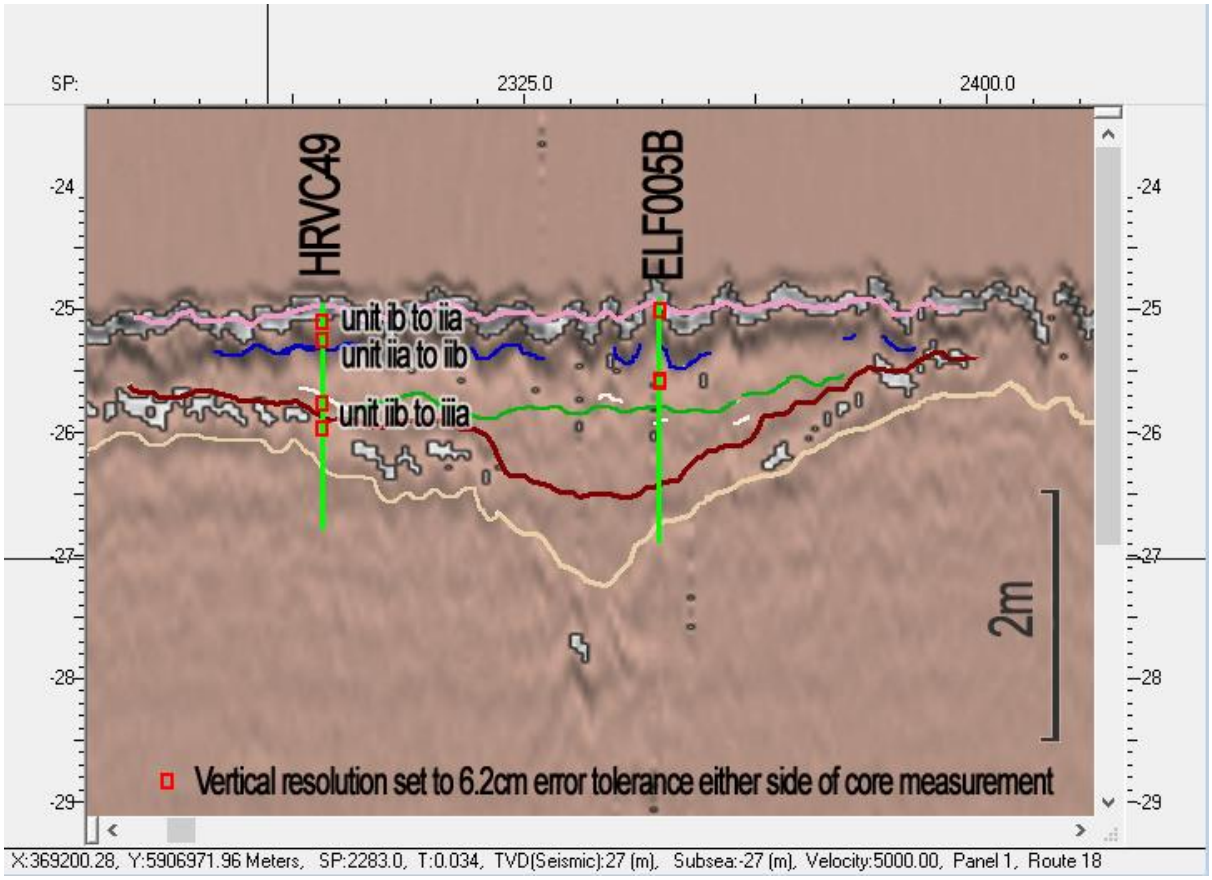

Figure 6.21 Depth Converted Seismic Data magnified to show precision of analysis

ELF005B failed to follow suit. The three main boundary interfaces apparent in the cores at 0.13m, 0.64m and 0.68m did not show on the seismic amplitude depth conversion. The first of these may have been due to its proximity to the seafloor and the velocity model being unable to contextualise itself with the shallow volume. There was a strong seafloor signal which, despite being outside the 12.4cm rang of vertical resolution issues, smeared the seismic signal beyond 13cm and this may have prevented the isolation of and individual response. The contacts at 0.64 and 0.68m surrounding Unit IIb, a single thin but distinct, organic layer were perhaps too small to show up as individual signals due to the Fresnel resolution. The contact should still have demonstrated a significant, contrasting change in material type to register a response. Expectation would have been for a single peaked amplitude wave even if it remained

undifferentiated between two more distinct boundaries. The problem, as discussed in Chapter 5, may stem from the lack of proximity of the core to the seismic line against which it was being assessed. Precise analyses may not always be possible up to 8.2m away from the interpreted data.

Figure 6.22 Phase Function shows very strong defined polarity between negative (blue) and positive and the zero charge variance peaks

However, following on from the Q-Factor and phase analysis, this research examined the new depth converted data in a phase function view. It also applied a bandpass filter to eradicate high and low frequency 'noise' and set variance 'wiggle' peaks to view the wave forms at zero phase to give further visibility of bedding and deposition. Initially, the view was complex and required a simplification of the colour bar to show extreme phase polarities. In this way, it was possible to isolate the zero-phase wavelet, the negative and positive polarities and the variance peak that ran through the middle. When viewed in conjunction with the depth conversion and a regular bandpass filter a definite pattern appeared (Figure 6.22).

The phase analysis on this palaeo feature gave strong signals. The polarity was equally balanced between positive and negative with the simplified colour bar showing the division of phase characteristics along the variance fill wave forms. In Figure 6.22 the strong variance fill signified by the pink peaks always led with a strong negative polarity of over 150 (blue) followed by a thin line of neutral polarity in which the variance peak lay. This was then followed by a positive polarity equal to the negative signal.

As indicated earlier in the chapter, this equality of signal polarity signified a zero-phase wavelet, not a linear phase wavelet as would be the case with a typical amplitude peak (Sheriff 2012).

In regard to core *HRVC49*, the core evidence of organic units at a depth of 0.3m again did not hold in the phase analysis. There appeared to be no phase variance peak at 0.3m, no negative to positive polarity switch and no zero-phase wavelet. Each of these was present, within error tolerance, at the 0.83m depth mark. It was here that the core reported clay-silt with organics had a gradated boundary contact with brown clay. The research therefore can show that this phase view supports the original interpreted result of no organic signal at 0.3m but an organic signal 0.83m. It also validated the depth analysis, but it did not identify the higher organic signal.

Similarly, in ELF005B, no organic layer was picked in the phase character despite the presence of peat in the core. However, a small variance peak immediately to the right of the core location at precisely the right depth may indicate a misaligned location. Certainly, this would be within the error tolerance of the vibrocore and GNSS horizontal accuracy measurements as set out in chapter 5.3 above. Unfortunately, the variance peak was not of a significant order and the polarities of the phase wavelets were not extreme in their differentiation at this point to be conclusive.

6.8.2 ELF002

Depth analysis of ELF002 (Figure 6.24, page 164) correlated with the original interpretation and to the core lithology within vertical error tolerances. The abrupt contact boundary at 1.95m between unit Ib and IIa appeared strong on the survey. Likewise, the strong reflectors at 3.10m, measuring a significant amplitude peak of -29,000 p-waves corresponded to the core boundary of unit IIb to IIc at the same depth. The core report specified this contact between peat and silt as abrupt. The 62cm unit Ia to Ib boundary of gradated contact from coarse shell and sand, to sand and gravel did show on the seismic though it was partially obscured within the bright seafloor signal.

An unconformity registering -17,000 p-wave was interpreted on the survey at 1.2m (in blue, Figure 6.23) but no corresponding unit distinction could be found within the core evidence. A further and more distinct high energy reflector measuring -23,000 p-wave (marked in gold Figure 6.23) was interpreted as depositional fill but did also had no matching unit boundary in the core evidence. It would have placed at 1.65m (±6.2cm) and a further one measuring a less impressive -18,000 p-wave, in green at 2.60m (±6.2cm) which again did not fall into the precise unit boundaries found within the core. The latter could have been a reflected multiple and the phase function would eliminate the problem. The former however were more of an issue and would need discussion.

The abrupt contact at 2.85m between unit IIa and IIb that was so evident in the core report did not readily appear in the survey. The interface between laminated clays overlying peats was not reported but the peat itself was described as compact, amorphous and firm and measured 0.15m in thickness. The next interpreted boundary identified by the velocity model was that of the 3.10m Unit IIb to IIc peat to fine silty sands. This could be corelated as it fit within the tolerance bars and the peat to silty sands would deliver a higher negative p-wave signal (Wang 2016). This would be further tested in the phase function but overall, the velocity model mapped the seismic data to the core evidence well for *ELF002*.

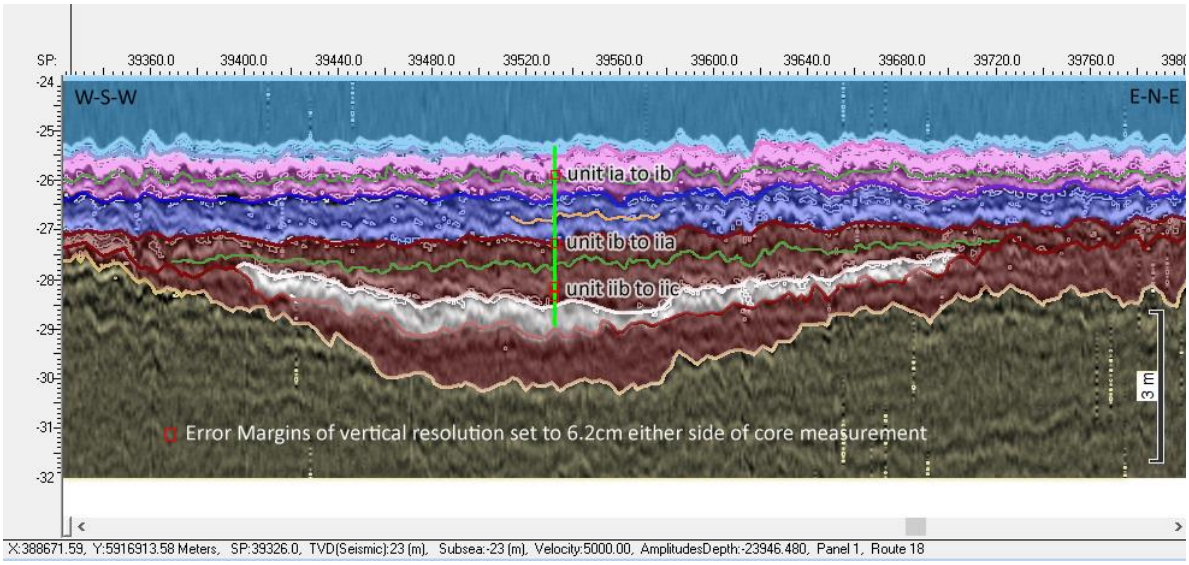

Figure 6.23 Depth Conversion and Ground Observation of Core ELF002

Within the phase function, the simplification of the colour bar proved revealing (Figure 6.24) in that the peat to silty sand boundary (3.10m) was one of only two strongly defined regions. The variance fill line with strong negative / positive polarity either side formed an almost solid bedding of zero phase signal at the confirmed depth of the core peat to silty sand contact. The issue here was that the variance fill was present either side of the core location on the survey but was explicitly absent in the area over and surrounding the core itself. This did not suggest that the core did not contain peat – it patently did. It also did not say that the interpretation results were incorrect in suggesting the phase analysis was not detecting organic matter. On the contrary this research interpreted the seismic data to have picked a contiguous bed of valley fen peat in this palaeo feature and the evidence of peat within the core, some 1.9m distance from the survey line supported this claim (Ekono 1980; Bates Pers Comm 2019).

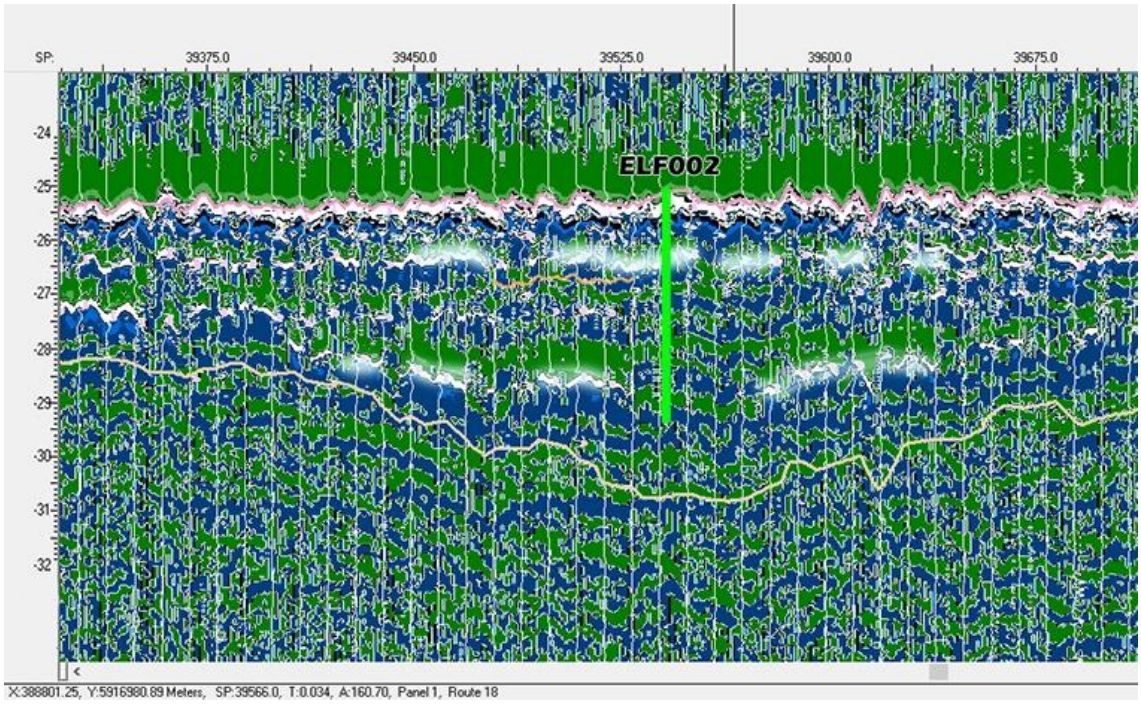

Figure 6.24 Phase Function with Variance reveals 2 layers of organic boundaries (in white)

Though the 2.6m multiple line had been eradicated in the phase analysis, the reflector at 1.2m (in blue, Figure 6.23, page 163) was now displaying strong variance fill of zero phase signal. The interpreted reflector here passed directly through the core location. Therefore, it must be assumed that the zero-phase wavelet coupled with the high reflective p-wave response at this precise depth were interpreting a significant signal within unit Ib of the core. This can only be attributed to noted large shell

fragments within this unit (Bates ELF Report 2019) or the core missing the precise material picked up in the survey.

6.8.3 ELF009

Depth Conversion (Figure 6.25) for this core initially proved difficult. 2.83m of 3.53m were assigned to Unit IIb (a greyish brown silty sand). This single material type out-weighed all other lithostratigraphical units in the velocity model to fractional proportions and caused the model to calculate sonic speed through sediment too fast. This skewed the depths in relation to the other cores. To do this, the unit IIb was divided into two and recomputed evenly as a combination of sandy-silts and silty-clays which were only stepped by granularity of material (see Appendix 2). This could be rationalised due to the descriptive Troels-Smith markers within the lithostratigraphical report which specified a gradated change from one to the other as the unit progressed.

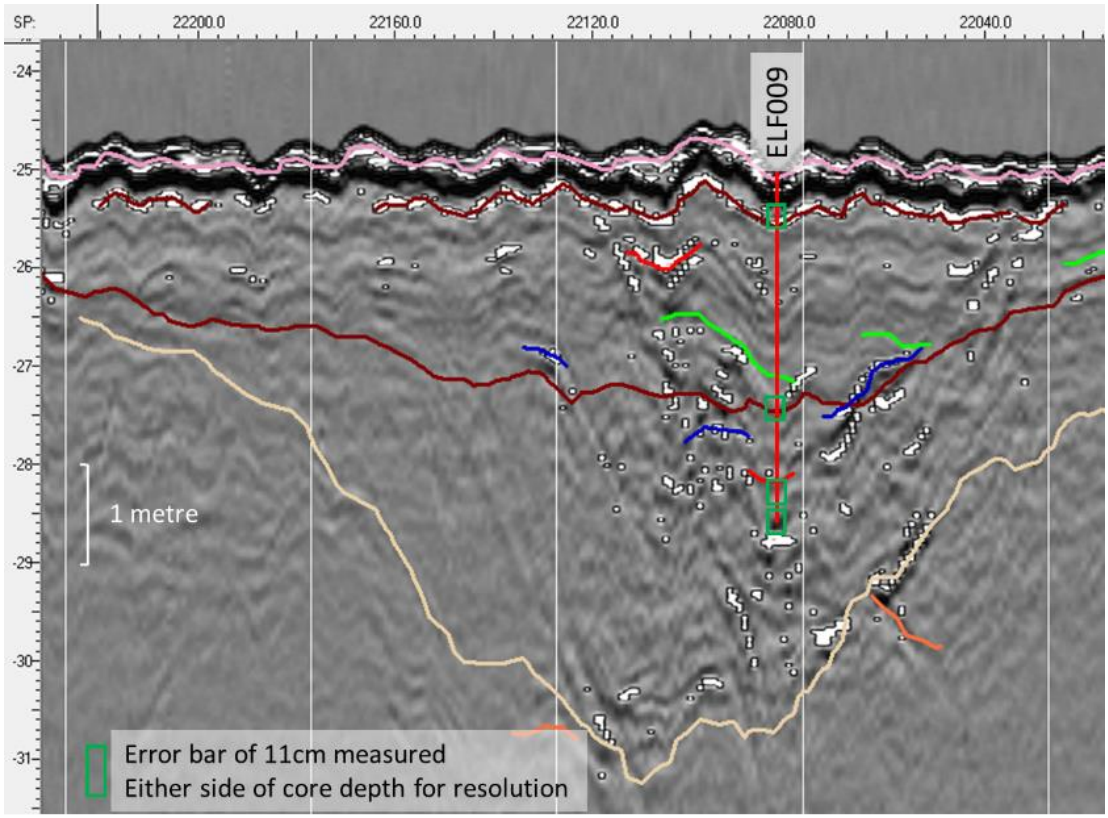

Figure 6.25 ELF009 Depth conversion. Note the error bars are 5.5cm either side of core measurements or 11cm in total

Another reason for doing this was to account for the descriptors 'occasional thin <2mm black laminated peat, from 2.20m – 2.38m' (M

Bates, Europe's Lost Frontiers Project Report 2017) that were intercalated within the unit. Due to their incorporation, they could not be individually modelled, but their organic nature could be classified between 5.25 and 5.5 φ using the new system as per Table 6.3.

Once this had been achieved the velocity model worked perfectly, bringing the depth conversion within centimetre precision of the unit boundaries found in the core. The very high amplitude reflective signal located in the interpretation view, still proved to be too deep at 3.87m. That did not mean however that the reflection was not indicative of organic material, or even that it was not part of the same organic peat layer present at the base of core ELF009 – there was no termination boundary found within the core. The signal in the seismic line may be evidence of a deeper, base boundary. Unit Ia and Ib tended to merge together within the vertical resolution smear of the seabed, however the boundary for Unit IIb at 0.43m was almost perfectly aligned as was the 2.40m contact boundary. The abrupt contact that occurred at 3.26m fell just within the error tolerance.

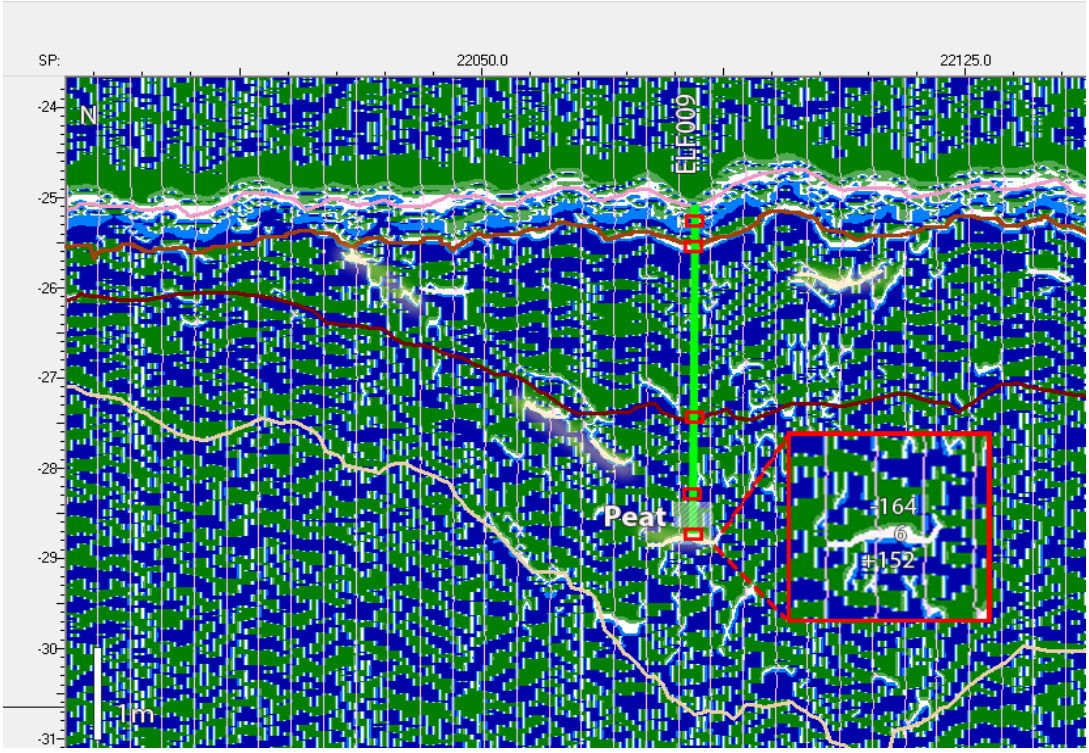

Figure 6.26 Phase function with inset showing possible peat bed and deeper boundary within core ELF009

An examination in phase function (Figure 6.26) supported the idea that the 3.87 bright reflector boundary was part of the same peat layer as had

been discovered in the core. The variance peaks appeared thin but clear on the insert along the white zero polarity line. Above and below this were signature negative and positive polarity of the zero phase wavelets measuring -164 and +152 respectively. Both right and left of the core were upward variance slopes with similar zero phase wavelets. In all of these cases, the negative and positive values were between -/+153 to -/+ 176. The neutral polarity of the variance peak ranged between -2 and +8. The plane at which these phase signals were aligned matches so uniformly it could be classified as a contiguous soligenous peat bed with an estimated depth to the 3.87m lower boundary of 62cm.

The reasons behind the phase function not detecting the unit IIb to unit IIc boundary is unpacked further in the Concluding chapter. Suffice it to say that, in the initial interpretation there were no strong negative reflectors that touched the core location 2.1m from the survey line. Many of the reflectors in the interpretation seemed perturbed or even misaligned for an organic signal. In the depth conversion, bandpass filters were applied that amplified weaker negative amplitudes that may have otherwise been missed. However, it was clear from the phase analysis that organic signals were detected throughout this area but not at this contact. So, within the core was there anything unusual? The only material difference was the description of Sh1 present at the base of Unit IIb and within Unit IIc. If peat existed in both units then the contact cannot have been abrupt, the boundary was unlikely to have been sharp and the material types would have been uniform, in which case the seismic data would have found the context difficult to separate. However, this can only be conjectured for this particular core.

6.8.4 ELF007, HRVC29, ELF020

The depth conversion for the three cores located within the one feature were run independently. The interpretation of the palaeo feature, the geomorphology of their location and their environmental situation however suggested they should be considered together. The three cores had differing lengths and were cored on different occasions. The reports were addressed to differing standards with differing levels of detail. However, they were all weighted against the same velocity model and depth converted against the same background data (Figure 6.27). Unit Ia was ignored due to the seabed smearing that occurred on *ELF007*, after which all three cores initially plotted well, lining up within the error

tolerance of the first two units. The boundary contact between unit Ib and Unit IIa was detected for each core (south to north at 0.73m, 0.75m, descending to 0.91m for *ELF007*). The units within the cores deviated from this point. Both *ELF007* and *ELF020* contained approximately 1m of fine silted sands with laminations before abrupt interfaces between Unit IIa and IIb. In both cores, this latter unit was reported as an organic peat layer.

The organic signal interpreted at 2.19m as part of core *ELF007* did not coincide with the 2.01m core boundary. This was too deep for the silt and $Gmin_2$ sands to peat contact and was entirely missed in the depth analysis. The negative reflectors at 2.19m however, did fall within error tolerance of the base of the core at 2.15m which contained peat and did not terminate with the end of the coring length. It was entirely possible a further peat boundary was located at 2.19m depth. This would be consistent with previous results in which the lower boundary contact had been identified with the velocity model.

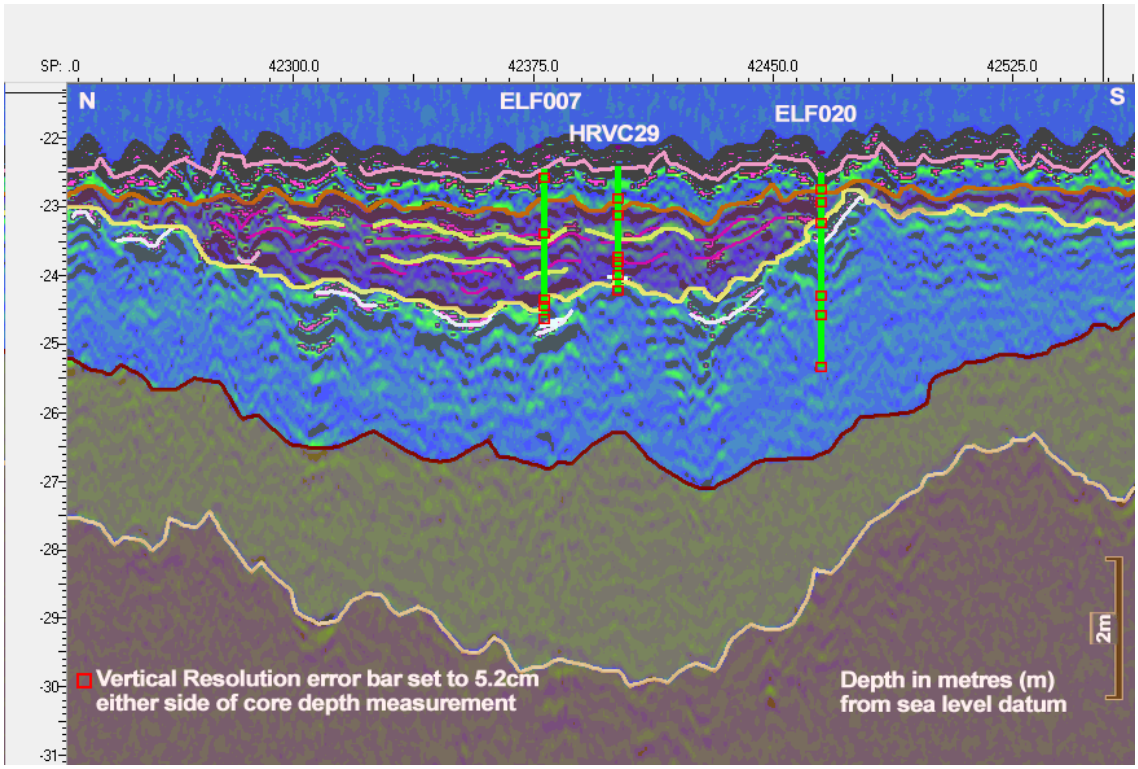

Figure 6.27 Depth analysis including error bars for vertical resolution & bright reflectors (Whitewright 2015).

Core *HRVC29*, which lay between the other core locations, reported only 0.6m of clayey silt without lamination before its boundary with IIb. Unit IIb

is reported as an organic peat layer, similar in reflectivity peak to that of both *ELF007* and *ELF020* but in core *HRVC29* it occurred at a depth of only 1.42m below sea floor as opposed to 2.19m as measured in its closest neighbour, *ELF007*.

Error tolerance of 5.2cm allowed the 1.42m negative p-wave peak to have been interpreted as either the contact between Unit IIa and IIb at 1.36m or the sub-division of Unit IIb (humified silty peat to organic silt with organic detritus) at 1.44m. The resolution was not sufficient to differentiate. Therefore, on the basis of previous results, the highest negative response would most likely have occurred from the greatest material change. This would have placed the depth analysis pick at the Unit IIa to Unit IIb boundary where silt changed to peat (Ag_3 ->Ag_1->Sh_2).

Furthermore, the description of the second subdivision of Unit IIb with organic humified silts and detritus Sh_1 was marked as As+, though from the description it may have been possible to classify this as As+ and DT. Organic sediment may contain detritus, including wood, seeds, grasses etc but the composition of such detritus cannot be accounted for in a velocity model nor the volume of detritus.

Finally, for core *HRVC29,* strong reflectors at 1.60m denoted the boundary of unit IIb and IIc. No further signals were detected through the base of the core despite the presence of silts and chalky gravel which respond well.

The peat layer in *ELF020* proved more complex. The core report stated it began at 1.78m and ran for 0.26m, demonstrating abrupt boundary contacts both above and below. Of the three cores, it should have had the greatest potential to interpret on the survey. Unit Ib indeed placed precisely at 0.73m. However, the next strong negative reflector boundary picked in the seismic interpretation plotted outside the error tolerance range at 1.15m. This would have placed it in the centre of unit IIa in the core. There was no boundary change within the core at this depth. There was certainly no organic boundary within the core at this depth. The peat boundary in ELF020 began at 1.78m.

Unfortunately, below 1.15m on the survey, there were no further high amplitude reflectors. There was a potential erosional channel in the side of the valley at 1.40m, but again, this did not correlate to any boundary in the core and was too close to the valley side to provide peat accommodation space.

The co-ordinates of the core, which were verified for the research, did indeed seem to place the core on the valley side where a depth of 1.78m would have passed through the valley base and beyond any depositional sediment. Even within the resolution error maximum range of 11cm there were no high negative reflector amplitudes on the seismic survey within reach of the core at this depth. It can be observed from the core evidence that depositional sediment and peat was cored at this site, so either the survey data or the depth analysis is incorrect.

The depth analysis of other cores within this feature suggested the velocity model used could be accepted. Therefore, the issue must be attributed to the survey data. In particular, the location of the core upon the line. This has been verified with the Gardline Report to be within 4.63m distance of the seismic survey. The fact that the Unit Ib is extremely close on all 3 cores in this area, suggest that the sedimental bedding is flat in this area. However, core *ELF020* is not located quite on the slope of the river valley as the survey suggested. The phase function also corroborated the above results (Figure 6.28). As in previous survey lines, the reflectors demonstrated definite zero phase wave characteristics. These reflectors led with a negative polarity signal uniformly between -160 to -180 and were matched by an equally charged positive signal. The neutral signal between the two varied between +2 to +4 with corresponding variance fill peaks that overlay the neutral zero phase amplitude. This variance fill coincided precisely with the strong negative amplitude reflectors in the p-wave view.

In Figure 6.28 these variance fills could be seen running contiguously across the valley bottom, picked up in the bottom of Core ELF007. The Variance peak signals were then traced steeply up the valley side on a soligenous bed through the location of ELF020. However, the evidence, as explained above, was not present in this core. Interestingly, while there was the smallest variance kick over *HRVC29* at 1.39m, directly between the two organic layers Unit IIb, there was no zero-phase wavelet over the core location. So, despite a double layer of organic peats and silts in the

core evidence no zero phase wavelet evidence supported it in the survey. This was likely due to the lack of differentiation between units IIa and IIb in the lithostratigraphy. In addition to the results for the cores, a wider view of the palaeo feature revealed a semi-continual layer of organic sediment approximately 2.25m to 2.5m below the sea floor. Taking this into account, there was enough detail to conclude a semi-continuous band of peat existed before the marine inundation. This would suggest a well-established mire or marsh, possibly of some depth.

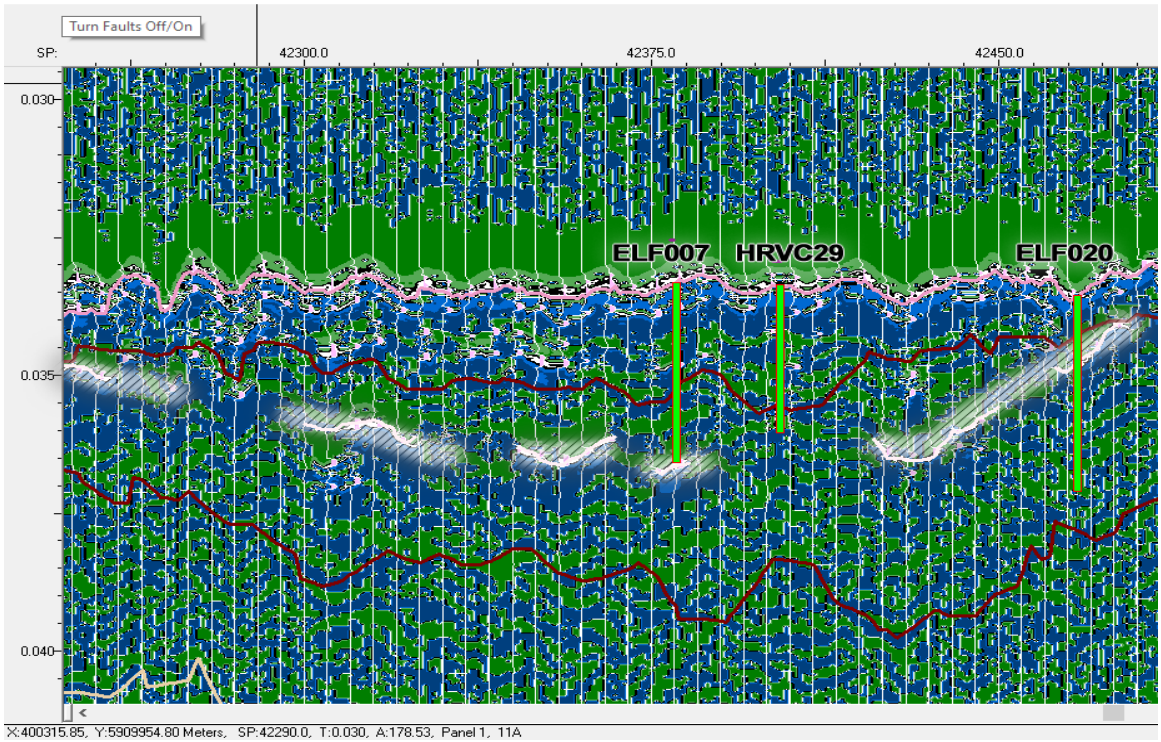

Figure 6.28 Phase Function and picked peat horizons(white). Hatched area shows extent of potential peat bed.

6.8.5 ELF054

Despite the poor imaging on the entire line (Figure 6.15) due to poor weather while shooting, the depth conversion was able to verify and clarify many details with the initial interpretation. Figure 6.29 shows the depth analysis overlain against the interpretation. It showed the contact between sands and clays immediately below the highly reflective seafloor was independently bright. Two parallel horizons appeared to display with sufficient amplitude to warrant marking on the seismic data. However, on depth conversion the uppermost proved to be a seabed multiple. The modern erosional surface identified on the interpretation did not appear

in the core or hold any validity in the depth analysis. This must also be attributed to faulty interpretation. There was a terminated amplitude signal present within the data, but no core unit boundaries coincided within a metre of the lines. These clinoforms were obvious in the surveys but not present in the core. This could signify a misreading of the data or that the core distance was too far from the erosional surface for that to appear in the data.

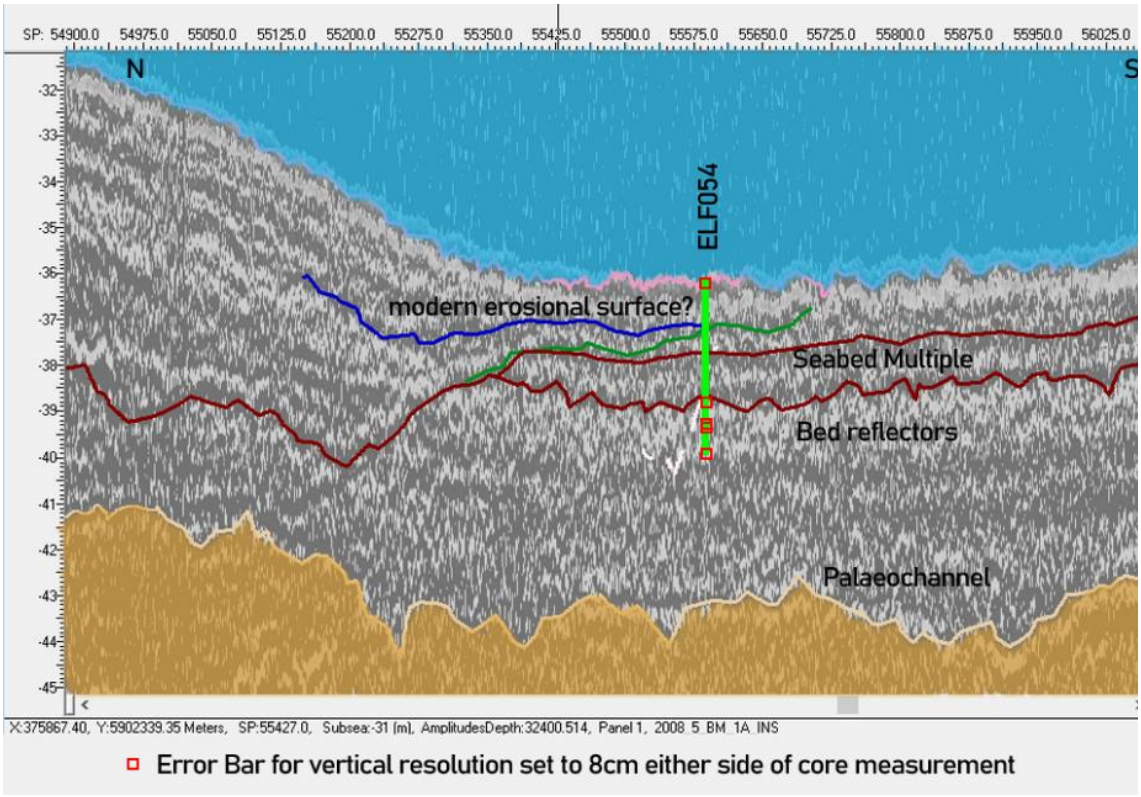

Figure 6.29 Depth analysis for ELF054. Initial interpretations made difficult due to inclement weather

The velocity model was unable to distinguish between Unit Ia and Unit IIa due to the vertical resolution limits. The error tolerance was set to ±7.7cm (See Figure 6.31 and calculation, page 175) which meant the first unit boundary of 0.11m could not be differentiated from the seabed. The material in unit IIa was precisely the archaeologically ideal laminated fine clay silts (As_2) that could act as impermeable caps for organic preservation, therefore the boundary below would be critical to pick out. In fact, two boundaries of distinct peat layers were picked. The p-wave amplitudes were low and even with bandpass filtering there was a lot of background noise. However, the velocity model weighted the reflected amplitudes precisely and the depth results produced were within tolerances. The first; Unit IIa to Unit IIb at 2.94m, placed 0.1m below that of

the core evidence but within the 15.6cm error tolerance of this survey line (see calculation, page 175).

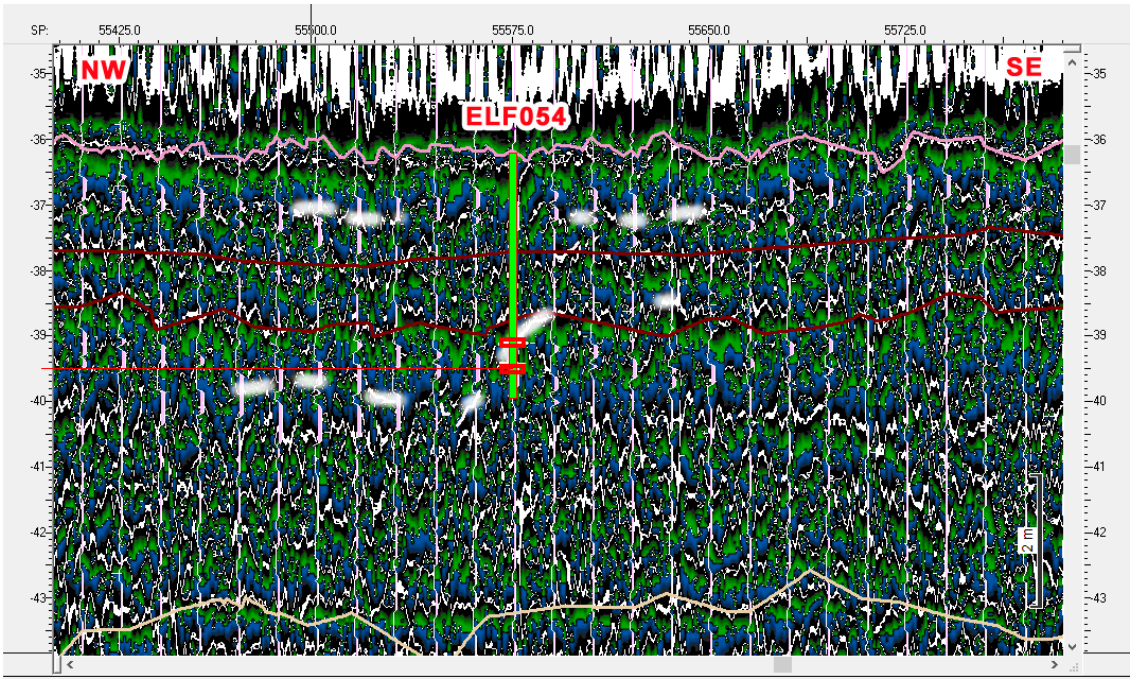

Figure 6.30 The phase Function is of poor quality but shows distinct variance peaks below clay limit.

The second signal, which was very poorly represented in the time amplitude view, even with bandpass filters to eradicate noise, was visible via the phase function at 3.30m. Given the large vertical resolution error tolerance and the thin nature of the 0.05m interim unit of clay silt between the two peat layers, this contact may have referred to the core contact at 3.25m or at 3.30m. It was impossible to differentiate this as the peat unit could not be separated on the seismic survey. This depth conversion may have also benefitted from Unit IIa being split into two sub-units for the velocity model to prevent once single 2.63m weighted sediment overbearing the model. The descriptor mentioned the material gradated from Ag to As (clay silt to brown organic silts) towards base.

The phase function (Figure 6.30) showed the two distinct boundaries as per the core. The distinct variance peaks displayed at 2.91m within error tolerance of the Unit IIa to Unit IIb clay to peat boundary and 3.30m Unit IIb to IIIb, clay silt to peat boundary. This was despite the silt layer only measuring 0.05m thick, well below the vertical resolution bar. Below the zero-phase wave line at 3.30m the signal became heavily attenuated. This may have been due to the weather conditions, but it could also have

been attributable to considerable depths of organic material deposition. The base of the core at 3.80m did not signify the termination of the peat bed at this location and the sand flecks did not suggest a boundary was imminent.

Though the signals were attenuated, the polarity sparse (Figure 6.30) and there were little to no variance peaks to overlay except on the higher polarity lines where extremely sharp contact boundaries were detected, what was visible worked extremely well within the research framework. It was noted that the boundary between Unit IIa and Unit IIb at 2.84m, although described as grey clay silt to Peat, was extremely strong in both p-wave and phase. There was an argument however – to be made in the concluding chapter – that it was the gradating silts in Unit IIa that signalled the boundary change to Unit IIb, not the clays.

When considering this survey line, the vertical resolution must be considered. The poor amplitude response achieved made interpretation of the line data difficult and timed response at specific cycle frequency must be calculated to engender a reasonable expectation of the results.

In Chapter 5.3 Vertical, horizontal and Fresnel Zone resolutions were accounted for, and in here, the research explicitly sets out the calculations for the survey *line 5 BM_1A*. In the Frequency (Time) breakdown (Figure 6.31) it was seen that 35% of the frequency was in the sub 1kHz range, only 3% over 2kHz or over range and 0.7% of the total amplitude range was 5.3kHz.

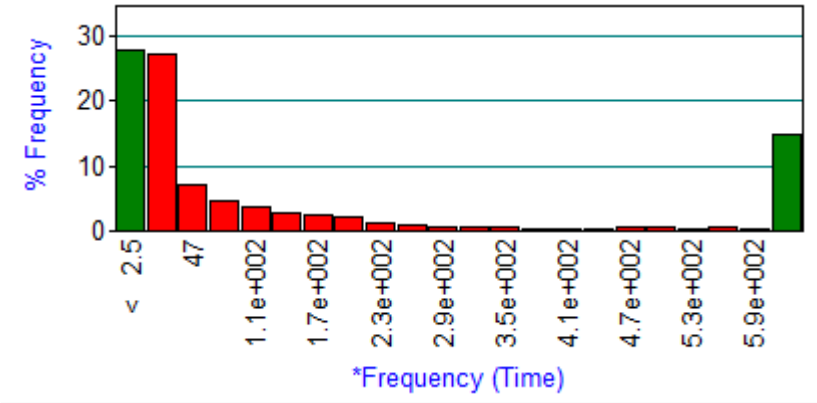

Figure 6.31 Cycle frequency (time) against target percentage frequency achieved

This would equate to a vertical threshold limit of

$$\lambda/4 = v/4f.$$

(Sheriff 2012)

where

λ = wavelength resolution

v = velocity through sediment, using the average weighted velocity model for ELF054 this will be 1530.751387m/s

f = upper limit of frequency range (Hz) = 5300

= 0.077m

This meant that the best possible vertical resolution available on *line 5 BM_1A* was 7.7cm. At that resolution less than 1% of data would be detailed enough for differentiation within the spatial limit. Applied to the coring evidence, this would mean a 7.7cm error bar either side of any boundary within which it would be impossible to guarantee differentiation of individual signal.

Therefore the results from the new velocity model could be measured against the core reports to gauge its effectiveness. The correspondence overall was high with interpreted horizons in the seismic picking unit changes in the core evidence 63% of the time. This meant that the horizons picked in the seismic matched the depth of material contacts in the core evidence within a resolution error bar of between ±5 and ±7.7cm. Where they did not match, a logical reason generally was presented – in the majority of cases this was distance of the core location from the seismic line.

The distance of the core from the seismic line gave highly variable results. Of course, even at a distance of a few centimetres the geostratigraphy can change but with noted conformities in the seismic data, the layers of organic sediment and overlying silts or sands should be relatively widespread in most feature locations. It is however, when the cores are located metres away from the seismic data that issues expectedly occur. The positive results from this case study were in spite of the distances and future investigation would be expected to return even more positive correlations if the cores were taken during the same mission and along the same seismic lines.

The phase polarity results were also highly effective and enabled the creation of a single seismic interpretation process that could identify organic sediments, if not peat. It demonstrated that palaeo features and cores in the seismic record did not have to exactly overlie the seismic lines to suggest larger areas of organic sediment. Due to the nature of the Elbow Formation and its associated peat layers, these organic sediments may be identified with peat. This process has been implemented to try and identify areas of high peat potential for future coring. The principles were also utilized to extend the landscape and propose potentiality maps for the location of peat beds and Holocene peats eroding to the surface.

7 SPATIAL ANALYSIS OF POTENTIAL PEAT BEDS IN SOUTHERN NORTH SEA

7.1 A Characterisation of the Study Area from a Spatial Perspective

In order to take the positive results from a small pilot such as the study area and interpolate this over a larger region, the interpreted data needed to be overlayed onto a map. Only by doing so could the correlations between organic interpretation and evidence seen within localised features be extended beyond the immediate range of the survey lines. As has been well documented (Van Heteren et al. 2014a; Cotterill et al. 2017), peat beds, similar to those investigated in the study area have been recorded throughout the southern North Sea region.

Glacial changes that affected terrestrial landscape features in river valleys and estuarine delta were followed by climatic changes that brought gradual rising groundwater and tidal transgression. As shown in Chapter 5, this combination of factors on a shallow basin landscape proved excellent for peat development. Evidence for soligenous deposits on the slopes, valley and marsh fens in slow or still-water valley bottoms, leading to saddle peat beds on higher grounds were all present in the interpretations. The seismic lines that were available in the study area included three specifically employed for the interpretations (*Line_11A, Route_18, Line 5 BM_1A*), the survey 100m north of Route 18 (*Route_18_100N*), a line 100m west of Line 11A (*Line 11A_100W*) and a line that directly bisected Route 18 (*Line 14*). This allowed the study area to use the interpretations from the original three lines in a wider environment and interpolate the results into a larger spatial context.

7.2 Mapping the Organic Signature

It was possible to plot the organic signal results from the research as values over the survey line. This allowed a quantitative spatial analysis over the immediate area for certain values such as amplitude and frequency to depth. The first of these, shown in Figure 7.1 overlayed the survey lines on

coloured modern bathymetry. The amplitude value for each marked horizon was then displayed as a colour. Colours represented the p-wave negative amplitude intensity of the bright organic reflectors as marked using the velocity model introduced in Chapter 5 of this research. They ranged from yellow as low intensity (approximately -10,000) through pink to blue at the higher negative amplitude.

It must be noted however, that the surveys achieved varying frequencies of attainment which meant that conformity of data was an issue here. One survey line may have wavelength amplitude ranges between -33,000 and +33,000 while another may have had -18,000 and +18,000. Without a common baseline, it cannot be explicitly stated whether this model demonstrates the same material types in differing locations, differences in material or in the shooting of the survey.

That said, significant organic activity with high amplitude responses were observed on the western end of *Route 18* and, by interpolation, this extended through to *Route 18_100N*. Areas of especially high numbers of high amplitude responses were marked in red in Figure 7.1. It is significant that these red boxes cover locations of cores *ELF004* which was rejected from this study due to only containing organic silts, not peat and *ELF001A* which, though it contained occasional organic fragments deeper in the core, had no peat either (M Bates 2017). Both of these cores occur on survey lines at points where the palaeo features looked favourable for peat interpretation, though the cores themselves did not prove to contain sufficient evidence of peat. *ELF001A* especially was a complicated core with a large layer of reworked, broken and mixed brackish and marine deposits, which may have been produced by a large storm surge or tsunami during inundation (Walker et al. 2020). Its inclusion in the research would have confused rather than explained the organic interpretations.

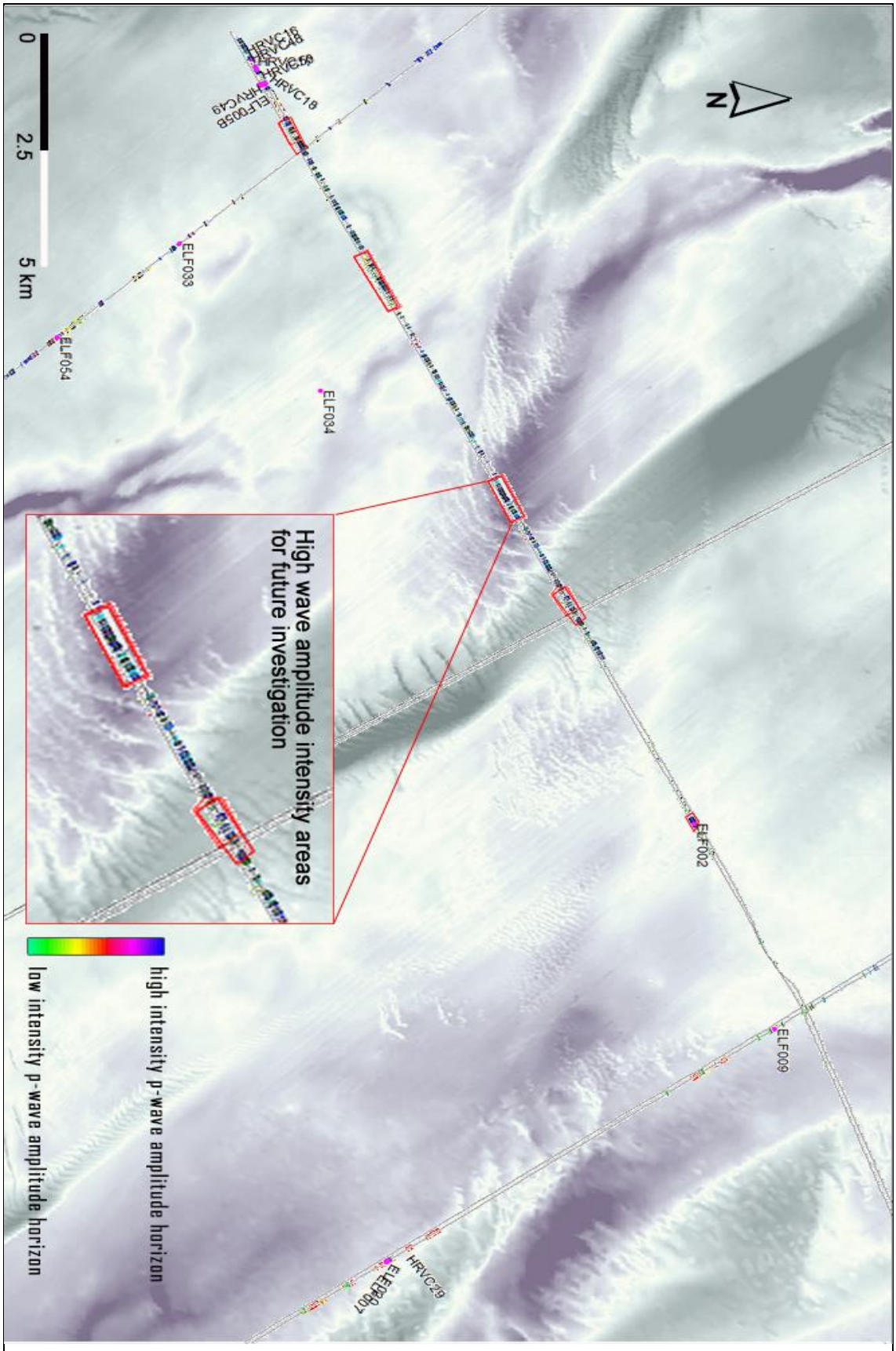

Figure 7.1 Organic Signature Occurrences by Amplitude Intensity

With respect of the other interpreted features that displayed an organic signature, the results from *Line 5 BM_1A* suggested large beds of peat. Here the signals were definitely of lower intensity, though this can also be explained by the weather conditions on the day the survey was shot (Tappin et al. 2011). This result suggests beds on flatter, open ground that cease once the terrain becomes riverine and finally estuarine in nature toward the southern end. Cores *ELF034* and *ELF035*, situated either side of the 'southern river' channel cut through the southern end of *Line 5 BM_1A* and are visible on the modern bathymetry. Both lines recorded peat in the cores and were part of a putative raised saddle peat bed (M Bates 2017 ELF Project Report). However, neither of these cores were located on a survey line to test this hypothesis. It would have been interesting view data from a seismic line traversing a north to south route between *Line 5_BM_1A* and *LINE_14N* that passed through *ELF034*.

A second spatial analysis based on the survey lines took the number of occurrences of phase variance signature and used a buffer function to display all locations of contiguous occurrences within 50m (Figure 7.2). It then used a depth conversion at the Holocene Horizon to establish a base marker for the depth below sea level. The velocity model used was a general two step model as used for mapping interpolation in Chapter 3. This was used because the specialised three-step velocity model, used in Chapter 6, was only applied to certain features containing cores and not the entire survey line. Ideally, the horizon used to build the gridded depth interpolation would have been that of the picked phase variance signature. However, this horizon was too infrequent and incomplete to deliver a cogent result, therefore the early Holocene horizon, which had been marked throughout the area, was used in preference.

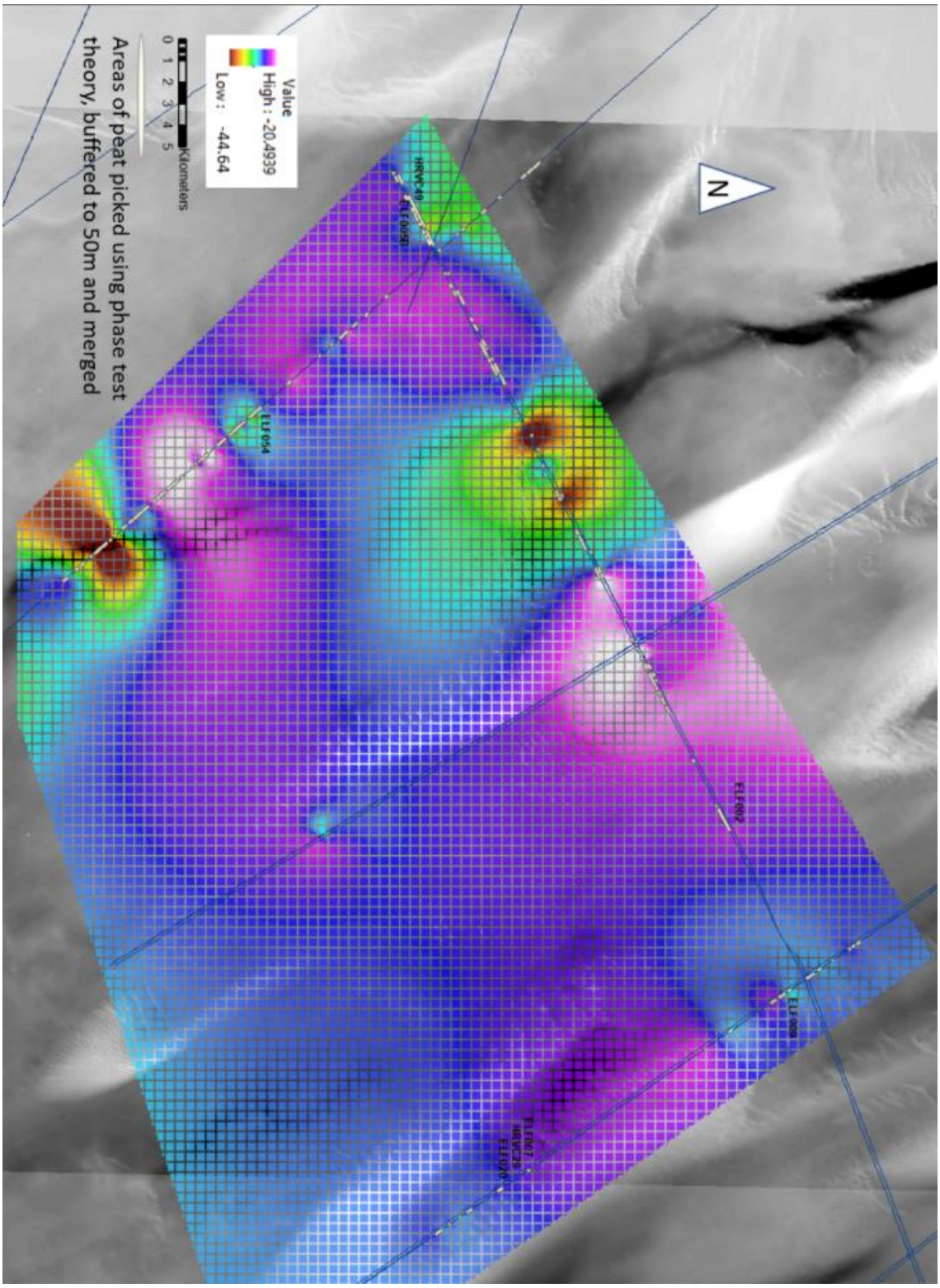

Figure 7.2 Depth of potential Peat beds below modern sea level. This may give some indication of locations where peat may be eroding onto the seabed.

The output gave an impression of the correlation between the location of the potential peat beds and the depth below current sea level. The surface was not necessarily parallel to the bathymetric shape of the

modern sea floor. Some obvious errors did show dips on the survey lines where the point-to-point interpolation encountered aberrations, also the imprecision became more obvious and the data more generalised the further from any particular survey line. This was expected due to the distances between the lines. However, it did illustrate the wide, flattened marsh plains at the west of *Route 18* and the northern end of *Line 5 BM_1A* well, through to *ELF054* where it gave way to deeper mudflats. Also noticeable was the rise of terrestrial land through the saddle upon which *ELF034* sat.

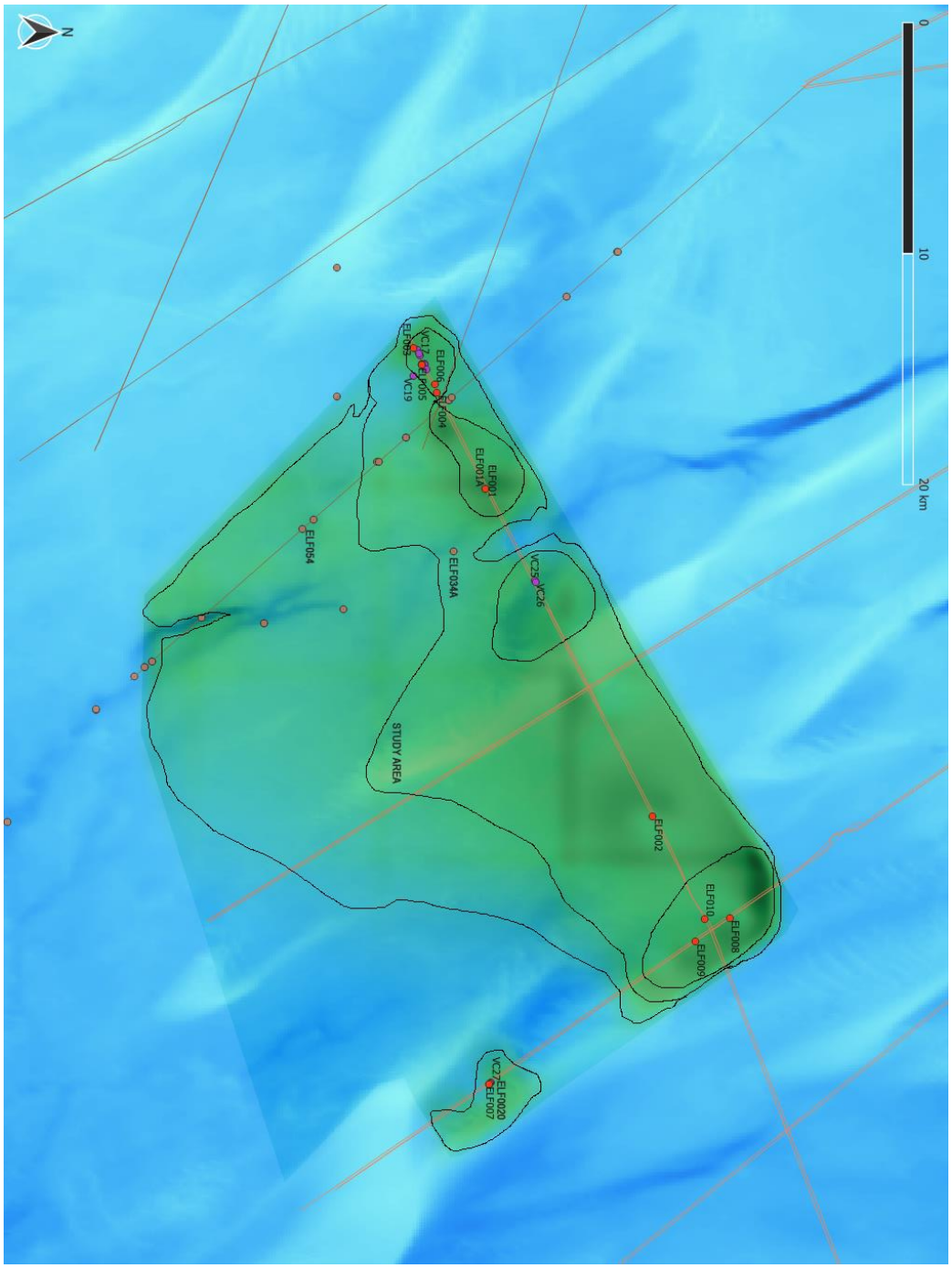

Figure 7.3 Extrapolated heatmap of Organic Signature by intensity. These contours are not topographic but by frequency of signal.

This could then be extrapolated from the immediate surrounding survey lines and, while the peat beds need not be consistent throughout the entire area, the potential for peat bed occurrence could be inferred. Therefore, a contoured heatmap such as the one in Figure 7.3 was used to determine the likely areas of potential peat bed intensity. As opposed to previous potentiality maps that base themselves on bathymetry, this was based on organic seismic signals extrapolated from core observed data and interpolated mapping from depth converted analysis. Combining the previous two spatial analyses (Figures 7.1, page 179 and 7.2, page 181) made this the strongest potential peat model currently available.

This analysis took an interpolated grid of the picked organic reflector signal amplitudes and plotted them against the occurrences of phase variance in green. The amplitude intensity was overlain on the number of occurrences to create a gradient pixel heatmap. The darker the green, the more frequent and intense the signature. The contour lines were added for clarity. There were some issues with grid blocking during interpolation so that the model appeared stepped and blocky in places.

While *Route 18* still dominated the study area in the number of high amplitude occurrences, *Line 5 BM_1A*, despite lower amplitude responses, proved consistent throughout. The phase variance distinction remained greater in *Line 5 BM_1A* than in *Line* 11A to the east and the negative amplitude p-wave of *Line 11A* was inconsistent. In fact, very high amplitude responses from *Line 11A occurred* at the crossline with *Route 18* and locally around the core locations for *ELF020, ELF007* and *HRVC029* but not elsewhere. This gave the line a broken contoured effect. The evidence in the cores of chalks and gravels, which did not reflect such high amplitude signals suggested that this may have been the coastal edge. Where peats were able to continue to develop in river and estuarine deposits, possible beaches, eroding cliffs and coastal edges may had prevented the formation of peat from advancing further.

Such spatial analyses and potentiality mapping of organic sediments was used to build a wider scale perception of the extensive Naaldwijk peat deposits by means of interpolation of data from the small case study area to surrounding regional scale features. By doing so, coastal, riverine and

estuarine beds could be suggested and mapped for a greater understanding of the receding land mass. It also provided a focus for further examination and coring within areas of high archaeological potential.

8 DATA ANALYSIS & NEURAL NETWORKS

8.1 Introduction to Analysis by means of Neural Networks

The identification of data capable of classification as organic sediments occurred within seismic interpretations by means of quality velocity modelling (Chapter 5). The addition of ground truthing to support such interpretations using a phase and variance 'signature', as set out in Chapter 6, helped differentiate sediment from gases and even provided a focus on specific types of peat formations. In Chapter 7, spatial analysis aided in showing wider scale potential for the distribution of these organic beds. Looking back to the geology section in Chapter 2.3, it is also important to bear in mind the possibility of the ubiquity of the Nieuwkoop peat beds across the southern North Sea (Cotterill et al. 2017).

To this end, an automated classificatory or 'pattern recognition' process would greatly assist archaeological landscape analysis. Similar needs are required by the rapidly expanding Windfarm and shallow gas enterprises that must run surveys for organic shallow bedding sediments as preliminary investigative work before siting installations (Thal et al. 2018).

8.2 Available technologies for the automation of geophysical machine learning

The theory behind using a network of neurons or logical containers to launch logic responses has been in use for many years. Handwriting recognition and CCTV facial identification software has been used to create patterns that weight positive or negative results in response to comparisons to a database catalogue (Wechsler et al. 2012). This allows AI unsupervised networks to create loops for pathfinding and pattern recognition which make up an ever-increasing number of algorithms in our modern world. Refinement in such fields is increasingly complex as the processing power of modern computers allows this technology to enter the mainstream of research.

Oil and Gas industry research has always created more datasets than it has the ability to manually interpret, store and process (Coléou et al. 2003). Therefore, the use of machine learning analytic workflows have become very important to the investigation of constructing synthetics and recognising patterns in substrates. Previously, traditional human interpretation of seismic data has been performed in two ways; deductive and inductive (Chopra et al. 2018). The former uses logic and reason to surmise links between one piece of evidence and another for which there are little or no supporting data. Machines find deductive learning extremely difficult. Inductive workflows, using examples to map a direct causality, are, however, iterative, validatory and repeatable. Machine AI excels at such tasks and can use these processes to successfully predict extremely complicated outcomes that human interpreters would find repetitive and arduous. This is known as pattern recognition.

When investigating existing seismic pattern recognition techniques, they tended to fall into two broad categories. The first were those that were prone to changes in fluid and lithology and the second those that worked well with curvature and coherence of waveform (Zhao et al. 2015). These were not directly applicable to this research. Stratigraphic differentiation, especially of shallow depositional material and facies analysis was poorly represented. Therefore, it was deemed necessary to create a bespoke network model.

To create the foundations for any neural network, it was necessary to identify the parameters which any given AI would need, in order to work. These would include:

a) Fixed criteria – unchanging aspects of the physical world which could be hard coded.
b) Changing criteria – any aspect that could change depending on an individual query and would only be valid within the current environment (dataset).
c) Input criteria – any aspect of the query that was dependent on the output of an event or multiple events from which an outcome may be achieved.
d) Output criteria – any aspect of the query that relied on the outcome of an entire loop (epoch) of the neural network to influence the input criteria and weighting of the next parameterisation.

The difference between the final two was vital to understand. The former c) was a parameter that could be weighted at the start or as an outcome

of any event within the process. These input criteria could also be employed at the hidden, AI stages of an epoch. The latter d) was set as an evaluation of the epoch and used to adjust the weighting of the next epoch accordingly.

8.3 Supervised Machine Learning – Theoretical Models

Machine learning can be broken down into supervised and unsupervised networks. These relate to the methodology in question. The primary supervised (*a priori, learn by example)* model for this was the Multi-layer Perceptron network (MLP) or Artificial Neural Network (ANN) as in Figure 8.1 (Chopra et al. 2018).

The strengths of the Artificial Neural Network lie in its speed and robust computational power for machine learning when data are incomplete, noisy or incomprehensible. These characteristics make them inherently useful for real-world problems such as pattern recognition (Van der Baan and Jutten 2000; Schalkoff 2007). Their use in marine geophysics has been demonstrably proven over the last thirty years in the energy industry. Research in the use of ANNs for reservoir characterisation (An and Moon 1993; Aminzadeh et al. 2000; Ouenes 2012), seismic event classification (Dysart and Pulli 1990) and even the auto-location of buried objects using backscatter have been pursued with interest (Brown and Poulton 1996). Recent work by Haber and Ruthotto (2017) and Peters, Haber and Granek (Peters et al. 2019) implemented routines of chain ANNs could be used to interpret entire survey lines and interpolate data between observed and classified borehole wells based on the lithology. Such a neural network would have been the ideal basis for this research. However, the code for this ANN was not available and re-creating the necessary code, while briefly pursued, was beyond the scope of this thesis.

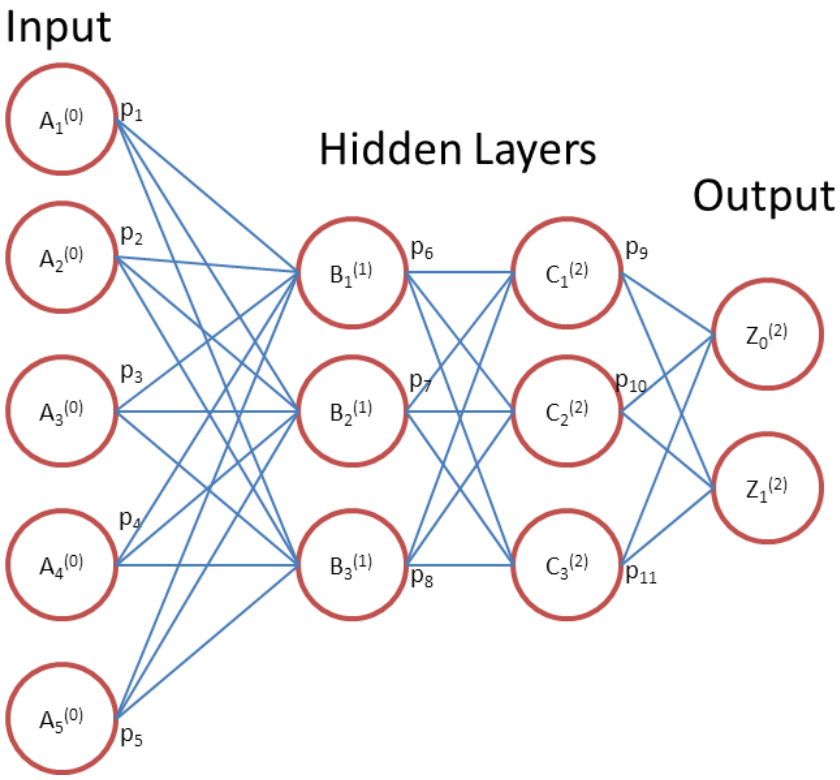

Figure 8.1 An illustrative model of an ANN or MLP neural network with 4 levels of logical depth.

The theory behind such a model, would require a minimum of one set of manually picked correct data and one incorrect set of data. The training would then run reiteratively with a set of biases to enable improvement. To do this the model would employ a number of hidden layers in order to act as logic gates in a back-propagation routine. Data under parameterisation would be fed into the model via neural nodes (A_1 to A_5 in Figure 8.1) and would propagate to as many neural nodes at the next level (B1 to 3 in Figure 8.1) as passed the threshold of the input criteria. These would be subject to logic commands (NOT, OR, AND, NOR, NAND). The outcome of each step would be assigned a weighting. This weighting (p for the blue arrows in Figure 8.1) could be assigned as a result of an event outcome or a cost analysis at the end of a training epoch.

The weightings, after the initial input parameter entry of the model, would be entirely controlled by the AI which is why the neural nodes for all intermediary stages are classed as 'hidden' (B and C in Figure 8.1). The decisions made and the weightings involved at each progressive level became more complex based on the weightings assigned so that initially, many nodes will fulfil every criterium but as the model progresses, loops

and is refined, ultimately, in the ideal model, only a single output would fulfil the output criteria (Z in Figure 8.1).

To achieve this level of efficiency, the model would employ two methods of weighting data on each set of nodes and for each iteration of the process. The first is the 'feed-forward' cost function which is a gradient descent method. This allows the AI to subtract a cost weighting from each step and on each loop to find the most efficient, logical cost saving from each process iteration. It could then apply this weighting to every node and eliminate any inefficient nodes, or any node which had been activated in error. This reduces the overall processing cost of the model. The second method is back propagation in which the AI runs the process backwards from the outputs through the hidden layers, but only applies the logic and the weighting. It does not process any of the data. In doing so the AI activates the nodes to trace the cost efficiency of the neural pathways taken without the overhead of data processing. This demonstrates the efficiency of the weighting itself and flags up any improvements that could be made in the structure and weighting system. It is important to note that these methods do not detect or correct errors in the neural network. If the design is incorrect, the workflow compromised or the parameters set incorrectly, the AI will not detect this.

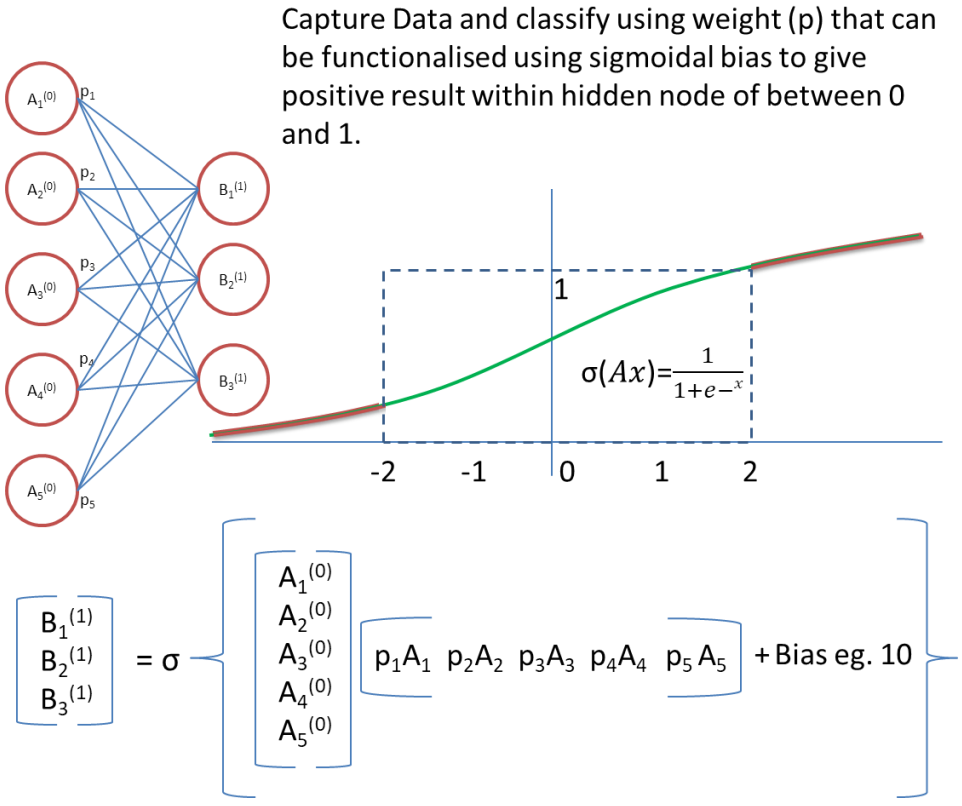

Figure 8.2 Using a sigmoid bias to weight neurons allows integer outputs (Smith 2013).

As computers prefer to work in positive integers, the biases that are applied to the neural nodes are most commonly sigmoidal (Figure 8.2). Sigmoidal biases are used in order to eliminate negative parameterised data and data greater than 1 into a range between 0 and 1 (Smith 2013). Alternatively, inserting large biases to the initial nodal weights in order to flatten all of the data into positive ranges can be effective, e.g. they may have assigned a weighting of +10 across all nodes to give a range of between 8.3 and 11.7. For this thesis, the neural network would have employed a sigmoidal bias as the input parameters were in the form of both event and equation criteria. It would have proved impossible to apply the same logic operators to these differing sets of values. Therefore, confining all input parameters to a weighted range between 0 and 1 ensures no issues with unexpected out-of-range results.

Another consideration when constructing an ANN is one of planning. Due to the nature of hidden layers and nodes, the entire model must be considered as a closed box, and, while the initial parameters can be set manually, the overall design of the model cannot be changed once created. Therefore, the number of levels including hidden nodes, the creation of the initial logic gates and their parameters, as well as the number and functionality of the outputs must be considered and set up correctly at the outset. Once the model is initiated and the first weights and biases set it becomes 'too late to merely tweak the model' (Nielsen 2015).

The vast majority of work with ANNs has focused on the use of image recognition for which these networks are extremely robust. However, the methods set out in Chapter 5 and the small dataset of results meant that this research posed problems for such an image recognition-based network. The problems fell into three major areas:

The first was that the results from Chapter 6 relied heavily on interpretation of seismic data. Variations in the frequency, number of traces and resolution of data between surveys meant that little consistency could be determined to build up a set of images. Amplitudes, even for the brightest of organic reflectors, ranged from -18,000 to -30,000 p-wave. Even when viewed in phase function, where the polarity crossover was more uniform

between surveys; attenuation, tuning and resolution issues could still make the visual identities of similar signals appear very different.

The model would therefore require numerous examples to capture all parameters and conditions. Such seismic image catalogues exist with extensive libraries of thousands of facies data images (Ouenes 2012). In recent years seismic pattern recognition and facies analysis modelling using machine learning technology has advanced in this regard with large datasets now available on subscription for common interpretive features (Figure 8.3). These have been used to establish algorithmic parameters for the pre-processing of data that has allowed simpler classification of seismic facies to be studied (Wrona et al. 2018). Unfortunately, no image library was available to this research and, as will be discussed later, the stock 100 x 100-pixel image catalogue was not practical for detailed, shallow sediment research.

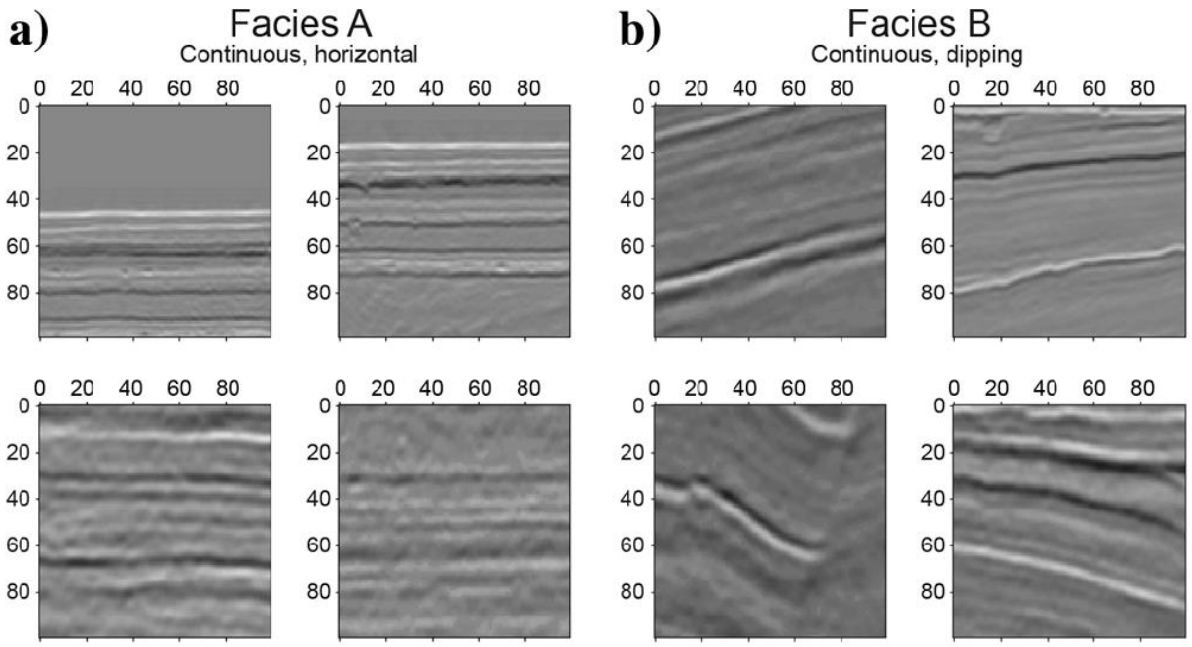

Figure 8.3 2 x examples of the 4 seismic facies divisions from the 100x100 pixel image catalogue (Wrona et al. 2018).

This thesis would have required both better resolution images and a processing power for the image identification and subsequent pattern matching technology, that would have stretched this already advanced technology. In the specific targeting of an organic fascia via image recognition the challenge perhaps has more in common with the work of Jesper Dramsch's in his PhD *Deep Computational Geophysics and*

Machine Learning (Dramsch 2018). Here he explores the methodologies of AI interpretation for Oxford University Visual Geometric Group's VGG-16 and other generative adversarial networks. The ability to create virtual synthetic seismic data for the training of networks was a vital part of the evolution of deep learning where multiple networks competed with each other for efficiency (Mosser et al. 2018).

The second issue was the image size, resolution and quality for the purposes of this research. A standard ANN uses industry agreed architecture resident networks (ResNets) tailored to the tasks of image vectorisation input and output using variations of Deng's Grey Incidence Analysis model (e.g. Keras and Tensorflow). However, as has been discussed in recent papers (Luo et al. 2016; Peters et al. 2019), these ResNets were specifically intended for small, self-contained images, where downscaling images to greyscale vectors also meant a downscaling in dimensionality. However, in larger scale datasets where segmentation may be necessary and reduction of the image does not necessarily equate to a reduction or a downscaling of parallel, convolutional data (such as peak frequencies, amplitudes or spatial relationships), this coarsening of the dataset may have profound effects. Newer, non-standard architectures, such as U-Net, Fast FCN and Gated SCNN, which may be upscaled or downscaled while maintaining such convolutional algorithms, are coming on-stream but are not yet in common usage (Peters et al. 2019).

Finally, the ANN required for use in this research was required to look at the study area from which the peat coring evidence, and thus the seismic signature was attained. It was therefore limited by both the geographic and seismic availability of that study area, resulting in a dataset of only 8 confirmed (cored) peat sites and a further 17 high potential peat / clay or peat / silt interfaces located by means of the phase variance identification method adopted in the previous chapters. This gave very few data sets for a working pattern matching neural network to work with. With more time resource and technical ability available to the research, the option of generating virtual synthetic seismic data could have been advantageous but this was not an option at the time.

Sufficient coverage for supervised neural network learning of well core data has been the subject of previous papers (Johann et al. 2001). Here, discussions over increasing geographical areas and decreasing

resolutions resulted in ever lower statistical confidence intervals and incomplete or missing data for accurate predictions. This was especially true when attempting to interpolate a 2.5D or 3D surface from 2D seismic data over an extensive area (Kohonen 2006). In such cases it was proposed that an unsupervised model such as a Self-Organising Map (SOM) may be a preferred alternative.

8.4 Unsupervised Machine Learning (via an SOM)

Two unsupervised learning algorithms can be used for pattern recognition. The first; K-means Clustering was developed in the 1960s (Forgy 1965) and used no interpretation attributes. It was a mathematical model based purely on the vector and number of desired clusters. The issue with this solution was that the resulting pattern cluster had no consistent structure (Zhao et al. 2015). For seismic interpretation this would mean that facies with similar reflective properties could not be relied upon to be interpreted as the same pattern cluster each iteration.

The second unsupervised learning algorithm for pattern recognition was devised by Tuevo Kohonen in 2001 and built a structured topography into the clustering. He named this the Self-Organising Map (SOM) and this solution was demonstrated to be more efficient and consistent than the K-means clustering (Coléou et al. 2003). Unlike the supervised ANN, the SOM does not require a catalogue of data against which to compare results. Instead, the code in a SOM utilises pixels or, in the case of seismic horizon picking, vector characterisation. The model relies on only one set of clustered manual data in a user-defined number of vector classes. It does not feature any input parameterisation or logic weighting. Each iteration of the routine process establishes a number of 'cluster centres' that the model posits as the baseline from which all other vectors are measured on a cost-basis analysis. These are then compared to the previous iteration. By constantly moving this baseline and recalculating the costs, the AI is able, over a number of training loops, or epochs, to cluster together - like patterns with like.

Because the reiterative process does not use weighting or logical based parameterisation such as are employed by a supervised ANN, the reference samples must be isolated manually before running an unsupervised SOM. These manual seeds are classified (m_i) and stored as

vector points in space including X, Y and possible Z co-ordinates. When the SOM is run, these co-ordinates are generated in proximity to their neighbours, thus creating a weighting system within a proximity, with the smallest distance (m_b) to the central vector (χ) being computed as the Best Matching Unit (BMU) for that cluster. This is based on the original SOM algorithm first suggested by Kohonen in 2001:

$$|\chi - m_b| = \min_i\{|\chi - m_i|\}$$

The process is then repeated with the each of the interconnected vectors being moved closer to the previous BMU. The updating rule is given as:

$$m_i(t+1) = m_i(t) + \lambda(t)h_{bi}(t)[\chi - m_i(t)]$$

(Kohonen 2006)

Where λ is the rate of improvement while t is the iteration or epoch. So, while the epoch number increases, with each manual classified seed, the neighbouring cluster size $h_{bi}(t)$ shrinks. The movement of vectors in respect to the location dependent on the neighbouring cluster size is governed by a sigmoidally reducing sub-routine:

$$h_{bi}(t) = \frac{e - |r_b - r_i|^2}{2\sigma^2(t)}$$

(Kohonen 2006)

More refined forms of weighting are available in order to move the vector co-ordinates in specific groups or to target specific clusters. U-Matrix, Von Neumann and Moore Neighbourhoods all target different groups of vectors in square, triangular or hexagonal based connections. Each train the model to move the vectors to different BMU positions in map space without changing the topology. Thus, the AI is able to compute the costs associated with the weighting proximities.

8.5 Methods and Requirements for machine learning.

For the purposes of this thesis three methodologies were attempted for automation of peat detection and interpretation from seismic (SEG-Y) data. For the sake of simplicity, only reflective impact seismic geophysical data was investigated in this research. This included Boomer, Sparker and, from literature, chirper SEG-Y data. Boomer data was taken from the study area outlined in previous chapters. Sparker and Boomer data was taken from the East Coast REC survey data (Birchenough et al. 2011) and sparker

data used in supporting evidence from Fugro Holland Kust Noord Wind Farm (Thal et al. 2018).

The software used, in addition to the geophysical analysis software and Geographical Information System software already mentioned in previous chapters, included the following:

Python 3.4, Jupyter Notebook, Tensorflow and Matlab 2 were used in the creation of a basic image recognition ANN. The MNIST handwriting recognition database was used to train the coded image recognition ANN and the bulk of the Python code originated from open source tutorials online at GitHub. The full code is attached as Appendix 3 Python Script for Keras Image Recognition. For the Supervised parameter based ANN and the Unsupervised SOM based machine learning, here called an Unsupervised Vector Quantiser Network (UVQ), a specific piece of software called OpendTect was used for the specific reason that it possessed a module capable of running neural networking on geophysical data surveys. OpendTect from dGB Earth Sciences is an open source software with a number of commercial 'professional' plugin licences and was used specifically for the interpretation and analysis of seismic data. The neural networking plugin was part of the commercial licence and required the OpendTect Professional release of the software. The release version used in this research is 6.4 under academic licence.

The graphical and memory requirements of the software proved quite intensive and even with a workstation equipped with an i5-3Ghz processor, 64 GB RAM, Nvidia GTX 1080 graphics card and dual monitor capability, the research pushed it beyond the limits of the computers processing power resulting in frequent crashes and memory corruption.

8.6 Method 1: Image Recognition (Python & Tensorflow)

The most straight-forward method for the implementation of such a routine was to be coded in a language called Python where a number of examples of Artificial Neural Networks have been developed for many different purposes and are freely available online for deep learning and machine learning training purposes (cf. www.github.org).

Python makes use of open source modules such as Matlab for plotting results and Jupyter Notebook for online cell code structuring and widget control. The use of Keras and Tensorflow in modern python coded ANNs has turned simple machine learning image recognition into a mainstream investigative tool. Everything from CCTV crime detection to online patient self-diagnosis now employ image recognition. Implementation of such a model was the most straight-forward as there were numerous examples of Artificial Neural Networks built for a wide range of different purposes and freely available online for deep learning and machine learning purposes. Although none were specifically directed toward seismic research, theoretically, patterns matching images of phase polarity within a seismic survey is not dissimilar to a routine for handwriting recognition or camera pixel identification (Schmidhuber 2015). Therefore, it was an obvious place to start development.

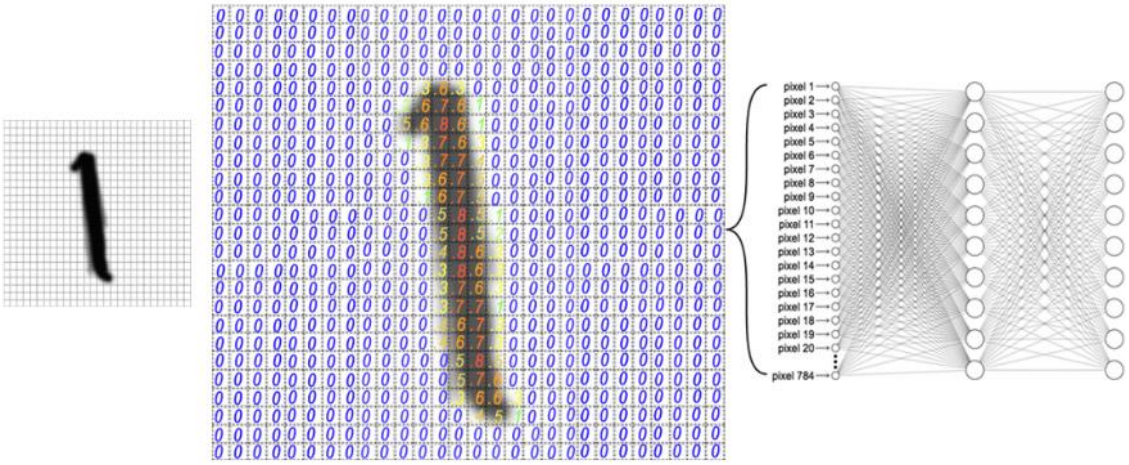

Figure 8.4 Simple image recognition using Tensorflow based on 28x28 pixel imagery and 10 outputs with one hidden neural layer (after collaborative model Pytorch hub)

In order to utilise code from a basic handwriting image recognition script and adapt it to read images of seismic interpretation it was necessary to build up a basic library. In this case the script required images of 28 x 28 pixels, giving a total input of 784 pixels as in Figure 8.4. These were given an initial sigmoidal bias based on the level of black in each pixel from 0 to 1.

Even in the theoretical stage of development there were issues with an out-of-the-box solution. First, the solution for the detection of peat via seismic investigation, as detailed in Chapter 5 relied on a measurement of the crossover of negative to positive polarity either side of the zero-phase wavelet. The phase variance study required this to lead with a negative polarity. Such functionality cannot be accomplished within an image without a representative key. Variance peaks were also vital to the method described in Chapter 5. These were overlayed onto the phase function and had a tendency, depending on the display quality, to obscure any interpretation of the survey data behind. A separate image would be required to preserve both datasets. Not only this but the 28x28 standard greyscale pixels as employed by the simplified Tensorflow network would be an impractical solution for the purposes of seismic interpretation without a high degree of pre-normalisation of imagery. Therefore, this needed to be factored into the methodology.

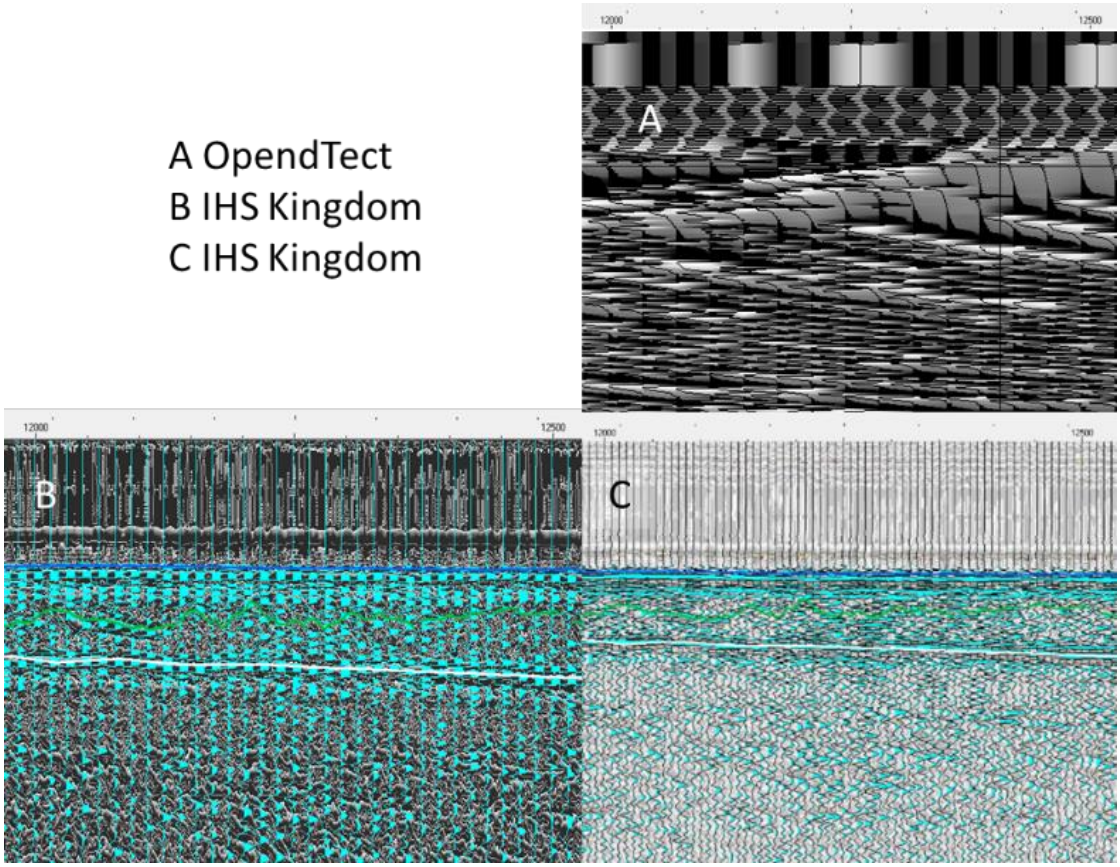

Figure 8.5 The same section of survey line V5-X-S3000 in phase view with variance peak overlay. A) on OpendTect B) and C) on IHS Kingdom on different PCs. Data courtesy of FUGRO RVO (Thal et al. 2018).

It became apparent that imagery not only varied between differing pieces of software and different versions of the software but could even look different on two machines running the same software. Figure 8.5 illustrates how the same line of survey data can be displayed by default in

A) and B) two different pieces of software and between B) and C) the same line as displayed in IHS Kingdom but on two different PCs.

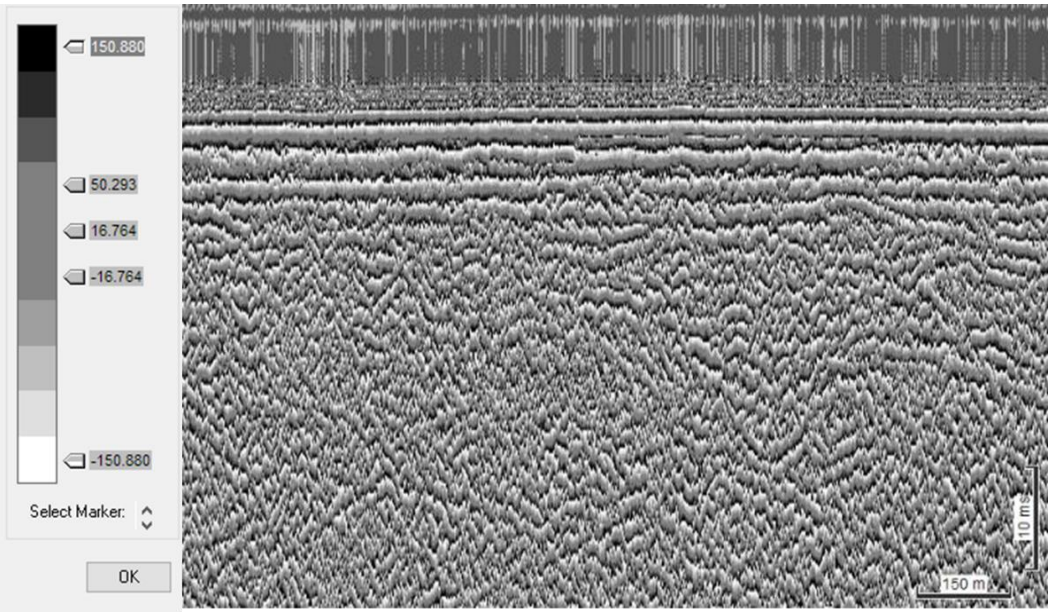

Figure 8.6 (above) Employing a uniform and simplified colour bar and (below) variance peaks set to white may still obstruct detail. Therefore there needs to be a function to run with variance on, variance off and compare

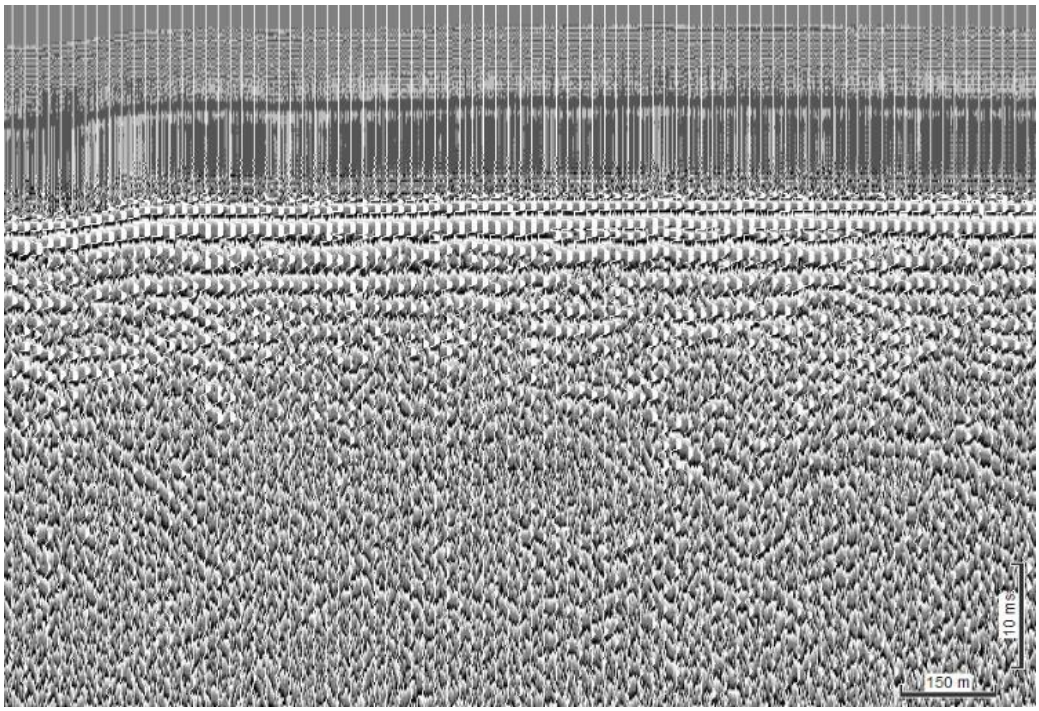

Therefore, the first steps in the normalisation process would need to be to a) create a baseline for all images and b) allow the analyses from the previous chapter to take place in an uncluttered workspace. To do this, the surveys were displayed in a phased function mode with a colour bar set to a basic 10-colour grayscale ramp with white as extreme negative and black as extreme positive and a wide range of grey in the centre (see Figure 8.6).

Frequency ranges may differ between individual surveys, but a bandpass filter was then employed to remove any frequencies that play little or no part in the phase display and further normalise and simplify the image. Phase degree usually peaks by 300Hz and tails off after 500Hz. Cutting the range of 700+Hz removes excess display variation as in Figure 8.7.

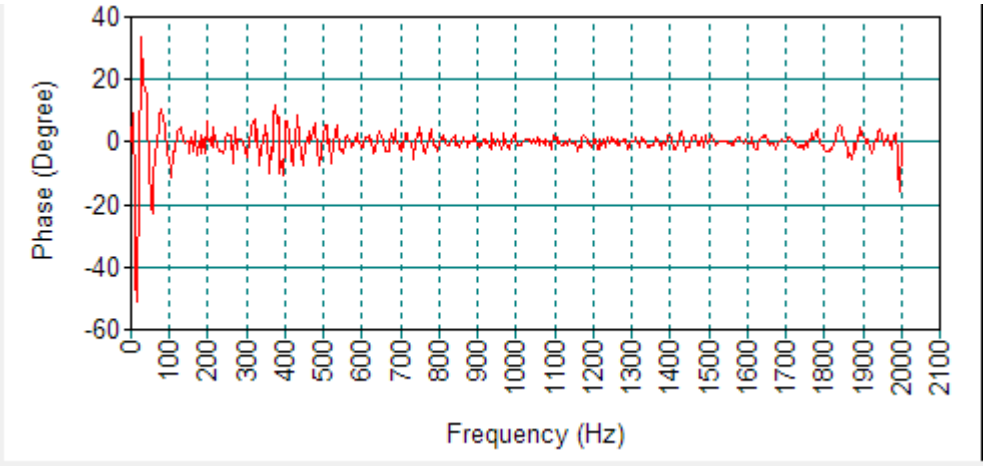

Figure 8.7 The Phase Degree against frequency of a typical Sparker survey (Thal et al. 2018)

There was also a need to consider the variance peaks carefully. Their inclusion was very important in the determination of the zero-phase wave boundary location for organic facies, and therefore had to be considered crucial for the inclusion in any AI routine. However, as shown in Figure 8.6, the variance peaks obscured the details of the reflectors so that Tensorflow or Keras image identification routine proved unable to pick the phase polarity beneath. Therefore, it was necessary to run the routine twice, to create two images and compare the two results. This added a layer of complexity to the network above that of the handwriting recognition ANN.

Finally, reduction to a minimum pixel size required attention. 28x28 pixels proved to be too small to provide any resolution (Figure 8.8). Direct size capture (Figure 8.8a) did not provide enough data to establish the existence or not of a peat fascia. Downsizing of pixels from a larger image (Figure 8.8b), lost all useful definition. The differentiation between the variance fill and the negative wave form behind was negligible. In fact, to separate these features to any meaningful degree required either the use of full colour or a multiplying of the pixel resolution in greyscale. The minimum size that could practically work for this purpose was 128x128pixels (Figure 8.8c) to allow direct pixel by pixel capture and recognition. It must be noted here that Thilo Wrona was able to work with a dataset employing images only 100 x 100 pixels in resolution see Figure 8.3, page 191 (Wrona et al. 2018).

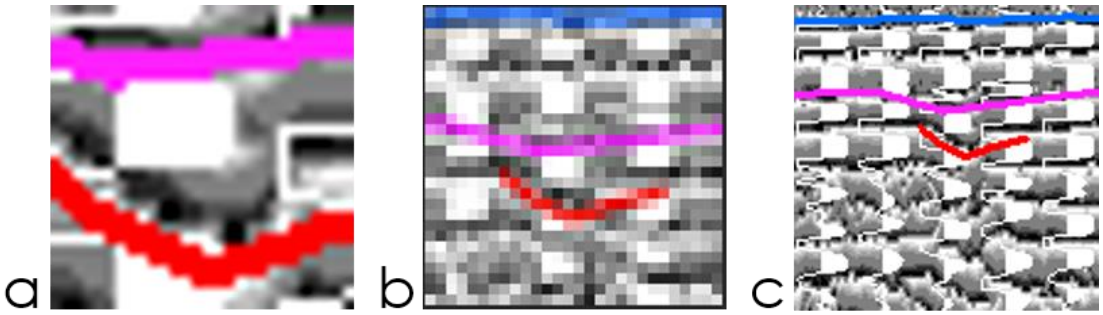

Figure 8.8 Three examples of input data for image recognition ANN. a) direct 28x28pixel capture. b) Capture downsized to 28x28pixels in photo-editing software c) 128x128 pixel direct capture.

The CGG catalogue of surveys from which Wrona's images were taken was of ultra-high resolution 3D seismic surveys with bin sizes in the kilometre ranges. So, the sample sizes displayed in Wrona's 100 x 100-pixel images while looking very compact, actually had a resolution equal to around 1 pixel per 100m. This resolution whilst justifiable for facies recognition for oil and gas prospection is not suitable for the purposes of this research. The detail required for manually picking of peat beds in river channels, would make vertical resolution of sub-metre scales impossible in these images.

Utilising larger resolution images in the research would create its own problems. Upscaling the input nodes to accommodate 128x128 pixel resolution would require a neural network comprising 16,384 inputs and the exponential number of required weighted biases required per iteration. At such complexity, more efficient methods would be necessary than employed by simple ANN models using Keras or Tensorflow. Such models employ algorithms applied to a standardised set of images in order to create a baseline of mean, Gaussian and standard deviation images which are then used as comparison for assessing cost and

weighting. Input images tend to be divided into portions which are processed with their own logic and recombined using transferred learning processes defined by an iterative layering of the mean, Gaussian, and standard deviation weights. This has been achieved successfully in complex facial recognition networks to identify key features such as eyes and mouths (e.g. Beniaguev. 2018) This may yet be of use in the visual analysis of seismic surveys but the technology is far in advance of this research.

Therefore, the results of this method were inconclusive. The research was unable to move past a theoretical stage of ANN creation due to the following complexities:

- tutorials existed to create simple ANN coding using Keras for stock image recognition functionality. However, anything that required the slightest complexity increased the coding difficulties exponentially.
- image recognition could not be run on a full line of survey data, only on specific images that would require intensive pre-processing to work for Keras. An amount of work that would negate the benefits of its use.
- to be of use to archaeologists, the peat facies not only needed to be auto interpreted, but also placed in context. An interpreted image cannot accomplish this.
- the phase variance signature calculated in the previous chapters relied on the measurement of wave polarity and overlain variance peaks. This could not be isolated within one single image.
- the time and limits of research meant it was not be possible to mobilise the multiple personnel and skillsets that would be required to achieve this goal.

Ultimately, though the research was not able to create a working code, it was able to demonstrate the potential for future ANN design work. By following tutorials on the GitHub website and using examples of code on various forums, demonstrating more advanced ANN models, the research created a working Keras image recognition AI in Python script (See Appendix 3 for code). The same basic concepts would apply to the groundwork for a coded seismic facies recognition model.

8.7 Method 2: Unsupervised Vector Quantiser (via OpendTect)

dGB OpendTect Pro was considered for this stage of research as it possessed a commercial module for seismic stratigraphic neural networking cluster classification UVQs. These Unsupervised Vector Quantisers are a type of proprietary SOM in which manually classified vectors cluster together by means of a cost analysis dependent on the attributes assigned to the input and the output nodes.

In its simplest form, this means it is possible to set a number of attributes against specific facies points at co-ordinate vector points x, y and z and have the machine propagate those classifications along a set horizon or dataset. The network establishes a number of cluster centres and sets a cost analysis weighting for the next iteration to use as an input attribute for those clusters. The 'winning' cluster then receives a match and the others in that segment are moved to a minimum quantised vector distance from it before the test is repeated. This continues ad-infinitum or for a set number of 'epochs' defined by the network. The UVQ needs to be refined after each run to establish a final trained network before it is run on a horizon or volume.

For the purposes of this research, the benefits the UVQ offered was the application of attribute parameterisation on the input nodes. OpendTect not only allowed the application of attribute sets to the survey data but also to the classification elements manually assigned for use in the UVQ. In order to test the UVQ potential, the study set out to try and classify two types of marine geophysical feature:

1) The first test – a straight horizon line. The data used was from the East Coast REC (Birchenough et al. 2011). The straightest line in the survey was the sea surface reflector. This reflector was marked manually on 2 of 3 interconnected 2D survey lines with the intention of the UVQ identifying the same classification and interpolating it over the interconnecting 2.5D space.
2) The second test was to seed multiple peat deposits on a single survey alongside facies of non-peat materials. The UVQ would then classify the peat deposits and identify similar deposits, classifying them as peat while differentiating these from other material facies.

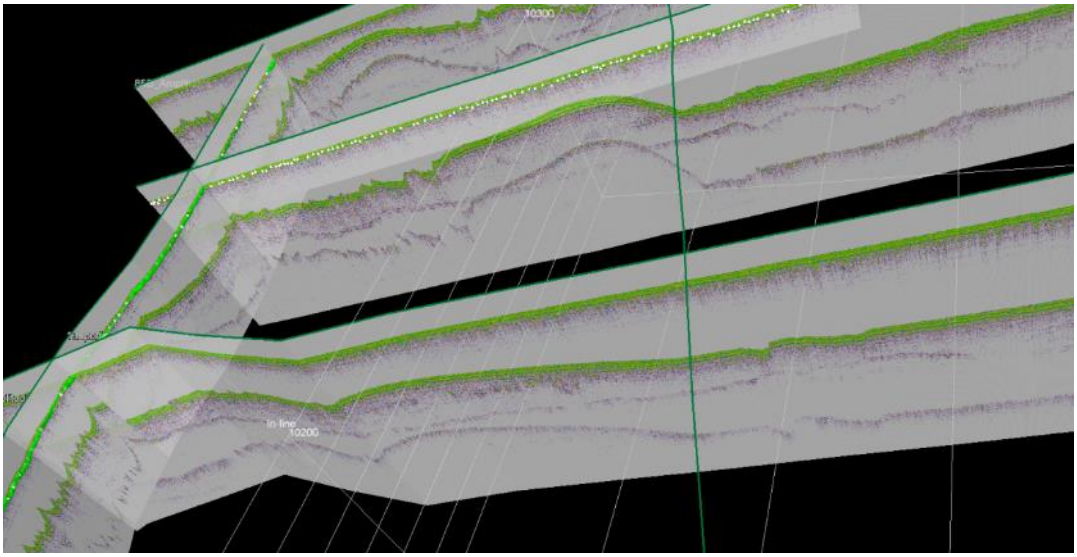

Figure 8.9 Manual picked vector sea horizon on crossline and inline, for SOM pattern recognition

To do this the following attributes were applied to an intersection of 4 data lines (Figure 8.9) in the following order:

Line Attribute Set 1:

Instantaneous Analysis -> Phase View

1-kHz Band-pass filter for normalisation

Line Attribute Set 2:

Instantaneous Analysis -> Q Factor

1-kHz Band-pass filter for normalisation

Least-Square Estimation Calculation based on frequency

Class Attribute Set:

Narrow class to time window (ms) 1class per 10 ms = 5 classes (50ms) x2*.

OpendTect set the window equally to positive and negative integers. To reach a two-way travel time of 50ms the window default was -24 to +24ms. In the sea horizon test, the window was set to run iteratively. The UVQ's aim was to set the number of classes and the time window at the correct level to capture the correct attributes selected in the 4 data line pickset. This would result in a trained network with the best number of matches. This was at best a system of trial, error and experience. Several tests showed that, 10 samples and 12 classes provided the optimum spread of samples and gave a practical window of -8 to +24ms.

An additional class attribute that would have proved useful would have been a negative to positive phase filter as one of the frustrating aspects of OpendTect was that UVQ could not be run using wave amplitude and variance fill views simultaneously. Therefore, the UVQ had to be run in phase function and the variance fill peaks overlaid separately in a 2D viewer. There were no opportunities to utilize the variance peaks in attribute analysis for the UVQ. An additional issue for this research was the inability to filter for direct crossover of negative to positive phase values at the zero-phase wavelet that was such an integral part of the results found in Chapter 6.

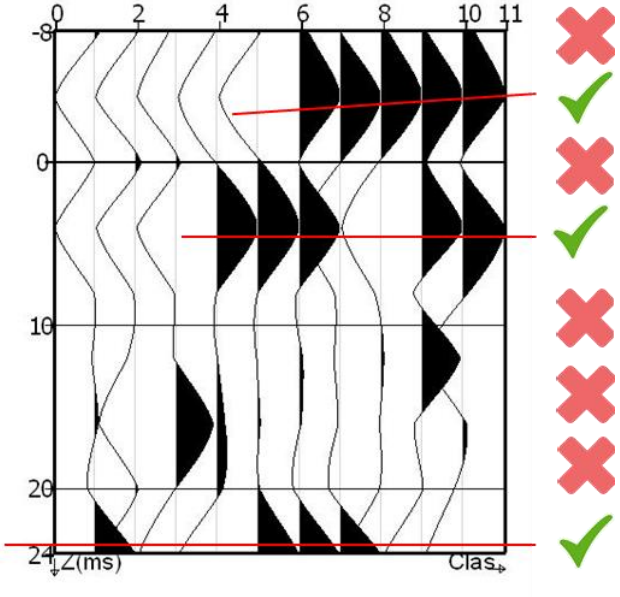

Figure 8.10 The sample UVQ claimed to return a 55% match over 10 samples and 12 classes. However, the wave sample comparison only matched in 35% samples and classes.

Manual picking of the sea horizon from the East Coast REC data (Birchenough et al. 2011) was performed in two ways as both were available as options in OpendTect. A solid manually picked horizon line was chosen on Survey *Line 13B* (far left), while a seeding system was used on *line 35B* (2nd crossline). These were classified as two different horizon events as shown in Figure 8.9: the first as a VD 2D horizon (solid green) and the second as a seeded pointset (white dotted). It was advised when creating a pointset that it should ideally contain between 200 – 1000 points. The pointset on 35B was estimated to contain 200 points.

In the seabed horizon run, the Q-Factor analysis was not employed as there was no peat fascia expected. The simplicity of the horizon suggested

the seeds themselves should be used as the only samples in line attribute set 2. By requesting the AI take certain number of samples at positions in the time window the classification could be propagated.

Once the attributes sets were assigned, from within the Design Neural Network module, the pickset, from which the seeds used in horizon classification, could be identified. The UVQ would have the sample range -12 to Sample 24 assigned to the appropriate input attributes. The samples were made up from the horizon pickset and the solid manual horizon, chosen above and below 0 (being the picked horizon time itself). Because this horizon line was so near to the top of the survey, very little data appeared above it, therefore variation above was less likely than the likelihood of errors occurring below, so more attention was paid to samples occurring below this line. Therefore, more samples were taken below the horizon than above. 10 samples were the recommended number as cited by the software guides.

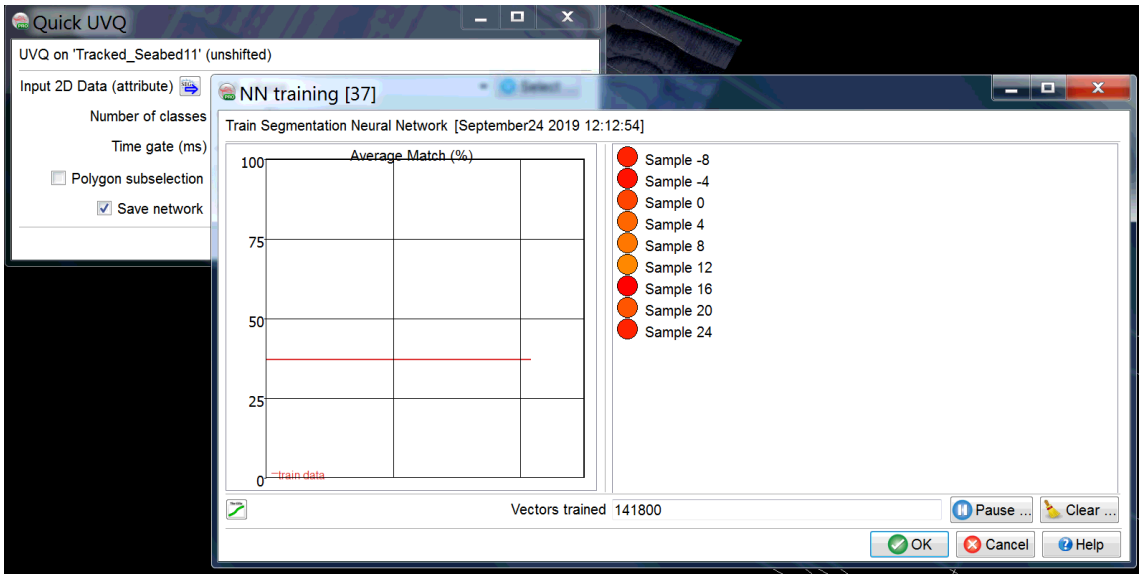

Figure 8.11 Training the UVQ by samples, steady at 37% Average match after 141800 vectors trained

Training the network was performed per 2D survey line using the horizon and pickset in samples. The UVQ then ran reiteratively for the time window per sample ad-infinitum. Over this time the average match (Figure 8.11) would be expected to rise as the networked trained and became more efficient. The Samples to the right should have changed from red to green as their best matching unit criteria changed and the wave segmentation improved.

Once the system ran through 200,000 epochs, the UVQ had been trained. OpendTect now allows interpolative horizons to be created from the trained data. The resultant 3D horizon created from the combination of handpicked horizon and seeded horizon and UVQ created data was promising but not 100% foolproof for an entirely flat basic horizon (Figure 8.12). It did not stretch as far as the survey line *85B* (far back) where no horizon had been manually picked. However, where there were part horizons, or part seeds, such as on line 37B where a partial horizon did pre-exist, the UVQ managed to perfectly align the horizon. It also successfully continued the horizon lines through the junction with *13B* despite no horizon or seed being present on the left side section line *37B*. This was regarded as a positive. The values of the colour bar, however, seem to be meaningless. They ranged in Z values from 0.002 to 0.0334ms which made no sense either in depth or with reference to itself.

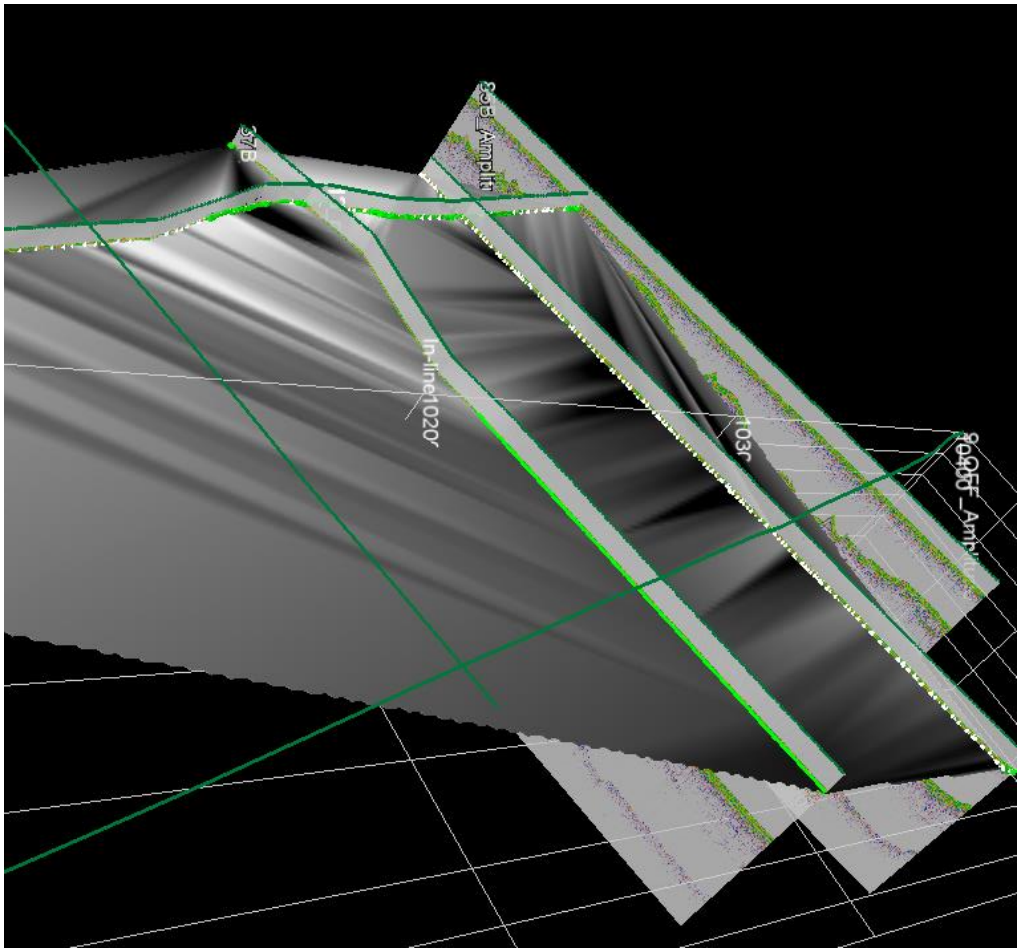

Figure 8.12 Sea Horizon as a UVQ 2.5D surface

The second UVQ analysis looked for peat deposits by classifying multiple peat facies identified via the phase variance signature and Q-Factor, as

demonstrated in Chapter 5. The UVQ would attempt to cluster these facies from other marine material interfaces as well as from unconformable horizons and features. This was originally intended to be run on multiple surveys within the study area. For this reason, the research returned to the study area used in Chapter 5 and 6.

Unfortunately, OpendTect struggled to display the 3 lines of survey data required for this test. Even with 64GB of RAM, OpendTect would often freeze or leak over 30GB of physical memory in displaying the traces required for the survey data. The first solution attempted was to reduce the number of traces read from the survey lines. Approximately half the traces per shotpoint were removed before the surveys would display together. At this resolution however, much of the individual feature detail at the material interface level was missing (Figure 8.13).

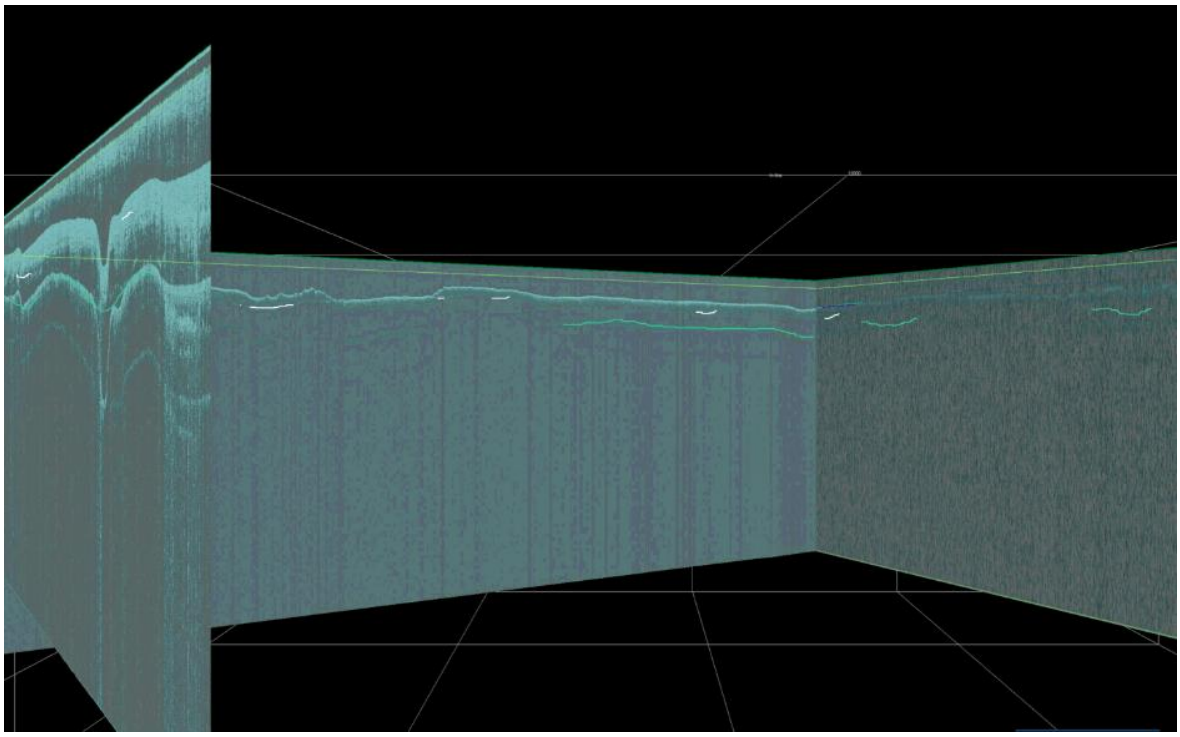

Figure 8.13 Study Area in simplified Q-Factor and Band-pass Filter view with picked features.

A final solution was reached isolating the CPU and memory for the tasks, and allowing sufficient time to run the test on only a single survey line at one time, whilst this worked, the software often crashed due to the system requirements and thus repeat processing was required.

Due to the lack of a variance peak overlay on the OpendTect phase functionality, the zero-phase wavelet peak could not be traced by the UVQ. However, the UVQ was able to overlie the Q-Factor range at the same point in the window as the zero-phase wavelet if the negative to positive polarity crossover was classified as an event. In doing so, the UVQ could be set to look for Q-Factor values at specific phase crossover events. This did not bear out the results of the phase variance signature in Chapter 6, but after repeated tests the outcomes appeared very similar. If a UVQ could be developed that worked with this combination, it may prove a useful first step to the future development for introducing the variance element.

In combination, the features, horizons and seismic facies were picked manually as both horizons and as classified picksets (as in Figure 8.14). The seabed horizon formed the top boundary of the UVQ window while the lower boundary of the UVQ window was the sub surface feature. Both of these horizons were picked in solid green. Between these were two distinct picksets – the cream picksets marked out an unconformity line while the crimson pickset marked out an area of parallel sediment deposition of similar composition. Within this were 3 small areas of phase-picked peat picked in white (Figure 8.14).

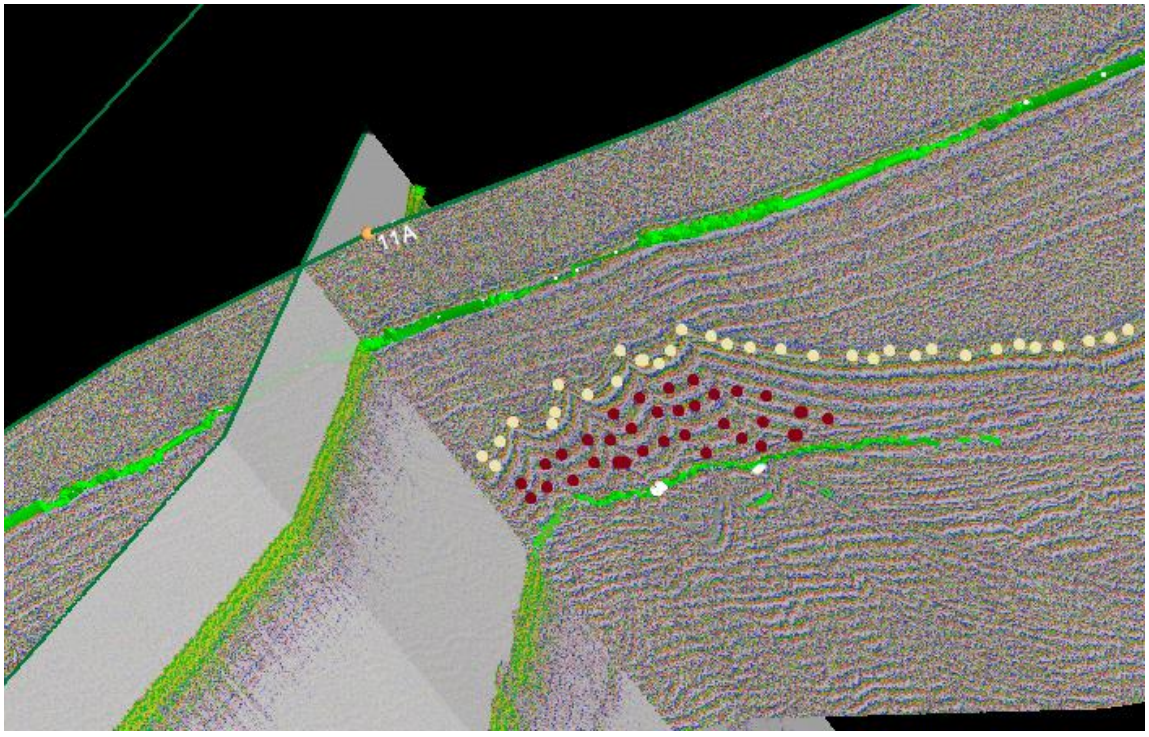

Figure 8.14 Line 11A picksets and horizons in phase view in OpendTect

The phase picked peat markers were small but close together and gave good polarity crossover from negative to positive phase. The Q-Factor values in each location were those indicative of organic silty sands (See chapter 5) in the range of -35 to -70 Q-F. Alongside these small areas of seeded peat, were 11 hand-picked limited horizons of signature peat marked out on both line 5 BM_1A and Route 18A that could be used as training matches for detecting peat on line 11A. However, OpendTect would only be able to use these as library references if the system could run on multiple lines, which unfortunately posed a constant problem.

Further along line 11A – at shotpoint 39,000, were two larger landscape features with hand-picked facies of phase variance detected peat. One of these however had a Q-Factor of -32 at the phase crossover, which would place it outside the silty sands and within the silty clay organic sediment range. This range had not been identified to the AI and would present a challenge. It was hoped that the network would attempt to classify the phase crossover event and Q-Factor value as a match with the manually picked peat facies despite their having different Q-Factor values. The attribute sets should still allow the pattern match to work.

Running the training data required the training segmentation to be run on the survey lines as opposed to classes and samples used in the previous case. Therefore, the original attribute sets, as described above were used with 5 classes employed at 10ms sample intervals for the phase attribute set and 5 classes employed at 10ms sample intervals for the Q-Factor attribute set. As explained above, due to lack of processing power, the training was run for only survey line *11A* and for a limit of 100,000 shotpoints.

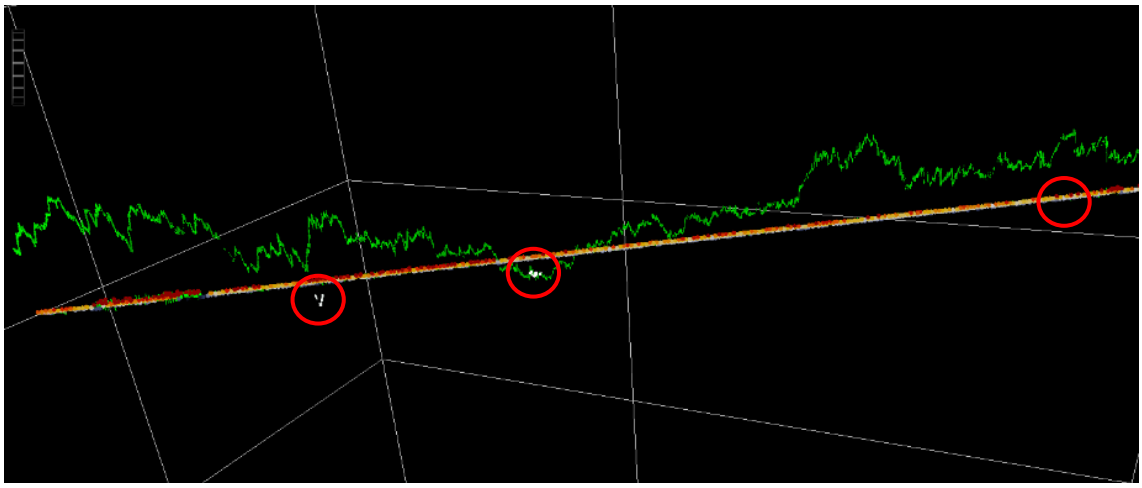

Figure 8.15 Creation of UVQ surface was unsuccessful and failed to identify the organic deposits (in white, circled).

This classification appeared less successful than the original UVQ test. Whilst there was undoubtedly a large element of user error involved in the design process, identifying where that error lay proved impossible to trace. The training process never achieved above a 25% match, which suggests the routine identified no clusters of note. The option of OpendTect producing an interpolated horizon based on the collected data from the seeded cluster did not produce a result that answered any question raised (Figure 8.15). Instead it created a simple straight line that ignored all the clustered seed data, the horizons and the picked organic deposits but created a multi-coloured pickset horizon across the entire survey with no z-dimension reported. A number of the original coloured pickset values were contained in this horizon but there was no way to separate them out. The UVQ also removed the ability to view the original survey data when displaying this horizon. This prevented the plotting of any new information against the features except for the three organic deposits (ringed in red, Figure 8.15).

8.8 Method 3: Supervised Artificial Neural Networking (via OpendTect)

Another option available within OpendTect was to run a full MLP supervised neural network. This was not as flexible as the python coded ANN option and ran within a strictly structured framework of input nodes with manually created parameters (attribute sets). Outputs were also set manually (usually true\false) and then a set number of hidden layers were built into the architecture based on the quadratic cost of the number of initial decision nodes. The more complex the initial input logic, the more hidden layers were required to process the decisions. This would ultimately provide less transparency or control over the network.

Consequently, the solution was to make the network only as complex as required for the task while keeping it as simple as possible. This was especially true when considering the back-propagation and autonomous gradient descent, as those were the elements that would train the network, not the initial parameterisation. However, the overall design of the network was the key to obtaining the correct result.

In the case of this study, the auto-identification of organic / clay, organic / silt facies, the back-propagation and autonomous gradient descent would be the area where most problems would occur. Keras' handwriting and Tensorflow's facial recognition ANN networks are well founded and have access to thousands of images on database catalogues (Gulli and Pal 2017). OpendTect neural network has only a handful of examples accessible to the public (via the dGB forum). This research could find none that employed shallow sediment facies pattern recognition based on events. For this neural network it was decided to create an ANN from the bottom up using events as part of the initial attribute set. These events were defined as:

- taking place within a two-way travel time window of between 0.02 and 0.1s
- having a high amplitude reflective signal (against mean energy).
- having a Q-Factor range of -35 and -70 Q_{SR}
- having a cross balanced zero phase wave consisting of a negative to positive polarity
- falling below, and distinct from, the Seabed unconformity*
- lying above, and distinct from, the lower unconformity feature surfaces and \ or multiples*

* these boundaries could not be assigned as part of the attribute set for input nodes but rather used as guides for the running of the neural network.

A complicating factor in the MLP solution that did not affect the UVQ, was one of negative picking. The supervised network needed to have the option of both positive and negative outputs, in order to correctly categorise the data. In supervised networks the aim was not purely to match like-for-like but to recognise pattern formation in the data. At each node, there must be a decision made as to whether the output was required to activate ONLY on all aspects being positive. i.e. having a single output, or whether having multiple outputs and combinations of activated output possibilities could still be 'correct' and therefore still have produced positive outcomes. For instance, if two outcomes of the nodes proved positive, such as a high amplitude reflective signal plus the negative to positive zero phase crossover but the Q-Factor output failed, does the network still count this as a positive result? Would it class it as a negative outcome? Or could it have a third outcome?

This may be important when considering future versions of the network. For instance, if such networks are used on live survey vessels, for focused coring, they may have requirements to record the automated detection of all closely classified organic facies but only interpret those of peat / clay, peat / silt within coring depth.

When running the neural network, initial attribute sets should be kept as simple as possible. To avoid excessive mathematical complication at this stage therefore, no hard-coded functionality was applied to the initial attribute sets. Only a bandpass filter to normalise the data was included in each attribute set. Spectral analysis for acoustic attenuation on the Q-Factor was not used in the initial attribute set. Whilst, given the lack of variance peak data to work with in OpendTect, the omission of acoustic attenuation may have been justifiable in initial models, they would however, need to be introduced at a later date.

The complexity of hard-coding the spectral equation and velocity models from Chapter 3 as an input for this MLP would be impractical. It would also mean that the neural network would not be transferrable for any other survey work and would need redesigning for each project. Therefore, the removal of mathematical formula from the initial input was deemed appropriate. The combination of Q-Factor and phase polarity signature together at this stage would need to be sufficient for the given solution in order to keep the pattern recognition input nodes simple.

The next issue to consider within OpendTect was the careful structure of the nodes to ensure integer compatibility. The input nodes were all required to share the same integer format and range so that any weighting applied could be distributed uniformly. For the neural network to make sense of the output logic, it must be able to compare like integers so there was no value in comparing amplitudes to frequencies or phase energy to Q-Factor from different inputs. The purpose of creating events was to make a checksum of the attribute set which then output a logical integer which could then have a weighting applied.

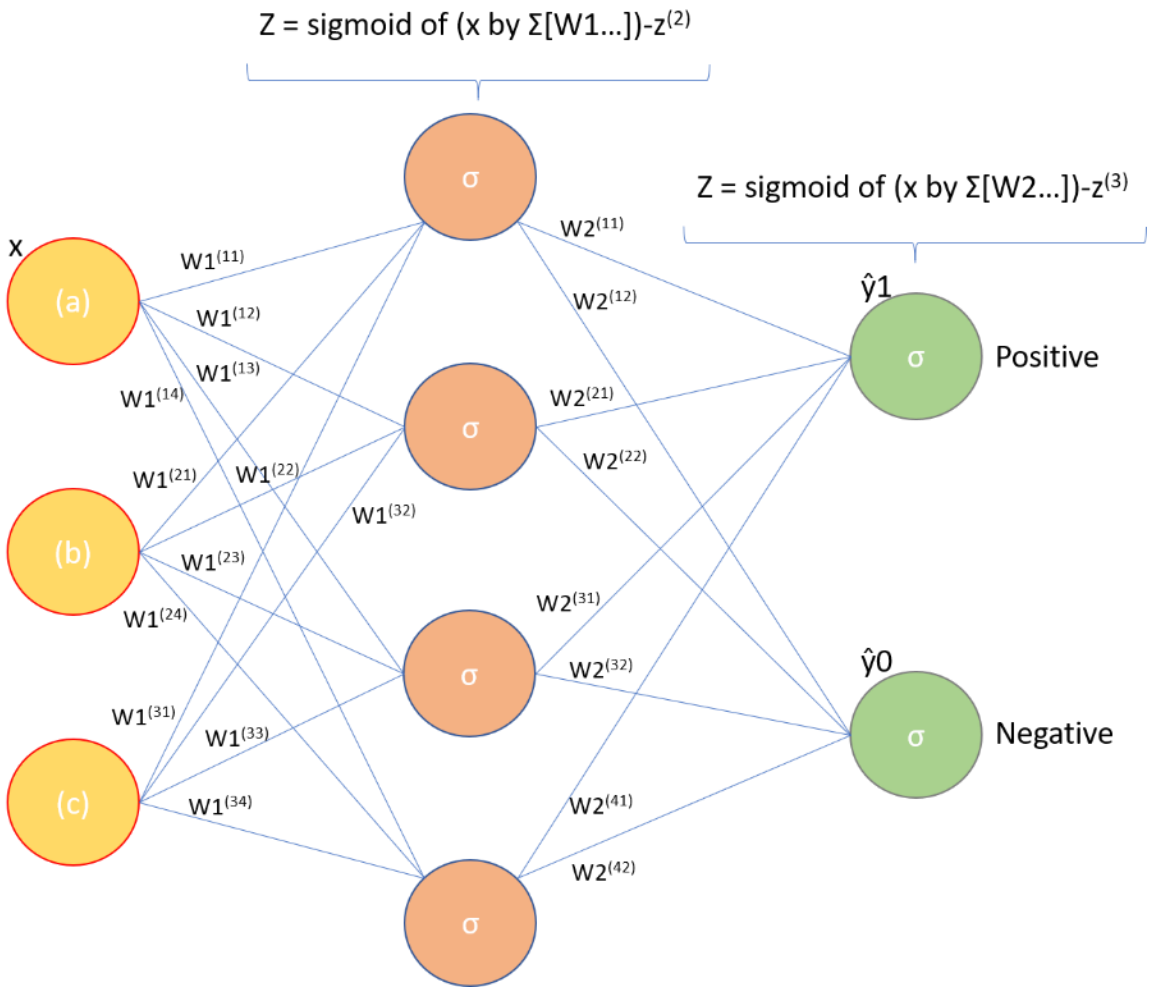

Figure 8.16 Diagrammatical representation of the OpendTect Supervised Neural Network as an MLP

The structure of the neural network was pre-defined and built as designed in the structure in Figure 8.16, such that the number of inputs (x) were all based on events (a), (b) and (c) that shared the same integer format. These events (Figure 8.17 below) such as (a) checksum for zero-phase negative to positive crossover, (b) checksum for Q-Factor events within time window, and (c) checksum for amplitude ranges for mean and peak energy in time window. The connectors in Figure 8.16 (W) were the actuators and these provided the biases by which over repeated runs could alter results to affect the outcome. The two output nodes for the pattern recognition of peat facies were a simplified positive 1 or negative 0 (yes / no) response. This process was not looking to determine what the response would be if the network did not detect a peat facies, merely that it did or did not detect one and also the resolution at which this occurred. The simplicity of the three inputs and two outputs meant that the network could be expressed with only a single hidden layer of 4 neurons (Z). Forward propagation was maintained by a sigmoidal sum of all possible

W actuators to the hidden neurons. From each of these, a simplified positive or negative (yes or no) response was propagated from each of the second actuators (W2).

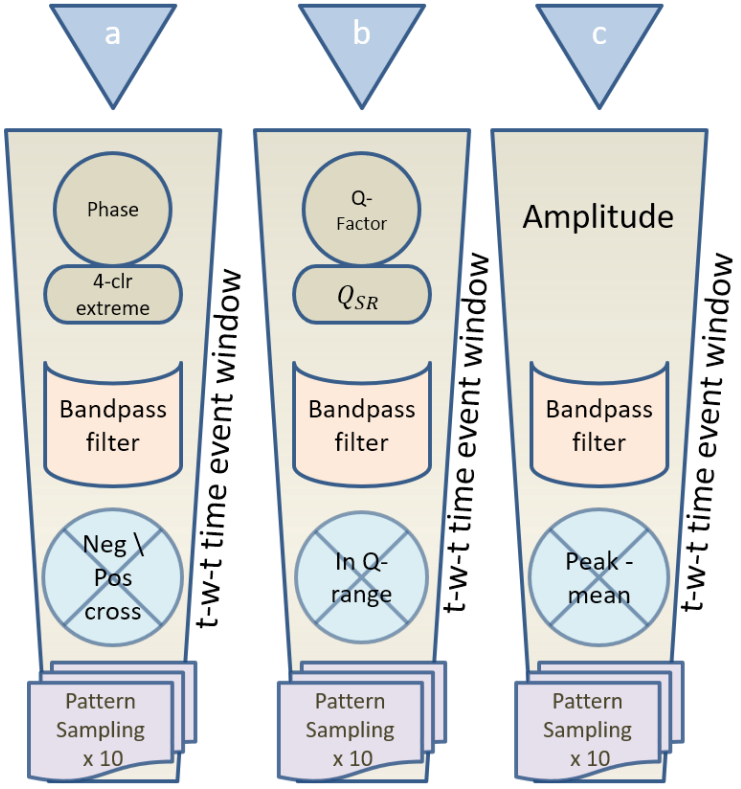

Figure 8.17 The Event Attribute Set workflows.

The event attribute sets (Fig. 8.17) were created as follows:

The first event was created using an instantaneous phase and a bandpass filter. The bandpass filter was set with a low cut below 80Hz and a high cut above 1200Hz - according to the survey spectra averages taken in the phase analysis. The Horizon event within this attribute is a negative to positive crossover event in the zero-phase wave within a threshold tolerance window of -10 to 10 (i.e. within a 10ms tolerance either side of the sample). There were 10 pattern samples taken within the two-way-travel time window of 0.02s (20ms) and 0.1s (100ms) and this same window size was used for all of the attribute sets as a useful guide to capture all activity from below the seabed and above the first main reflection multiples for the entire study area.

The second event based attribute set used the same bandpass filter, two-way-travel time window and pattern sampling, was based upon an instantaneous Q-Factor attribute SR calculation. The event looked for

signals within the Q value estimated range of (-)30 and (-)70. This value alone would not prove conclusive as the material type remained unresolved and there was no velocity model upon which interpret the analysis. However, as shown by Wang (2016) and supported by this research in Chapter 6, the Q-Factor range was a strong indicator of modulus change sufficiently different enough from other materials to suggest organic silts or clays.

The final event attribute set was present as a control and was a simple amplitude horizon event set. This analysis ran using the same bandpass filter in the same two-way travel time window. The analysis also ran with the same number of pattern samples as the other event attribute sets, but this time simply looked for a high negative amplitude response from the mean. This eliminated the problems of different intensities of surveys by normalising all amplitude data in reference to themselves.

The three attribute sets were trained by a classification and misclassification outcome of vectors. The vectors were weighted depending on the closeness of the data to the reference horizon and pointset data the AI had available. For this reason, the attribute sets were intentionally kept open as there were limited examples for the AI to use as evidence. In an ideal world, OpendTect would have allowed the import of the numerous phase variance signature horizons already picked in IHS Kingdom. However, where OpendTect did permit the successful import and display of one such horizon without crashing the machine, the attribute set seemed unable to utilise these horizons for any classification / misclassification training of vectors. Despite much investigation, no reason could be found for this failure.

If a solution were to be found to this and the import of interpreted survey lines to OpendTect were possible, sampling would be vastly improved. By importing lines already picked with phase variance data into OpendTect, it would be possible to expand the catalogue of examples, both positive and negative many times over.

Unfortunately, this was not possible for the research and it was necessary to recreate each phase variance signature picks and the negative picks within OpendTect. However, due to the limitations of the overlays, as described earlier, it was necessary to perform this without the aid of

variance peaks as the integration of the wiggle overlay proved a hindrance to the process. An added issue was machine response time when picking manual horizons, which, could result in a lag of up to five seconds per mouse click. As this was a memory intensive task, failures due to lack of memory even on a high-performance system were commonplace. For these reasons, survey line Line 14A proved unable to load at all and had to be removed from the study area. Line 5 BM_1A could not be opened concurrently with Route 18, which posed a problem as they shared a common crossline.

Despite this, eleven phase picked peat boundaries were created as both horizons and seeded picksets (located as per Figure 8.18). Obviously a great many more would be required for a robust testing of the AI capabilities of this software, but for an initial test of the training classification ability the selected data was sufficient.

The network was trained for 200,000 epochs on ten separate runs. On each run three attribute sets ran for each of three surveys, twice. While the root-mean square deviation in all cases eventually reduced to below 0.25 which was within tolerance for standard deviation error, the percentage of misclassification throughout did not fall as would have been expected. It fluctuated between 20% and 50% of all samples misclassified (Figure 8.19, page 218). The confusion matrix showed that the confidence level in positive classification was low and misclassification was high. Unfortunately, positive classification never attained suitable confidence levels for pattern recognition to be achieved and, despite running 200,000 epochs, the training did not successfully complete. Due to this, no results were output, and no self-interpretation or horizon division could be attempted. The full results can be found in Appendix 3 – Artificial Intelligence Results.

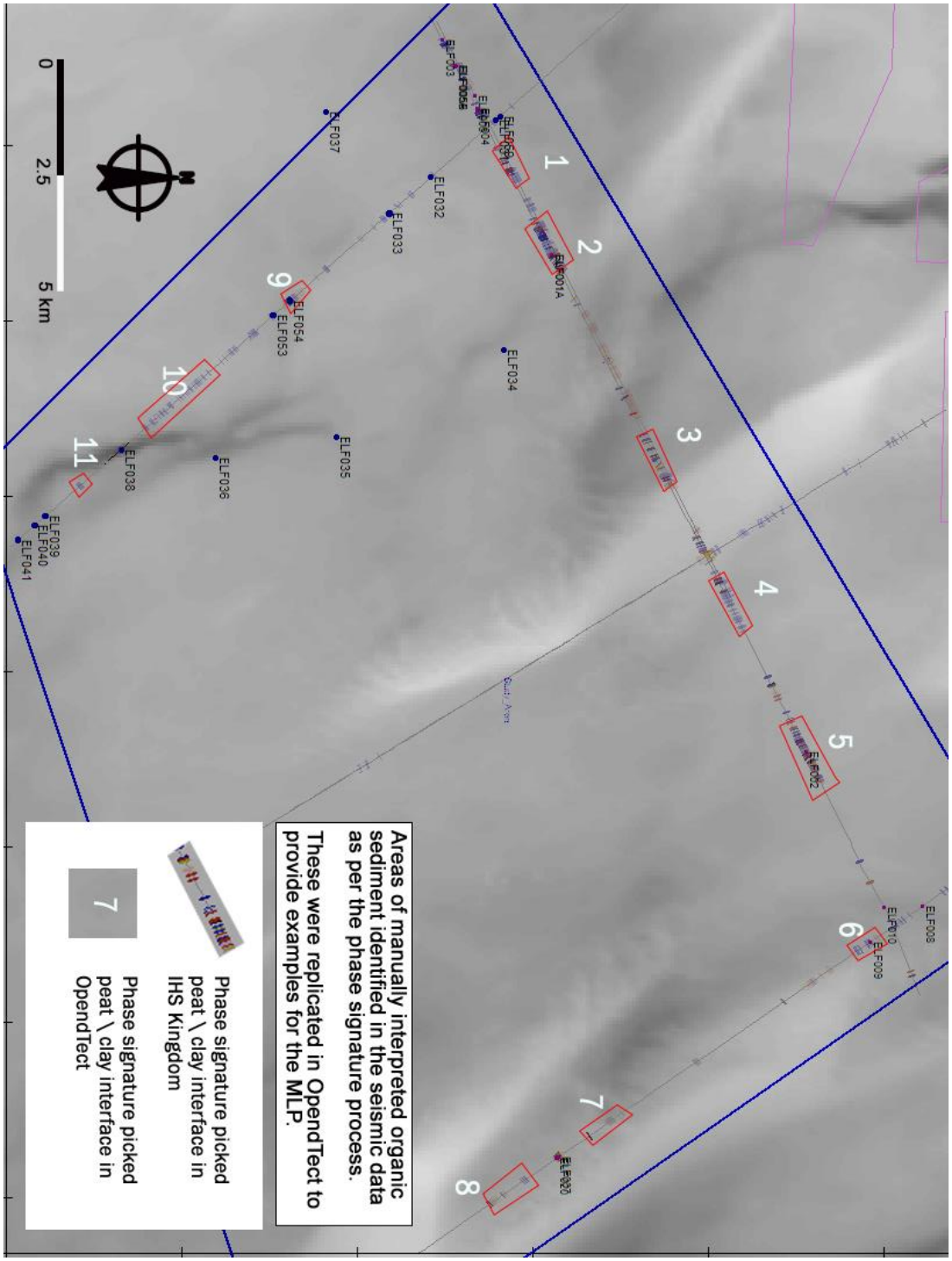

Figure 8.18 Organic / Clay Silt interface locations as picked in IHS Kingdom and OpendTect.

8.9 Discussion on improving neural networking model results

A fuller discussion on the conclusions of the neural networking aspect of this research appears in the Concluding Chapter (Chapter 9). However, at no point was the potential benefit of a successfully implemented neural network solution ever in doubt. The only issue for this research was the implementation, which suffered shortcomings in available resource and scope. Therefore, it is worth a brief discussion on ways in which the current methods were not sufficiently robust and how this may be improved for future research.

Figure 8.19 Training monitor showing dropping RMS but highly erratic percentage of misclassification

The first issue that should be considered is the use of larger, more representative datasets. The access to a larger selection of evidential data would have allowed for a far higher matching of positive (and negative) classifications. The limitations imposed in this research by a) the data available and b) the technological restraints imposed by OpendTect mitigated against a successful outcome. A dataset with tighter gridding and a more extensive example of extant feature peat, e.g. the Hollandze Kust Noord windfarm area investigated and interpreted by Fugro in 2018 and which became publicly available shortly after the research ended, would have been beneficial. This dataset would have provided extensive picked organic boundaries, classified as 'peat anomalies' for analysis.

Further, resources must also be assigned for understanding and troubleshooting the errors received from the training sets. It was recognised that in the running of the OpendTect ANN, the majority of the errors were due to problems in the implementation of the event-based attribution sets. Understanding what lay at the root of these problems and how to solve them proved insurmountable due to a perceived lack of visibility within the software functionality.

If this analysis were repeated using future versions of the OpendTect software, it would be recommended that smaller test sections of low resolution data are presented and tests are run using only organic reflectors without other horizons to confuse the issue. Tests would need to be kept simple and utilising the minimum amount of data necessary. In this regard, the research was too ambitious given the limitations of the software and the computing resources available.

A move away from proprietary software such as OpendTect, toward scripted coding in Python or C++ would aid with the data processing issues that came with the survey resolution sizes. Bespoke coded ANN development that could accept direct import of interpreted horizon picks from IHS Kingdom would be able to focus on only the required window of data to analyse.

While the methods and application here failed to produce trained networks and repeatable, validatory or reiterative results, it did not mean they did not hold potential for future work. Given more time and resources for the coding aspect of these neural networks, there is a strong possibility that significant outcomes could be achieved in this area. This is discussed further in Chapter 11.

9 CASE STUDY CONCLUSIONS – PEAT IDENTIFICATION IN INUNDATED PALAEOLANDSCAPES

9.1 Identification and Classification of Organic Reflectors

'Bright reflectors' of high negative amplitude may have been misclassified for years. Interpretations have categorised them as ubiquitous peats without differentiating between the silts and clays at the measured boundaries (Comas et al. 2004; Kreuzburg et al. 2018). By using ground observations of individual unit boundaries to accurately tie into core samples, it has been possible to analyse the correlation between such bright reflectors in the seismic data and the sediments in the cores. These can provide exact readings for the amplitude, polarity, variance, density and therefore attenuation of signal through material. This in turn allows for a determination of differing sediment material types in some – though not all – cases. Additionally, it allows compressional accommodation space or gas pockets to be considered as alternative responses to peat.

The first issue identified by the research was the immediate discrepancy between the reflector signal and any picked seismic event. For, whilst the reflector may have demonstrated a strong negative amplitude, significant to the organic material, this was represented as a trough in the seismic data. In seismic interpretation, when using wave peaks and troughs, the material boundary demarcation is to be found as close to the zero Reflection Coefficient (RC) as feasibly possible (Bradley 1984). When interpreting wave peaks and troughs dependent on the phase polarity, zero RC falls in line with zero amplitude crossing. Thus, changes in interfaces between material types were picked as close to zero p-wave amplitude – neither positive nor negative. Usually however, the definition at zero amplitude is poor and can be an issue when picking, therefore it is common for the peak (or the positive amplitude) to be used when manually selecting a sequence. One of the defining features of the 'bright' reflectors are their strong negative amplitude which gives them

their bright quality. This reflectivity is therefore an intrinsic feature of the material and will complicate the division of unit types at boundary levels.

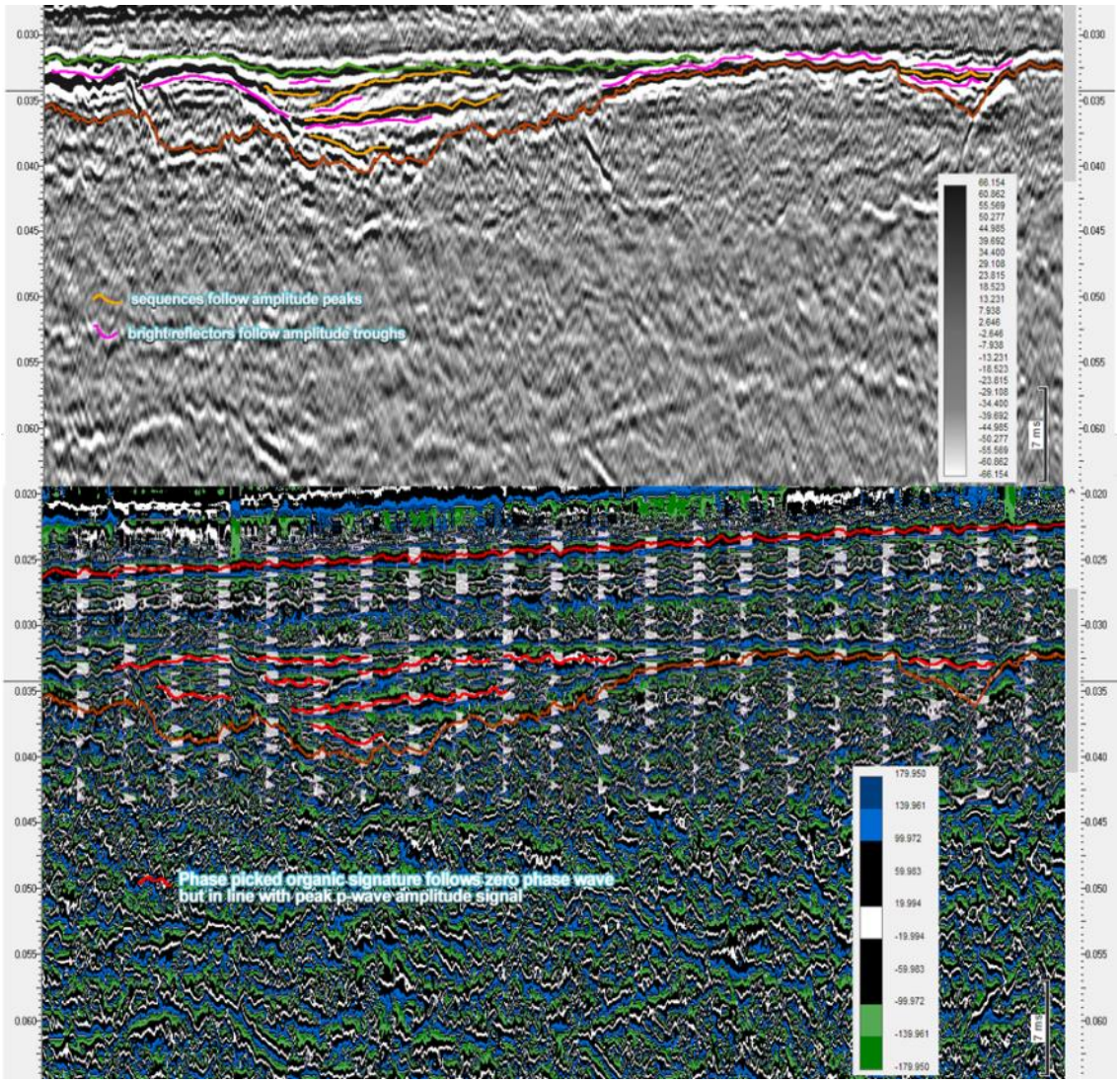

Figure 9.1 A (above) p-wave amplitude and B (below) the same data in phase function. Survey data by Fugro (Thal et al. 2018)

The phenomena are demonstrated in Figure 9.1a. The amplitude peaks are marked in gold, while amplitude troughs (the negative bright reflectors) are marked in pink. In Figure 9.1b the phase and variance signature model for the same feature clearly shows that the organic facies (red lines) overlie the p-wave amplitude peaks (positive waves - gold lines in 9.1a) and not the troughs. Such a situation illustrates that bright reflectors often used to signify peat in seismic interpretations are not representative of unit boundaries. However, the reflector may represent the upper surface of the organic material itself, below the boundary contact. For this reason, and with all other contributing factors remaining constant, the

attenuation scatter and Q_{SR} values as predicted in Chapter 5 may be an important consideration in the identification of material type.

To examine this in detail, three cores were selected for further analysis that gave direct evidence for definitive matching of bright reflector signals to the specific unit boundaries. Within core *ELF005B*, four unit divisions were picked out in the seismic survey and all were matched to the depths in the core within accepted error tolerances (±6.2cm) using the depth conversion set out in Chapter 5 (Figure 9.2).

The boundaries directly above and below the central core peat unit were not noted for their sharp contacts or material change. Both were silt to peat unit boundaries – at contact IIa to IIb (dark grey, 1-2mm thick laminated silt ranging to brownish grey organic silt / peat with brown woody fragments) and IIb to IIc (from peat to a lower structureless mid-brownish grey silty fine sand). These contacts occurred at 0.64m and 0.68m in the core and were located at a depth of 25.48m to 25.59m on the depth converted seismic survey. Two organic bright reflectors, only 12cm apart at depths of 25.50m and 25.62m would fit these boundaries almost perfectly within the vertical resolution error bar of ±6.2cm above and below the converted depth).

The fact that the material types within the core were very similar between Unit IIa Organic silts (Ag) and Unit IIb Organic Silts (Ag) / Peats, was also of consequence. As discovered in Chapter 6, Silt to peat boundaries returned much stronger organic signals than those of clay to peat. It was also noted that 'woody fragments' were present in the organic layer (M Bates – ELF Project 2018). It is a possibility that the reflectors were responding to the difference of material types found between the organic sediments and these fragments. It is possible that the signals were a result of internal reflections from within the peat layer itself, due to the variable nature of this material. Determination of this proved difficult with this particular line as attenuation became an issue after the first 50cm of depth.

Unfortunately, the thickness of the unit layer makes it difficult to explore in any further detail. Unit IIb measured only 4cm in thickness between contacts which is less than the 6.2cm error tolerance. Therefore, any suggested visual differentiation was highly unlikely at this scale given the

vertical resolution mentioned. It is possible that one, or possibly both, of the bright reflectors could have been a false positive. This might have resulted from a multiple of another strong reflector further above this one in the seismic data. The modern sands of the late Holocene were very strong reflectors throughout the area, though these are likely too far above the bright reflectors to cause multiples. They also have not caused such problems elsewhere.

It is also worth noting, when considering the strong negative reflective properties of modern sands, that all data across all surveys contained strongly negative signals that were not derived from organic sediments. Most notably, this was found in the modern sands close to the seabed. A normal zero phase response should show strong reflectivity of the seabed to water column. These phenomena had little to do with organic materials, though gases could often account for a reflective blanking at shallow levels and an attenuation of signal below. It was common however, for a high reflectivity and attenuation coefficient from seabed materials in the modern sands to blank out very shallow signals. This blanking posed a problem in the trace testing carried out in Chapter 5. Further trace tests, in the future would be advised to run traces only within a window below the horizon of modern sands in order to avoid this modern marine 'noise'.

The fact that the phase signature process identified the silt – organic contact more readily than other unit contacts was significant when viewed in the context of the southern North Sea. The extent of the Naaldwijk Formation throughout the area means that in the majority of cases the organic layer identified does, indeed, refer to basal peat beds. The silts can be interpreted as of riverine or estuarine terrestrial origin as the environment turns steadily marine. The layers represent a prolonged inundation, possibly occurring over numerous low energy events. From this we are able to identify landscape change by means of the dating of buried peats.

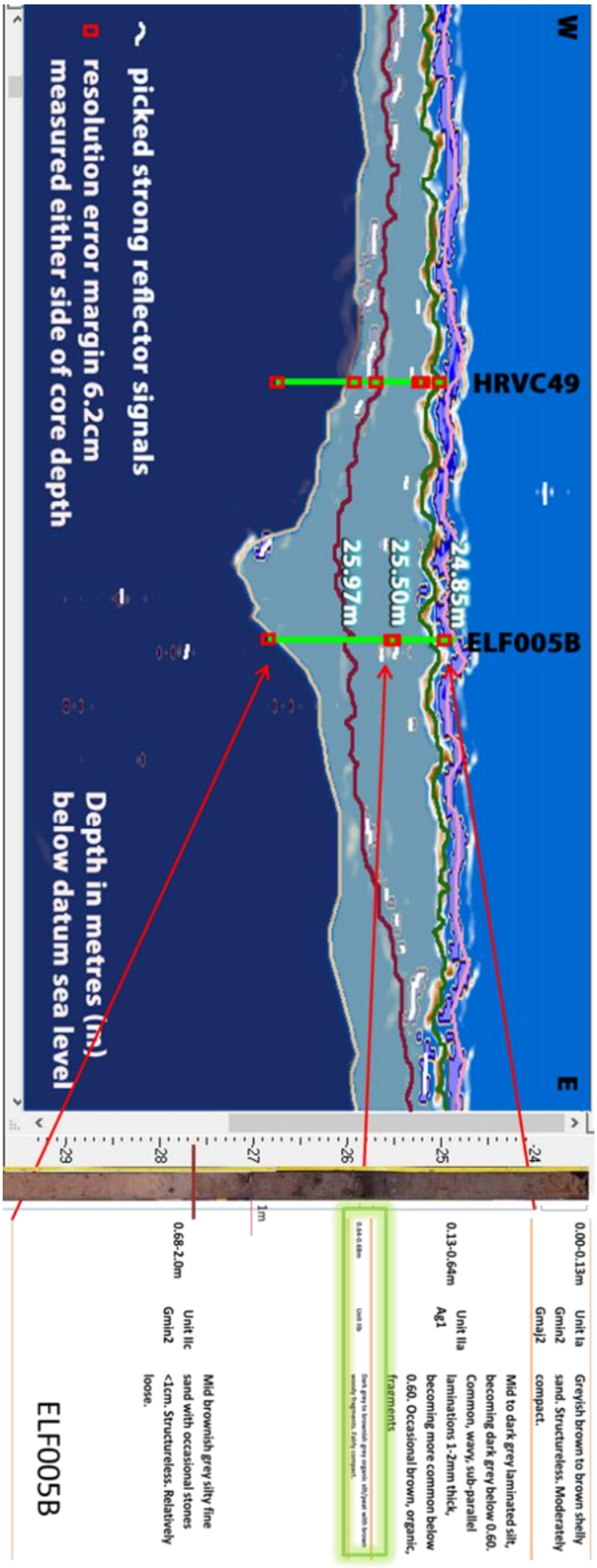

Figure 9.2 ELF005B analysis by depth

The second core for examination was *HRVC49*, (Figure 9.3 below) was part of the same shallow fen or marsh bed as ELF005B but this core was drilled into the chalky river side. Small but bright reflectors were bisected by the core at 25.30m which equated to 0.39m of measurable core depth. This corresponded well with the 0.36m abrupt contact between unit IIa and unit IIb - well humified silty peat and the clayey-silt with organics below.

A further, less well-defined reflector occurred at 25.73m (0.82m of measured core depth). This unconformity was observed across the entire feature with variable, but strong, reflections. However, the core evidence in *ELF005B* assigned no lithographic identity to the boundary. Core *HRVC49* on the other hand, gave a precise unit boundary between IIb and IIIa at 0.83m. This was interpreted as the H05 Elbow formation which represented the final terrestrial Holocene unit. To have depth converted this boundary to within a single centimetre was a great validation of the velocity model.

Despite this evidence, there cannot be a guarantee that this was the reflector correlating to the core boundary. The material composition of units IIb and IIIa were largely similar, the organic element was part of a clay sediment, not silts as may have been expected for a bright reflector. There was also a bright reflector below this horizon at 25.79m (0.88m in the core measurement, well within the error tolerance). Using the phase variance function applied in Chapter 5, the organic phase signature looked very strong on the zero-phase variance line. Although the vertical resolution prevents the definitive answering of which precise reflector is pertinent here, the number of other equally strong, bright reflectors nearby, suggested a soligenous fen peat accommodation had built up across this feature. The proximity to the terrestrial Holocene unconformity further suggested that this peat was still developing at the time of inundation. Therefore, it may be logical to assume that the clayey-silt with organics unit may well have contained an element of peat very close by.

It must be borne in mind that while the vertical error tolerance may be as low as ±6.2cm, the horizontal error may be far larger. As explained in Chapter 5, the vibrocore placement may drift by metres from the target location, the boat will experience drift while coring and satellite positioning may have tolerances of up to 12.5m. The fact that peat was

not present in a given core despite strong reflector signals does not mean the organic units are not there. It merely suggests the core is not at the same location as the seismic survey.

Other anomalies were observed in survey *Line_18* surrounding *ELF005B* and *HRVC49* where a prominent bright reflector was noted in the water column far above the seabed. This data error was a result of a shoal of fish or other submerged object within the water column.

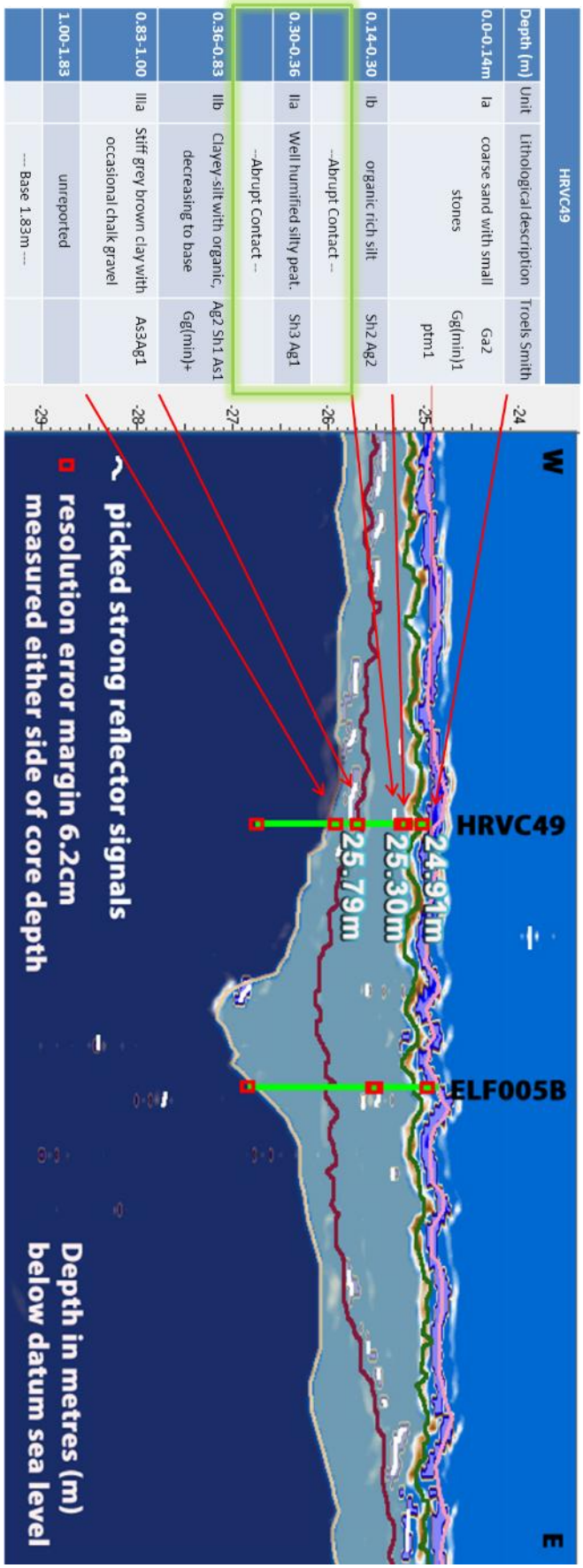

Figure 9.3 Analysis of HRVC49 bright reflectors and depth

The final core for analysis was *ELF002* (Figure 9.4). This core also had strong correlations between the seismic bright reflector signal and particular units in the core. The facia unit change at 28.29m (2.85m of core measurement) between unit IIa and unit IIb was not picked up well in the seismic data. However, at 28.53m (3.01m of core depth) a reflector cut across the core location in an almost continual response. There was no material change described in the core lithology at this measurement but at 3.08m a contact from unit IIb to unit IIc was noted. This boundary was from the base of one 15cm dark brown peat unit with horizontal phragmites to an abrupt sloping contact to silty sand and chalk. The material change between peats and silts, especially with chalks, responded strongly in the results of the tests in Chapter 6, so this was not a total surprise. However, the depth of 3.08m in the core, correlated to the 3.01m in the seismic data would have been just outside of the ±6.2cm error tolerance by less than a centimetre.

Interestingly, a further gradated contact existed within unit IIb of this core. The peat layer gave way to organic silts for a depth of 6cm before returning to a peat unit once more. This contact was measured at 3.0m in the core and correlates almost exactly with the bright reflector depth in the seismic data. Therefore, the correlation could be made at the base contact of the lower peat and the silty sand and gravel (unit IIb to IIc. The discrepancy with error tolerance being attributable to the dipping nature of the contact which begins higher at one side of the core than the other by almost 1.7cm. In which case, the lower boundary, at 3.06m, did fall within the tolerance and explained the single seismic signal for vertical resolution of unit IIb. Alternatively, the correlation may be made with the single bright material change within unit IIb where the thick peat gave way to organic silts.

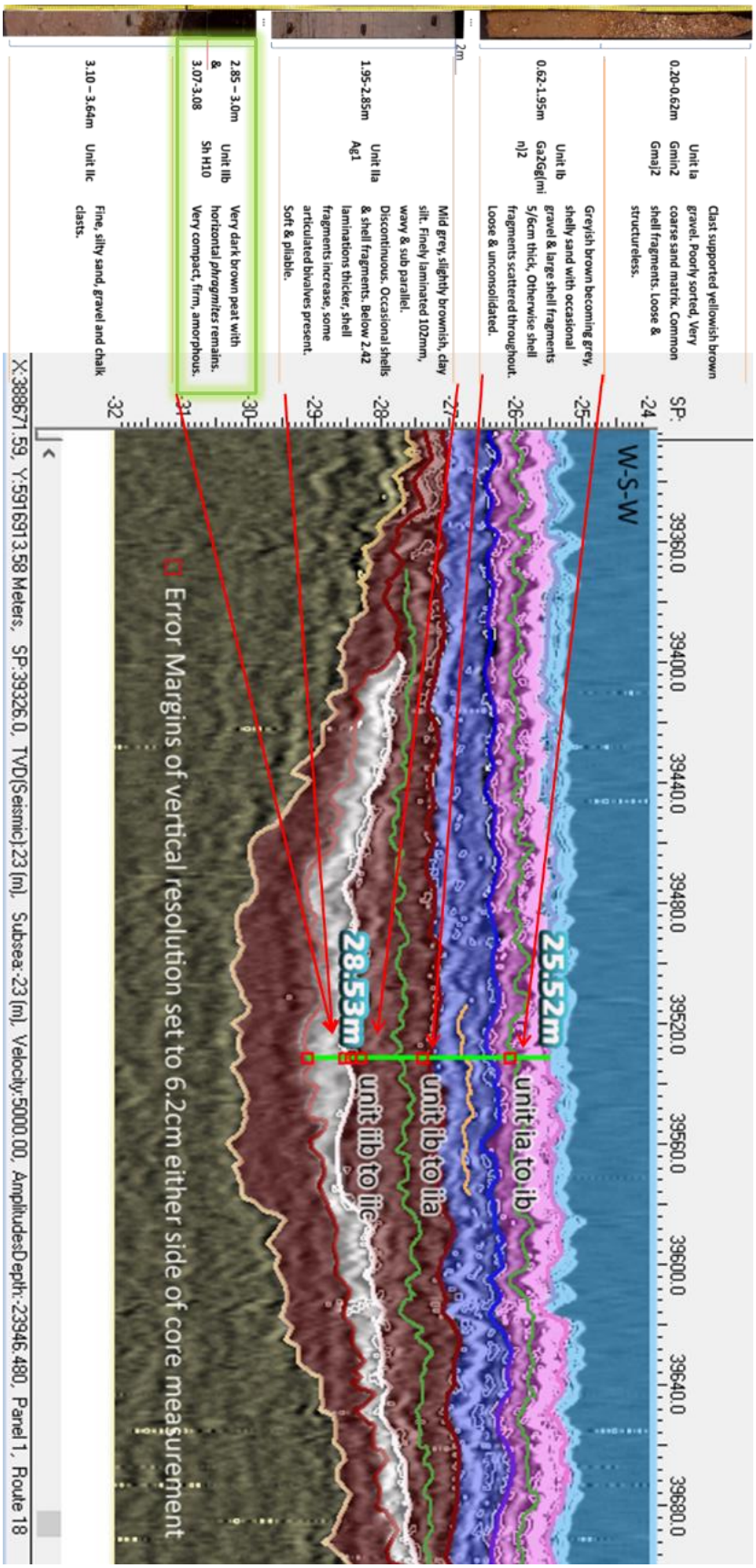

Figure 9.4 ELF002 Analysis by Depth

Between ELF005, HRVC49 and ELF002 (Figure 9.3 & 9.4 above) it could be concluded that the bright reflectors noted on seismic surveys, given an effective velocity model to demonstrate corrective depths, did indeed show up not only distinct organic signals but had a tendency to favour a particular material facies; that of the peat / silt interface. Where this did not hold true, the bright reflector could be identified as picking out the material within the organic layer rather than at the boundary due to the negativity of the signal rather than the zero crossing. In all cases a lower boundary seemed to be favoured where there was a vertical resolution limit to visibility.

9.2 Interpretation of boundary facies and depth precision employing a new velocity model

Vertical resolution between the different seismic surveys varied greatly due to weather conditions and the frequencies at which some lines were shot (Tappin, 2011). This variation could give error tolerances of between ±4.7cm and ±8cm. The ability to differentiate between individual signals within this error range made the interpretation of some elements of the data extremely difficult. This was especially true of the very shallow layers - in close proximity to the seabed, and the sub-layers within the peat units themselves. The peat layers were often small, the entire deposition measuring less than the vertical resolution error tolerance. In such cases the boundary contacts on either side could not be distinguished with any certainty. However, the results of the new velocity modelling in Chapter 6 did suggest that lower boundaries tended to be stronger than upper boundaries and these were picked out in the data. The ground observations to the core depths matched these lower boundaries if there were two within error tolerance.

In these cases, it was still important that a contextual velocity model could be designed that incorporated an organic element, peat, and could attempt to pick out at least one of the boundary contacts present in the core evidence. While shallow sediment velocity modelling had been undertaken in submarine, offshore and continental shelf locations (Hamilton 1970; Schock 2004), peat had never specifically been included amongst the sediments. No specific distinction had been made to model the boundaries between organic sediments of silts, clays, sands and peat. Therefore, before this research, no shallow sediment velocity modelling

had been performed. Further steps are still needed to refine the model further. The classification system was based on lithological descriptors matched against Troels-Smith (Folk 1954), Udden-Wentworth (Wentworth 1922) and Ekono (Kivinen 1980) models and using an adaptation of Hamilton's Continental shelf velocity model (Hamilton 1970). Core scanning XRF data, Loss on Ignition (LOI) processing, chemical composition and grain size composition data would all provide a more detailed classification system and therefore a more refined velocity model.

However, the new three-step velocity model as described in Chapter 5, incorporating a weighted volumetric calculation worked extremely well. The porosity fraction calculations based upon bulk density and grain size utilised the shallow sediment model created by Hamilton (Hamilton 1970), into which the 1980 Ekono organic classifications were inserted using the 1922 Udden-Wentworth scale as a guide. The results were therefore stepped but were observed to hold true to the original bulk density / porosity models that Hamilton devised. Additionally, the match to the cores was observed to work well within the study area. The comparison of interpreted picked horizon lines as well as bright reflectors to gauge unit boundaries and material facia changes was therefore deemed of importance. This enabled an understanding of the environmental context within the core and also within the landscape. Where the measurements did not match exactly, the model allowed for an understanding of why this may not have been the case.

Such an example was *ELF054* (Figure 9.5 below). Here the two peat layers in the core at 3.25m and 3.30m seemed to match the depth analysis at bright boundary contacts despite being only 5cm apart. The vertical resolution for this particular line, due to the bad weather at shooting was ±8cm (Tappin et al., 2011). It was therefore unlikely these were separate signals corresponding to individual peat layers. The higher of the two bright reflectors occurred at 3.14m which fell just outside of the error tolerance. The other, at 3.47m fell a long way outside the other range. It was not the final strong signal. A bright response was also detected very close to the base of the core depth at 3.78m. There was no corresponding organic layer in the core.

A similar problem occurred in the non-organic units in this particular core. The core reported that the deep Holocene unit (Unit IIa) was a continuous

layer of laminated clay silts for 2.6m. However, the seismic data displayed two strong reflective unconformities through this section. The topmost boundary contact was present, and the bottom contact was marked but the interpreted unconformities and infill sequences marked in the survey were nowhere to be seen in the core. In fact, of the 3.80m of core, the first 2.84m comprised of unchanging grey, 4mm laminated undulating clay.

Therefore, either the interpretation was wrong, or the core was positioned far from the survey line. While excuses can be made concerning the quality of the data due to the weather, there were strong enough amplitude peaks to follow conformities and sequences for interpretation. This leaves the location of the core. Validated co-ordinates placed the core at a distance of less than 1.1m from the survey line at this point. This must still be examined within the overall spatial horizontal tolerances as described earlier in this chapter of ±10m.

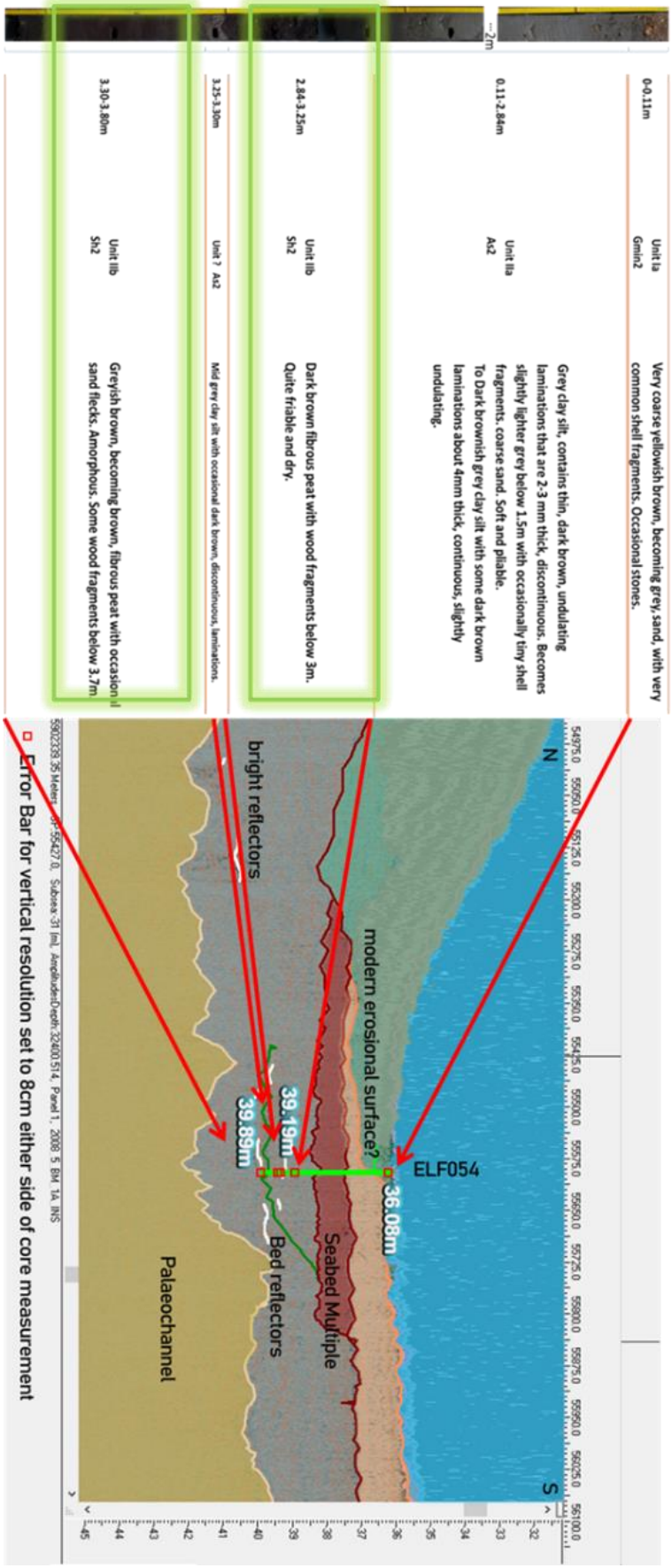

Figure 9.5 ELF054 with good matches for the peat to silt definition but poor definition elsewhere

Another problematic core was *ELF020* (Figure 9.6). Here, the depth analysis worked well initially, with this core but became unrecognisable to the interpreted feature after a certain point in the seismic data (See Chapter 6). The upper boundary and lower boundary between Units Ia and Ib were as shallow as 24cm and a sub-boundary that was picked in the seismic data. This sub-boundary was not noted in the lithostratigraphical report but was visible in the core. This was significant enough of a distinction to warrant the creation of an additional boundary surface for use in this thesis. This boundary surface (designated Unit Ib to Ib) at 0.43m was correctly depth converted on the seismic survey. The final boundary contact that matched between the seismic data and core was at 0.73m and consisted of Unit Ib to IIa, highly disturbed and mixed sands and shells. A high level of perturbation existed in this boundary and though the seismic data showed a strong facies reflector, the core revealed a more gradated contact.

To this point the velocity model was entirely validated. Beyond this point, there were no further matches. As can be seen in Figure 9.6, the seismic data shows the core dipping below the landscape feature into a formation within the valley. It would, therefore, have been expected to exhibit the properties of Unit IIc throughout the remaining depth. However, the core *ELF020* instead presented two further distinct units and 2m of laminated clays and dense black peats. This unexpected result within the core evidence could not be accounted for in the seismic survey. It could only have been due to errors in the reported location of the core with respect to the survey line. It is thought that this error occurred during core acquisition.

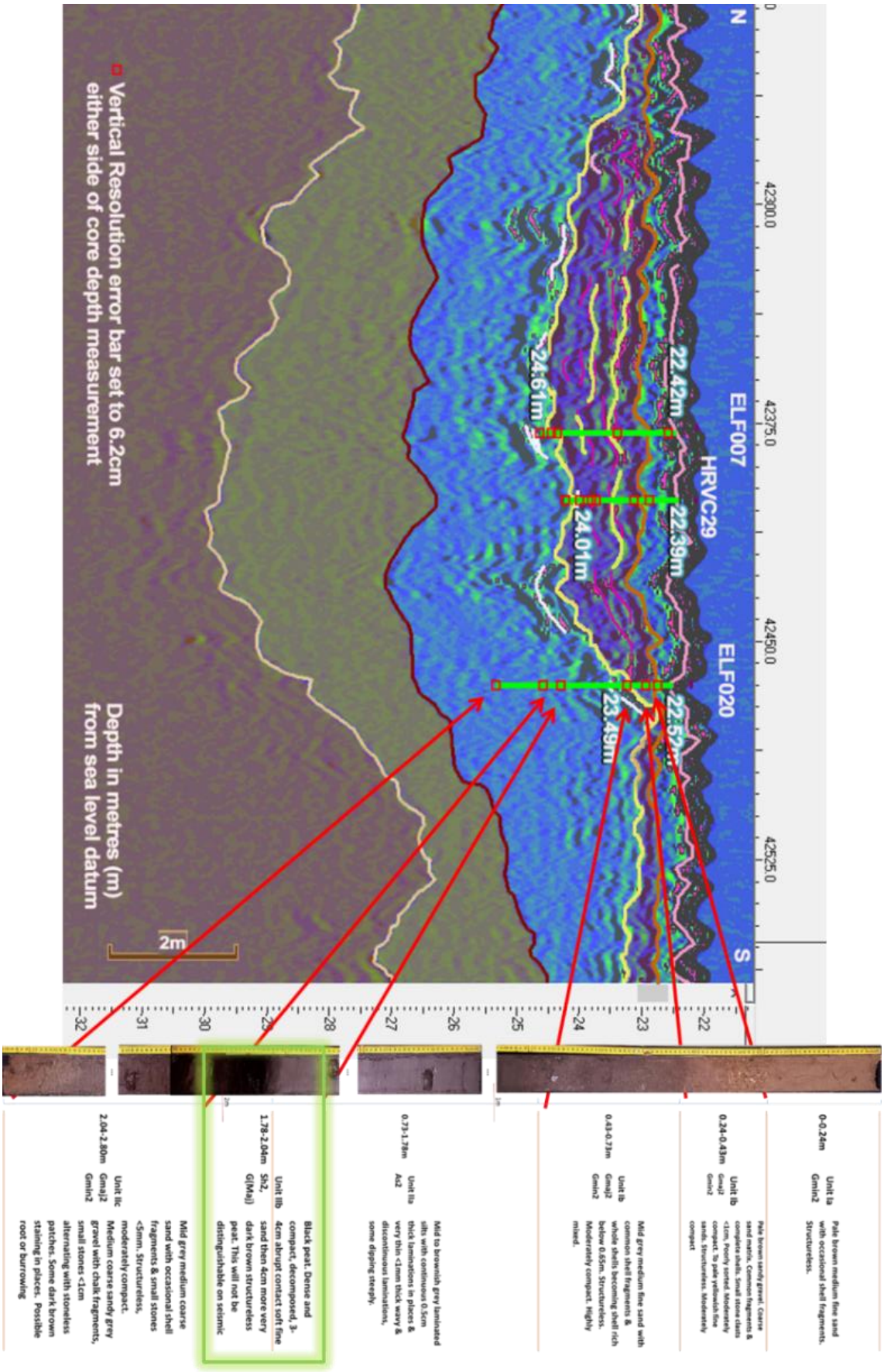

Figure 9.6 Depth Analysis of ELF020

In general, the plotting of an early Holocene boundary horizon was successful. For the majority of cores, the boundaries were precisely targeted, and the depth was well-defined. Peat layers were accurately interpreted to within the cm's and in an overwhelming number of cases, within the error tolerance. This is significant and suggests the process can be used as a focus for future coring programmes. Such programmes may target datable peat samples from the Holocene - Naaldwijk Formation that have the potential to contain useful environmental and archaeological proxies. This represents a significant achievement of this research.

9.3 Phase Variance Signature Research used for the location of Peat

It was assumed that bright reflectors were a signifier of organic sediment and, due to its abundance, peat was identified as the likely candidate in the southern North Sea (Van Heteren et al. 2014a; van Heteren et al. 2014b). However, proving this is problematic in a marine environment. The phase variance research undertaken by this thesis has taken a major step towards identifying both: a) precise locations of organic material facies in seismic submerged palaeo features and b) narrowing the identification between material types. This is especially true for the boundaries between peat and clays and peat and silts. The research has also been productive in identifying areas of phase gas, even if it was only used to eliminate area containing such gas from analyses within this study.

The visual core record provided the research with a physical understanding of where peat had the potential to develop. Additionally, it provided information on the rational extents of beds beyond the small palaeo features. Of course, good experimental models must have the ability to be repeatable, and also have reproducible results using different data. Thus, whilst pertaining directly to the methodology generated by this research, it was deemed useful to consider how this research could be additionally applied outside of the formal study area.

The thesis research methodology was applied in varying degrees around the Brown Bank. This was undertaken as part of a focused coring programme with the Netherlands Organisation for Research in Applied Natural Science (TNO) and the Flanders Marine Institute (VLIZ). The goal was to assist the understanding of the environmental potential in this area of high archaeological potential (Missiaen et al. 2020). The interpreted data discovered several sites of interest and coring took place in two locations. Both of these locations returned peat in the recovered cores. This success was followed up with further expeditions, with VLIZ. Analysis supplied further interpretation to the team and informed the surveying and coring mission. Through the knowledge garnered in this thesis, it was possible to provide information which proved extremely helpful in isolating areas with potential for coring Holocene peat within 4m of the seabed surface (the depth of the vibrocore). A total of eighteen cores from around the Brown Bank area have now been taken of which twelve

contain substantial Holocene peat layers – which represents a significant success and validation of the methodology presented here.

The ELF Project undertook environmental proxy analysis and further research, which provided material that is facilitating addition research into Seda DNA, the results of which may further improve future methodologies. This potential for future research has been greatly boosted by the bi-annual survey aboard the Belgian vessels the RV Simon Stevin and the RV Belgica, the most recent occurring in 2019 and 2020. During these partnered missions, areas which were once poorly surveyed have become well represented with sparker and PES coverage. This data could be utilised to develop the methods described here and potentially assist in the development of an AI for use in archaeological geophysical interpretations.

9.4 Acoustic Attenuation

Attenuation of signal was an issue during this research, but also proved beneficial under certain conditions. For instance, cores *ELF005B* and *HRVC49* shared a unit boundary - Unit Ia to Unit Ib, marked at 0.13m and 0.14m respectively. The boundary was described in the cores as from a structureless modern shelly sand to a moderately compact sand containing an element of gravel ($Gmin_2$ and $Gmaj_2$). Neither of these boundary contacts were visible in the seismic data due to the amplitude intensity of the seabed. This was as expected. However, immediately below these units the area was of interest, and could be further analysed due to the proximity of the cores to one another (34.1m).

The material types and boundaries within the cores are not dissimilar, therefore the reason for the discrepancy must be a combination of scattering and attenuation of signal which occurred at core *HRVC49* and not at *ELF005B*. This is likely due to a number of possible reasons, the primary one is thought to be free gas escaping from pockets of organic material found on the sides of the palaeo feature. Thus, rather than attenuation being a problem in this case, the issue is likely to be acoustic impedance. This may possibly be resolved through spectral decomposition and thin bed resolution; however, the feature may be too shallow for this to be successful.

If the degradation of signal was indeed due to acoustic attenuation, then the causes behind this could be multiple. It would be likely that not all of these would tie into the organic nature of the sediment but may be due to:

a) Seafloor masking – the reflections from the seafloor itself are very strong for a number of reasons including waterlogging. If seafloor masking causes too great a problem, if could be stripped out of any velocity model the depth conversion repeated without the seafloor horizon.
b) Visibility – the survey was shot at 3.5 kHz which gives a vertical resolution of approximately 5-6cm for a total of 10-12cm differentiation. In several cores of the study area, the peat layers were between 4cm and 6cm, which made isolation of individual signals difficult. Assumption must be made that this thickness of peat would be similar throughout the southern North Sea.
c) Material type – this method was designed to pick out the strong reflective responses at abrupt boundaries between distinct material types. Soft gradated contacts, say between organic silts and organic clays will show weakly in comparison, or may not appear at all. However, the material thickness would still attenuate in line with the Q-Factor rates for silts or clays for a material type judgement.
d) Phase gases could not identify at a boundary contact however they were able to produce bright reflections. These were identified by the masking effect they displayed in an acoustically impeded area below them and the scattering effect directly around the area that could result in seabed multiple reflectors.

While the results did not conclusively prove a simple and failsafe method of predicting peat within a submerged landscape, it did provide a strong method of suggesting the material types that could be present in a given organic boundary facies. It also, significantly, made recommendations for a method of predicting the location of organic material, and whether that particular boundary would be between peats, silts, clays or sands. The prediction provided still indicated the presence of organic deposits that could be directly related to a given depth within a survey. Any error was likely to be within a vertical tolerance of less than 12cm. This provides the opportunity to take the expensive world of archaeological marine coring

to a new level, making it more cost effective, and producing a higher hit rate for coring.

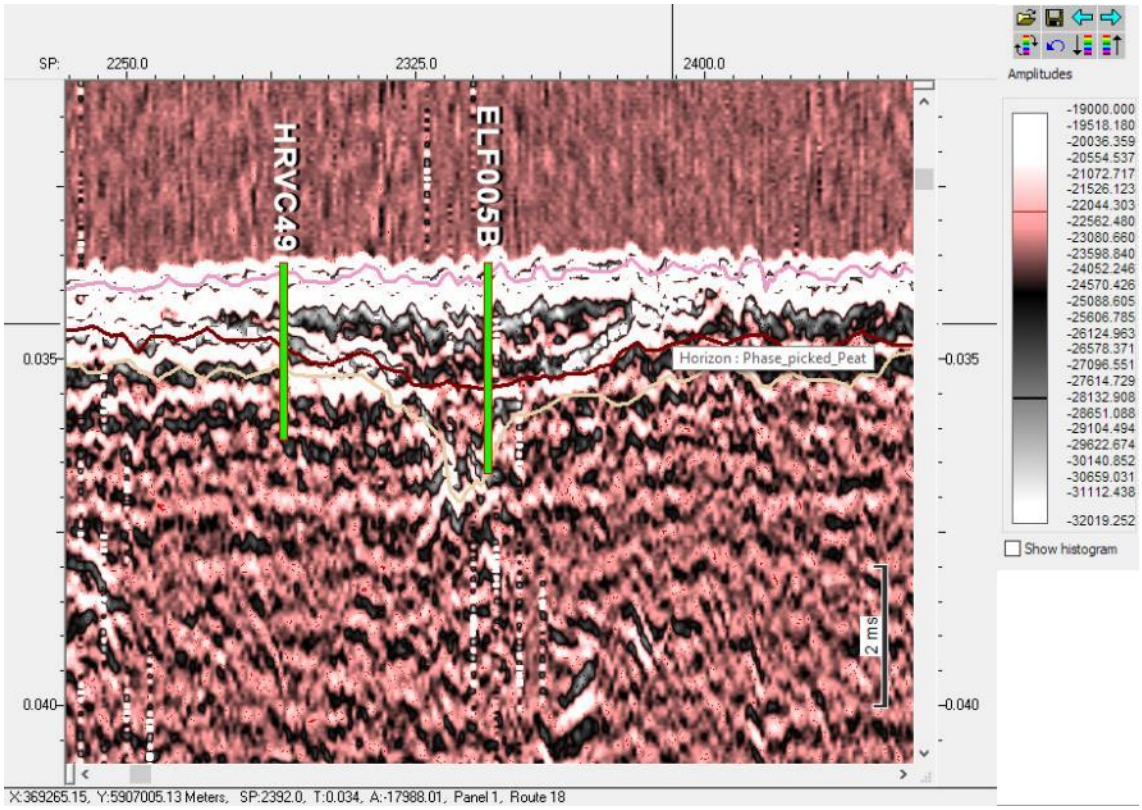

Figure 9.7 Bright boundaries smear at HRVC49 but sharp and defined at ELF005B

Fig 9.7 shows the proximity of the cores. An envelope function is applied to maximise the contrast of the amplitude signals. Following this, the negative amplitudes within the seismic data are enhanced by maximising the colour range exclusively for the negative amplitudes. What remains are the bright negative reflectors (in white) and all of the other amplitude peaks and troughs (in blacks and reds). What is evident from the figure is, that despite the proximity of the cores and the compatibility of their units, the clarity with which the signals at *ELF005B*'s location can be identified compared to those of *HRVC49* is unmistakeable. The latter show multiple confused bands of high negative amplitude reflectors bleeding into one another while other unit boundaries appear limited and weak. In phase function, there are no variance peaks at the 0.3m, instead the strong phase character picked comes at the boundary between IIc and IIIa – the clay-silt with organics abrupt contact with the brown clay beneath.

It was most likely that such gas locations would have been most easily located on boundaries immediately below laminated clays and these

would show more readily than those below sands due to the grain size, porosity and therefore permeability of the material. If gas rose directly up from an organic layer where it had been produced, it would travel through large grain, even waterlogged sands. Denser, finer, less voided clastic material would prevent upward passage and either force the gas horizontally or cap it within pocket in the sediment.

Therefore, it was worth considering the organic signal as a self-contained and capped response, a sharp contact boundary responding to a definitive boundary of material change. Below there must have been a source organic layer - most likely that of a peat, silt or clay. A solid material boundary. If however, the signal was not capped and appears to migrate up with the appearance of bright spots and masking – maybe the appearance of interference or multiples of the organic reflector or seabed above, then this was most likely attributed to free phase gas.

This is demonstrated in Figure 9.8 below. The data, taken from the windfarm surveys for HKN Hollandze Kust Noord by FUGRO for the Netherlands RVO in which they specified that certain highlighted areas were peat / clay anomalies. These would be potential geo-hazards for the pertinent reason that building wind turbines on peats and clays did not provide a solid foundation. However, given our understanding, the analysis used in the interpretation did not differentiate at a material level. This is an excerpt from the report of the data for survey line V5-S6300C, in which they state:

> 'This seismic anomaly show high amplitude, frequency attenuation of the reflector underneath and locally acoustic blanking of the deeper layers. The polarity is uncertain, locally reversed and in other zones normal.
>
> Due to possible thin bed tuning effects, both clay and/or peat can be possible at this level.'

Fugro Report GH216-R3. November 2017, RVO Netherlands

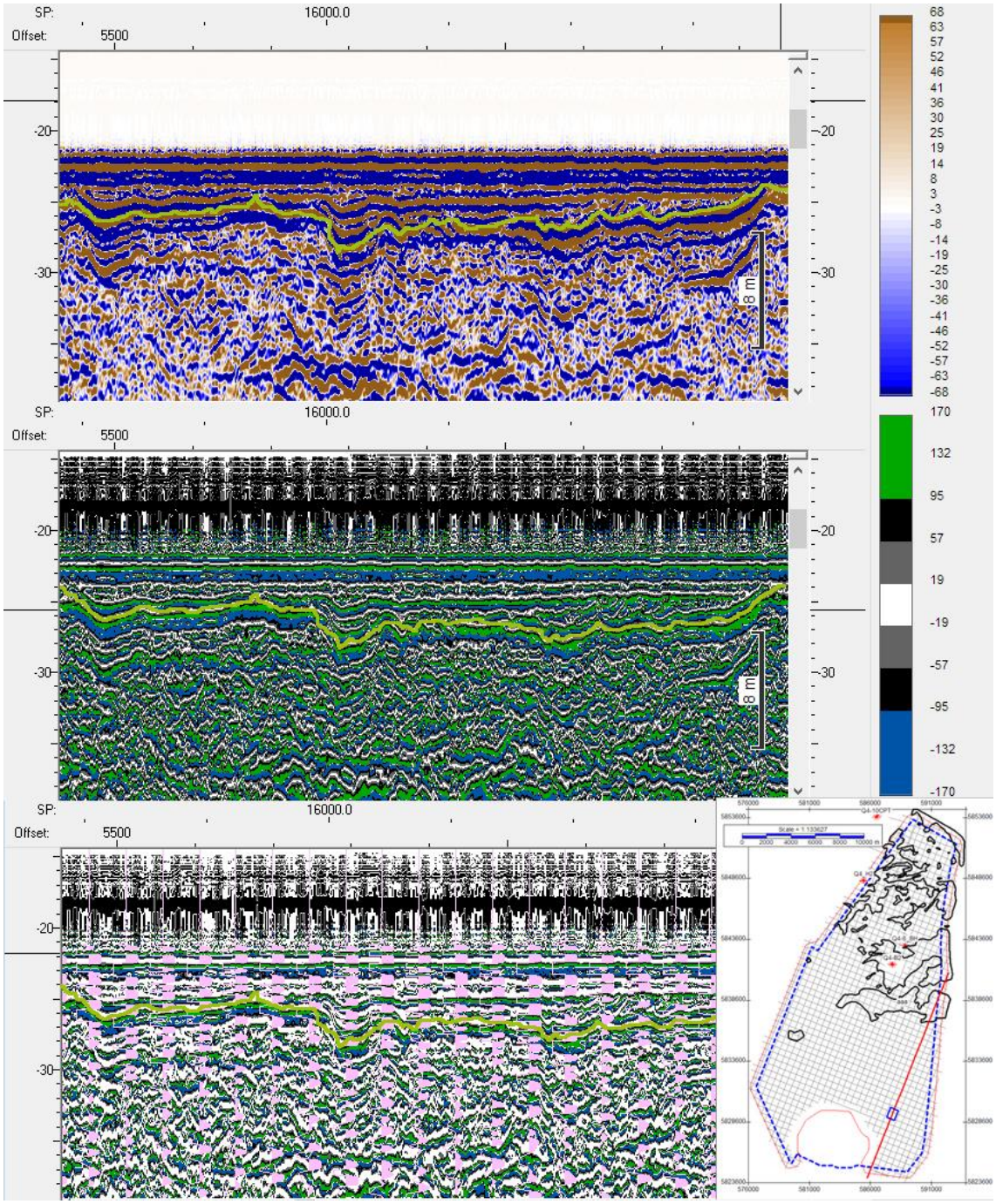

Figure 9.8 Fugro Windfarm data reinterpreted using this thesis research for same survey line V5-S63000C (Thal et al. 2018)

In Figure 9.8 the amplitude display for the same survey line V5-S63000C is shown above with the distinctive frequency attenuation that was referred to in the report. This would indeed indicate a peat layer overlain by clays or silts, but it could as easily refer to free phase gas. In the middle display, the phase function shows a distinct organic polarity with a strong negative to positive zero phase cross over (blue to green with thin white zero line between). These crossovers appeared in repeating bands above the strong reflector signal. While this was not conclusive, it suggested that the

reflector was not the only organic signature within this shallow area and the attenuation was not being caused by one single boundary but a cumulative effect. In the bottom display, with the addition of the variance peaks (in pink), strong parallel kicks along the zero-phase cross-over feature from the reflector signal all the way up to the seabed. This depth of signal uniformity, along with the parallel organic signatures and the definite attenuation below the horizon indicated that this was likely to be a bed of organic material of a permeable sediment with wide scale phase gas escape from or around this strong reflector. Whether or not the feature contains peat is therefore undetermined.

Aside from the problematic bright modern sands at seabed level, the phase variance method picked silt boundaries in preference to other contact boundaries. However, the next most picked was a potentially important archaeological boundary material in the southern North Sea; that of the clay boundary. As described in Chapter 3, these specialised laminated layers of clays that were laid as a result of repeated inundation episodes, can overlay the organic material preserving, isolating and contextualising proxy evidence (Gusick et al. 2019; Briggs et al. 2020). Peats were located between the silts and clays but could not be distinguished from the two by reflector strength, phase amplitude, polarity or variance. Only by means of interpretation of the sediment fill within a feature could an informed decision be made on whether the material was peat or an infilled riverine silt or depositional clay.

Silts were still the most picked, but it was possible to separate clays, silts and sands due to the porosity. It is possible that signals which showed up as potential peats at clay boundaries could in fact have been trapped gas. The bright reflectors in these instances may be caused by gases created in deeper organic layers rising through the porous sediments. The impermeability of the clay boundary halts or delays that escape.

High spike negative amplitudes combined with the bright reflective responses, demonstrate more success in the phase function tests for silt and clay interfaces than for the sands (due to grain size and therefore porosity). This suggests that gas reservoirs and gas production may have been the single most important cause of organic bright reflectors in these seismic shallow surveys. The signals and the potential predictability of peat and the upward mobility of free gas through sediments have implications on acoustic turbidity at all depths but especially for the shallow seismic

exploration. This is critical in archaeological prospecting where the potential for creating blind spots in very shallow (first 1.5m) of sediment can radically affect coring plans.

The presence or lack of bright negative amplitude signals can therefore be misleading at the shallowest of submarine depths. The highest amplitude peaks did not, as originally predicted, necessarily correlate with specific interface contacts as classified by Troels-Smith (Troels-Smith 1955). There were trends for certain boundaries to display higher negative responses than others - i.e. Sh_2 to As_2 or Sh_2 to Ag_2, but the Q-Factor, abruptness of the boundary itself and phase variance also played a significant part in any material prediction. As previously noted, bright negative amplitude signals can certainly signify peat deposits (Coughlan et al. 2018). However, Chapter 6 of this thesis has demonstrated they are also likely to correspond to pockets of free phase gas, directly above an organic layer rather than the layer of peat itself. It was likely, due to the large negative reflectivity and the impact of the Fresnel resolution (laterally and vertically), that the presence of such bright signals may have masked organic layers below (White 1992). This could cause problems for archaeological prospection and the testing of models such as the one in this research. A number of methods could be tested to resolve this, such as applying spectral decomposition on known areas of free phase gas or looking at thin-bed tuning. However, for the purposes of this research there was no gas contained in the core evidence and no definitive gas deposits within the study area seismic, so this avenue was not pursued.

10 OVERALL CONCLUSIONS & DISCUSSIONS

10.1 Introduction

The introduction to this research outlined a number of objectives centred around the identification of peat in a submerged landscape by means of geophysical seismic technologies. With respect of this goal, the research met with varying success. It has certainly increased our interpretive knowledge base in regard to organic responses of bright reflectors within seismic surveys. Additionally, it provided a method which, with a trained eye, allowed the identification of potential peat beds and was able to classify these to appropriate silt or clay interfaces. This is a significant result.

The phase variance signature, whilst still requiring a trained interpreter to understand the environment and context of peat development, did provide an indicator of peat bed potential. This requirement for experienced interpreter is the main reason why the creation of an automated neural network for pattern clustering turned out to be an issue and ultimately did not deliver the intended results.

Within the initial stages of the study, a number of objectives were considered. These were set out in the introduction to this thesis as follows:

> Objective 1 – To collate, collect and analyse available geophysical survey data in the project area and to interpret the results for a focused coring programme.
>
> Objective 2 – To identify, source and learn new software packages necessary for research purposes.
>
> Objective 3 – Interpret seismic data, pick terrestrial horizons for topographic grids, model depths and export 2.5D surfaces (DEMs) for use in GIS maps and models. Detail palaeo features in shapefiles for use in spatial models and scenarios.

Objective 4 – Construct a velocity model based on environmental core reports and statistical analyses and apply these to seismic data to predict peat contact locations and depth.

Objective 5 – Investigate 'bright' organic seismic reflectors and using velocity model attempt to construct a signature for detecting peat in seismic data.

Objective 6 – Construct a neural networking solution for automation of peat boundary detection and classification based on the tools built from the 'seismic signature' developed in the research.

2D and 3D seismic data were collected and collated covering the southern North Sea basin and in particular the study area of concern to this thesis. Geomorphological interpretations were made, and the data were used to create spatial analyses via GIS. Focused coring programmes as part of the ELF Project and those over the Brown Bank made use of such analyses (see Impact of Research in the next Chapter).

In doing this research, many new skills were learned and new software sourced. These ranged from specialised geophysical interpretation and spatial mapping applications to neural networking code that needed a level of mastery to operate. With this skill set it was then possible to create interpreted horizons, gridded, interpolated surfaces (-DEMs) and the OpendTect ANNs as described in the relevant chapters of this thesis.

The collected seismic data was used to construct a new velocity model based on environmental core reports as well as porosity and density calculations. This could be directly used to ascertain an organic 'peat' velocity which was used to investigate 'bright' organic seismic reflectors. Use of core ground observation alongside seismic velocity modelling of reflectors, allowed analysis of the attenuation and Q Factor. This in turn led to a phase variance 'signature' which, while not proving the existence of peat, gave very strong and precise predictors of peat / silt and peat / clay boundaries. It cannot be over-emphasised that through its use, the coring hit rate in the field improved significantly.

As noted in the discussion in Chapter 9, these organic reflectors could be the result of phase gas and not necessarily reflect a specific sediment

material boundary. However, it should be remembered that peat would still be a potential producer of such organic gases and the material at the base of the boundary is most likely to be peat.

Finally, the construction of a neural network employing a pattern recognition SOM was considered. Whilst in theory this should be a straight-forward automation, further investigation found that the current methods available and the practicalities associated with their implementation in the interpretative process, were far more complicated than anticipated. Approaches to both unsupervised artificial neural networking and supervised (manual vectored input) neural networking were undertaken. Whilst these were unsuccessful, they did demonstrate the potential of this field and, in this sense, the thesis provided an advance in archaeological methodology.

10.2 Summary of Results

The results clearly demonstrated that a new velocity model created specifically for the purpose, could link the bright organic reflectors found in seismic surveys directly to peat layers in the cores. The units matched closely in 60% of boundary measurements, which represents a significant achievement. In addition, the discovery that the boundary measurements tended toward the lower unit boundary rather than the higher unit boundary was an addition to our knowledge. In situations where more than one facies boundary occurs within the margin of vertical resolution, the velocity model was able to differentiate the bright organic signal on all but one core. Yet, the facies matched was always that of the lower core unit. This was a notable achievement in making interpretations more explanatory as previously the vertical resolution would have restricted the placement of such boundaries.

Before this thesis, most bright reflectors were identified by researchers as peat. After this study, these responses must be shown to also represent organic silts, clays and free phase gas (see results Chapter 6 and concluding discussions Chapter 9). From these results it has been possible to develop a process (below) that a knowledgeable interpreter may follow to significantly enhance the likely success for the prediction of peat locations for focused coring missions.

10.2.1 Outline Process for Peat Bed Location:

- Locate a palaeo feature – river valley, channel
- Select a time window between a picked seabed horizon and a palaeochannel horizon (no deeper than the Naaldwijk Formation)
- Use a phase function view (cosine phase).
- Run spectral decomposition with inverse Q. A range of between -30 - 75 increases resolution of organic signals within silt and clay but less so for sands.
- Employ a Bandpass Filter (based on the frequency of the survey to eliminate extreme high and low noise frequencies, (often an auto function).
- Simplify the colour bar – bold negative, bold positive, a colour for zero but little in the mid-ranges.
- The organic reflector appears strongly as a zero-phase wavelet, shaped with a negative polarity above. A zero polarity line in the centre and a positive polarity below. The negative and positive polarities will be equal.
- View with Variance 'wiggle' peaks turned on. Enhance if necessary.
- A variance peak appears at the zero polarity line. This is the line to pick.
- Note that the signal should have no interference or multiples above but may suffer from attenuation of signal below, especially if there is a presence of phase gas.

This multi-step process outlined above is still quite convoluted. Unfortunately, automating the procedure using neural networks was not achievable within the constraints of the current research. However, any streamlining of the process would have major benefits and could allow neural networking to be applied.

In its present form, the process still allows for a more focused interpretation of organic sediments and opens out opportunities for the mapping of potential peat beds to a more accurate level than has been achieved before. The process can be performed on multiple small palaeo features

discovered in seismic data, isolating areas of high potential organic to silt boundaries. This can then be combined with depth analysis to determine how close these are to the modern seabed to reveal where possible Holocene erosive contacts may outcrop on the surface. With the knowledge of how and where peat beds are likely created, this process may also be used to map high potential for estuarine development and thus a prograding coastline, prior to inundation (Fig. 10.1)

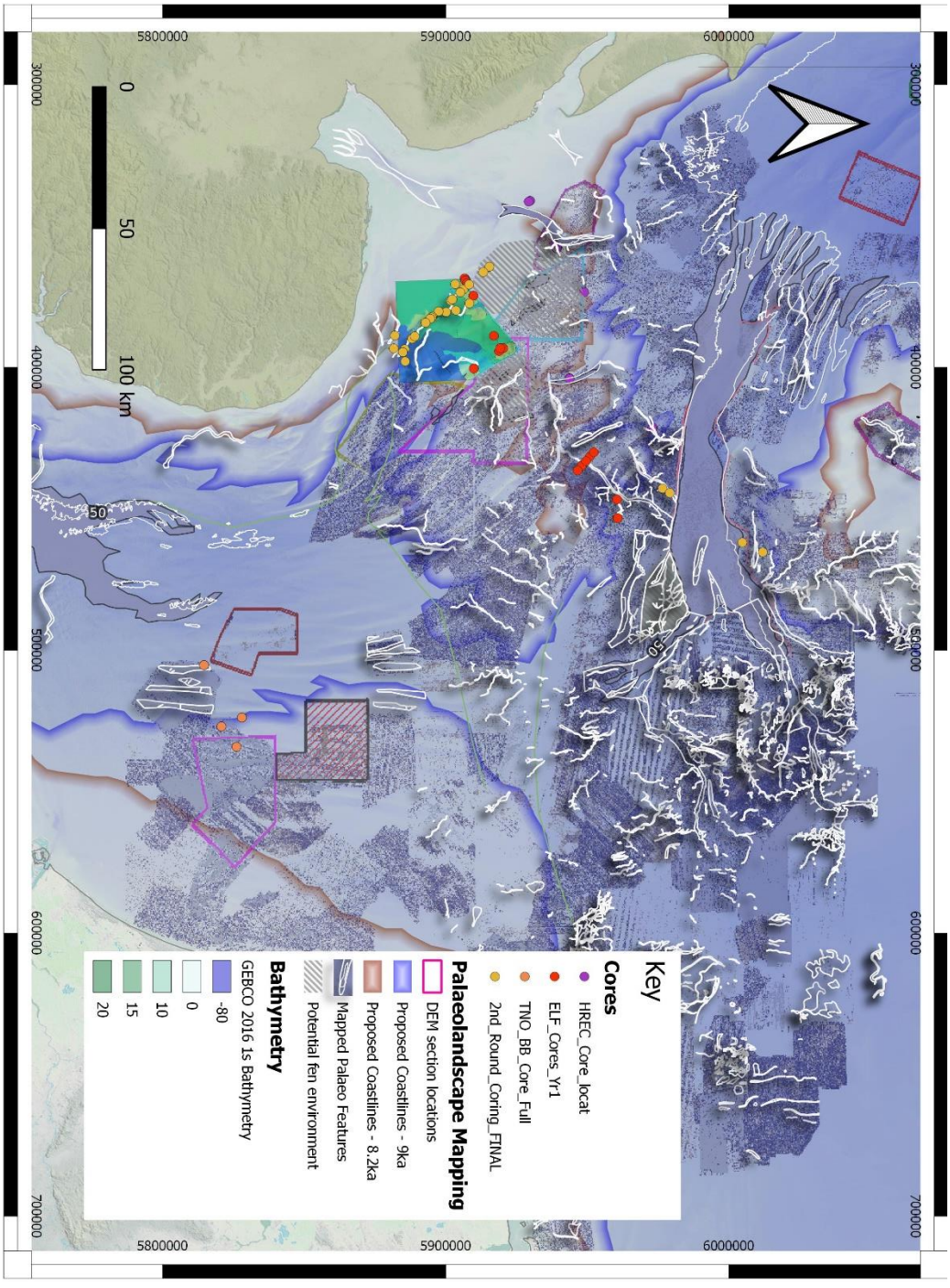

Figure 10.1 Potential palaeo environment predicted by the phase variance process (study area) and spatial analyses of wider potential.

10.3 Industrial Uses for Marine Organic Seismic Modelling

While the focus of this thesis was on the archaeological uses of peat identification, it is worth noting the impact the results may have in the industrial arena. There are several areas of activity to which this may have fundamental value. These are Construction; Aggregate Extraction; Windfarms and the Oil and Gas energy sector.

10.3.1 Construction

Major marine construction developments such as docks and harbours require archaeological consultation, especially in the southern North Sea where the potential of what is understood but not always achieved (Rasmussen et al. 2014; Peeters et al. 2019). The extension of the Yangtze harbour at the Port of Rotterdam is a good example of development work that undertook high resolution seismic surveying and sub-bottom profiles to inform archaeological decision-making (Vos et al. 2015). The interpretive methods of research in this thesis would dovetail into such archaeological planning. Future applications may utilise this focus and efficiency demonstrated in this study as leverage to carry out more extensive geo-prospection and recovery in archaeologically sensitive areas.

10.3.2 Aggregate Excavation

Aggregate extraction sites occupy large tracts of the inshore, and to a lesser extent, offshore UK waters of the southern North Sea as illustrated in Figure 10.2. Such dredging zones are high in archaeological potential (Dellino-Musgrave et al. 2009; Bicket and Tizzard 2015). Between 2002 and 2011 a partnership between the Marine Aggregate Levy Sustainability Fund (MALSF), Wessex Archaeology, the Marine Environment Protection Fund and English Heritage researched the archaeological provenance of these zones. The reports (Balson and Harrison 1988; Bicket and Tizzard 2015) were detailed and showed the extent of archaeological potential. As further dredging continues to cut into the seabed these areas warrant further detailed sub-surface interpretation of the shallow sediment deposition. Revisiting the seismic profiles from the Thames and East Coast RECs would be of benefit as a starting point for further research in this area.

10.3.3 Windfarms

The site planning for windfarm development is an expensive and time-consuming process. Wind turbines are expensive to install and repair and siting them appropriately is of utmost priority. When planning, high definition seismic surveys are taken and interpreted by skilled seismic interpreters who report on 'anomalies' that may cause issues with the siting of a turbine such as boulders, outcropping rock, gas, peat and clay. The latter two are included due to their tendency for compaction and therefore unsuitability for loadbearing. Gas pockets are noted because, at present, it is difficult to differentiate between a signal of peat or gas. The interpreters are merely looking for the 'bright reflectors' and marking them as peat anomalies.

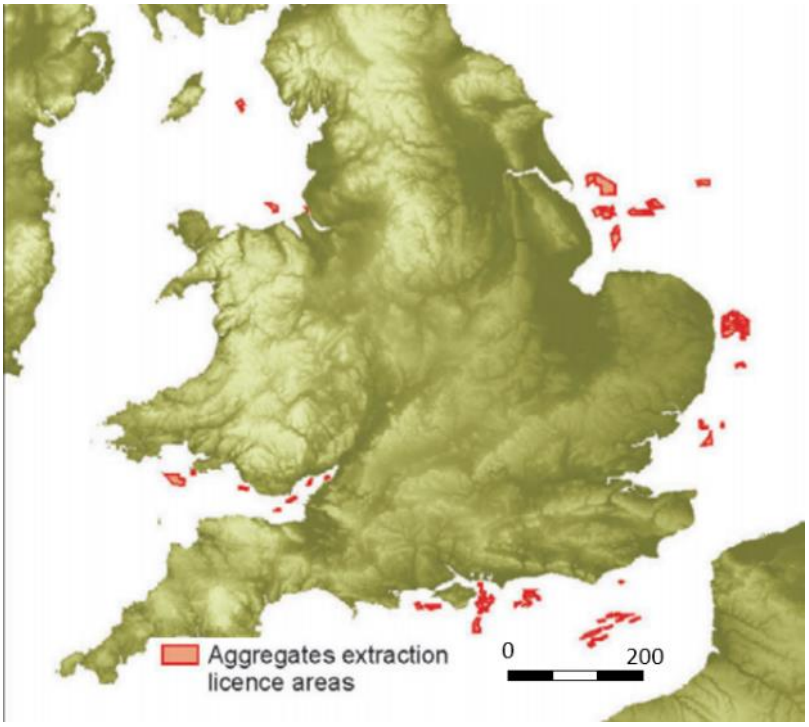

Figure 10.2 UK Aggregate Extraction Sites (Bicket and Tizzard 2015)

Using the process described in the research, not only does it become easier to differentiate between gas pockets and peat, clay or silt boundaries, it is also possible to determine their character in respect of:

a) the classification of material types at specific peat boundaries and;

b) which potential unit facies is being described by the reflector. The research reveals that the lower boundary is favoured, which can suggest to an interpreter whether the peat is bedded directly atop an unconformity signal, or overlain and possibly capped. The latter could

suggest the presence of gas rather than peat (see the discussion around Figure 9.8 in previous chapter).

With further work, an AI based clustering map that utilised the process set out in this research would be a valuable addition to the suite of tools available to this industry.

10.3.4 Energy Prospection

Phase gas at such shallow levels is not of interest as an energy source as the pockets are too small and the gas produced escapes through permeable modern sediments at too great a rate. It is considered a hazard however and must be prospected for when locating structures such as windfarms or oil platforms (Fleischer et al. 2001). Extensive areas of the southern North Sea are noted for the biogenic gas which occurs close to the seabed (Judd 2004; Kortekaas et al. 2010). Yet, apart from individual windfarm developments, regionwide reports are based on Cameron's original continental shelf profiling dating back to 1992 and few new data has become available since (Cameron 1992).

The potential identification of free phase gas in this research would undoubtedly benefit the spatial analysis for the location of turbines and oil platforms. By differentiating between peats, clays, silts and the acoustic turbidity of gases, an interpreter could utilise the research to avoid such hazards with greater certainty.

In addition, the theory underpinning the research could undoubtedly be extended to work on deeper interpreted features. There would be no reason that an experienced interpreter, or with further development, an AI Cluster Map, could not look for specific deposits at a greater depth as long as the window between horizons was still relatively well defined. There is reason to believe that larger capped gas deposits will demonstrate their boundary facies as clearly within the phase function as the shallow phase gases do. Again, the introduction of an AI pattern matching cluster map may be a great asset to this industrial solution.

10.4 Potentials for Archaeological Investigation

The ultimate focus of this research has been on producing methods and tools that are of use to the archaeological community. If this research can be successfully deployed to predict the location of peat beds and differentiate these from other signals, this will represent a significant step forward in how submerged landscape archaeology is undertaken within marine environments. This thesis has taken the first important steps forward, demonstrating that this is achievable. Through the provision of a working velocity model, a potential peat prediction model and the ability to spatially represent this over large areas, the research has provided valuable tools that will help direct archaeological research in this key area.

The research has also demonstrated that further interpretive insights may be achieved by the careful processing of landscape feature type, formation and depth. In this way, organic signals can be distinguished from non-organic reflectors, acoustically turbid gas can be differentiated from depositional organic material and specific boundary contacts can be recognised. Potential peat beds can then be identified and cored for archaeological proxy purposes.

By building spatial interpretations of peat potential, the research has allowed us to add a further layer to the GIS palimpsest as mentioned in Chapter 4 (Figure 4.3, page 97). Potential peat extents can suggest environment and landscape composition prior to and during inundation. When overlayed with other mapped features, changing coastlines, riverine and estuarine areas may be modelled, and the settlement focus may be interpreted with more certainty.

The identification of peat beds within landscape features in seismic data has two further, important implications for the investigation of sub-sea archaeological landscapes. The first is through the location of focused core sites. By refining the results of seismic analyses to allow for greater prediction of potential peat signals, it gives a much higher chance of successfully coring into these units. This will support efficient coring programmes and the cost of exploring submerged palaeolandscapes will be reduced, making research more cost effective.

The 'hit rate' of using non-focused coring programmes of non-archaeological led investigative marine coring compared to the research led, seismic interpretation driven archaeologically focused coring programme this research has been involved in, and continues to advise on, has been estimated at an 80% increase in proxy evidence return (Gaffney et al. 2017a). Such efficiency gains, combined with the methodologies suggested by the research presented here offer significant benefits for marine archaeological research.

The second implication of the research is in the support of environmental proxy evidence that may be sourced from such organic material. Coring programmes may be carried out for many reasons, including the provision of dated lithostratigraphies, but the opportunity to support palaeoenvironmental studies is of equal significance. Peats contain proxies such as pollen, plant remains, coleoptera, fauna, and sedimental ancient DNA and maintain a high level of preservation. In the case of SedaDNA, other sediments, such as clay, preserve equally well if not better and temperature seems to be the main consideration for lack of deamination (Kistler et al. 2017). A single core is a multi-disciplinary source of data for past environments as well as future sea-level rise.

11 FUTURE WORK

11.1 Use of Technologies for further Study – An Introduction

While this study has undoubtedly broken new ground in the prediction and interpretation of organic boundary signals in seismic data, it has only made the first steps into a much greater field of work. The study shows that, with the technology and tools now available, many new areas of study, previously thought impractical, have now opened up. Of these, some will require greater training, expertise and funding, whilst others are purely limited by time and resource. This section will identify the avenues for future research, either as part of post-doctoral study or as PhD subjects in their own right. This section will explore these in four sections focusing on 11.2) The North Sea 11.3) Worldwide Potential, 11.4) Sea Level Rise and Peat Cores and 11.5) Evidential Collection and Context before a final discussion on the impact the study has already achieved.

11.2 North Sea Research

11.2.1 Bright Reflectors

The first avenue for future study is on bright reflectors. As the results of this research revealed, bright reflectors corresponded to an organic signal which, in the correct environmental context, was likely to be peat but also had a high possibility of being gas. With development of shallow gas and windfarm technology in the North Sea set to increase dramatically over the next decade (PM Office 2020) it will be important to site these offshore structures efficiently and safely. Further development of the work in this thesis in differentiating between peat and phase gas could be useful to both archaeology and the British economy.

By looking at the boundaries where gas permeability is poor, such as those of silts and clays, the pressure and compressibility was high. This had the direct result of an increased bright response. Through highly permeable boundaries including sands and loose clastic mixes, the pressure was much lower and the bright response also appeared low. By understanding the material classifications and attenuation at such

boundaries, a more detailed interpretation could be made as to whether the reflector was representing a material sediment or a gas.

At present, the research uses Q-Factor to establish a broad organic sediment type for the boundary contact. Consequently, whilst the results can be characterised as highly predictive, they cannot be said to identify peat specifically at a level of 100% certainty within a submarine context. This also requires additional refinement to identify peat within these organic unit boundaries.

11.2.2 Peat Location

This leads onto the second avenue for further study in the southern North Sea. The location of submerged peat beds. As discussed in Chapter 5, the environmental conditions, especially within the shallow palaeochannels, during the time of inundation were beneficial for the development of peat beds throughout an extensive region south of the Dogger Bank. The phase variance organic signature method, as set out within this thesis, is a useful tool for the shallow seismic interpreter as a means of predictive interpretation of core sites for archaeological prospection. The method has been employed successfully to aid in focused coring missions on the Brown Bank, an area of high archaeological potential in the southern North Sea (see Table 2.1). The method needs further refining and development. As a further study area, the Brown Bank region has great potential. There are already seismic data covering the banks in detail and cores from previous missions (Missiaen et al. 2020).

11.2.3 Parametric Echosounder Integration

One technology that was available for use in the research during the Brown Bank surveys was the parametric echosounder (PES). This technology showed great potential and a third avenue of study would be to investigate this high resolution SEG-Y data in a comparable study. Attempts were made during this research to assimilate lines of echosounder and sparker data to determine optimal coring locations both prior to, and on board the boat. Whilst the organic reflectors displayed with the same amplitude intensity in both the PES data as in the sparker data, they behaved very differently in the phase variant view. When subjected to the same frequency bandpass filters and employing the same phase function as set out in the methods, Chapter 5, there was

no zero-phase wavelet in the PES data. It was replaced with an asymmetrical wave function which was not a simple phase wavelet and had no obvious negative to positive polarity crossover.

This phenomenon may have been a result of the PES technology itself – a parametric echosounder emits a pulse that fires not one but two signals at different frequencies. These are designed to interact; one at a high frequency range and one at a lower frequency. The waves are modulated to create new frequencies within the water column (both a primary and a differential). More work is required to understand these results but presently there is not the time or resource to investigate this. Future research may allow an adaptation to the methodology to cater for the PES.

11.2.4 Artificial Intelligence

The fourth avenue of future development leading from this research concerns the coding of an artificial neural network. Image identification was shown to be lacking in flexibility when it came to the identification of the many differing types of organic facies that could be accounted for in the phase variance method. However, the event pattern matching showed that similar results could theoretically be achieved and clustered using events rather than comparing images.

By setting simple sampling parameters within a two-way time window, an artificial neural network could be developed. This ANN would detect suitable feature unconformities at a suitable depth and then attempt to classify reflectors based on the phase variance method in Chapter 5 of this study. Such similarly classified responses would be cluster in a similar manner to a pattern matching self-organising map.

The issue encountered in this study resulted from using proprietary software in its approach to creating the self-organising map instead of direct coding. The need for bespoke event parameters and the ability to import specific data direct from source software such as IHS Kingdom, suggests that a bespoke coded solution should perhaps have been identified earlier. Such research would have the potential for very positive predictive interpretation of organic seismic facia and may even be developed to run ‘on-the-fly’ aboard a shipboard mission. This could fundamentally

change marine archaeological investigation by making 'live' guided surveys running alongside coring programmes on inundated landscapes across the world in a cost-effective manner.

11.3 Worldwide Application

The methodologies developed through this study are not limited in applicability to the North Sea. Further afield there are many areas of the world that have continental shelves that were terrestrial for great periods of time after the LGM. For example, the Sunda straits, was a shallow continental shelf that connected Indonesia to Sahul (the combined landmass of Australia and New Guinea). Until 9 kya these straits comprised of island archipelagos each one visible, and therefore navigable, from the last (Clarkson et al. 2017). Recent work undertaken by Southampton University on the Australian Continental Shelf independently compliments many of the seismic methods employed in this research (Fogg et al. 2020). Such seismic interpretation and mapping is only the first step. A focused coring operation is necessary to enhance the archaeological understanding of this area. The greater success rate and efficiency that is brought to focused archaeological coring via the results of this research would benefit future project proposals in this area of expanding archaeological interest.

Similarly, the east and west coasts of the United States have, in the last decade, woken to the importance of submerged continental shelf archaeology. Investigations in the Gulf of Mexico (Gusick et al. 2019) and the Pacific continental shelf off California are now producing significant results (Laws et al. 2020). Research in both Russia and the US on the Bering Strait shelf is casting new light on the migration of man following hunting pathways into the Americas (Graf and Buvit 2017). Likewise, research into the origins of human occupation throughout the South China and Yellow Seas are being explored for the first time by means of core sediments from the submerged continental shelf (Li et al. 2016). Each of these areas have huge archaeological potential for submerged landscape research. At the heart of this lies marine based archaeological coring, driven by seismic interpretation and peat identification. Development of the methodologies described here within these areas would not only benefit the individual archaeological projects, but, by building up a seismic database, it will aid in the global understanding of peat development, inundation and the submerged environment.

11.4 Sea-Level Rise & Peat Cores

Peat is ubiquitous across the world from northern mires to mangrove swamps and, because it contains organic material, it can be dated. These samples can be used to indicate final terrestrially aerated dates and, though there are issues with using peat as a lone proxy in this manner, such dates can be used in combination to build up complex sea level rise index points for localised areas (Shennan et al. 2015). This has been achieved in the North Sea as described in Chapter 2 and could be achievable in other areas of the world where peat coring is a viable option.

By creating a series of sea-level rise index points, the focus of peat identification and coring is not purely an archaeological pursuit but extends the audience to present and future climate modellers and environment researchers. In turn, this widens the data frames that inform our archaeological models (Törnqvist and Hijma 2012: 2012). It is therefore important to understand what climatic change meant at the time and how it may affect us now. At the same time, understanding evidence of climate change now, may allow us to interpret our palaeoenvironmental evidence in a different light.

The temperature increase and deglaciation between 11.6 and 7 kya was the most recent period of rapid, perhaps catastrophic, sea level rise recorded (Hansen et al. 2016). During this period, annual sea level rise measured in Tahiti was estimated to have been around 12 mm per year (Bard et al. 2010), reducing to around 0.6 mm per year after 7 kya (Flemming et al. 2014). By means of a parallel, this year-on-year sea-level rise in Tahiti remained relatively constant until the Twentieth Century. At the beginning of the Twenty-First Century (2003) sea-level rise estimates increased to 3.1 mm per year and by 2099 Tahiti's sea-level rise was expected to be at 6 mm per year (Cazenave et al. 2009).

For a full understanding of the implications of future sea level rise, a robust understanding of sea level curves may help us to tackle present sea level rise concerns. To do so, a fuller programme of marine peat cores from continental shelves across the globe is required to build a catalogue of isostatic index points on a world-wide scale. The cost effectiveness of such a coring programme could be improved significantly with the help of the methods set out in this study. New localised sea-level curves devised from

those cores may inform of potential risks for coastal settlements and safeguards put in place.

11.5 Collection & Context of Samples

The collection of archaeological samples from the seabed is a complex and difficult process. In depths or conditions unsuitable for diving, archaeologists frequently use grabs, cores or dredge areas to try and recover material. However, in submerged landscape research, there is rarely a confirmed site location on which to focus. Even detailed information on the location of organic deposits and their accessibility is not immediately available, meaning these missions often rely on chance to locate such deposits.

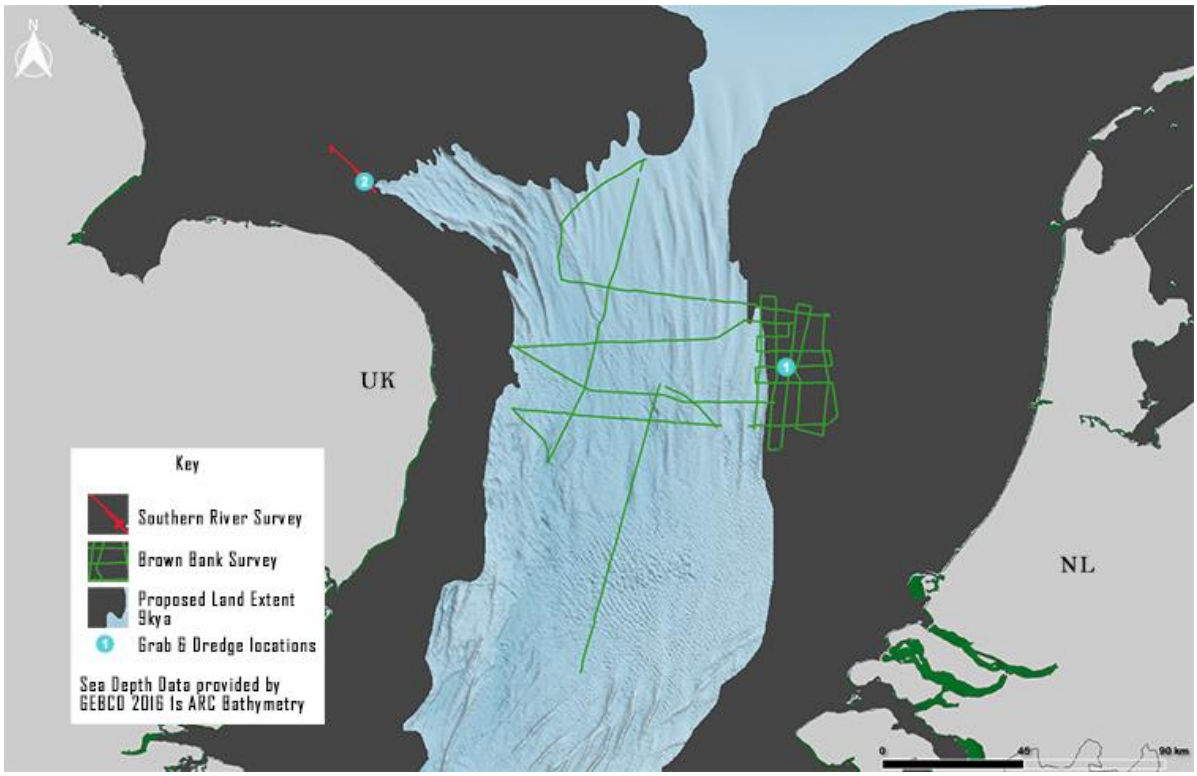

Figure 11.1 Grabs and dredging were tried at two locations interpreted as high potential for erosional or outcropping of peat

The author was given the opportunity to test the results of the analysis presented here and interpret seismic data during a surveying and coring mission. This took place in May 2019 aboard the Belgian research vessel RV Belgica. By identifying locations where potential peat outcropped at the seabed, it was possible to experiment with a range of collection methods such as grabs and dredges to sample the focused area. This was

attempted in two distinct study areas (Figure 11.1) The first, on the Brown Bank, was known from previous cores, to have layers of early Holocene peat eroding to the modern surface in certain areas as discussed in Chapter 2 (Figure 2.12, page 39). The second was across the mouth of a river in an area provisionally titled the Southern River (Number 2 in Figure 11.1). A dredge was run concurrently with the sparker survey on lines where potential outcropping peat from the Naaldwijk formation lay just below the modern sands and could be furrowed by the teeth of the dredge and the peat samples collected in the net.

The methods employed were successful and peat was recovered at both locations (Missiaen et al. 2020). Further refinement is still required, however. Grabbing by means of a Hamon Grab was not well suited to the task of peat collection as the mechanism could not close with sufficient pressure. Attaching a fixed camera to record movement and GPS location on a beam dredge, meanwhile, did provide rudimentary recovery location data and as such has potential. A finer degree of precision would be beneficial for the logging and recording of finds in order to contextualise them on a long dredge line. However, the success of identifying peat from seismic interpretation through to extracting peat samples – all during one shipboard mission is both a valediction of this study and a tantalising taste of what may be achieved in the future.

11.6 Impact of this Research

Without even recovering a single artefact, this study has already had significant impacts upon archaeological research. This is because peat cores contain a wealth of information about the land, the environment, the climate and the dating of an area that is otherwise inaccessible. These data are invaluable to assist an archaeologist predict potential settlement areas, hunting routes even dispersal patterns. In doing so research activity can move from wide supra-regional scales to localised areas, and, perhaps, even site-specific scale targets (Missiaen et al. 2020).

The methodologies presented in this study have provided results which led to a robust step-by-step analytical process. This has been tested and shown to work in providing an improved coring (and dredging) success rate for recovery of organic sediments. Developments of the methods and some results from this study have been presented at the CAA (Computer Aided Archaeology) Conference 2017, and the Europa 2018 Conference. Implications of the work and issues surrounding it played a key role in

plenary sessions and poster displays at other smaller post-Graduation symposia and seminar sessions. These generated high levels of interest both in the UK and Europe about the potential impacts of this thesis' methodologies on future research.

The clearest evidence for the impact of this research is in the work at the Brown Bank. As stated in section 11.5 above, the study methods presented here were used in the location of cores which returned a 75% success rate for peat content. The study was also used in the location of eroding peat onto the modern seabed surface as a trial for the practical application of an archaeologically focused dredge for potential settlement sites. A small number of dredge runs recovered large samples of intact ancient wood roots and blocks of peat. These targeted organic materials are an impressive vindication of the thesis' interpretations of the seismic signals. In addition to this organic material, the project also dredged two possible worked flints as shown in Figure 11.2 (Keys 2019; Gaffney et al. 2020), which clearly show the archaeological potential of these landscapes and the impact that this research's methods may have on the targeted recovery of material in offshore regions.

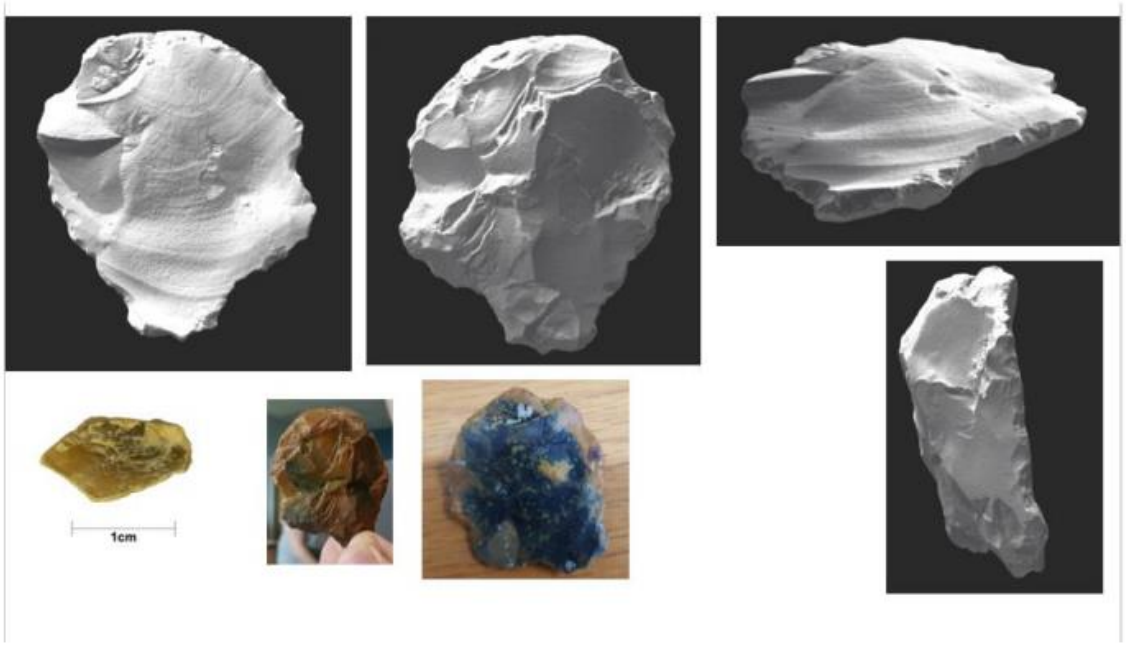

Figure 11.2 Bottom Left flint debitage, Above and Right, worked fragment, probably from hammer stone (3D Scan courtesy of Tom Sparrow, Visual Heritage University of Bradford)

It is important to emphasise that these are the first archaeological artefacts retrieved from a submerged palaeolandscape beyond 12 nm from the shore as a direct result of focused investigation and retrieval.

While some improvement is required in the collection and processing of data, as presented here, it cannot be denied that methods for discovery have been enhanced by this study and are a major step forward in our understanding of inundated palaeolandscapes. This knowledge will enhance our ability to undertake effective archaeological research at sea.

12 WORK CITED

A2S, Southampton, G. a. U. o., Adramar, VIOE, Centre, N. O., Trust, M. A. and DRASSM (2010) *Archaeological Atlas of the 2 Seas.* University of Southampton: Accessed 2nd September 2016.

Aaby, B., Fischer, A. and Pedersen, L. (1997) *The Danish Storebaelt since the Ice Age: man, sea and forest.* Storebælt Fixed Link.

Aki, K. and Richards, P. G. (2002) *Quantitative seismology*.

Alexander, L. M. (2020) *The North Sea.* [online] 02/04. *https://www.britannica.com/place/North-Sea* Accessed 09/04.

Aminzadeh, F., Barhen, J., Glover, C., Toomarian, N. J. C. and Geosciences (2000) Reservoir parameter estimation using a hybrid neural network. 26 (8), 869-875.

Amkreutz, L. and Spithoven, M. (2019) Hunting beneath the waves. Bone and antler points from North Sea Doggerland off the Dutch coast.

An, P. and Moon, W. M. (1993) Reservoir characterization using feedforward neural networks. *SEG Technical Program Expanded Abstracts 1993.* Society of Exploration Geophysicists. 258-262.

Andrews, J., Boomer, I., Bailiff, I., Balson, P., Bristow, C., Chroston, P., Funnell, B., Harwood, G., Jones, R. and Maher, B. (2000) Sedimentary evolution of the north Norfolk barrier coastline in the context of Holocene sea-level change. *Geological Society, London, Special Publications* 166 (1), 219-251.

Archaeology, W. (2007) Historic environment guidance for the offshore renewable energy sector. *Commissioned by COWRIE Ltd, Ref: ARCH-11-05*.

Ashton, N., Lewis, S. G., De Groote, I., Duffy, S. M., Bates, M., Bates, R., Hoare, P., Lewis, M., Parfitt, S. A. and Peglar, S. (2014) Hominin footprints from early Pleistocene deposits at Happisburgh, UK. *PLoS One* 9 (2), e88329.

Astrup, P. M. (2018) *Sea-level change in Mesolithic Southern Scandinavia: long-and short-term effects on society and the environment.* Vol. 106. ISD LLC.

Athy, L. F. (1930) Density, porosity, and compaction of sedimentary rocks. *Aapg Bulletin* 14 (1), 1-24.

Baeteman, C., Waller, M. and Kiden, P. (2012) 'Reconstructing middle to late Holocene sea-level change: A methodological review with particular reference to "A new Holocene sea-level curve for the southern North Sea" presented by K.-E. Behre': Reply to comments: Boreas Reply to Comments. *Boreas* 41 (2), 315-318.

Bailey, G., Barrett, J., Craig, O. and Milner, N. (2008) Historical ecology of the North Sea basin. *Human impact on ancient marine ecosystems: a global perspective. University of California Press, Berkeley and Los Angeles, California*, 215-242.

Bailey, G. e., Galanidou, N., Peeters, H., Jöns, H. and Mennenga, M. (2020) *The Archaeology of Europe's Drowned Landscapes.*

Bailey, G. N. and Flemming, N. C. (2008) Archaeology of the continental shelf: marine resources, submerged landscapes and underwater archaeology. *Quaternary Science Reviews* 27 (23), 2153-2165.

Balson, P., Butcher, A., Holmes, R., Johnson, H., Lewis, M. and Musson, R. (2001) *Technical Report 008 - North Sea Geology*.

Balson, P. and Harrison, D. (1988) Marine Aggregate Survey. Phase 1, Southern North Sea.

Barber, D., Dyke, A., Hillaire-Marcel, C., Jennings, A., Andrews, J., Kerwin, M., Bilodeau, G., McNeely, R., Southon, J. and Morehead, M. (1999) Forcing of the cold event of 8,200 years ago by catastrophic drainage of Laurentide lakes. *Nature* 400 (6742), 344-348.

Barcelo, J. A., Barcelo, J. A. and Del Castillo, F. (2016) *Simulating prehistoric and ancient worlds.* Switzerland: Springer.

Bard, E., Hamelin, B. and Delanghe-Sabatier, D. J. S. (2010) Deglacial meltwater pulse 1B and Younger Dryas sea levels revisited with boreholes at Tahiti. 327 (5970), 1235-1237.

Barlow, N. L. M., Long, A. J., Saher, M. H., Gehrels, W. R., Garnett, M. H. and Scaife, R. G. (2014) Salt-marsh reconstructions of relative sea-level change in the North Atlantic during the last 2000 years. *Quaternary Science Reviews* 99, 1-16.

Barton, N. and Roberts, A. (2004) The Mesolithic period in England: current perspectives and new research.

Barus, C. (1892) *The compressibility of liquids.* Vol. 92. Govt. Print. Off.

Bates, M. R., Bates, C. R. and Whittaker, J. E. (2007) Mixed method approaches to the investigation and mapping of buried Quaternary deposits: examples from southern England. *Archaeological Prospection* 14 (2), 104-129.

Bayliss, A. and Woodman, P. (2009) A new Bayesian chronology for Mesolithic occupation at Mount Sandel, Northern Ireland. *Proceedings of the Prehistoric Society*. Vol. 75. Cambridge University Press.

Behre, K.-E. (2007) A new Holocene sea-level curve for the southern North Sea. *Boreas* 36 (1), 82-102.

Bell, M., Brunning, R., Batchelor, R., Hill, T., Wilkinson, K., Banerjea, R., Young, D., Brown, A., Carson, S. and Maslin, S. (2016) The Mesolithic of the wetland/dryland edge in the Somerset Levels.

Bell, M., Caseldine, A. and Neumann, H. (2000) *Prehistoric intertidal archaeology in the Welsh Severn Estuary.* Council for British Archaeology.

Benjamin, J., Bonsall, C., Pickard, C. and Fischer, A. (2011) *Submerged prehistory.* Oxbow Books Oxford.

Benjamin, J. and Hale, A. (2012) Marine, maritime, or submerged prehistory? Contextualizing the prehistoric underwater archaeologies of inland, coastal, and offshore environments. *European Journal of Archaeology* 15 (2), 237-256.

Berglund, B. E., Björck, S., Lemdahl, G., Bergsten, H., Nordberg, K. and Kolstrup, E. (1994) Late Weichselian environmental change in

southern Sweden and Denmark. *Journal of Quaternary Science* 9 (2), 127-132.

Bicket, A. and Tizzard, L. (2015) A review of the submerged prehistory and palaeolandscapes of the British Isles. *Proceedings of the Geologists' Association* 126 (6), 643-663.

Billette, F. and Brandsberg-Dahl, S. (2005) The 2004 BP velocity benchmark. *67th EAGE Conference & Exhibition*. European Association of Geoscientists & Engineers.

Biot, M. A. J. T. J. o. t. a. S. o. a. (1956) Theory of propagation of elastic waves in a fluid-saturated porous solid. II. Higher frequency range. 28 (2), 179-191.

Birchenough, A., Limpenny, Barrio Froján, C., Cotterill, C., Foster-Smith, Pearce, B., Tizzard, L., Long, D., Walmsley, Kirby, Baker, Meadows, Rees, J., Hill, Wilson, C., Leivers, M., Churchley, Russell, Birchenough and Law, R. (2011) *The East Coast Regional Environmental Characterisation*.

Blackford, J. (2000) *Palaeoclimatic records from peat bogs*. England, Elsevier Ltd.

Blockley, S. P., Blaauw, M., Ramsey, C. B. and van der Plicht, J. (2007) Building and testing age models for radiocarbon dates in Lateglacial and Early Holocene sediments. *Quaternary Science Reviews* 26 (15-16), 1915-1926.

Bocherens, H., Polet, C. and Toussaint, M. (2007) Palaeodiet of Mesolithic and Neolithic populations of Meuse Basin (Belgium): evidence from stable isotopes. *Journal of archaeological Science* 34 (1), 10-27.

Bondevik, S., Løvholt, F., Harbitz, C., Mangerud, J., Dawson, A. and Svendsen, J. I. (2005) The Storegga Slide tsunami—comparing field observations with numerical simulations. *Marine and Petroleum Geology* 22 (1), 195-208.

Bos, I. J., Busschers, F. S. and Hoek, W. Z. J. S. (2012) Organic-facies determination: a key for understanding facies distribution in the basal peat layer of the Holocene Rhine-Meuse delta, The Netherlands. 59 (2), 676-703.

Botch, M., Kobak, K., Vinson, T. and Kolchugina, T. (1995) Carbon pools and accumulation in peatlands of the former Soviet Union. *Global Biogeochemical Cycles* 9 (1), 37-46.

Bradley, R. (1984) *The social foundations of prehistoric Britain: themes and variations in the archaeology of power*. London: Longman.

Bradley, S. L., Milne, G. A., Shennan, I. and Edwards, R. (2011) An improved glacial isostatic adjustment model for the British Isles. *Journal of Quaternary Science* 26 (5), 541-552.

Brandt, R., Groenewoudt, B. J. and Kvamme, K. L. J. W. A. (1992) An experiment in archaeological site location: modeling in the Netherlands using GIS techniques. 24 (2), 268-282.

Brew, D. S. (1996) Late Weichselian to early Holocene subaqueous dune formation and burial off the North Sea Northumberland coast. *Marine Geology* 134 (3-4), 203-211.

Briggs, N., Dall'Olmo, G. and Claustre, H. (2020) Major role of particle fragmentation in regulating biological sequestration of CO2 by the oceans. *Science* 367 (6479), 791-793.

Broecker, W. S. (2006) Was the Younger Dryas triggered by a flood? *Science* 312 (5777), 1146-1148.

Bronk-Ramsey, C., Hedges, R. E. M., Housley, R. A. and Law, I. (1990) Radiocarbon dates from the Oxford AMS system: Archaeometry datelist 10. *Archaeometry* (32), 101 - 108.

Brown, M. P. and Poulton, M. M. (1996) Locating buried objects for environmental site investigations using neural networks. 1 (3), 179-188.

Brück, J. (2005) Experiencing the past? The development of a phenomenological archaeology in British prehistory. *Archaeological dialogues* 12 (1), 45-72.

Bruck, J. and Goodman, M. (2012) *Making places in the prehistoric world: themes in settlement archaeology*. Routledge.

Bryn, P., Berg, K., Forsberg, C. F., Solheim, A. and Kvalstad, T. J. (2005) Explaining the Storegga slide. *Marine and Petroleum Geology* 22 (1-2), 11-19.

Buckingham, M. J. (2005) Compressional and shear wave properties of marine sediments: Comparisons between theory and data. *The Journal of the Acoustical Society of America* 117 (1), 137-152.

Buiron, D., Stenni, B., Chappellaz, J., Landais, A., Baumgartner, M., Bonazza, M., Capron, E., Frezzotti, M., Kageyama, M. and Lemieux-Dudon, B. (2012) Regional imprints of millennial variability during the MIS 3 period around Antarctica. *Quaternary Science Reviews* 48, 99-112.

Bull, J. M., Quinn, R. and Dix, J. K. (1998) Reflection coefficient calculation from marine high resolution seismic reflection (Chirp) data and application to an archaeological case study. *Marine Geophysical Researches* 20 (1), 1-11.

Burkitt, M. C. (1932) 138. A Maglemose Harpoon dredged up recently from the North Sea. *Man* 32, 118-118.

Bynoe, R. (2018) The submerged archaeology of the North Sea: Enhancing the Lower Palaeolithic record of northwest Europe. *Quaternary Science Reviews* 191, 1-14.

Bynoe, R., Dix, J. K. and Sturt, F. (2016) Of mammoths and other monsters: historic approaches to the submerged Palaeolithic. *Antiquity* 90 (352), 857-875.

Byrne, D. (2002) *Interpreting quantitative data*. Sage.

Calvo, E., Grimalt, J. and Jansen, E. (2002) High resolution U37K sea surface temperature reconstruction in the Norwegian Sea during the Holocene. *Quaternary Science Reviews* 21 (12-13), 1385-1394.

Cameron, T. (1992) *The geology of the southern North Sea*. Balogh Scientific Books.

Carleton, W. C., Conolly, J. and Ianonne, G. (2012) A locally-adaptive model of archaeological potential (LAMAP). *Journal of Archaeological Science* 39 (11), 3371-3385.

Cazenave, A., Dominh, K., Guinehut, S., Berthier, E., Llovel, W., Ramillien, G., Ablain, M., Larnicol, G. J. G. and Change, P. (2009) Sea level budget over 2003–2008: A reevaluation from GRACE space gravimetry, satellite altimetry and Argo. 65 (1-2), 83-88.

Chapman, H. (2015) The landscape archaeology of bog bodies. *Journal of Wetland Archaeology* 15 (1), 109-121.

Charman, D. J., Barber, K. E., Blaauw, M., Langdon, P. G., Mauquoy, D., Daley, T. J., Hughes, P. D. and Karofeld, E. (2009) Climate drivers for peatland palaeoclimate records. *Quaternary Science Reviews* 28 (19-20), 1811-1819.

Childe, V. G. (1925) *The Dawn of European Civilization... 1925.* Routledge and Kegan Paul.

Chopra, S. and Alexeev, V. (2006) Applications of texture attribute analysis to 3D seismic data. *The Leading Edge* 25 (8), 934-940.

Chopra, S., Lubo-Robles, D. and Marfurt, K. J. (2018) GCSome Machine Learning Applications in Seismic Interpretation.

Chotiros, N. P. and Isakson, M. J. (2004) A broadband model of sandy ocean sediments: Biot–Stoll with contact squirt flow and shear drag. *The Journal of the Acoustical Society of America* 116 (4), 2011-2022.

Clapham, M. (2014) *Fluvial Transport and Sedimentology*. YouTube.

Clark, G. (1932) *The mesolithic age in Britain.* Cambridge Univ Press.

Clark, G. (1936) *The Mesolithic Settlement of Northern Europe: The Food-gathering Peoples of Northern Europe During the Early Post-glacial Period.* The University Press.

Clark, G. (1954) *Excavations at Star Carr: an Early Mesolithic site at Seamer near Scarborough, Yorkshire*. Vol. Rev. Cambridge 1971- Book: Cambridge University Press.

Clark, G. and Clark, J. G. D. (1975) *The earlier stone age settlement of Scandinavia.* CUP Archive.

Clarke, G. K., Leverington, D. W., Teller, J. T. and Dyke, A. S. (2004) Paleohydraulics of the last outburst flood from glacial Lake Agassiz and the 8200BP cold event. *Quaternary Science Reviews* 23 (3), 389-407.

Clarkson, C., Jacobs, Z., Marwick, B., Fullagar, R., Wallis, L., Smith, M., Roberts, R. G., Hayes, E., Lowe, K. and Carah, X. (2017) Human occupation of northern Australia by 65,000 years ago. *Nature* 547 (7663), 306-310.

Coetsiers, M. and Walraevens, K. (2006) Chemical characterization of the neogene aquifer, Belgium. *Hydrogeology Journal* 14 (8), 1556-1568.

Cojan, I. and Renard, M. (2002) *Sedimentology.* Abingdon;Lisse;: A.A. Balkema.

Coléou, T., Poupon, M. and Azbel, K. (2003) Unsupervised seismic facies classification: A review and comparison of techniques and implementation. *The Leading Edge* 22 (10), 942-953.

Coles, B. J. (1998) Doggerland: a Speculative Survey. *Proceedings of the Prehistoric Society* 64, 45.

Coles, B. J. (2000) Doggerland: the cultural dynamics of a shifting coastline. *Geological Society, London, Special Publications* 175 (1), 393-401.

Comas, X., Slater, L. and Reeve, A. (2004) Geophysical evidence for peat basin morphology and stratigraphic controls on vegetation observed in a Northern Peatland. *Journal of hydrology* 295 (1-4), 173-184.

Conneller, C., Bayliss, A., Milner, N. and Taylor, B. (2016) The resettlement of the British landscape: Towards a chronology of Early Mesolithic lithic assemblage types.

Conneller, C., Milner, N., Taylor, B. and Taylor, M. (2012) Substantial settlement in the European early mesolithic: new research at Star Carr. *Antiquity* 86 (334), 1004-1020.

Conolly, J. and Lake, M. (2006) *Geographical information systems in archaeology*. Cambridge University Press.

Cordain, L., Miller, J. B., Eaton, S. B., Mann, N., Holt, S. H. and Speth, J. D. (2000) Plant-animal subsistence ratios and macronutrient energy estimations in worldwide hunter-gatherer diets. *The American journal of clinical nutrition* 71 (3), 682-692.

Cotterill, C. J., Phillips, E., James, L., Forsberg, C. F., Tjelta, T. I., Carter, G. and Dove, D. (2017) The evolution of the Dogger Bank, North Sea: a complex history of terrestrial, glacial and marine environmental change. *Quaternary Science Reviews* 171, 136-153.

Cottrell, A. M. (1993) The law of the sea and international marine archaeology: abandoning admiralty law to protect historic shipwrecks. *Fordham Int'l LJ* 17, 667.

Coughlan, M., Fleischer, M., Wheeler, A. J., Hepp, D. A., Hebbeln, D. and Mörz, T. (2018) A revised stratigraphical framework for the Quaternary deposits of the German North Sea sector: a geological-geotechnical approach. *Boreas* 47 (1), 80-105.

Council of Europe, C. (1992) European Convention on the Protection of the Archaeological Heritage (Revised) Valletta 1992. *Council of Europe Treatises, series 143*. .

Crombé, P. (2018) Abrupt cooling events during the Early Holocene and their potential impact on the environment and human behaviour along the southern North Sea basin (NW Europe). *Journal of Quaternary Science* 33 (3), 353-367.

Dasgupta, R. and Clark, R. A. (1998) Estimation of Q from surface seismic reflection data. *Geophysics* 63 (6), 2120-2128.

Davison, K., Dolukhanov, P., Sarson, G. R. and Shukurov, A. (2006) The role of waterways in the spread of the Neolithic. *Journal of Archaeological Science* 33 (5), 641-652.

De Groote, I., Lewis, M. and Stringer, C. (2018) Prehistory of the British Isles: A tale of coming and going. *Bulletins et Mémoires de la Société d'Anthropologie de Paris* 30 (1-2), 1-13.

Deegan, A., Oakey, M. and van den Toorn, D. (2004) *SUMMARY REPORT: Lower Wharfedale National Mapping Programme Project*. WYAS for National Monuments Record.

Delefortrie, S., Saey, T., Van De Vijver, E., De Smedt, P., Missiaen, T., Demerre, I. and Van Meirvenne, M. (2014) Frequency domain electromagnetic induction survey in the intertidal zone: Limitations of low-induction-number and depth of exploration. *Journal of Applied Geophysics* 100, 14-22.

Dellino-Musgrave, V., Gupta, S. and Russell, M. (2009) Marine aggregates and archaeology: a golden harvest? *Conservation and management of archaeological sites* 11 (1), 29-42.

Deravignone, L., Blankholm, H. P., Pizziolo, G. J. M. and archaeology (2015) Predictive modeling and artificial neural networks: from model to survey. 335-351.

Dixon, S. (2015) *UK Sea Fisheries Statistics 2014*. Office of National Statistics.

Dolukhanov, P. M. (1996) The Pleistocene—Holocene Transition on the East European Plain. *Humans at the End of the Ice Age*. Springer. 159-169.

Dramsch, J. (2018) Deep Computational Geophysics and Machine Learning.

DTI, U. (2002) *Strategic Environmental Assessment of Parts of the Central & Southern North Sea SEA 3*. Industry, D. O. T. A. Consultation Document: HM Goverment.

Duin, E., Doornenbal, J., Rijkers, R., Verbeek, J. and Wong, T. E. (2006) Subsurface structure of the Netherlands-results of recent onshore and offshore mapping. *Netherlands Journal of Geosciences* 85 (4), 245.

Dunn, M. and Hickey, R. (1998) The effect of slope algorithms on slope estimates within a GIS. *Cartography* 27 (1), 9-15.

Dysart, P. S. and Pulli, J. (1990) Regional seismic event classification at the NORESS array: seismological measurements and the use of trained neural networks. *Bulletin of the Seismological Society of America* 80 (6B), 1910-1933.

Emery, D. and Myers, K. (2009) *Sequence stratigraphy*. John Wiley & Sons.

Engler, N. J., Scassa, T. and Taylor, D. F. (2013) Mapping traditional knowledge: digital cartography in the Canadian North. *Cartographica: The International Journal for Geographic Information and Geovisualization* 48 (3), 189-199.

Esestime, P., Browning-Stamp, P. and Hewitt, A. (2015) Evidence of early halokinesis in the Zechstein Group suggests the formation of Permian-Triassic carbonates build-ups offshore UK (Quad. 20-21). *First Break* 33 (12), 69-75.

Ferrier, K. L., Austermann, J., Mitrovica, J. X. and Pico, T. (2017) Incorporating sediment compaction into a gravitationally self-consistent model for ice age sea-level change. *Geophysical Journal International* 211 (1), 663-672.

Ferrier, K. L., Li, Q., Pico, T. and Austermann, J. (2018) The Influence of Water Storage in Marine Sediment on Sea-Level Change. *Geophysical Research Letters* 45 (5), 2444-2454.

Fischer, A. (1995) An entrance to the Mesolithic world below the ocean. Status of ten years' work on the Danish sea floor. *OXBOW MONOGRAPH*, 371-384.

Fischer, A. (2004) Submerged stone age-Danish examples and North Sea potential. *CBA RESEARCH REPORT* 141, 21.

Fitch, S., Thomson, K. and Gaffney, V. (2005) Late Pleistocene and Holocene depositional systems and the palaeogeography of the Dogger Bank, North Sea. *Quaternary Research* 64 (2), 185-196.

Fitch, S. E. J. (2011) *The mesolithic landscape of the Southern North Sea*. University of Birmingham.

Fleischer, P., Orsi, T., Richardson, M. and Anderson, A. (2001) Distribution of free gas in marine sediments: a global overview. *Geo-Marine Letters* 21 (2), 103-122.

Flemming, N. (2003) The scope of Strategic Environmental Assessment of North Sea area SEA4 in regard to prehistoric archaeological remains.

Flemming, N., Bailey, G. N., Sakellariou, D., Arias, P., Canals, M., Chiocci, F. L., Cohen, K., Erlandson, J., Faught, M. K. and Flatman, J. (2012) Early Human Dispersals and Submerged Landscapes: comment on news feature" Migration: value of submerged early sites" in Nature's May 2012 special issue" Peopling the Planet". *Nature* 34.

Flemming, N. C., Çağatay, M. N., Chiocci, F. L., Galanidou, N., Jöns, H., Lericolais, G., Missiaen, T., Moore, F., Rosentau, A. and Sakellariou, D. (2014) *Land beneath the waves: submerged landscapes and sea level change: a joint geoscience-humanities strategy for European Continental Shelf Prehistoric Research.* Vol. 21. European Marine Board.

Flemming, N. C., Harff, J., Burgess, A., Bailey, G. N. and Moura, D. (2017) *Submerged landscapes of the European continental shelf: Quaternary paleoenvironments.* Vol. 1. John Wiley & Sons.

Fletcher-Tomenius, P. and Williams, M. (1999) The draft UNESCO/DOALOS Convention on the protection of underwater cultural heritage and conflict with the European Convention on Human Rights. *International Journal of Nautical Archaeology* 28 (2), 145-153.

Fogg, A., Dix, J. and Farr, H. (2020) Late Pleistocene Palaeo Environment Reconstruction from 3D Seismic data, NW Australia. The ACROSS project-Australasian Research: Origins of Seafaring to Sahul.

Folk, R. L. (1954) The distinction between grain size and mineral composition in sedimentary-rock nomenclature. *The Journal of Geology*, 344-359.

Forgy, E. W. (1965) Cluster analysis of multivariate data: efficiency versus interpretability of classifications. *biometrics* 21, 768-769.

Fraser, A. (2016) Characterising a Submerged Landscape – Making Archaeological Sense of Submarine Data using a Geographic Information System. University of Bradford Masters Thesis.

French, J. R. (1993) Numerical simulation of vertical marsh growth and adjustment to accelerated sea-level rise, North Norfolk, UK. *Earth Surface Processes and Landforms* 18 (1), 63-81.

Frenzel, P. and Boomer, I. J. P., Palaeoclimatology, Palaeoecology (2005) The use of ostracods from marginal marine, brackish waters as bioindicators of modern and Quaternary environmental change. 225 (1-4), 68-92.

Gaffney, V., Allaby, R., Bates, R., Bates, M., Ch'ng, E., Fitch, S., Garwood, P., Momber, G., Murgatroyd, P. and Pallen, M. (2017a) Doggerland and the Lost Frontiers Project (2015–2020). *Under the Sea: Archaeology and Palaeolandscapes of the Continental Shelf*. Springer. 305-319.

Gaffney, V., Fitch, S., Bates, M., Ware, R. L., Kinnaird, T. and Gearey, B. (2017b) Proceedings of the Inaugural Conference for the Europe's Lost Frontiers ERC Funded Project

Gaffney, V., Fitch, S., Bates, M., Ware, R. L., Kinnaird, T., Gearey, B., Hill, T., Telford, R., Batt, C. and Stern, B. (2020) Multi-Proxy Characterisation of the Storegga Tsunami and Its Impact on the Early Holocene Landscapes of the Southern North Sea. *Geosciences* 10 (7), 270.

Gaffney, V. and Van Leusen, M. (1995) Postscript-GIS, environmental determinism and archaeology: a parallel text. *Archaeology and geographical information systems: a European perspective*, 367-382.

Gaffney, V. L., Fitch, S. and Smith, D., (2009) *Europe's lost world: the rediscovery of Doggerland.* Vol. 160;no.160;. York: Council for British Archaeology.

Gaffney, V. L., Thomson, K. and Fitch, S. (2007) *Mapping Doggerland: the Mesolithic landscapes of the southern North Sea.* Archaeopress.

García-Artola, A., Stéphan, P., Cearreta, A., Kopp, R. E., Khan, N. S. and Horton, B. P. J. Q. S. R. (2018) Holocene sea-level database from the Atlantic coast of Europe. 196, 177-192.

Garrison, T. S. (2012) *Oceanography: an invitation to marine science*. Cengage Learning.

Garton, D. (2017) Prior to Peat: Assessing the Hiatus between Mesolithic Activity and Peat Inception on the Southern Pennine Moors. *Archaeological Journal* 174 (2), 281-334.

Gauss, C. F. (1828) *Disquisitiones generales circa superficies curvas.* Vol. 1. Typis Dieterichianis.

Gautier, D. L. (2005) *Kimmeridgian shales total petroleum system of the North Sea graben province.* Geological Survey (US).

Gearey, B., Bermingham, N., Chapman, H., Charman, D., Fletcher, W., Fyfe, R., Quartermaine, J. and Van de Noort, R. (2010) Peatlands and the Historic Environment.

Glimmerveen, J., Mol, D. and van der Plicht, H. (2006) The Pleistocene reindeer of the North Sea—initial palaeontological data and archaeological remarks. *Quaternary International* 142, 242-246.

Glob, P. V. and Bruce-Mitford, R. L. S. (1975) *The bog people: Iron-Age man preserved.* New York,: Cornell University Press.

Graf, K. E. and Buvit, I. (2017) Human dispersal from Siberia to Beringia: assessing a Beringian standstill in light of the archaeological evidence. *Current Anthropology* 58 (S17), S583-S603.

Graham, A. G., Stoker, M. S., Lonergan, L., Bradwell, T. and Stewart, M. A. (2011) The Pleistocene glaciations of the North Sea basin. *Developments in Quaternary Sciences.* Vol. 15. Elsevier. 261-278.

Groenendijk, H. A. (2015) Mesolithic hearth-pits in the Veenkoloniën (prov. Groningen, the Netherlands), defining a specific use of fire in the Mesolithic. *Palaeohistoria* 29, 85-102.

Groß, D., Lübke, H., Schmölcke, U. and Zanon, M. (2019) Early Mesolithic activities at ancient Lake Duvensee, northern Germany. *The Holocene* 29 (2), 197-208.

Grover, S. and Baldock, J. (2013) The link between peat hydrology and decomposition: Beyond von Post. 479, 130-138.

Gulli, A. and Pal, S. (2017) *Deep learning with Keras.* Packt Publishing Ltd.

Guo, Z., Berger, A., Yin, Q. and Qin, L. (2009) Strong asymmetry of hemispheric climates during MIS-13 inferred from correlating China loess and Antarctica ice records. *Clim Past* 5 (1), 21-31.

Gusick, A. E., Maloney, J., King, R. B. and Braje, T. J. (2019) Emerging Technologies in the Search for the Submerged Cultural Landscapes of the Pacific Continental Shelf. *Offshore Technology Conference.* Offshore Technology Conference.

Haber, E. and Ruthotto, L., (2017). Stable Architectures for Deep Neural Networks. *Inverse Problems, 34(1),* p.14004

Hagelund, R. and Stewart, L. (2017) SEG-Y revision 2.0 Data Exchange format. *Society of Exploration Geophysicists.* January 2017 (January 2017).

Hall, K. (2014) 14. Locating Potential Mesolithic Fish Sites in Britain using Predictive Modelling: Applying the 'fishing site model'to British conditions. *Wild Things: Recent advances in Palaeolithic and Mesolithic research*, 175.

Hamilton, E. L. (1970) Sound velocity and related properties of marine sediments, North Pacific. *Journal of Geophysical Research* 75 (23), 4423-4446.

Hansen, J., Petersen, H. C., Frei, K. M., Courtaud, P., Tillier, A.-m., Fischer, A. and Allentoft, M. E. (2017) The Maglemosian skeleton from Koelbjerg, Denmark revisited: identifying sex and provenance. *Danish Journal of Archaeology* 6 (1), 50-66.

Hansen, J., Sato, M., Hearty, P., Ruedy, R., Kelley, M., Masson-Delmotte, V., Russell, G., Tselioudis, G., Cao, J. and Rignot, E. (2016) Ice Melt, Sea Level Rise and Superstorms: Evidence from Paleoclimate Data, Climate Modeling, and Modern Observations that 2 {\deg} C Global Warming is Dangerous. *arXiv preprint arXiv:1602.01393*.

Harrison, S., Smith, D. E. and Glasser, N. F. (2019) Late Quaternary meltwater pulses and sea level change. *Journal of Quaternary Science* 34 (1), 1-15.

Hazell, Z. J. (2013) Offshore and intertidal peat deposits, England—a resource assessment and development of a database. *Environmental Archaeology*.

Hedges, R. E., Housley, R., Law, I. and Bronk, C. (1990) Radiocarbon dates from the Oxford AMS system: Archaeometry datelist 10. *Archaeometry* 32 (1), 101-108.

English Heritage. (1998) *Identifying and protecting Palaeolithic remains: Archaeological guidance for planning authorities and developers.* English Heritage.

Hublin, J.-J., Weston, D., Gunz, P., Richards, M., Roebroeks, W., Glimmerveen, J. and Anthonis, L. (2009) Out of the North Sea: the Zeeland Ridges Neandertal. *Journal of human evolution* 57 (6), 777-785.

Hunt, E. D. (1992) Upgrading site-catchment analyses with the use of GIS: Investigating the settlement patterns of horticulturalists. *World Archaeology* 24 (2), 283-309.

Innes, J. B. and Blackford, J. (2003) The ecology of late Mesolithic woodland disturbances: model testing with fungal spore assemblage data. *Journal of Archaeological Science* 30 (2), 185-194.

Innes, J. B., Blackford, J. J. and Simmons, I. G. (2011) Mesolithic environments at Star Carr, the eastern Vale of Pickering and environs: local and regional contexts. *Journal of Wetland Archaeology* 11 (1), 85-108.

Jacobi, R. (1976) Britain inside and outside Mesolithic Europe. *Proceedings of the Prehistoric Society*. Vol. 42. Cambridge University Press.

Jacobi, R. M., Tallis, J. H. and Mellars, P. A. (1976) The Southern Pennine Mesolithic and the ecological record. *Journal of Archaeological Science* 3 (4), 307-320.

Jelgersma, S. (1961) *Holocene sea level changes in the Netherlands.* Uitgevers-maatschappy" Ernest Van Aelst.

Jelgersma, S. (1979) Sea-level changes in the North Sea basin. *The Quaternary history of the North Sea. Symposia Universitatis Upsaliensis annum quingen-tesimum celebrantis.* Vol. 2. Almqvist och Wiksell.

Jelgersma, S. and Tooley, M. J. (1995) Sea-Level Changes During the Recent Geological Past. *Journal of Coastal Research*, 123-139.

JNAPC (1995) JNAPC code of practice for sea bed developers.

Jochim, M. A. (1976) *Hunter-gatherer subsistence and settlement: a predictive model.* Studies in Archaeology. London;New York. Academic Press - Book: Academic Press.

Johann, P., de Castro, D. D., Barroso, A. S. and SA, P. (2001) Reservoir geophysics: Seismic pattern recognition applied to ultra-deepwater oilfield in Campos basin, offshore Brazil. *SPE Latin America and Caribbean Petroleum Engineering Conference*.

Judd, A. G. (2004) Natural seabed gas seeps as sources of atmospheric methane. *Environmental Geology* 46 (8), 988-996.

Kearey, P., Brooks, M. and Hill, I. (2013) *An introduction to geophysical exploration.* John Wiley & Sons.

Kelley, J.T., Cooper, A., Plets R. and Belknap, D.F., (2018). Measuring the Most Complicated Post-Glacial sea-level Changes in the World: Northern Ireland.

Kent, P. (1967) Outline geology of the southern North Sea Basin. *Proceedings of the Yorkshire Geological Society* 36 (1), 1-22.

Keys, D. (2019) Britain's Atlantis: Evidence of Stone Age Human activitiy found beneath North Sea. *Independent*, Tuesday 11th June 2019, *https://www.academia.edu/39610914/The_first_archaeological_artefacts_found_during_the_search_for_lost_prehistoric_settlements_in_the_North_Sea*

Kinsler, L. E., Frey, A. R., Coppens, A. B. and Sanders, J. V. (1999) Fundamentals of acoustics. *Fundamentals of Acoustics, 4th Edition, by Lawrence E. Kinsler, Austin R. Frey, Alan B. Coppens, James V. Sanders, pp. 560. ISBN 0-471-84789-5. Wiley-VCH, December 1999.*, 560.

Kistler, L., Ware, R., Smith, O., Collins, M. and Allaby, R. G. J. N. a. r. (2017) A new model for ancient DNA decay based on paleogenomic meta-analysis. 45 (11), 6310-6320.

Kivinen, E. (1980) Proposal for a general classification of virgin peat. *Proceedings of the 6th International Peat Congress, Duluth, Minnesota, USA. International Peat Society, Duluth, USA*.

Klavins, M., Sire, J., Purmalis, O. and Melecis, V. (2008) Approaches to estimating humification indicators for peat. *Mires & Peat* 3.

Kohler, T. A. and Parker, S. C. (1986) Predictive models for archaeological resource location. *Advances in Archaeological Method and Theory, Volume* 9. Elsevier. 397-452.

Kohonen, T. J. N. n. (2006) Self-organizing neural projections. 19 (6-7), 723-733.

Kontorovich, V. A., Surikova, E. S. and Ayunova, D. V. (2019) Seismogeological criteria for the gas potential of Aptian–Cenomanian sediments in the north of West Siberia (by the example of the Yubileinoe field). *Russian Geology and Geophysics* 60 (5), 570-582.

Kortekaas, S., Sens, E. and Sarata, B. (2010) Shallow gas hazard linked to worldwide delta environments. *Frontiers in offshore geotechnics II*, 221-225.

Kreuzburg, M., Ibenthal, M., Janssen, M., Rehder, G., Voss, M., Naumann, M. and Feldens, P. (2018) Sub-marine continuation of peat deposits from a coastal peatland in the southern baltic sea and its holocene development. *Frontiers in Earth Science* 6, 103.

Kristiansen, I. L., Mangerud, J. and LOMO, L. (1988) Late Weichselian / Early Holocene Pollen and Lithostratigraphy in Lacks in the Aitsurud Area, Western Norway.

Krüger, S., Dörfler, W., Bennike, O. and Wolters, S. (2017) Life in Doggerland–palynological investigations of the environment of prehistoric hunter-gatherer societies in the North Sea Basin. *E & G Quaternary Science Journal* 66 (1), 3-13.

Kuiper, J. A. and Wescott, K. L. (1999) A GIS Approach for Predicting Prehistoric Site Locations. *Nineteenth Annual ESRI User Conference, San Diego, California, USA, July*.

Lambeck, K. and Chappell, J. (2001) Sea level change through the last glacial cycle. *Science* 292 (5517), 679-686.

Lamotte, K. R. (2002) UNESCO: Convention on the Protection of the Underwater Cultural Heritage. *International Legal Materials* 41 (1), 37-56.

Larsson, L. (2013) Tooth-beads, antlers, nuts and fishes. Examples of social bioarchaeology. *Archaeological Dialogues* 20 (2), 148.

Laws, A. W., Maloney, J. M., Klotsko, S., Gusick, A. E., Braje, T. J. and Ball, D. J. Q. R. (2020) Submerged paleoshoreline mapping using high-resolution Chirp sub-bottom data, Northern Channel Islands platform, California, USA. 93 (1), 1-22.

Leary, J. (2014) *Past mobilities: Archaeological approaches to movement and mobility*. Ashgate Publishing, Ltd.

Leary, J. (2009) Perceptions of and responses to the Holocene flooding of the North Sea lowlands. *Journal of Archaeology* 28 (3), 227-237.

Lecours, V., Dolan, M. F., Micallef, A. and Lucieer, V. L. (2016) A review of marine geomorphometry, the quantitative study of the seafloor. *Hydrology and Earth System Sciences* 20 (8), 3207.

Lewis, J., Ryves, D., Rasmussen, P., Olsen, J., Knudsen, K.-L., Andersen, S., Weckström, K., Clarke, A., Andrén, E. and Juggins, S. (2016) The shellfish enigma across the Mesolithic-Neolithic transition in southern Scandinavia. *Quaternary Science Reviews* 151, 315-320.

Lewis, L. F. (1967) *Speed of sound in unconsolidated sediments of Boston Harbor, Massachusetts*. Massachusetts Institute of Technology.

Li, G., Li, P., Liu, Y., Qiao, L., Ma, Y., Xu, J. and Yang, Z. (2014) Sedimentary system response to the global sea level change in the East China Seas since the last glacial maximum. *Earth-Science Reviews* 139, 390-405.

Li, X., Zhao, Y., Feng, Z., Liu, C., Xie, Q. and Zhou, Q. (2016) Quaternary seismic facies of the South Yellow Sea shelf: depositional processes influenced by sea-level change and tectonic controls. *Geological Journal* 51, 77-95.

Li, Z., Zhu, C. and Gold, C. (2004) *Digital terrain modeling: principles and methodology*. CRC press.

Lisiecki, L. E. and Raymo, M. E. (2005) A Pliocene-Pleistocene stack of 57 globally distributed benthic δ18O records. *Paleoceanography* 20 (1).

Long, D., Wickham-Jones, C. R. and Ruckley, N. (1986) A Flint Artefact from the Northern North Sea in Studies in the Upper Palaeolithic of Britain and Northwest Europe. *BAR. International Series* (296), 55-62.

López-Dóriga, I. L. (2015) An experimental approach to the taphonomic study of charred hazelnut remains in archaeological deposits. *Archaeological and Anthropological Sciences* 7 (1), 39-45.

Louwe Kooijmans, L. (1970) Mesolithic Bone and Antler Implements from the North Sea and from the Netherlands.

Lowry, C. S., Fratta, D. and Anderson, M. P. (2009) Ground penetrating radar and spring formation in a groundwater dominated peat wetland. *Journal of Hydrology* 373 (1-2), 68-79.

Luo, W., Li, Y., Urtasun, R. and Zemel, R. (2016) Understanding the effective receptive field in deep convolutional neural networks. *Advances in neural information processing systems.*

Lurton, X. (2002) *An introduction to underwater acoustics: principles and applications.* Springer Science & Business Media.

Maarleveld, T. J. (2020) Beam Trawls and Bones: A Reflection on Dutch Fisheries. *The Archaeology of Europe's Drowned Landscapes.* Springer. 521-535.

Malim, T., Morgan, D. and Panter, I. (2015) Suspended preservation: particular preservation conditions within the Must Farm–Flag Fen Bronze Age landscape. *Quaternary International* 368, 19-30.

Marchand, G., Dupont, C., Laforge, M., Le Bannier, J.-C., Netter, C., Nukushina, D., Onfray, M., Querré, G., Quesnel, L. and Stéphan, P. (2018) Before the spatial analysis of Beg-er-Vil: A journey through the multiple archaeological dimensions of a Mesolithic dwelling in Atlantic France. *Journal of Archaeological Science: Reports* 18, 973-983.

Martin J Head, I. U. o. G. S. I. (2018) IUGS ratifies Holocene subdivision. *Minutes of ICS Meeting 14th June 2018*.

Matero, I., Gregoire, L., Ivanovic, R., Tindall, J. and Haywood, A. (2017) The 8.2 ka cooling event caused by Laurentide ice saddle collapse. *Earth and Planetary Science Letters* 473, 205-214.

Matte, P. (2001) The Variscan collage and orogeny (480–290 Ma) and the tectonic definition of the Armorica microplate: a review. *Terra Nova* 13 (2), 122-128.

Mazur, S., Porębski, S. J., Kędzior, A., Paszkowski, M., Podhalańska, T. and Poprawa, P. (2018) Refined timing and kinematics for Baltica–Avalonia convergence based on the sedimentary record of a foreland basin. *Terra Nova* 30 (1), 8-16.

Meese, D., Gow, A., Alley, R., Zielinski, G., Grootes, P., Ram, M., Taylor, K., Mayewski, P. A. and Bolzan, J. (1997) The Greenland Ice Sheet Project 2 depth-age scale: Methods and results. *Journal of Geophysical Research: Oceans* 102 (C12), 26411-26423.

Megaw, J. V. S. (2007) L.P. Louwe Kooijmans, P.W. van den Broeke, H. Fokkens & A.L. van Gijn (ed.). The Prehistory of the Netherlands. 2 volumes, 844 pages, 501 illustrations, 48 colour plates, 12 tables. 2005. Amsterdam: Amsterdam University Press; 90-5356-160-9 (both volumes) hardback €89.50. *Antiquity* 81 (311), 230-231.

Miller, K. G., Kominz, M. A., Browning, J. V., Wright, J. D., Mountain, G. S., Katz, M. E., Sugarman, P. J., Cramer, B. S., Christie-Blick, N. and Pekar, S. F. (2005) The Phanerozoic record of global sea-level change. *science* 310 (5752), 1293-1298.

Milne, G. A., Gehrels, W. R., Hughes, C. W. and Tamisiea, M. E. (2009) Identifying the causes of sea-level change. *Nature Geoscience* 2 (7), 471-478.

Milner, N., Conneller, C. and Taylor, B. (2018) Star Carr Volume 2.
Missiaen, T., Evangelinos, D., Claerhout, C., De Clercq, M., Pieters, M. and Demerre, I. (2018) Archaeological prospection of the nearshore and intertidal area using ultra-high resolution marine acoustic techniques: Results from a test study on the Belgian coast at Ostend-Raversijde. *Geoarchaeology* 33 (3), 386-400.
Missiaen, T. and Feller, P. J. J. o. a. g. (2008) Very-high-resolution seismic and magnetic investigations of a chemical munition dumpsite in the Baltic Sea. 65 (3-4), 142-154.
Missiaen, T., Fitch, S., Muru, M., Harding, R., Fraser, A., De Clercq, M., Moreno, D. G., Versteeg, W. and Gaffney, V. (2020) Targeting the mesolithic: Interdisciplinary approaches to archaeological prospection in the Brown Bank area, southern North Sea. *Quaternary International*.
Missiaen, T., Slob, E. and Donselaar, M. J. N. J. o. G. (2008) Comparing different shallow geophysical methods in a tidal estuary, Verdronken Land van Saeftinge, Western Scheldt, the Netherlands. 87 (2), 151-164.
Mithen, S. J. (2003) *After the ice: a global human history 20,000-5000 BC*. London: Weidenfeld & Nicolson.
Mol, D., Post, K., Reumer, J. W., de Vos, J. and Laban, C. (2003) Het Gat: preliminary note on a Bavelian fauna from the North Sea with possibly two mammoth species. *Advances in Mammoth Research. Deinsea* 9, 253-266.
Momber, G. (2000) Drowned and deserted: a submerged prehistoric landscape in the Solent, England. *The International journal of nautical archaeology* 29 (1), 86-99.
Morgan, E. C., Vanneste, M., Lecomte, I., Baise, L. G., Longva, O. and McAdoo, B. J. G. (2012) Estimation of free gas saturation from seismic reflection surveys by the genetic algorithm inversion of a P-wave attenuation model. 77 (4), R175-R187.
Mörner, N.-A. (1980) The northwest European "sea-level laboratory" and regional Holocene eustasy. *Palaeogeography, Palaeoclimatology, Palaeoecology* 29, 281-300.
Morozov, I. B. (2008a) Geometrical attenuation, frequency dependence of Q, and the absorption band problem. *Geophysical Journal International* 175 (1), 239-252.
Morozov, I. B. J. G. J. I. (2008b) Geometrical attenuation, frequency dependence of Q, and the absorption band problem. 175 (1), 239-252.
Morrison, A. (1980) *Early man in Britain and Ireland: an introduction to Palaeolithic and Mesolithic cultures*. Taylor & Francis.
Mosser, L., Dubrule, O. and Blunt, M. (2018) Stochastic seismic waveform inversion using generative adversarial networks as a geological prior. *First EAGE/PESGB Workshop Machine Learning*.
Müller, S., Reinhardt, L., Franke, D., Gaedicke, C. and Winsemann, J. (2018) Shallow gas accumulations in the German North Sea. *Marine and Petroleum Geology* 91, 139-151.

Nafe, J. E. and Drake, C. L. (1961) *Physical properties of marine sediments*. Lamont Geological Observatory Palisadesny.

Nielsen, M. A. (2015) *Neural networks and deep learning*. Determination Press.

Okabe, A. (2016) Spatial tessellations. *International Encyclopedia of Geography: People, the Earth, Environment and Technology: People, the Earth, Environment and Technology*, 1-11.

Ouenes, A. J. C. R. (2012) Seismically driven characterization of unconventional shale plays. 37, 22-28.

Paramor, O., Allen, K., Aanesen, M., Armstrong, C., Piet, G., Hal, R. v., van Hoof, L. and van Overzee, H. (2009) MEFEPO North Sea Atlas, 2nd Edition.

Parfitt, S. A., Ashton, N. M., Lewis, S. G., Abel, R. L., Coope, G. R., Field, M. H., Gale, R., Hoare, P. G., Larkin, N. R. and Lewis, M. D. (2010) Early Pleistocene human occupation at the edge of the boreal zone in northwest Europe. *Nature* 466 (7303), 229.

Parfitt, S. A., Barendregt, R. W., Breda, M., Candy, I., Collins, M. J., Coope, G. R., Durbidge, P., Field, M. H., Lee, J. R. and Lister, A. M. (2005) The earliest record of human activity in northern Europe. *Nature* 438 (7070), 1008-1012.

Parkes, G. and Hatton, L. (2013) *The marine seismic source*. Vol. 4. Springer Science & Business Media.

PAUS, A. (1988) Late Weichselian vegetation, climate, and floral migration at Sandvikvatn, North Rogaland, southwestern Norway. 17 (1), 113-139.

Peeters, J. and Momber, G. (2014) The southern North Sea and the human occupation of northwest Europe after the Last Glacial Maximum. *Netherlands Journal of Geosciences-Geologie en Mijnbouw* 93 (1-2), 55-70.

Peeters, J. H. M. (2007) Hoge Vaart-A27 in context: towards a model of Mesolithic-Neolithic land use dynamics as a framework for archaeological heritage management.

Peeters, J. H. M., Amkreutz, L. W. S. W., Cohen, K. M. and Hijma, M. (2019) *North Sea Prehistory Research and Management Framework (NSPRMF) 2019: Retuning the research and management agenda for prehistoric landscapes and archaeology in the Dutch sector of the continental shelf*. Vol. 63. Rijksdienst voor het Cultureel Erfgoed.

Peltier, W. R. (2004) GLOBAL GLACIAL ISOSTASY AND THE SURFACE OF THE ICE-AGE EARTH: The ICE-5G (VM2) Model and GRACE. *Annual Review of Earth and Planetary Sciences* 32 (1), 111-149.

Peters, B., Granek, J. and Haber, E. (2019) Multi-resolution neural networks for tracking seismic horizons from few training images. 7 (3), 1-54.

Petit, J.-R., Jouzel, J., Raynaud, D., Barkov, N. I., Barnola, J.-M., Basile, I., Bender, M., Chappellaz, J., Davis, M. and Delaygue, G. (1999) Climate and atmospheric history of the past 420,000 years from the Vostok ice core, Antarctica. *Nature* 399 (6735), 429.

Philippsen, B. and Meadows, J. (2014) Inland Ertebølle Culture: the importance of aquatic resources and the freshwater reservoir

effect in radiocarbon dates from pottery food crusts. *Internet Archaeology* 37, 573-600.
Pielou, E. C. (1974) *Population and community ecology: principles and methods.* CRC Press.
Pinson, L. J. W. (2008) Estimating quality factor and mean grain size of sediments from high-resolution marine seismic data. *GEOPHYSICS* 73 (4), G19-G28.
Pinson, L. J. W. (2010) *Derivation of Acoustic and Physical Properties from High Resolution Seismic Reflection Data*. PhD.
Plets, R., Dix, J., Bastos, A. and Best, A. (2007) Characterization of buried inundated peat on seismic (Chirp) data, inferred from core information. *Archaeological Prospection* 14 (4), 261-272.
PM Office, G. B. (2020) New Plans to make UK World Leader in Green Energy.
Post, K. and Reumer, J. W. (2016) History and future of paleontological surveys in the Westerschelde Estuary (Province of Zeeland, the Netherlands). *Deinsea* 16, 1-9.
Price, T. D. and Brown, J. A. (1985) Aspects of hunter–gatherer complexity. *Prehistoric Hunters-Gatherers.* Elsevier. 3-20.
Rasmussen, E. S., Dybkjær, K. and Piasecki, S. (2010) Lithostratigraphy of the upper Oligocene–Miocene succession of Denmark. *Geological Survey of Denmark and Greenland Bulletin* 22, 92.
Rasmussen, S. O., Bigler, M., Blockley, S. P., Blunier, T., Buchardt, S. L., Clausen, H. B., Cvijanovic, I., Dahl-Jensen, D., Johnsen, S. J. and Fischer, H. (2014) A stratigraphic framework for abrupt climatic changes during the Last Glacial period based on three synchronized Greenland ice-core records: refining and extending the INTIMATE event stratigraphy. *Quaternary Science Reviews* 106, 14-28.
Raynaud, D., Loutre, M., Ritz, C., Chappellaz, J., Barnola, J.-M., Jouzel, J., Lipenkov, V., Petit, J.-R. and Vimeux, F. (2003) Marine Isotope Stage (MIS) 11 in the Vostok ice core: CO2 forcing and stability of East Antarctica. *Washington DC American Geophysical Union Geophysical Monograph Series* 137, 27-40.
Reid, C. (1913) *Submerged forests.* Cambridge University Press.
Renfro, B. A., Stein, M., Boeker, N. and Terry, A. (2018) An analysis of global positioning system (GPS) standard positioning service (SPS) performance for 2017. *See https://www. gps. gov/systems/gps/performance/2014-GPS-SPS-performance-analysis. pdf*.
Reynier, M. (2005) *Early Mesolithic Britain: origins, development and directions.* Vol. 393. Oxford: Archaeopress.
Richards, M. P. and Schulting, R. J. (2006) Touch not the fish: the Mesolithic-Neolithic change of diet and its significance. *Antiquity* 80 (308), 444-456.
Rijsdijk, K. F., Passchier, S., Weerts, H., Laban, C., Van Leeuwen, R. and Ebbing, J. (2005) Revised Upper Cenozoic stratigraphy of the Dutch sector of the North Sea Basin: towards an integrated

lithostratigraphic, seismostratigraphic and allostratigraphic approach. *Netherlands Journal of Geosciences* 84 (2), 129-146.
Roberts, D. H., Grimoldi, E., Callard, L., Evans, D. J., Clark, C. D., Stewart, H. A., Dove, D., Saher, M., Ó Cofaigh, C. and Chiverrell, R. C. (2019) The mixed-bed glacial landform imprint of the North Sea Lobe in the western North Sea. *Earth Surface Processes and Landforms* 44 (6), 1233-1258.
Robson, H. K., Little, A., Jones, A. K. G., Blockley, S., Candy, I., Matthews, I., Palmer, A., Schreve, D., Tong, E. and Pomstra, D. (2018) Scales of analysis: Evidence of fish and fish processing at Star Carr. *Journal of Archaeological Science: Reports* 17, 895-903.
Schalkoff, R. J. (2007) Pattern recognition.
Schlitzer, R. (1989) Modeling the nutrient and carbon cycles of the North Atlantic: 2. New production, particle fluxes, CO2 gas exchange, and the role of organic nutrients. *Journal of Geophysical Research: Oceans* 94 (C9), 12781-12794.
Schmidhuber, J. (2015) Deep learning in neural networks: An overview. *Neural networks* 61, 85-117.
Schock, S. G. (2004) A method for estimating the physical and acoustic properties of the sea bed using chirp sonar data. *IEEE Journal of Oceanic Engineering* 29 (4), 1200-1217.
Schoeninger, M. J. and DeNiro, M. J. (1984) Nitrogen and carbon isotopic composition of bone collagen from marine and terrestrial animals. 48 (4), 625-639.
Schroot, B. M., Klaver, G. T. and Schüttenhelm, R. T. (2005) Surface and subsurface expressions of gas seepage to the seabed—examples from the Southern North Sea. *Marine and Petroleum Geology* 22 (4), 499-515.
Sebastian, L. and Judge, W. (1988) *Quantifying the present and predicting the past: theory, method, and application of archaeological predictive modeling.* US Department of the Interior, Bureau of Land Management.
Shennan, I. and Andrews, J. (2000) An introduction to Holocene land-ocean interaction and environmental change around the western North Sea. *Geological Society, London, Special Publications* 166 (1), 1-7.
Shennan, I. and Coulthard, T. F. R., Horton, B., Macklin, M., Rees J. and Wright M. 2003. Integration of shelf evolution and river basin models to simulate Holocene sediment dynamics of the Humber Estuary during periods of sea-level change and variations in catchment sediment supply. *Science of the Total Environment* 314 (316), 737-754.
Shennan, I., Lambeck, K., Flather, R., Horton, B., McArthur, J., Innes, J., Lloyd, J., Rutherford, M. and Wingfield, R. (2000) Modelling western North Sea palaeogeographies and tidal changes during the Holocene. *Geological Society, London, Special Publications* 166 (1), 299-319.

Shennan, I., Long, A. J. and Horton, B. P. (2015) *Handbook of sea-level research.* John Wiley & Sons.

Sheriff, R. E. (2012) *Seismic stratigraphy.* Springer Science & Business Media.

Sier, M., Cohen, K., Kooistra, L., Kubiak-Martens, L., Moree, J., Niekus, M., Peeters, J., Schiltmans, D., Verbaas, A. and Verbruggen, F. (2014) Twenty metres deep! The Mesolithic period at the site Yangtze Harbour in the Rotterdam Maasvlakte, the Netherlands. Early Holocene landscape development and habitation.

Slater, L. and Reeve, A. (2002) Understanding peatland hydrology and stratigraphy using integrated electrical geophysics. *Geophysics* 67 (2), 365-378.

Smith, D., Firth, C., Turbayne, S. and Brooks, C. (1992) Holocene relative sea-level changes and shoreline displacement in the Dornoch Firth area, Scotland. *Proceedings of the Geologists' Association* 103, 237-257.

Smith, O., Momber, G., Bates, R., Garwood, P., Fitch, S., Pallen, M., Gaffney, V. and Allaby, R. G. (2015) Sedimentary DNA from a submerged site reveals wheat in the British Isles 8000 years ago. *Science* 347 (6225), 998-1001.

Smith, S. (2013) *Digital signal processing: a practical guide for engineers and scientists.* Elsevier.

Sørensen, M. (2003) Rethinking the lithic blade definition: towards a dynamic understanding. *Skilled production and social reproduction*, 277.

Stevens, T., Jestico, M. J., Evans, G. and Kirkham, A. (2014) Eustatic control of late Quaternary sea-level change in the Arabian/Persian Gulf. *Quaternary Research* 82 (1), 175-184.

Stoker, M., Balson, P., Long, D. and Tappin, D. (2011) An overview of the lithostratigraphical framework for the Quaternary deposits on the United Kingdom continental shelf.

Sturt, F., Garrow, D. and Bradley, S. (2013) New models of North West European Holocene palaeogeography and inundation. *Journal of Archaeological Science* 40 (11), 3963-3976.

Systems, J. (2020) *GNSS (GPS) ACCURACY EXPLAINED.* [Web Page] April 2020. Online: *https://junipersys.com/support/article/6614#:~:text=Most%20receiver%20manufacturers%20do%20not,of%20the%20stated%20horizontal%20accuracy* Accessed 13/08/2020.

Tappin, D., Pearce, B., Fitch, S., Dove, D., Gearey, B., Hill, J., Chambers, C., Bates, R., Pinnion, J. and Diaz Doce, D. (2011) *The Humber regional environmental characterisation.* Marine Aggregate Levy Sustainability Fund.

Taylor, J. (1990) Upper Permian—Zechstein. *Petroleum Geology of the North Sea: Basic Concepts and Recent Advances, Fourth Edition*, 174-211.

Thal, J., Socko, L., Feldmann, S. and Brock, J. P. (2018) *Geological Desk Study for the Hollandse Kust (west) Wind Farm Zone.* RVO.NL.

Thomson, K. (2004) Overburden deformation associated with halokinesis in the Southern North Sea: implications for the origin of the Silverpit Crater. *Visual Geosciences* 9 (1), 39-47.

Tizzard, L., Baggaley, P. and Firth, A. (2011) Seabed Prehistory: investigating palaeolandsurfaces with Palaeolithic remains from the southern North Sea. *Submerged prehistory*, 65-74.

Tizzard, L., Bicket, A., Benjamin, J. and Loecker, D. D. (2014) A Middle Palaeolithic site in the southern North Sea: investigating the archaeology and palaeogeography of Area 240. 29 (7), 698-710.

Tolan-Smith, C. (2008) Mesolithic Britain. *Mesolithic Europe*, 132-157.

Törnqvist, T. E. and Hijma, M. P. (2012) Links between early Holocene ice-sheet decay, sea-level rise and abrupt climate change. *Nature Geoscience* 5 (9), 601-606.

Trizio, I., Savini, F. and Giannangeli, A. (2018) Integration of 3D Digital Models and 3D GIS: The Documentation of the Medieval Burials of Amiternum (L'Aquila, Italy). *International Archives of the Photogrammetry, Remote Sensing & Spatial Information Sciences* 42 (2).

Troels-Smith, J. (1955) Karakterisering af lose jordarter. Characterization of unconsolidated sediments.

Turney, C. S. M. and Brown, H. (2007) Catastrophic early Holocene sea level rise, human migration and the Neolithic transition in Europe. *Quaternary Science Reviews* 26 (17-18), 2036-2041.

Underhill, J. R. (2009) Role of intrusion-induced salt mobility in controlling the formation of the enigmatic 'Silverpit Crater', UK Southern North Sea. *Petroleum Geoscience* 15 (3), 197-216.

UNESCO (2020) *UNESCO NPL Tech Guide Acoustic Speed of Sound Equations.* Online: UNESCO NPL. *http://resource.npl.co.uk/acoustics/techguides/soundseawater/content.html* Accessed 28/05/2020.

Van de Noort, R. (2011) North Sea Archaeologies.

Van der Baan, M. and Jutten, C. J. G. (2000) Neural networks in geophysical applications. 65 (4), 1032-1047.

Van Heteren, S., Meekes, J., Bakker, M., Gaffney, V., Fitch, S., Gearey, B. and Paap, B. (2014a) Reconstructing North Sea palaeolandscapes from 3D and high-density 2D seismic data: An overview. *Netherlands Journal of Geosciences-Geologie en Mijnbouw* 93 (1-2), 31-42.

van Heteren, S., Meekes, J. A. C., Bakker, M. A. J., Gaffney, V., Fitch, S., Gearey, B. R. and Paap, B. F. (2014b) Reconstructing North Sea palaeolandscapes from 3D and high-density 2D seismic data: An overview. *Netherlands Journal of Geosciences - Geologie en Mijnbouw* 93 (1-2), 31-42.

Van Lancker, V., Du Four, I., Mathys, M., Versteeg, W. and De Batist, M. (2009) Towards a high-resolution 3D-analysis of sand-bank architecture on the Belgian Continental Shelf (RESOURCE-3D).

Veenstra, H. J. (1965) Geology of the Dogger bank area, North Sea. *Marine Geology* 3 (4), 245-262.

Verhagen, P., Rensink, E., Bats, M. and Crombé, P. (2013) Establishing discovery probabilities of lithic artefacts in Palaeolithic and Mesolithic sites with core sampling. *Journal of Archaeological Science* 40 (1), 240-247.

Verhagen, P. and Whitley, T. G. J. J. o. A. M. a. T. (2012) Integrating archaeological theory and predictive modeling: a live report from the scene. 19 (1), 49-100.

Verhegge, J., Missiaen, T. and Crombé, P. (2016) Exploring integrated geophysics and geotechnics as a paleolandscape reconstruction tool: Archaeological prospection of (prehistoric) sites buried deeply below the Scheldt Polders (NW Belgium). *Archaeological Prospection* 23 (2), 125-145.

Vink, A., Steffen, H., Reinhardt, L. and Kaufmann, G. (2007) Holocene relative sea-level change, isostatic subsidence and the radial viscosity structure of the mantle of northwest Europe (Belgium, the Netherlands, Germany, southern North Sea). *Quaternary Science Reviews* 26 (25), 3249-3275.

Vos, P. C., Bunnik, F. P., Cohen, K. M. and Cremer, H. (2015) A staged geogenetic approach to underwater archaeological prospection in the Port of Rotterdam (Yangtzehaven, Maasvlakte, The Netherlands): A geological and palaeoenvironmental case study for local mapping of Mesolithic lowland landscapes. *Quaternary International* 367, 4-31.

Waddington, C. (2007) *Mesolithic Settlement in the North Sea Basin: a case study from Howick, north-east England.* Oxbow Books.

Waddington, C. and Pedersen, K. (2007) *Mesolithic studies in the North Sea Basin and beyond: proceedings of a conference held at Newcastle in 2003.* Oxbow Books Limited.

Waddington, C. and Wicks, K. (2017) Resilience or wipe out? Evaluating the convergent impacts of the 8.2 ka event and Storegga tsunami on the Mesolithic of northeast Britain. *Journal of Archaeological Science: Reports* 14, 692-714.

Wal, W. v. d. and IJpelaar, T. (2017) The effect of sediment loading in Fennoscandia and the Barents Sea during the last glacial cycle on glacial isostatic adjustment observations. *Solid Earth* 8 (5), 955-968.

Walker, J., Gaffney, V., Fitch, S., Muru, M., Fraser, A., Bates, M. R. and Bates, C. R. (2020) A Great Wave: The Storegga Tsunami and the end of Doggerland. *Antiquity* (In Review).

Wang, Y. (2016) Generalized viscoelastic wave equation. *Geophysical Journal International* 204 (2), 1216-1221.

Ward, I., Larcombe, P. and Lillie, M. (2006) The dating of Doggerland–post-glacial geochronology of the southern North Sea. *Environmental Archaeology* 11 (2), 207-218.

Wechsler, H., Phillips, J. P., Bruce, V., Soulie, F. F. and Huang, T. S. (2012) *Face recognition: From theory to applications.* Vol. 163. Springer Science & Business Media.

Wenban-Smith, F. (2002) Palaeolithic and Mesolithic Archaeology on the Sea-bed.

Weninger, B., Schulting, R., Bradtmöller, M., Clare, L., Collard, M., Edinborough, K. and Hilpert, J. (2008) The catastrophic final flooding of Doggerland by the Storegga Slide tsunami. *Documenta Praehistorica* 35, 1-24.

Wentworth, C. K. (1922) A scale of grade and class terms for clastic sediments. *The journal of geology* 30 (5), 377-392.

Wheatley, D. and Gillings, M. (2013) *Spatial technology and archaeology: the archaeological applications of GIS.* CRC Press.

Wheeler, M. (1954) *Archaeology from the Earth.* Vol. 356. Oxford University Press.

White, R. (1992) The accuracy of estimating Q from seismic data. *Geophysics* 57 (11), 1508-1511.

Whitehouse, P. L. (2018) Glacial isostatic adjustment modelling: historical perspectives, recent advances, and future directions. *Earth surface dynamics.* 6 (2), 401-429.

Whitewright, J. (2015) Heritage Partnership Agreements for Undesignated (Marine) Sites: A Pilot.

Willey, G.R. (1953). Prehistoric Settlement Patterns in the Virú Valley, Peru. *Bureau of American Ethnology Bulletin*

Wiltshire, P. E. and Edwards, K. J. (1993) Mesolithic, early Neolithic, and later prehistoric impacts on vegetation at a riverine site in Derbyshire, England. *Climate change and human impact on the landscape.* Springer. 157-168.

Wong, G. S. and Zhu, S. m. J. t. J. o. t. A. S. o. A. (1995) Speed of sound in seawater as a function of salinity, temperature, and pressure. 97 (3), 1732-1736.

Wrona, T., Pan, I., Gawthorpe, R. L. and Fossen, H. (2018) Seismic facies analysis using machine learning. 83 (5), O83-O95.

Wunderlich, J. and Muller, S. (2003) High-resolution sub-bottom profiling using parametric acoustics. *International Ocean Systems* 7 (4), 6-11.

Wymer, J. and King, J. E. (1962) Excavations at the Maglemosian sites at Thatcham, Berkshire, England. *Proceedings of the Prehistoric Society.* Vol. 28. Cambridge University Press.

Xia, J. (2014) Estimation of near-surface shear-wave velocities and quality factors using multichannel analysis of surface-wave methods. 103, 140-151.

Zaccone, C., Sanei, H., Outridge, P. and Miano, T. (2011) Studying the humification degree and evolution of peat down a Holocene bog profile (Inuvik, NW Canada): a petrological and chemical perspective. *Organic Geochemistry* 42 (4), 399-408.

Zhao, T., Jayaram, V., Roy, A. and Marfurt, K. J. (2015) A comparison of classification techniques for seismic facies recognition. *Interpretation* 3 (4), SAE29-SAE58.

Zorn, J. R. (1994) Estimating the Population Size of Ancient Settlements: Methods, Problems, Solutions, and a Case Study. *Bulletin of the American Schools of Oriental Research* (295), 31-48.

Zurita Hurtado, O. J. (2014) Comparative seismic source study for buried palaeolandscape investigations in the Southern North Sea. *1st Applied Shallow Marine Geophysics Conference, Part of Near Surface Geoscience 2014*.

12.1 Websites Referenced:

ALEXANDER, L. M. 2020. *The North Sea* [Online]. Available: https://www.britannica.com/place/North-Sea [Accessed 09/04 2020].

BELLIS, K: *Untitled UTC Map image*. Creative Commons Wikimedia. [Accessed 18/09/2020]

BENIAGUEV, D., 2017. The Selfish Gene Project: Neuron as Deep Net. *Github Python Network* [Accessed 23/06/2020] https://github.com/SelfishGene?tab=repositories

SYSTEMS, J. 2020. *GNSS (GPS) ACCURACY EXPLAINED* [Online]. Online. [Accessed 13/08/2020 2020]. https://junipersys.com/support/article/6614#:~:text=Most%20receiver%20manufacturers%20do%20not,of%20the%20stated%20horizontal%20accuracy

SPLASHCOS Viewer – COST Action TD0902 Initiative online archaeological database. [Accessed site on multiple occassions 2017 – 21]. http://splashcos.maris2.nl/

UNESCO npl acoustic speed in water. [Accessed multiple occassions 2017 – 2021]

http://resource.npl.co.uk/acoustics/techguides/soundseawater/content.html

R Schlitzer 1989. Ocean Water Density Calculator. [Accessed multiple occassions 2017 – 2021]

http://www.csgnetwork.com/water_density_calculator.html

based on

Millero, F, C. Chen, A Bradshaw, and K. Schleicher, 1980: *A new high pressure equation of state for seawater*, Deep Sea Research, Part A, 27, 255-264.

13 Appendices

13.1 APPENDIX 1 – SEDIMENT CLASSIFICATION SYSTEMS

FOLK and Troels-Smith Classification of sediment as used within lithological core modelling research.

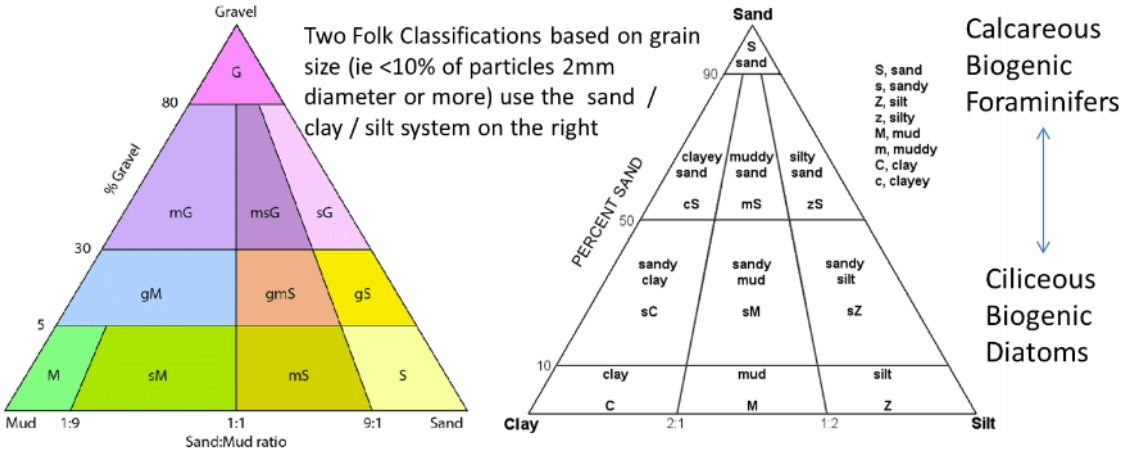

Figure 13.1 Classification by sediment class (derived from Folk - left, 1954 and Troels-Smith – right, 1955)

To the Folk Model of Sedimental Classification (Folk 1954), Troels-Smith (Troels-Smith 1955) added additional factors for organic sediments to be included in lithological descriptions for northern temperate lakes, covering 3 elements:

- Composition; these were recognised as turfa – pieces of wood still attached to the tree (Troels-Smith 1955; Kristiansen et al. 1988; Törnqvist and Hijma 2012); *detritus* – plant fragments not attached to the plant such as leaves, bark, seeds (*granosus*), fungus (*lignosus*), grasses (*herbosus*) designated with a D(Dg, Dl, Dh etc.); *limus* – like a gyffa, a non conformable, organic mud (L) consisting of small particles of *detritus* (LD) or entirely of '*substantia humosa*' (Sh); *argilla* – minerogenic sediments either of silts (Ag) with grain sizes of 0.06 – 0.02mm or clays (As) with grain sizes of <0.02mm; finally there is *grana* which comprises large, macroscopic particles – sands and gravels (gMin and gMaj) that do not roll when wet and crumble when dry.
- Degree of Humification; this is based on a 5-point scale of decomposition of observable macrofossils and uses the Von Post criteria as discussed in Chapter 5.

- Physical properties; the properties that should be included are degree of darkness on a scale of nig.4 (black) to nig. 0 (Whitewright 2015); degree of dryness on a scale of sicc.4 (very dry) to sicc. 0 (water); degree of elasticity on a scale of elas.4 (very elastic) to elas. 0 (non-elastic) and degree of stratification on a scale of strf.4 (well stratified) to strf. 0 (no stratification)

In this research, the lithological unit classifications use both Folk and Troels-Smith terminology, however they do not use the complete classification systems of either suite.

13.2 APPENDIX 2 – VELOCITY MODEL COMPUTATIONS

See ATTACHED SPREADSHEET – Velocity Model Calculations.xls

13.3 APPENDIX 3 – PYTHON SCRIPT FOR KERAS IMAGE RECOGNITION

The Neural Networking Appendices comes in two separate sections. Section 1 is the actual code created for learning Python 3 image recognition. Though this never advanced to the point of imaging seismic facies as the manipulation of images became too complex, the processes for the building of the ANN are sign posted within the code.

Python for Keras.html

The second part of the appendix is the OpendTect report on the supervised neural network. This failed to match any of the sample lines and despite 200,000 epochs of training did not improve the efficacy of the matching parameterisation. However, despite running the training several times, the report could not clarify the errors sufficiently.

```
Number of classes:    10

Vectors classified: 1202
Class 1 vectors: 149. Average match: 0.698344
Class 2 vectors: 89.  Average match: 0.732409
Class 3 vectors: 76.  Average match: 0.726385
Class 4 vectors: 148. Average match: 0.702187
Class 5 vectors: 151. Average match: 0.703631
Class 6 vectors: 147. Average match: 0.700626
Class 7 vectors: 138. Average match: 0.70131
Class 8 vectors: 151. Average match: 0.697866
Class 9 vectors: 75.  Average match: 0.735857
Class 10 vectors: 78. Average match: 0.741448


Input node relative importances:
 10.5    ( Sample -8 )
 99.6    ( Sample -4 )
  6.1    ( Sample 0 )
100.0    ( Sample 4 )
  9.5    ( Sample 8 )
 25.1    ( Sample 12 )
 22.9    ( Sample 16 )
 10.9    ( Sample 20 )
 94.3    ( Sample 24 )
```

```
   Node  \ Class   Center 1    Center 2    Center 3    Center 4
      Center 5    Center 6    Center 7    Center 8    Center 9
      Center 10
   Sample -8 9.55823326   3.23447585   -19.17640877 -7.76707077  2.19749808
      16.79426193  -2.25161171  13.34115887  7.78840351   23.05752373
   Sample -4 -89.19706726 -88.93844604 -87.77290344 -87.05986023 -
87.57297516  88.17922974  87.6470871   88.04319763  88.78469086  89.1650238
   Sample 0  -1.42366982  10.97377777  6.22381067   -7.07239723  5.49782801
      -4.27475882  -1.77433598  -8.75527477  6.41801834   -9.92746735
   Sample 4  -88.56599426 -87.53422546 -88.77284241 87.36676025  87.79534912
      87.60972595  -86.55667114 -88.057724   87.87948608  88.51043701
   Sample 8  -3.06436062  -6.63726091  -6.95482254  -3.98720694  -3.80904388
      -8.45701694  -15.01521111 -16.84402466 -22.90056801 7.69272137
   Sample 12 -8.37533951  -20.64115906 -7.56595469  -2.06726241  -6.00937557
      5.45929527   -16.34329796 2.8311522    80.76268005  -84.32266998
   Sample 16 6.5772872    -81.89868927 77.80245972  13.98993111  2.05480385
      1.53109527   -7.08083773  -6.30576372  -19.96149063 5.16209841
   Sample 20 -17.31902122 3.65159726   -5.40326929  9.06561184   0.34258717
      -15.46450901 -27.43945313 -6.2810688   -0.40021035  -22.14592552
   Sample 24 87.75682831  -84.43785858 -84.15466309 -86.45758057 85.97717285
      85.01824951  85.806633    -87.34324646 -85.13922882 -83.09951019
```

13.4 APPENDIX 4 – LEGISLATION SURROUNDING MARINE ARCHAEOLOGY

GUIDANCE & LEGISLATION FOR MARINE PALAEOLANDSCAPE ARCHAEOLOGICAL RESEARCH & INVESTIGATION

This Appendix is based on practice from the Standards and Guidance for Historic Environment Desk-based Assessment Document (Cottrell 1993), Wessex Technical Report Guidance for Dogger Bank Windfarms, UK Waters (Archaeology 2007), FUGRO Hollandze Kust Windfarm Environmental Reports (Thal et al. 2018), Infrastructure Planning Inspectorate 2015 & NSPRMF 2019 Guidelines.

This appendix attempts to bring together the most important UK and EU guidance documentation and legislation relating to the archaeological investigation of palaeolandscapes in submarine environments. It is compiled from reports by Wessex in the UK and FUGRO in the Netherlands as well as the NSPRMF (Peeters et al. 2019) 2019 Guidelines therefore taking into account archaeological, industrial and governmental concerns.

13.4.1 Terrestrial Legislation of Concern:

Each of the following apply equally in a marine environment as they do on land and are specific to the UK and UK waters.

Ancient Monuments and Archaeological Areas Act 1979 – This legislation has been amended to include offshore cultural heritage areas, though at present these are in coastal regions (Seahenge, submerged forests etc on accessible beaches)

Protection of Military Remains Act (1986) – Aircraft are specifically catered for in their own legislation (2002) and wrecked vessels are not covered automatically, though the MoD has the right to control a site they deem 'sensitive'. This act covers 'personnel' and 'items' such as unexploded ordnance.

Identifying and Protecting Palaeolithic Remains: Archaeological Guidance for Planning Authorities and Developers (Heritage 1998)

Military Aircraft Crash Sites (Lamotte 2002) – (see Protection of Military Remains above).

The Setting of Heritage Assets (English Heritage 2011) – Becomes important if an area becomes listed as a 'site'

13.4.2 UK Marine Legislation and Guidance:

The following apply only in UK waters

Protection of Wrecks Act (1973) – like the Military Aircraft Crash Sites, the discovery of a boat / shipwreck must be reported and investigated if unrecorded. If considered important it may be licenced. It may also be deemed dangerous due to cargo and / or ordnance.

Merchant Shipping Act (1995) – important for declaring the ownership of underwater finds. Defined as 'flotsam, jetsam, derelict and lagan found in or on the shores of the sea or any tidal water'. Within the 12nM limit of UK waters these must be reported to the Receiver of Wreck and the Maritime Agency.

Code of Practice for Seabed Developers (JNAPC 1995) – these are compliance guidelines for all industry development and were created with governmental approval. They are non-mandatory.

COWRIE: Historic Environment Guidance for the Offshore Renewable Energy Sector (Archaeology 2007) – Developed by Wessex Archaeology, these are again non-mandatory for the renewable energy sector.

13.4.3 European or International Waters Legislation:

United Nations Convention on the Law of the Sea (Cottrell 1993) – The UK ratified this Convention in 1997, stating a provision of protection of marine archaeological artefacts and sites to 24nM offshore.

International Council of Monuments and Sites Charter on the Protection and Management of Underwater Cultural Heritage (Fletcher-Tomenius and Williams 1999) (the Sofia Charter)

European Convention on the Protection of the Archaeological Heritage (Revised) (Council of Europe 1992) - The Valletta Convention was ratified by the UK Government in 2000. It binds the countries of the

EU to protect the archaeological heritage within their jurisdiction, therefore up to and including the Continental Shelf.

European Landscape Convention (2000) - UK signed up to this convention in 2007 covering terrestrial, and marine landscapes

UNESCO Convention on the Protection of the Underwater Cultural Heritage (Lamotte 2002) - The UK abstained and is not a signatory to this convention, however it was ratified and came into force in 2009, therefore must be considered as best practice throughout the archaeological world.

13.5 APPENDIX 5 – DIGITAL EXPANDED VERSIONS OF KEY IMAGES

Enclosed on the attached data media, a folder named Images. Within this folder are the following expanded images from the thesis:

- Chapter 4, Figure 4.3 DEM, Culture and Timeslice (0.07s) data in a palimpsest layered GIS. Also included as Digital Appendix 13.5 Section 5
- Chapter 6, Figure 6.1 Study Area within larger coring environment
- Chapter 7, Figure 7.1 Organic Signature Occurrences by Amplitude Intensity
- Chapter 8, Figure 8.18 Organic / Clay Silt interface locations as picked in IHS Kingdom and OpendTect.
- Chapter 10, Figure 10.1 Potential palaeo environment predicted by the phase variance process (study area) and spatial analyses of wider potential.

13.6 APPENDIX 6 – NEW CALIBRATED DATES FOR OFFSHORE ARCHAEOLOGICAL FINDS

The Table of archaeological finds from the southern North Sea (Table 2.4, page 37) provides new radiocarbon calibrated dates BC. These were performed using OxCal version 4.4 via the online resource at https://c14.arch.ox.ac.uk/oxcal.html

The individual results are presented here:

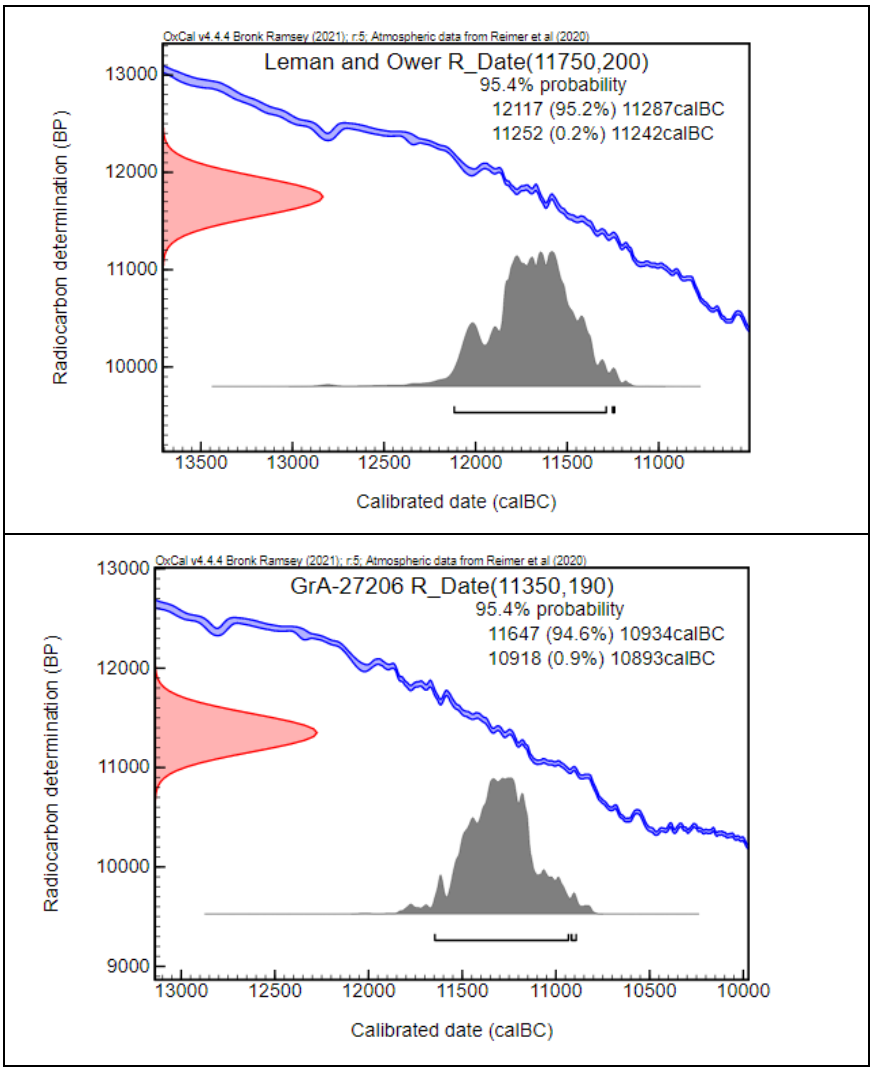

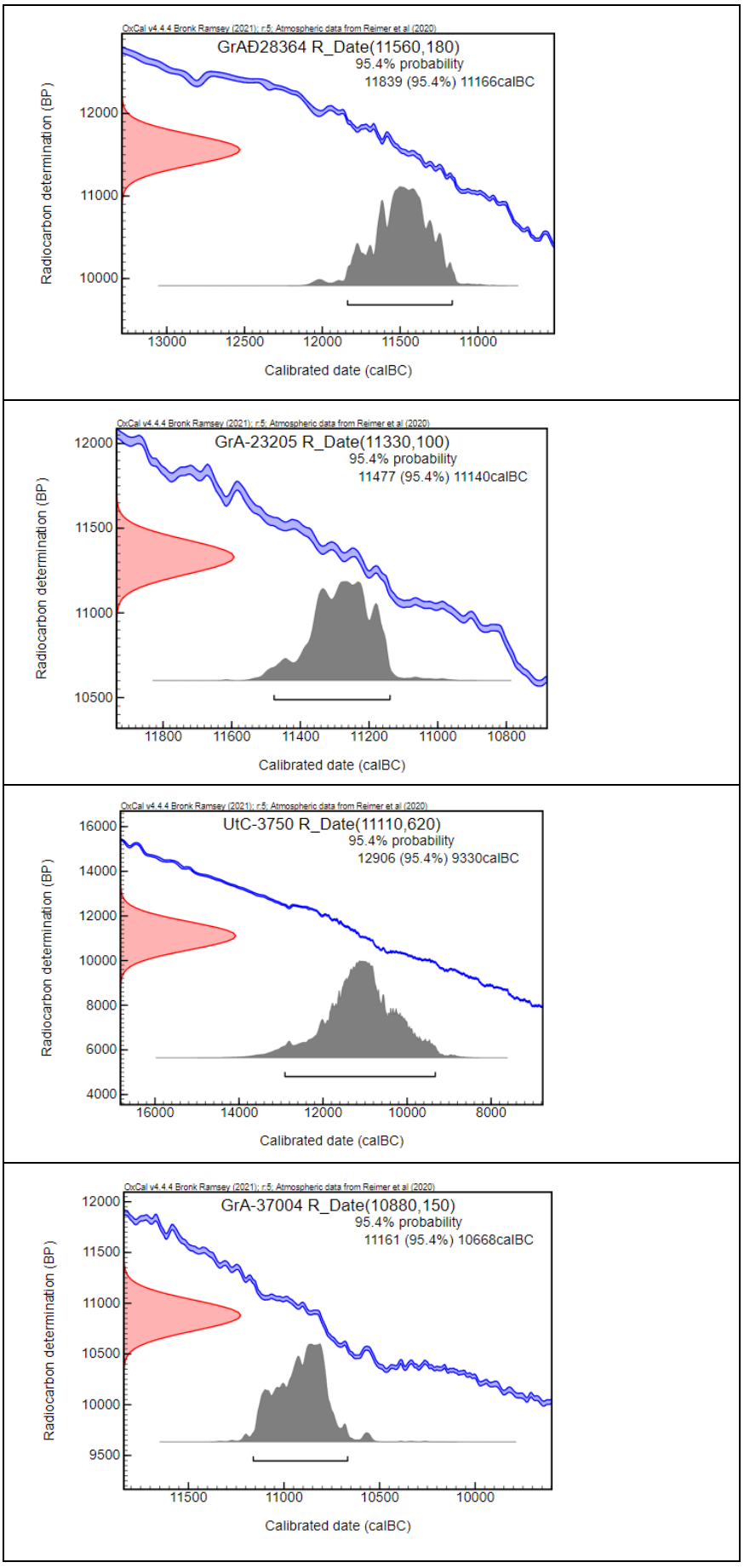
OxCal v4.4.4 Bronk Ramsey (2021); r:5; Atmospheric data from Reimer et al (2020)
GrAÐ28364 R_Date(11560,180)
95.4% probability
11839 (95.4%) 11166calBC
Radiocarbon determination (BP)
Calibrated date (calBC)
OxCal v4.4.4 Bronk Ramsey (2021); r:5; Atmospheric data from Reimer et al (2020)
GrA-23205 R_Date(11330,100)
95.4% probability
11477 (95.4%) 11140calBC
Radiocarbon determination (BP)
Calibrated date (calBC)
OxCal v4.4.4 Bronk Ramsey (2021); r:5; Atmospheric data from Reimer et al (2020)
UtC-3750 R_Date(11110,620)
95.4% probability
12906 (95.4%) 9330calBC
Radiocarbon determination (BP)
Calibrated date (calBC)
OxCal v4.4.4 Bronk Ramsey (2021); r:5; Atmospheric data from Reimer et al (2020)
GrA-37004 R_Date(10880,150)
95.4% probability
11161 (95.4%) 10668calBC
Radiocarbon determination (BP)
Calibrated date (calBC)

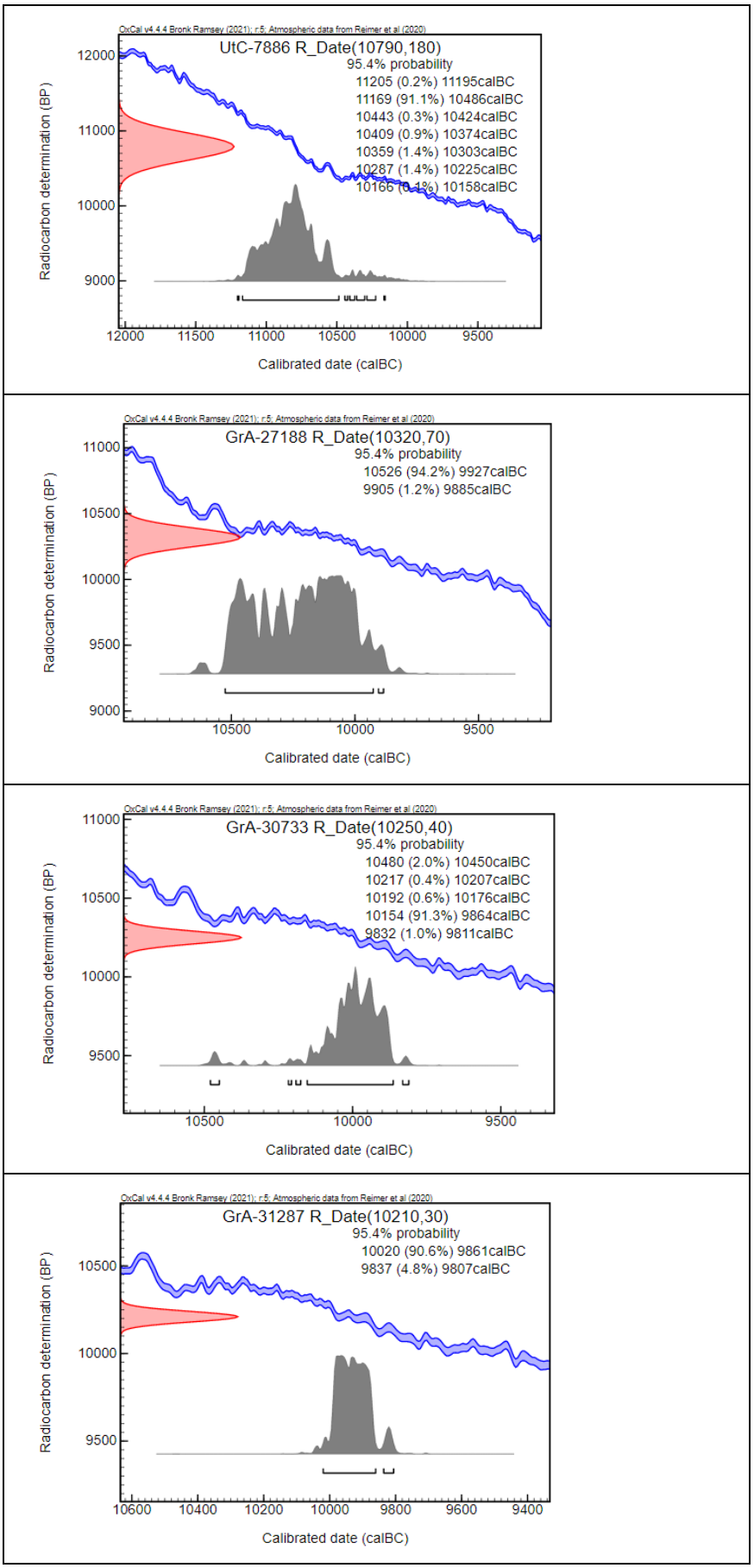
OxCal v4.4.4 Bronk Ramsey (2021); r:5; Atmospheric data from Reimer et al (2020)
UtC-7886 R_Date(10790,180)
95.4% probability
11205 (0.2%) 11195calBC
11169 (91.1%) 10486calBC
10443 (0.3%) 10424calBC
10409 (0.9%) 10374calBC
10359 (1.4%) 10303calBC
10287 (1.4%) 10225calBC
10166 (0.1%) 10158calBC
Radiocarbon determination (BP)
Calibrated date (calBC)
GrA-27188 R_Date(10320,70)
95.4% probability
10526 (94.2%) 9927calBC
9905 (1.2%) 9885calBC
GrA-30733 R_Date(10250,40)
95.4% probability
10480 (2.0%) 10450calBC
10217 (0.4%) 10207calBC
10192 (0.6%) 10176calBC
10154 (91.3%) 9864calBC
9832 (1.0%) 9811calBC
GrA-31287 R_Date(10210,30)
95.4% probability
10020 (90.6%) 9861calBC
9837 (4.8%) 9807calBC

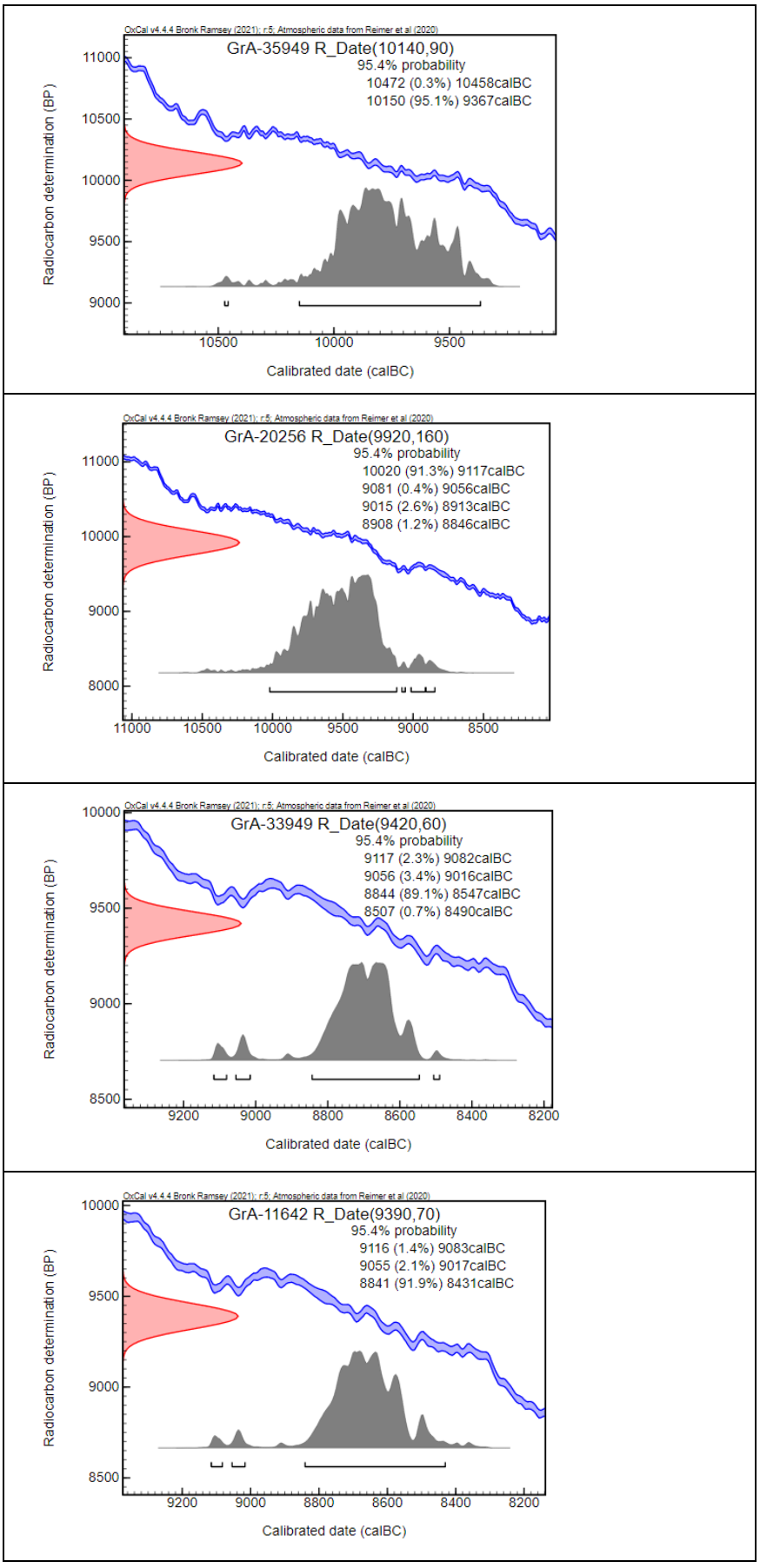
OxCal v4.4.4 Bronk Ramsey (2021); r:5; Atmospheric data from Reimer et al (2020)
GrA-35949 R_Date(10140,90)
95.4% probability
10472 (0.3%) 10458calBC
10150 (95.1%) 9367calBC
Radiocarbon determination (BP)
Calibrated date (calBC)
GrA-20256 R_Date(9920,160)
95.4% probability
10020 (91.3%) 9117calBC
9081 (0.4%) 9056calBC
9015 (2.6%) 8913calBC
8908 (1.2%) 8846calBC
GrA-33949 R_Date(9420,60)
95.4% probability
9117 (2.3%) 9082calBC
9056 (3.4%) 9016calBC
8844 (89.1%) 8547calBC
8507 (0.7%) 8490calBC
GrA-11642 R_Date(9390,70)
95.4% probability
9116 (1.4%) 9083calBC
9055 (2.1%) 9017calBC
8841 (91.9%) 8431calBC

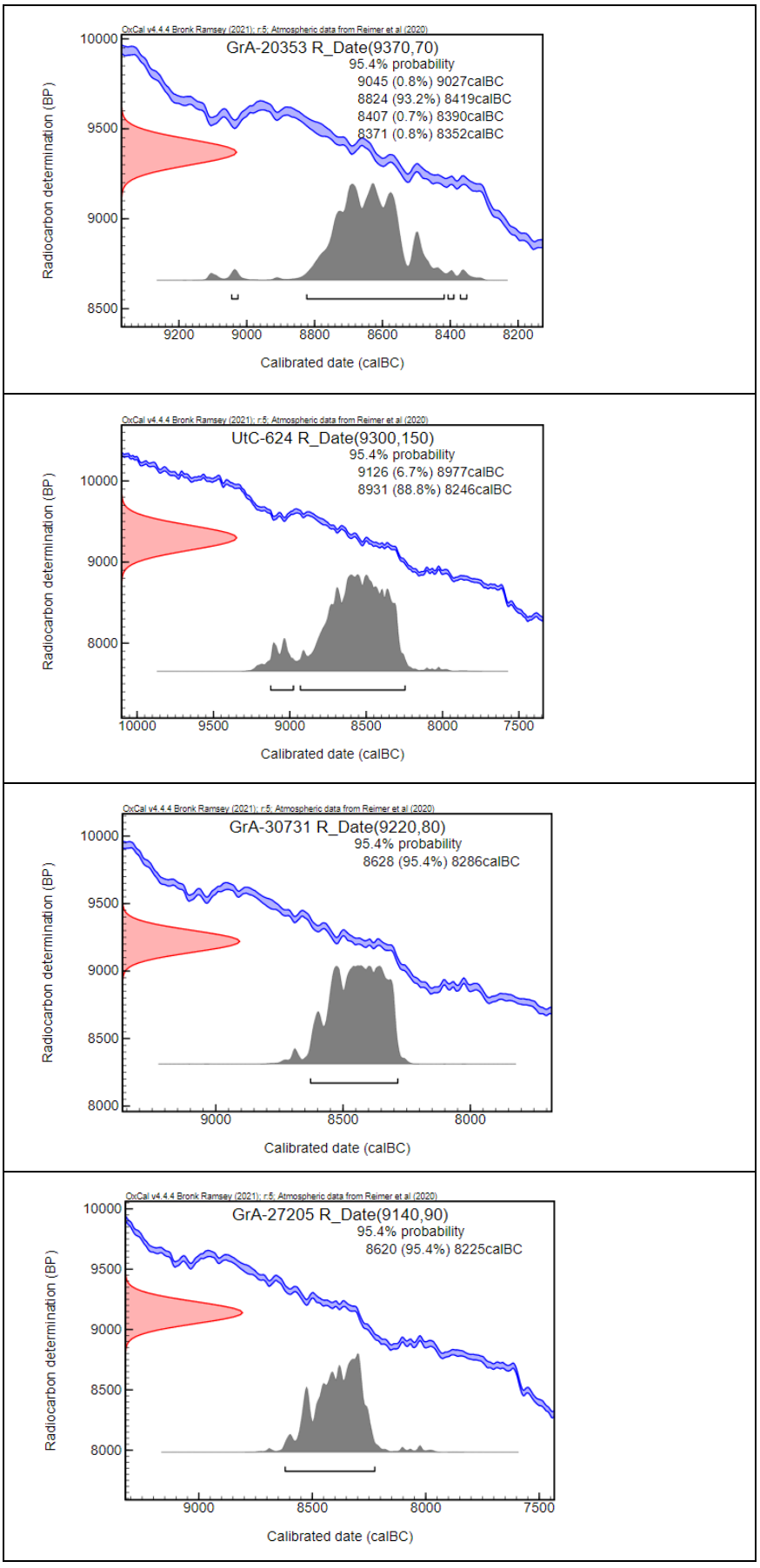
OxCal v4.4.4 Bronk Ramsey (2021); r:5; Atmospheric data from Reimer et al (2020)
GrA-20353 R_Date(9370,70)
95.4% probability
9045 (0.8%) 9027calBC
8824 (93.2%) 8419calBC
8407 (0.7%) 8390calBC
8371 (0.8%) 8352calBC
Radiocarbon determination (BP)
Calibrated date (calBC)
OxCal v4.4.4 Bronk Ramsey (2021); r:5; Atmospheric data from Reimer et al (2020)
UtC-624 R_Date(9300,150)
95.4% probability
9126 (6.7%) 8977calBC
8931 (88.8%) 8246calBC
Radiocarbon determination (BP)
Calibrated date (calBC)
OxCal v4.4.4 Bronk Ramsey (2021); r:5; Atmospheric data from Reimer et al (2020)
GrA-30731 R_Date(9220,80)
95.4% probability
8628 (95.4%) 8286calBC
Radiocarbon determination (BP)
Calibrated date (calBC)
OxCal v4.4.4 Bronk Ramsey (2021); r:5; Atmospheric data from Reimer et al (2020)
GrA-27205 R_Date(9140,90)
95.4% probability
8620 (95.4%) 8225calBC
Radiocarbon determination (BP)
Calibrated date (calBC)

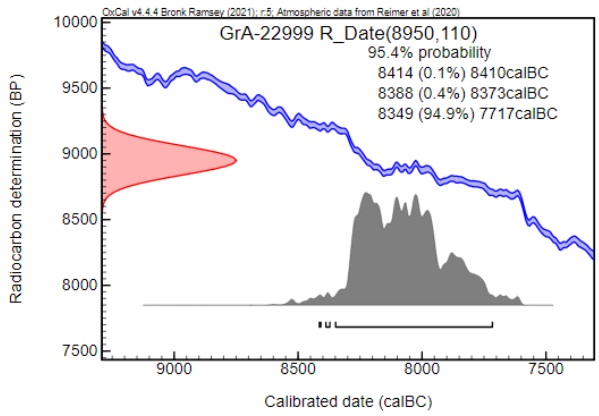
OxCal v4.4.4 Bronk Ramsey (2021); r:5; Atmospheric data from Reimer et al (2020)
GrA-22999 R_Date(8950,110)
95.4% probability
8414 (0.1%) 8410calBC
8388 (0.4%) 8373calBC
8349 (94.9%) 7717calBC
Radiocarbon determination (BP)
10000
9500
9000
8500
8000
7500
9000
8500
8000
7500
Calibrated date (calBC)

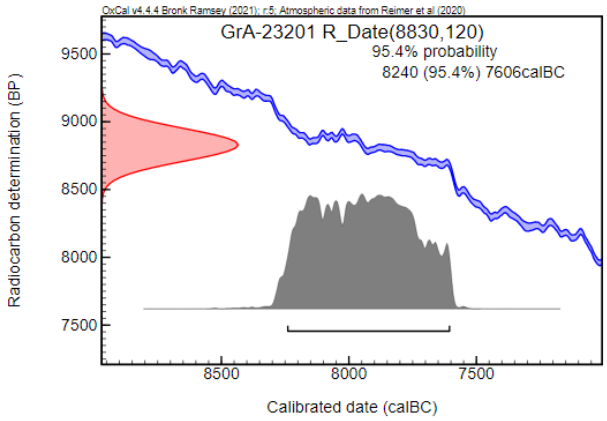
OxCal v4.4.4 Bronk Ramsey (2021); r:5; Atmospheric data from Reimer et al (2020)
GrA-23201 R_Date(8830,120)
95.4% probability
8240 (95.4%) 7606calBC
Radiocarbon determination (BP)
9500
9000
8500
8000
7500
8500
8000
7500
Calibrated date (calBC)